NAVOCEANO's Use of GOES-R and JPSS Data

Danielle Carpenter, Melissa Dykman, Harron Wise, Paul Lyon, Dan Olszewski, Valinda Kirkland, Michelle Little, Bruce McKenzie
Naval Oceanographic Office, NP321 Remote Sensing Branch

The Remote Sensing Branch of the Oceanographic Data Collection Division at the Naval Oceanographic Office (NAVOCEANO) is responsible for providing near-real-time oceanographic measurements to the US Navy, as well as other government agencies. With developmental assistance from the Naval Research Lab (NRL), numerous sets of GOES and JPSS satellite data are processed in house for input to the Navy's Global Ocean Forecast System (GOFS) and the Navy Global Environmental Model (NAVGEM).

MMSPS

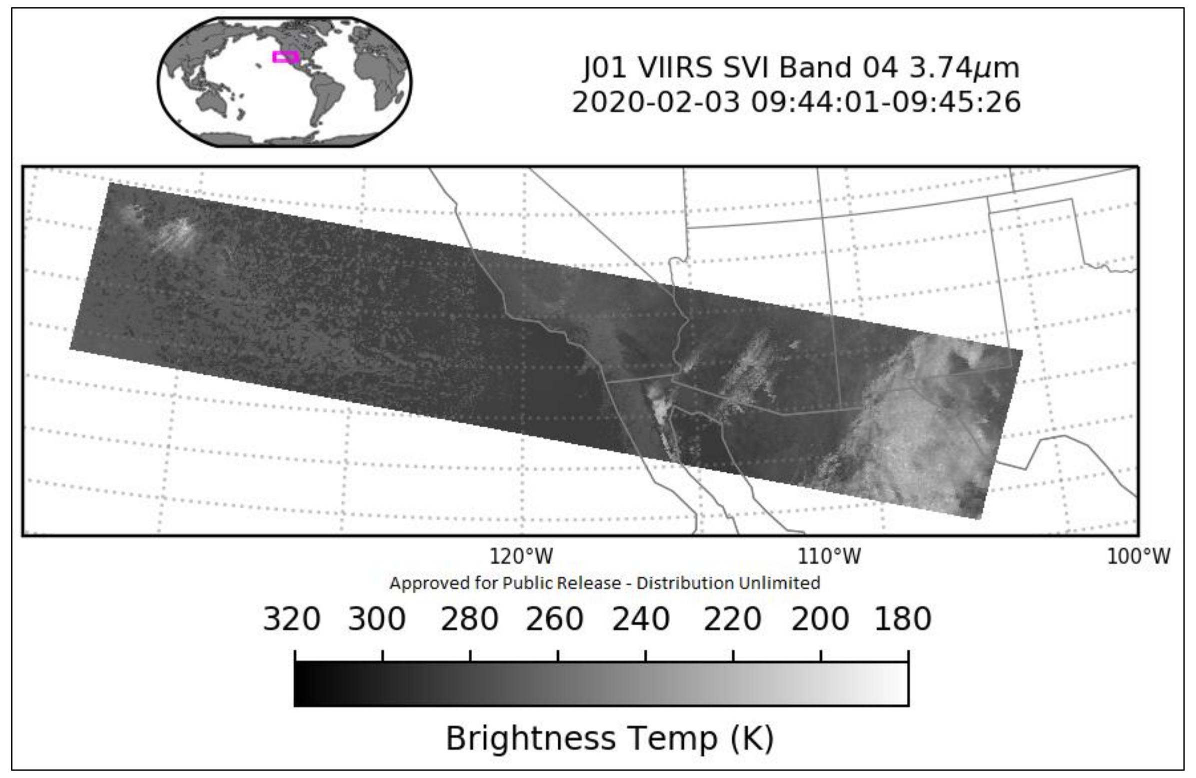

The Multi Mission Satellite Processing Segment (MMSPS) is a system that converts Suomi National Polar-orbiting Partnership (S-NPP), and Joint Polar Satellite System (JPSS-1, now NOAA-20) Extended Application Packet (EAP) raw files for the Visible Infrared Imaging Radiometer Suite (VIIRS) and Advanced Technology Microwave Sounder (ATMS) sensors into Raw Data Records (RDRs). Those are then fed through the Community Satellite Processing Package (CSPP), developed by the University of Wisconsin, to create Sensor Data Records (SDRs). Those SDRs are used by the NRL Ocean Surface Flux System (NFLUX), the Ice Concentration Processing System (ICPS), the Multi Channel Sea Surface Temperature System (MCSST), and the Automated Optical Processing System (AOPS) at NAVOCEANO for in-house data processing and product creation, to support naval operations.

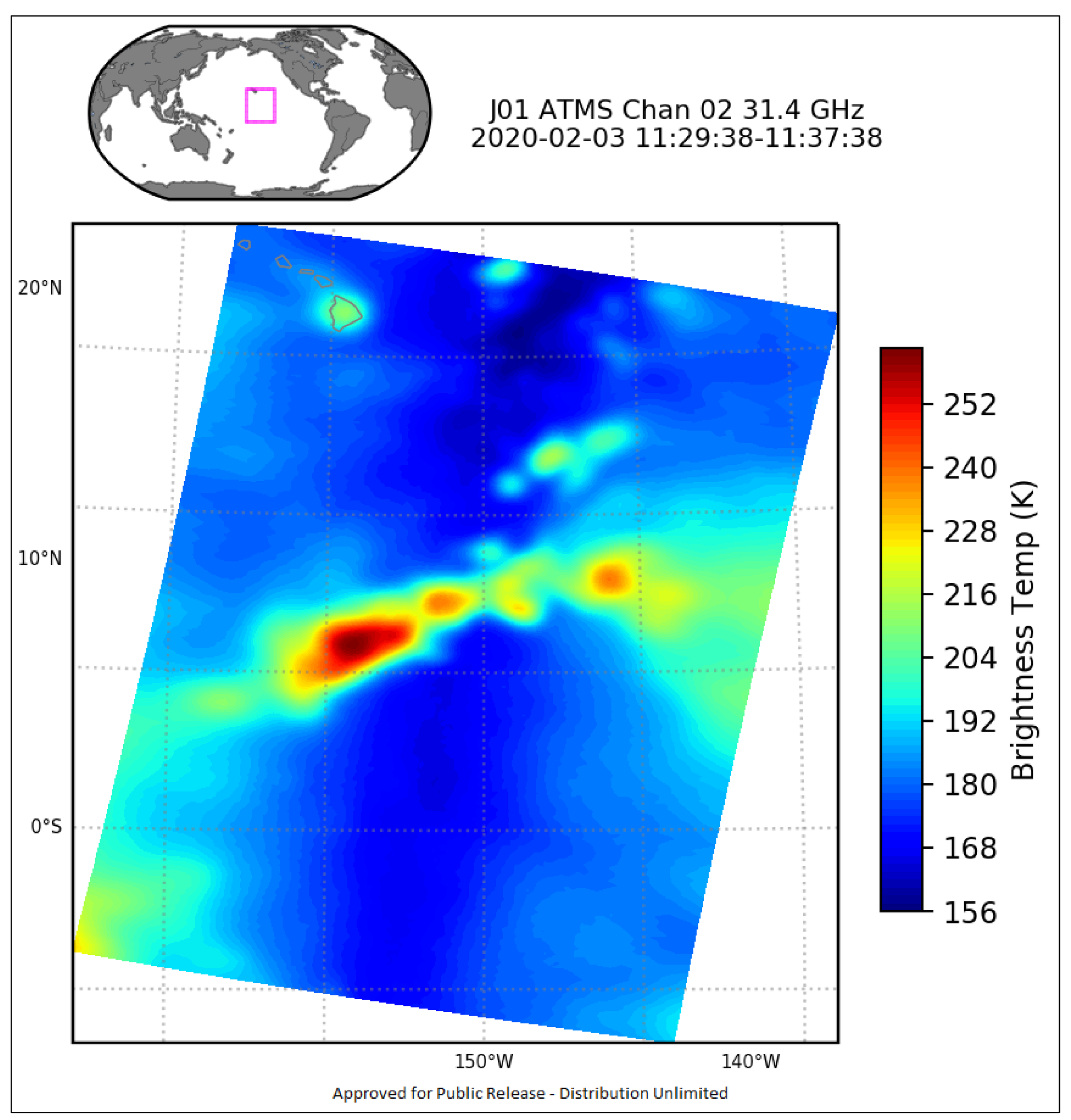

MCSST

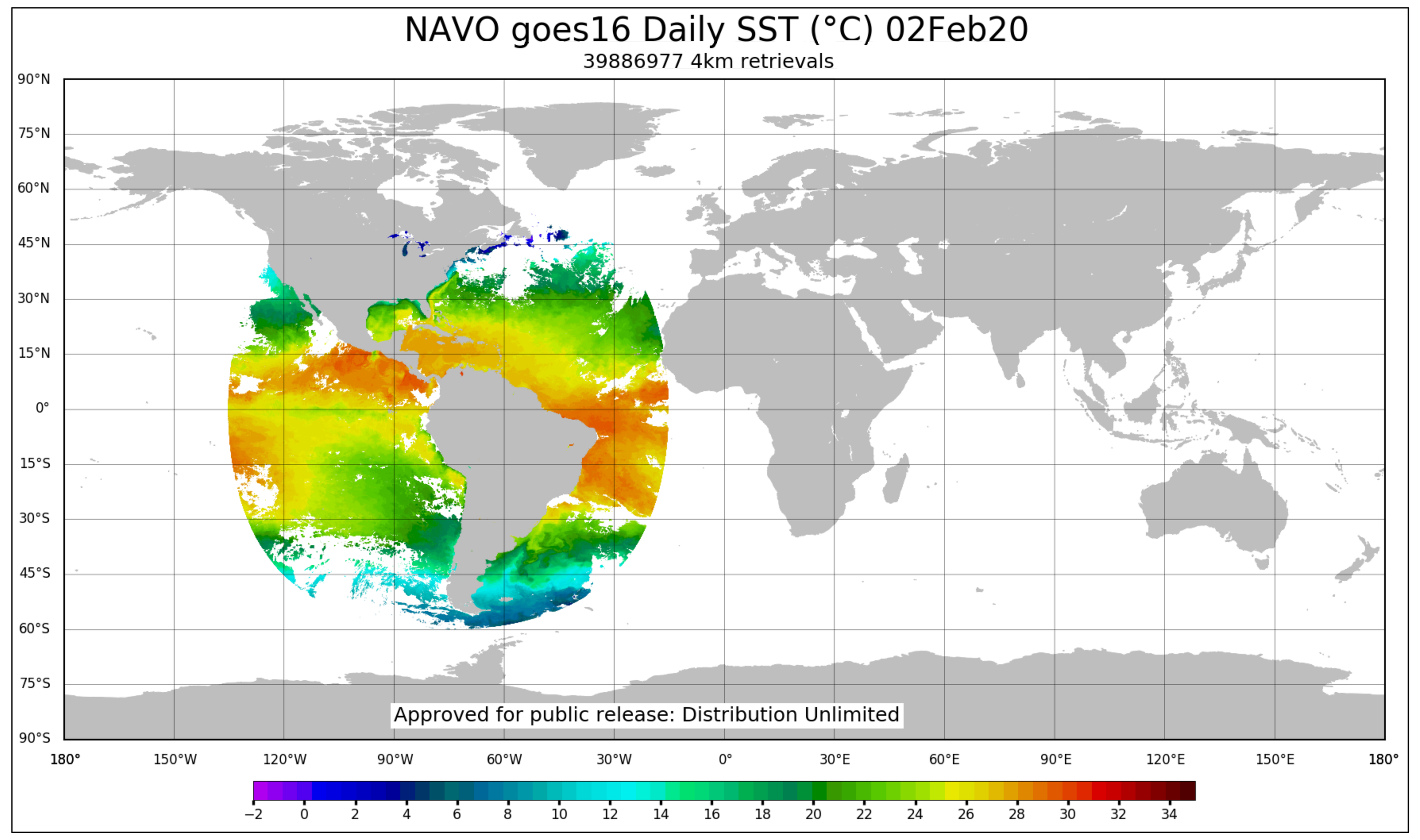

MCSST produces Sea Surface Temperatures (SST) using multiple polar orbiting and geostationary satellites with an in-house suite of software. GOES-16 data, acquired via NCEP College Park, is processed in-house utilizing channels 2, 3, 7, 13, 15, and 16, from the Advanced Baseline Imager (ABI). NAVO processes full disks every 10 minutes with 4km resolution SSTs (2x2 grid). VIIRS data is processed using channels 5, 7, 12, 15, 16, and associated geolocation data. NAVO processes 85 second granules in near-real-time resulting in daily global coverage with 1.5km resolution (2x2 grid of 750m). SST measurements are an important parameter assimilated into oceanographic and atmospheric forecasts, which constrain circulation model initial conditions and quantify the flux energy exchange between the ocean and atmosphere. Real-time ocean prediction systems readily assimilate SST, along with other oceanographic measurements, to generate mesoscale ocean forecasts for operational maritime activities.

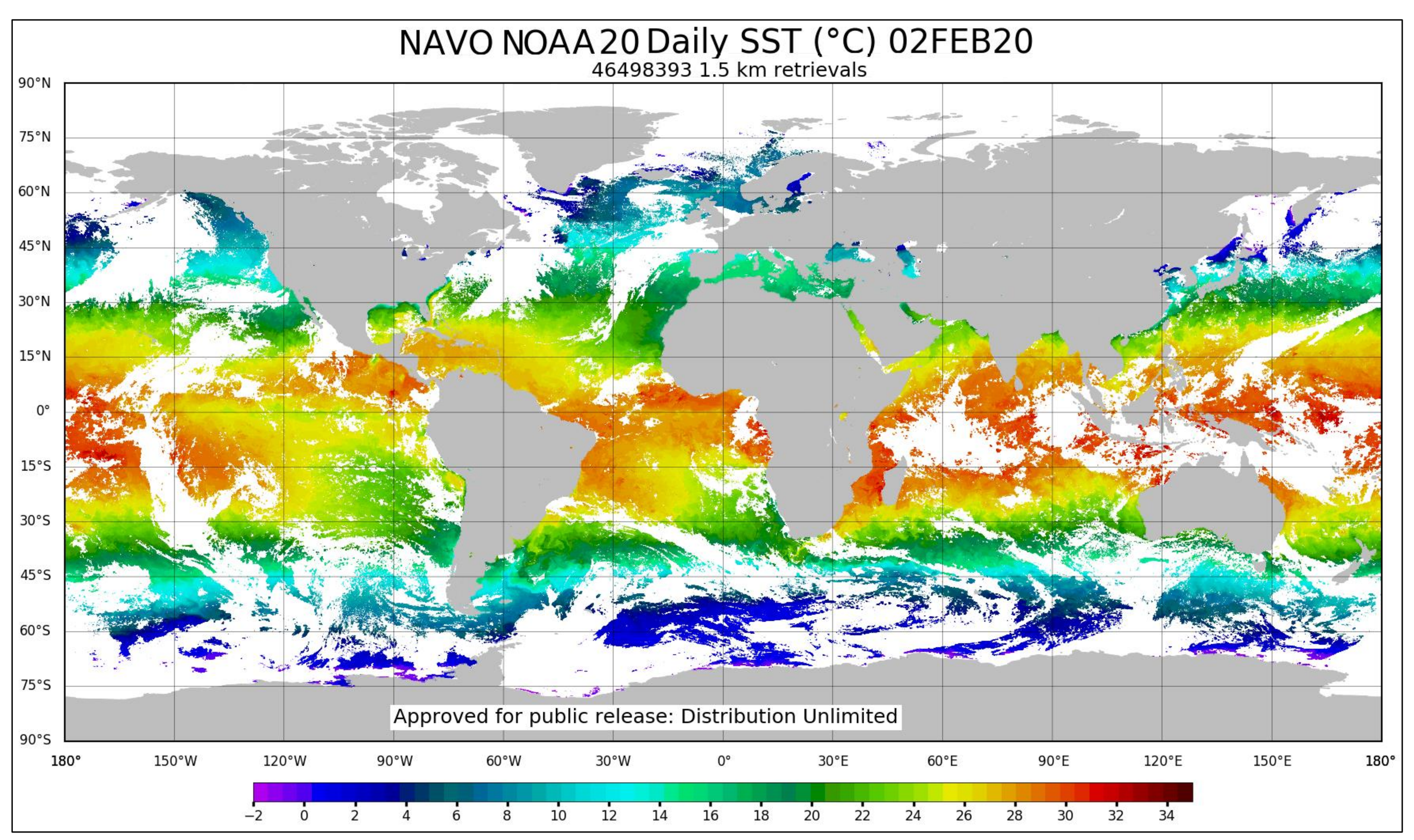

AOPS

The Automated Optical Processing System (AOPS) produces in-water water clarity and visibility from multiple satellite-borne sensors, including VIIRS. The near-real-time products are used by warfighters in the Navy to accomplish their tasks more safely, efficiently and effectively. Historical climatology products are also generated for mission asset scheduling. The in-water optical products are implemented in mission planning and naval operations around the globe.

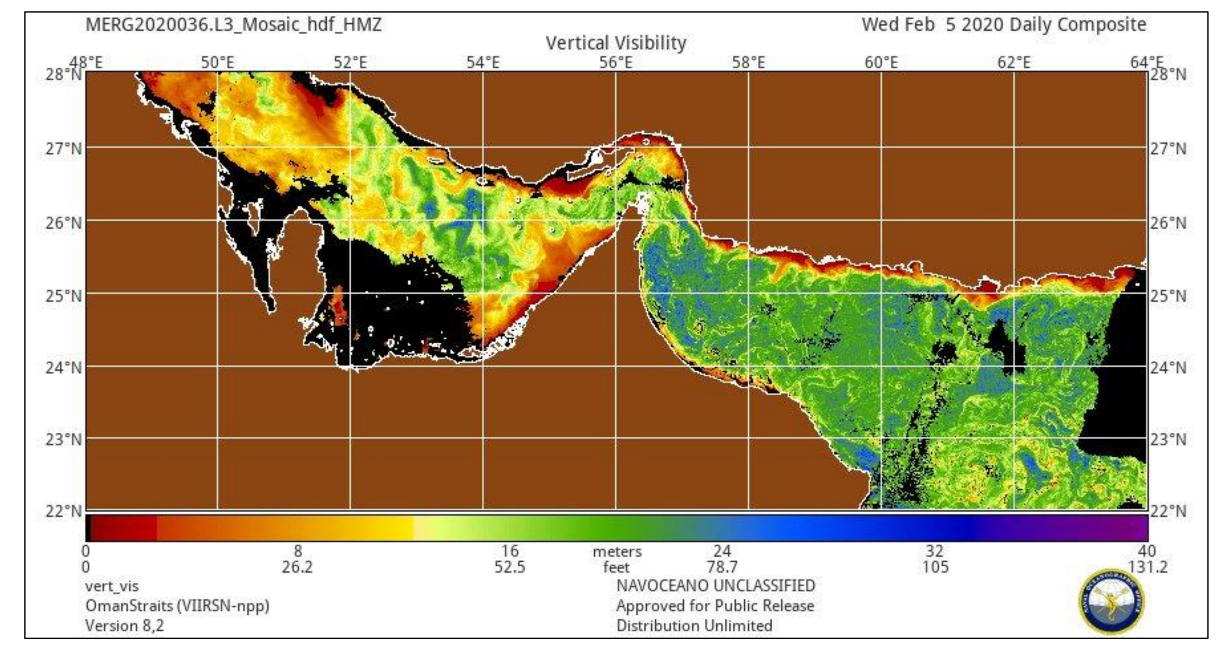

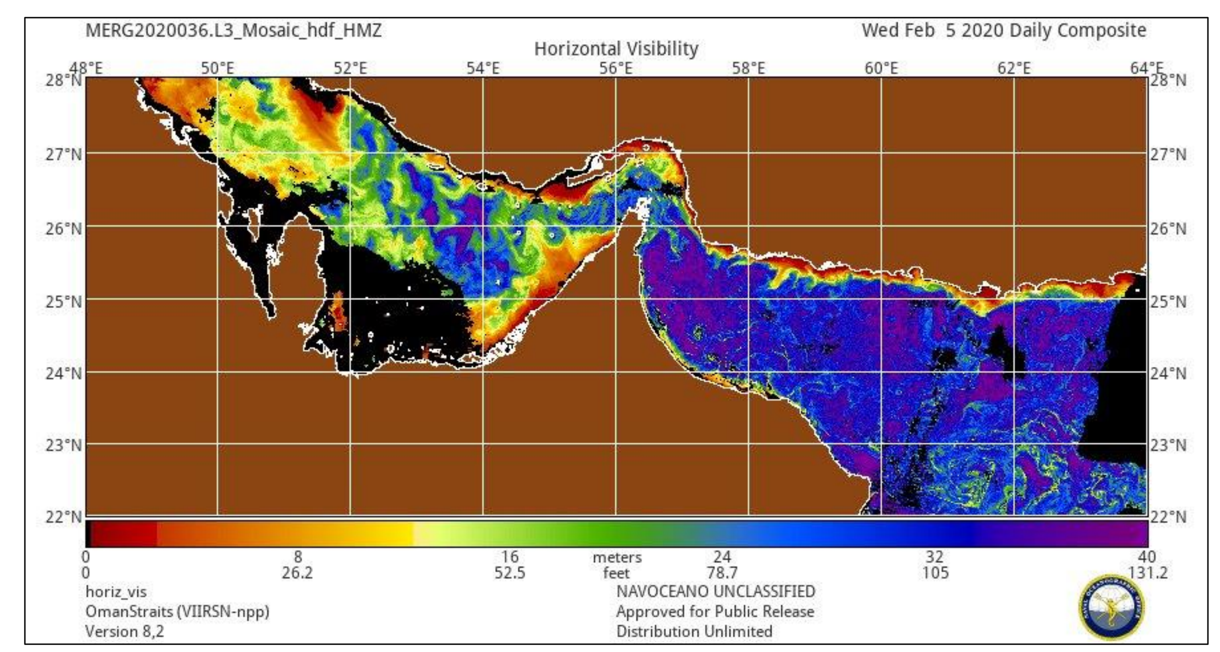

ICPS

ICPS is a system for operationally producing near-real-time ice concentration products from S-NPP, NOAA-20, and Global Change Observation Mission – Water "Shizuku" (GCOM-W1) satellites. Using VIIRS and Advanced Microwave Scanning Radiometer 2 (AMSR2) inputs, it creates ice concentration products for the northern and southern hemispheres. Future updates include higher resolution products and implementation of NOAA-20.

NFLUX

NFLUX is a data processing and assimilation system used to provide near-real-time satellite based surface heat flux fields over the ocean. This system provides satellite based 3-hourly gridded analysis fields over the global ocean for the near-surface parameters of air temperature, specific humidity, wind speed, solar radiation, and longwave radiation. NFLUX uses multiple inputs, including ATMS, from over a dozen different satellites to provide fluxes that will be used to determine NAVGEM bias corrections over the ocean in near-real-time.

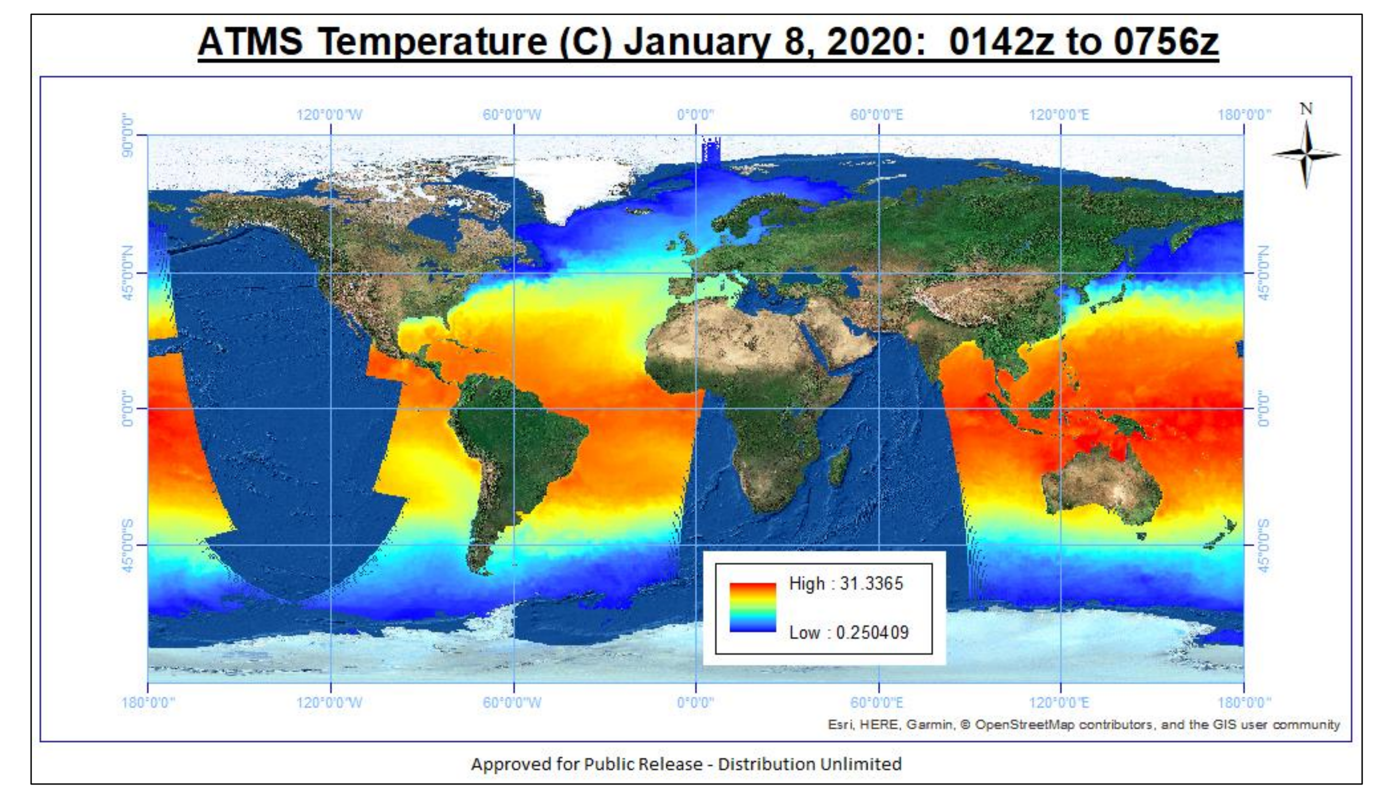

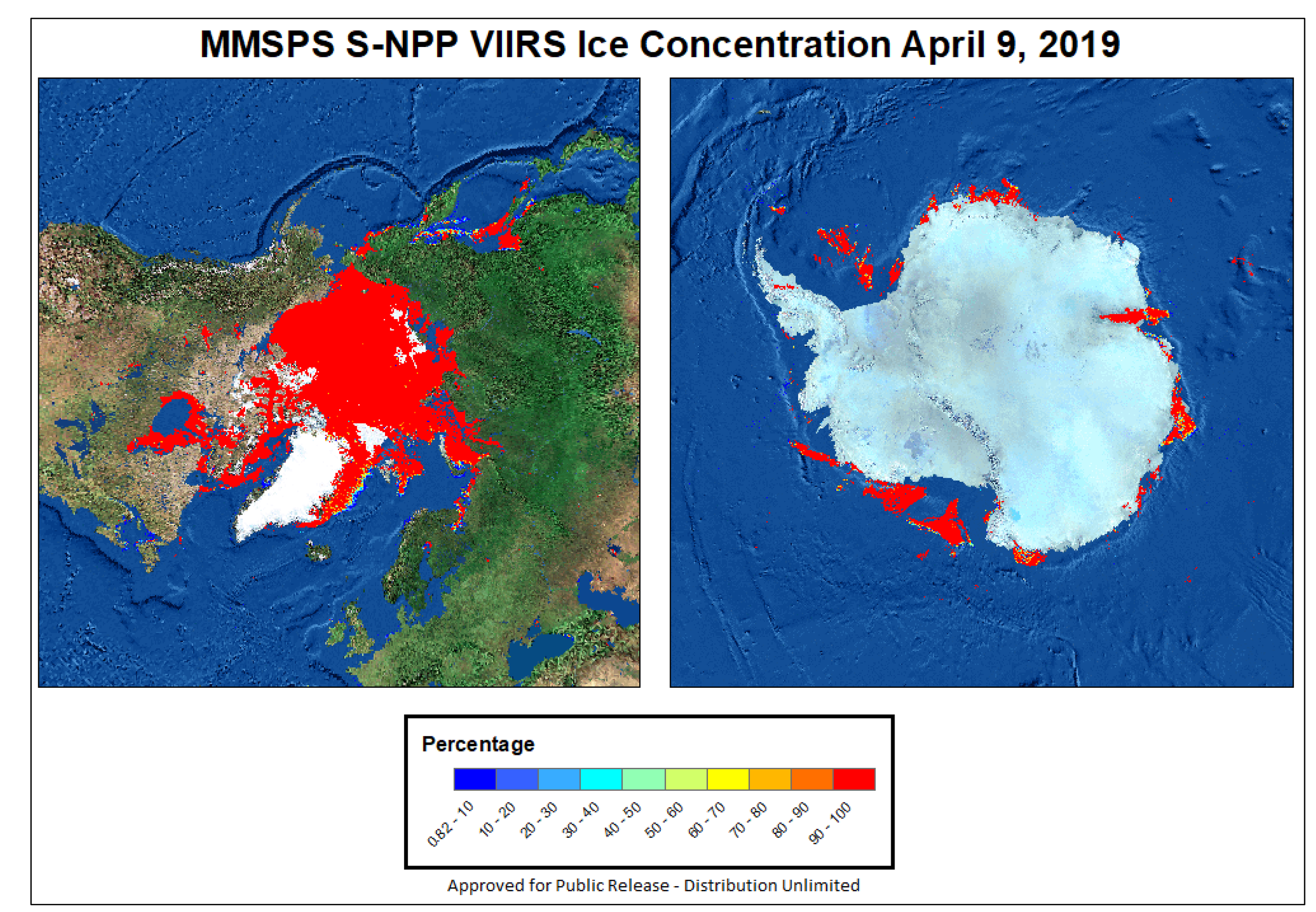

SNPP and NOAA-20 VIIRS Day/Night Band Calibration Performance Monitoring and Applications

Xi Shao[1], Sirish Uprety[1], Yalong Gu[2], Yan Bai[1], Slawomir Blonski[2], Wenhui Wang[1] and Changyong Cao[3]

1. Cooperative Institute for Satellite Earth System Studies (CISESS) , University of Maryland, College Park, MD

2. Global Science & Technology, Inc., Greenbelt, MD

3. NOAA/NESDIS/STAR, College Park, MD

Abstract

- The VIIRS Day/Night Band (DNB) sensors onboard NOAA-20 and SNPP satellites, being 50 minutes apart along the same orbit, provide nighttime imagery of clouds, nocturnal lights, aurora etc., and have been used for a variety of studies involving both geophysical and socio-economic activities.
- Recent SNPP and NOAA-20 DNB calibration algorithm updates focused improving imagery quality of DNB by addressing the striping in high aggregation zones due to residual nonlinearity.
- To synchronize with the improved DNB calibration algorithm, monthly DNB stray light correction LUTs for SNPP and NOAA-20 have also been updated. This poster reports updates that have been performed for SNPP and NOAA-20 DNB stray light correction and evaluates the improvements in DNB imagery product.
- Examples of applications of DNB data products in observations of aurora activities during severe solar storms, deep convective cloud monitoring, observation of light emission from lava flow during volcano eruption and monitoring of impacts of global event on social activities are also given.

SNPP and NOAA-20 DNB Calibration Update and Stray Light Correction

- Details on recent updates and development of SNPP and NOAA-20 DNB calibration can be found in the poster by Gu et al. presented in this session. The calibration algorithm improvements are mainly to reduce strong striping at the end aggregation zone.
- DNB stray light has been observed over both the Northern and the Southern Hemisphere. Origin of the DNB stray light may be due to the leaking of solar light near the extended zone and through the VIIRS Earth view and solar diffuser view aperture. To maintain consistency between DNB stray light correction and calibration algorithm update, monthly DNB stray light correction LUTs have been routinely generated by NOAA/STAR for operational DNB data production.

SNPP DNB Stray Light Correction

- There were remnant stray light of the magnitude ~1 nW/cm^2-sr in the SNPP DNB image over the southern hemisphere resulting from the use of static yearly-recycled stray light correction LUTs (twelve sets) generated during 2014 and 2015. To address this issue, the stray light correction algorithm was improved to support operational SNPP DNB calibration since May, 2019.

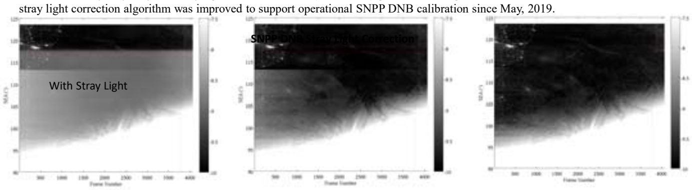

Figure 1. SNPP DNB image over Southern Hemisphere (Left) corrected with recycled stray light correction LUT (Middle) and corrected with improved stray light correction LUT (Right) developed by NOAA/STAR. City lights are better revealed with the improved stray light correction LUT.

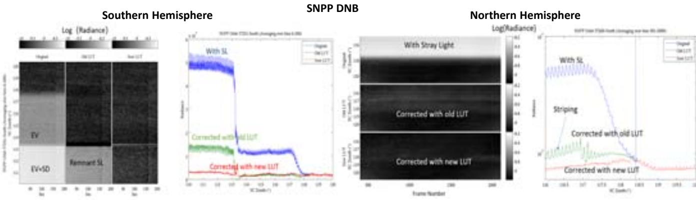

Figure 2: Comparison of stray light correction with recycled and new stray light correction LUT over northern and southern hemisphere indicates the remnant stray light magnitude is ~1 nW/cm^2-sr which were significantly reduced with improved stray light correction.

NOAA-20 DNB Stray Light Correction

- For NOAA-20 DNB, to synchronize with the improved DNB calibration algorithm and maintain consistency between DNB stray light correction and calibration algorithm update, monthly DNB stray light correction LUTs have been routinely generated for one additional full year until November, 2019.

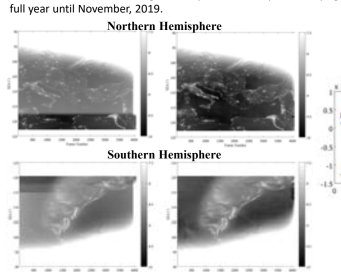

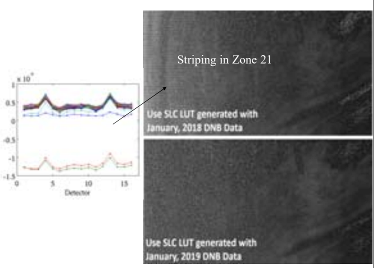

Figure 3: Example of NOAA-20 DNB correction over northern and southern hemisphere. Spatial distribution and radiometric features of nocturnal lights and aurora are better revealed after stray light correction.

Figure 4: Example of updating stray light correction LUT for NOAA-20 DNB to remove the strong striping in aggregation zone 21 after the update of calibration algorithm to address issues of detector nonlinearity in high aggregation zone.

Inter-Comparison of Radiometric Performance between SNPP and NOAA-20 DNB

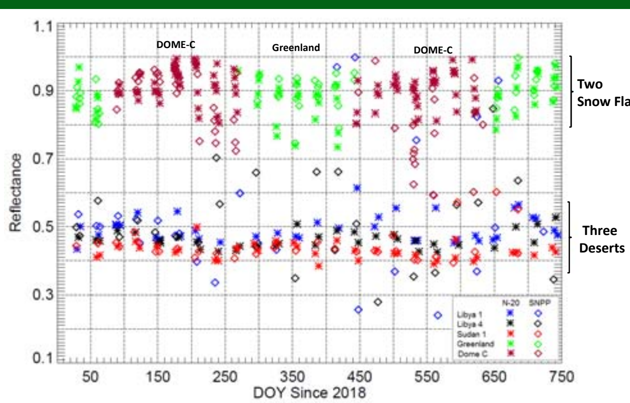

Figure 5: Radiometric consistency (within 3-5% over ~2 years) between SNPP and NOAA-20 DNB are demonstrated through long term monitoring of TOA reflectance derived from vicarious measurements over various pseudo-invariant calibration sites: two snow flats (~0.9 TOA Reflectance) and three desert sites, being illuminated by Moon Light. Lunar irradiance model from Miller and Turner, 2009 has been used to derive the TOA reflectance.

Applications of Day/Night Band

Aurora Activities during Severe Solar Storm Observed by SNPP DNB

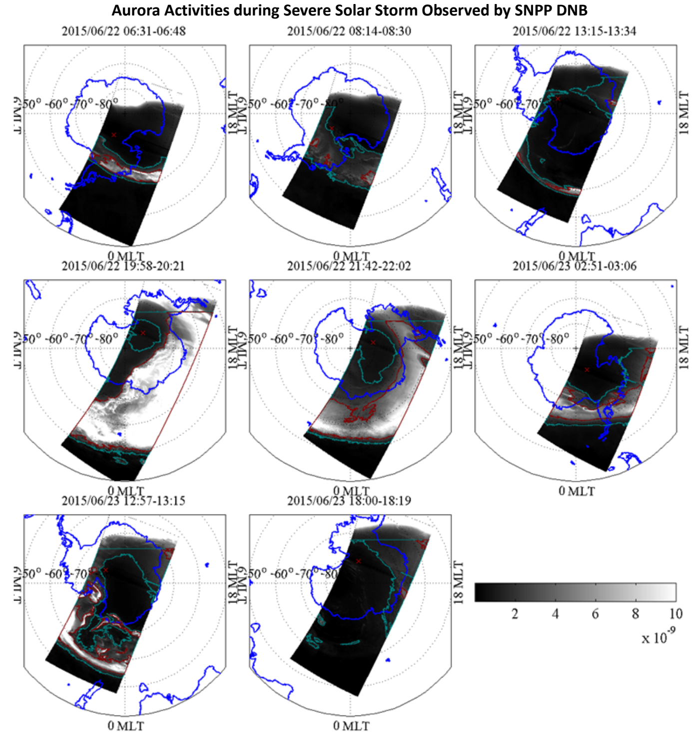

Figure 6: The DNB radiance map over southern hemisphere in solar-magnetic (SM) coordinates from UT 6:31 on June 22 to UT 18:19 on June 23, 2015. Two coronal mass ejections (CME) occurred on June 19 and 21, 2015 and had made their way to Earth to cause a G4 (severe) geomagnetic storm on June 22, 2015. Overall evolution of aurora such as initial appearance, growth, expansion and decay phases were observed in successive DNB overpasses. DNB observations monitored spatial and temporal variation of aurora activities and help understand particle/plasma flow and electromagnetic energy coupling in Sun-Magnetosphere-Ionosphere system during geomagnetic storms.

Deep Convective Cloud Observation under Moon Light

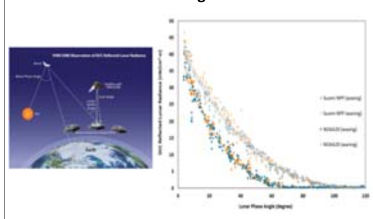

Figure 7: Night light observation of Deep Convective Cloud under moon light by DNB provides unique opportunity to perform inter-calibration of VIIRS DNB between SNPP and NOAA-20 using lunar radiances. (Cao et al., 2019)

DNB Observation of Lava Flow during Hawaii Kilauea Volcano Eruption

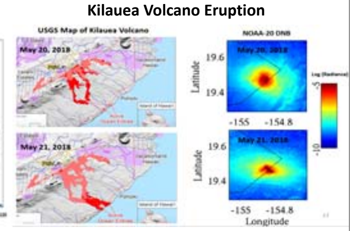

Figure 8: DNB data enable night time monitoring of natural disaster events. The observation of light emission from high temperature lava flow during Hawaii Kilauea volcano eruption by DNB shows the entry of lava into ocean on May 21, 2018, which is consistent with the in-situ measurements by USGS.

Global Event Impact Monitoring: Nocturnal Light Variation before and after Wuhan City Lockdown due to Coronavirus Outbreak

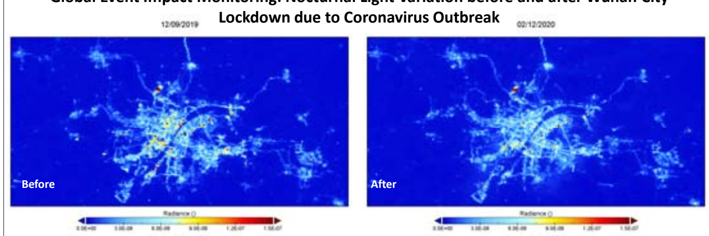

Figure 9: Comparison of night light distribution around Wuhan city, China observed by SNPP DNB before and after the coronavirus outbreak. City light reduction in both magnitude and spatial distribution after one third of city population left the city and with reduced socio-economical activities due to city lockdown on Jan. 23, 2020 can be clearly seen. DNB data provide unique capability for monitoring night light variation during global events.

Summary

- Maintained consistency between SNPP/NOAA-20 DNB stray light correction and recent DNB calibration algorithm update.
- Improved DNB data quality with updated stray light correction for SNPP by removing remnant stray light.
- Radiometric bias trending of SNPP and NOAA-20 DNB over pseudo-invariant calibration sites under moon light shows the radiometric consistency between SNPP and NOAA-20 DNB is within 3-5% with SNPP being higher. Part of the bias is due to the spectral response differences and the use of different solar irradiance spectra for DNB calibration. The rest may be from the calibration uncertainties.
- DNB observation of Deep Convective Cloud enables inter-calibration between SNPP and NOAA-20 DNB using lunar radiances.
- SNPP and NOAA-20 DNB data enable applications in monitoring large spatial scale and temporal variation of aurora light during severe solar storms, nocturnal light variation during global social event, and monitoring light emission variation during global natural disaster events such as lava flow due to volcano eruption.

References:

Cao, C., X. Shao, and S. Uprety, "Detecting light outages after severe storms using the S-NPP/VIIRS Day/Night Band radiances," IEEE Geosci. Remote Sens. Lett. **10**, 1582-1586 (2013).

Cao, C. et al., Radiometric Inter-Consistency of VIIRS DNB on Suomi NPP and NOAA-20 from Observations of Reflected Lunar Lights over Deep Convective Clouds. *Remote Sens.* 2019, *11*, 934.

Gu, Y. et al., Improvement of Visible Infrared Imaging Radiometer Suite Day/Night Band Image Quality, poster in this meeting, 2020.

Miller, S. D. and R. E. Turner, "A Dynamic Lunar Spectral Irradiance Data Set for NPOESS/VIIRS Day/Night Band Nighttime Environmental Applications," in *IEEE Transactions on Geoscience and Remote Sensing*, vol. 47, no. 7, pp. 2316-2329, July 2009.

Improvement of Visible Infrared Imaging Radiometer Suite Day/Night Band Image Quality

Yalong Gu[a], Sirish Uprety[b], Slawomir Blonski[a], Xi Shao[b], Bin Zhang[b], Wenhui Wang[b], and Changyong Cao[c]

[a]GST, [b]University of Maryland, College Park, MD, [c]NOAA/NESDIS/STAR.

Abstract

The Day/Night Band (DNB) is a panchromatic visible and near-infrared band of the Visible Infrared Imaging Radiometer Suite (VIIRS) on-board the Suomi National Polar-orbiting Partnership (S-NPP) and NOAA-20 satellites. Because of its three gain stage design, i.e., Low-Gain Stage (LGS) for daytime scenes, the Mid-Gain Stage (MGS) for twilight scenes, and the High-Gain Stage (HGS) for nighttime low light scenes, the DNB is capable of quantitative measurement of light radiances from 3×10^{-9} W·cm^{-2}·sr^{-1} to 2×10^{-2} W·cm^{-2}·sr^{-1}. The extreme sensitivity to low light enables numerous applications of environmental remote sensing and anthropogenic activities monitoring in nighttime. However, the three gain stage design makes radiometric calibration of the DNB's nighttime data complicated. Artifacts like striping are shown in the calibrated nighttime images. In this paper, we present our efforts for improving image quality of VIIRS DNB onboard both S-NPP and NOAA-20 by updating radiometric calibration algorithms. Our work is beneficial for applications that require high quality of DNB nighttime images.

Introduction

- The VIIRS DNB onboard S-NPP and NOAA-20 is a panchromatic visible and near-infrared band (0.5 ~ 0.9 μm) for Earth observation both day and night.
- The DNB is effectively an integration of three separate bands, i.e., Low-Gain Stage (LGS) for daytime scenes, Mid-Gain Stage (MGS) for twilight scenes and High-Gain Stage (HGS) for nighttime scenes.
- The HGS is able to detect lunar illuminated Earth surface, clouds and artificial lights such as city light, boat, ships, street light etc.
- The extreme sensitivity to low light enables many image based applications, including monitoring of power outages after natural disasters and automated fishing boat detection.
- The three gain stage design makes radiometric calibration of the HGS complicated. Artifacts like striping are shown in the calibrated nighttime images.
- The HGS is calibrated by two key parameters that is dark offset and gain.
- The HGS dark offset is determined by tracking on-orbit change on top of the baseline HGS dark offset by the DNB observation of deep space collected during the spacecraft pitch maneuver early in the mission.
- The HGS gain is obtained by transferring LGS gain through multiplying the MGS/LGS and HGS/LGS gain ratios evaluated in the twilight region.
- The HGS dark offset, MGS/LGS and HGS/MGS gain ratios are updated monthly using data collected during new moon nights.
- In this paper, we present our efforts for improving quality of the DNB nighttime images by radiometric calibration updates.

Correction of Striping due to Detector Nonlinearity

- Striping has been found in many aggregation zones of both the S-NPP and NOAA-20 VIIRS DNB nighttime imagery.
- Aggregation zone 21 of NOAA-20 VIIRS DNB is a typical example, shown in Figure 1.
- Because of the special aggregation option known as Option 21, about 30% pixels of a NOAA-20 VIIRS DNB image are in aggregation zone 21.
- Striping severely degrades the quality of the NOAA-20 VIIRS DNB nighttime imagery.

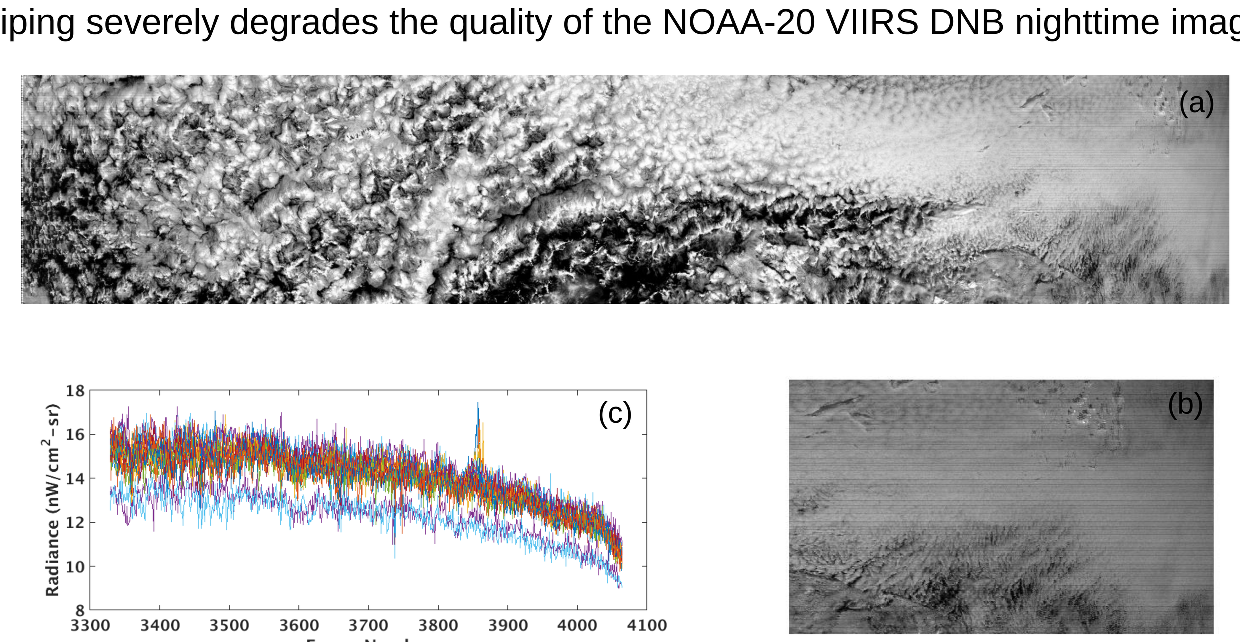

Figure 1. (a) NOAA-20 VIIRS DNB nighttime image recorded at 10:54 UTC, June 28, 2018. (b) striping in aggregation zone 21, right side of (a). (c) The detectors' radiances of a scan in (b).

- Image analysis shows that strips are from the DNB detectors with non-negligible nonlinearity in the low dynamic range.
- The MGS/LGS gain ratios of these detectors determined by the original algorithms are biased, consequently making the corresponding HGS gains biased ($G_{HGS} = G_{HGS/MGS} \times G_{MGS/LGS} \times G_{LGS}$, Figure 2).

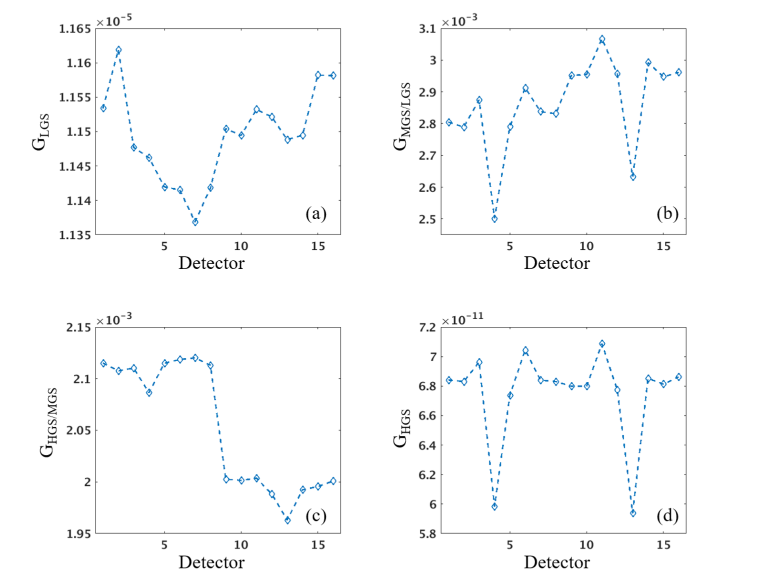

Figure 2. (a) LGS gain, (b) MGS/LGS gain ratio, (c) HGS/MGS gain ratio, and (d) HGS gain for all detectors of aggregation mode 21 used for radiometric calibration of the NOAA-20 VIIRS DNB nighttime image shown in Figure 1.

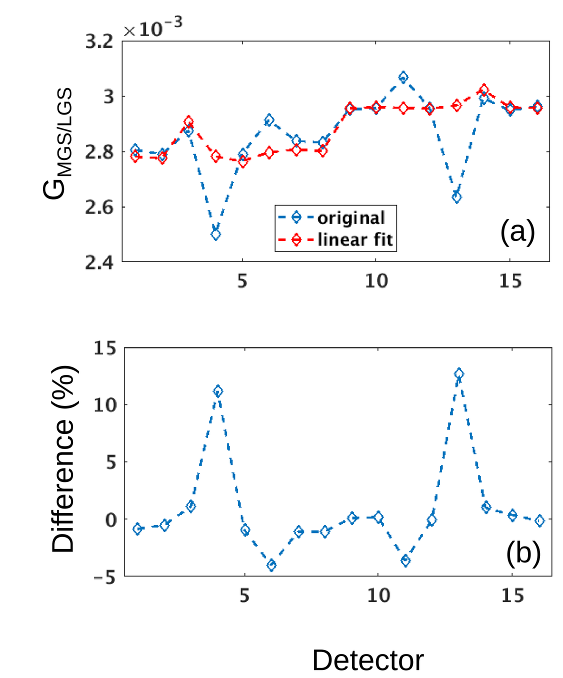

Figure 3. (a) $G_{MGS/LGS}$ determined by the original algorithm and the linear regression method. (b) Relative difference [100% × (linear - original)/linear]

- Such biased gain ratios can be corrected by the improved algorithm based on linear regression. (Figure 3).
- Striping in the reprocessed DNB nighttime images, in particular those under moonlight illumination, is significantly reduced (Figure 4).
- DNB gain ratios LUTs created by the improved algorithm have been used in operational calibration for both the S-NPP and NOAA-20 VIIRS DNB since March 2019 and November 2018 respectively.

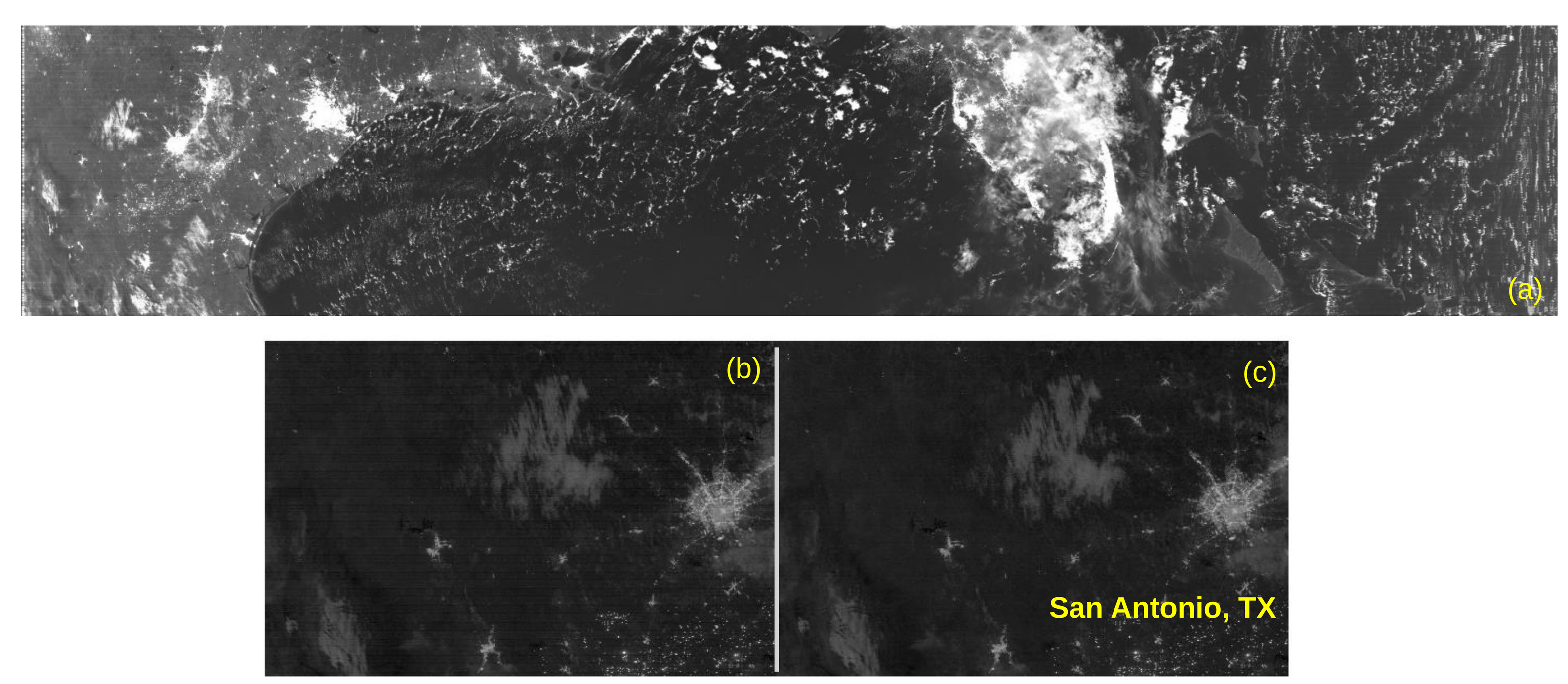

Figure 4. (a) NOAA-20 VIIRS DNB nighttime image recorded at 07:31 UTC, June 28 2018. (b) striping in aggregation zone 21, left side of (a). (c) reprocessed image by the updated gain ratios.

Improved SNPP VIIRS DNB Image Quality after Reprocessing

Reprocessed SNPP VIIRS DNB SDRs from early mission to March 2017 accommodate calibration updates since launch

- Continuous DNB LGS gain degradation using modulated relative spectral response (RSR) function, benefiting application of nightlight time series for study of socioeconomic changes (Figure 5).

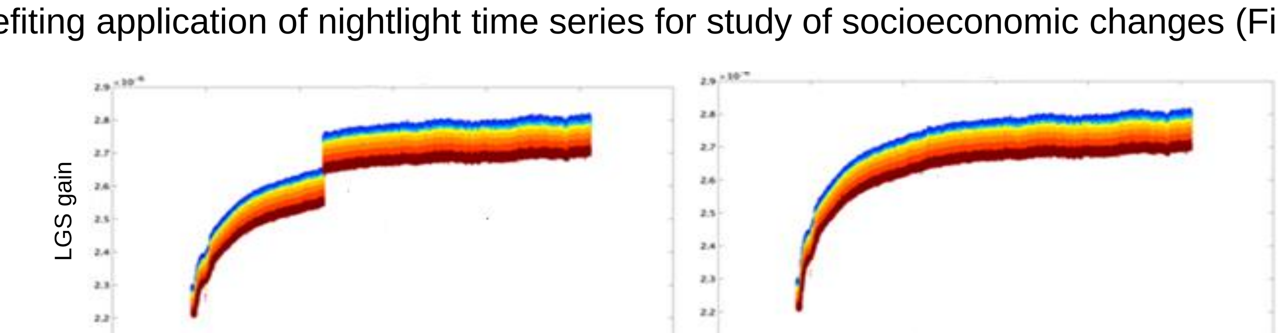

Figure 5 DNB LGS gain trends (aggregation mode 1). (a) Using only one update in RSR (April 4, 2013). (b) Using continuous sets of time-dependent RSRs for reprocessing.

- Significantly improved quality of the DNB data collected before March 20, 2012 which were originally calibrated with the prelaunch LUTs .

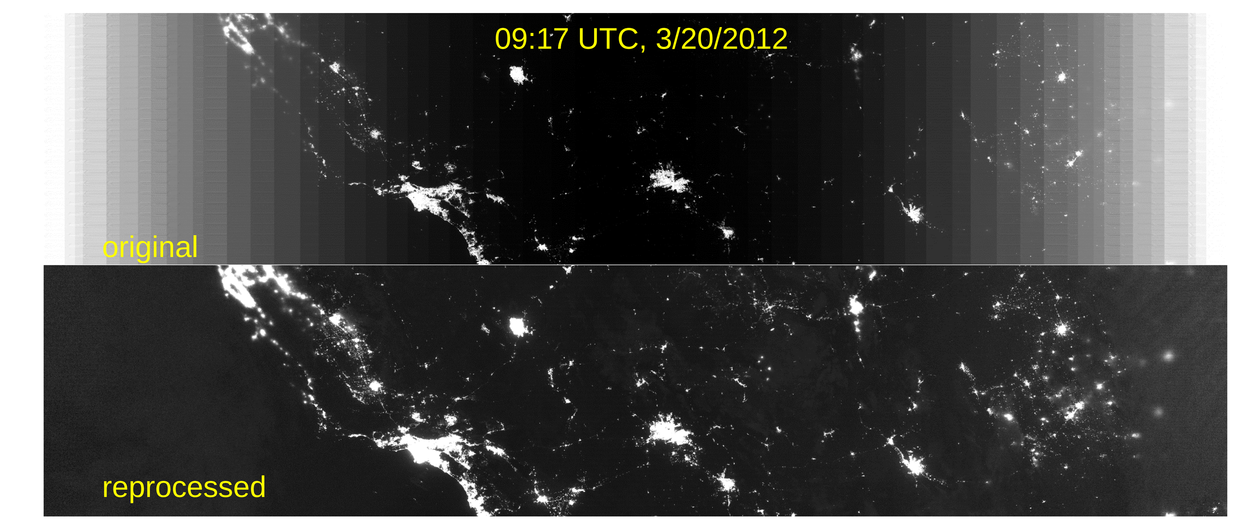

- Straylight corrected DNB data available since early mission of SNPP.

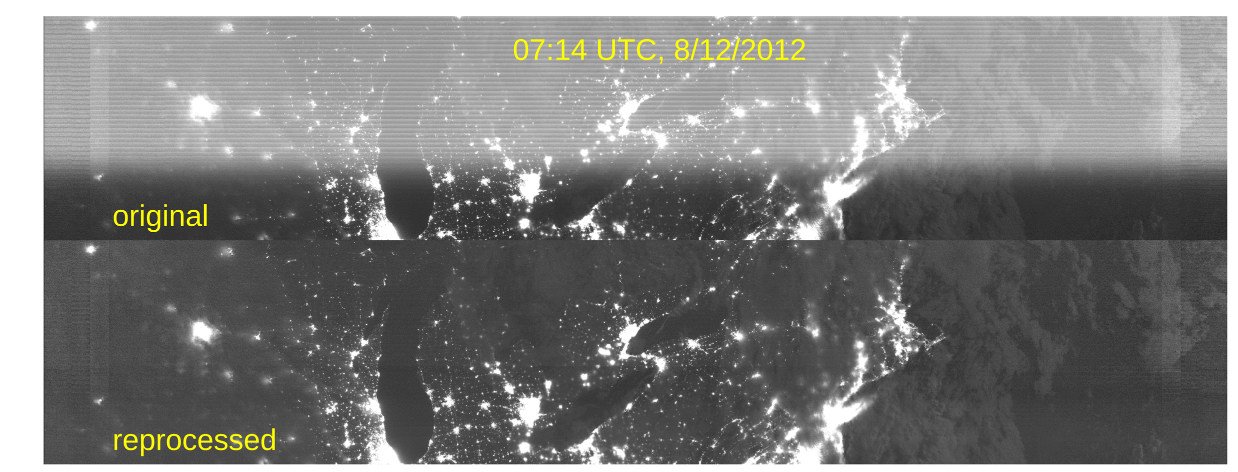

- Enhanced low light detection by the deep space based HGS dark offset

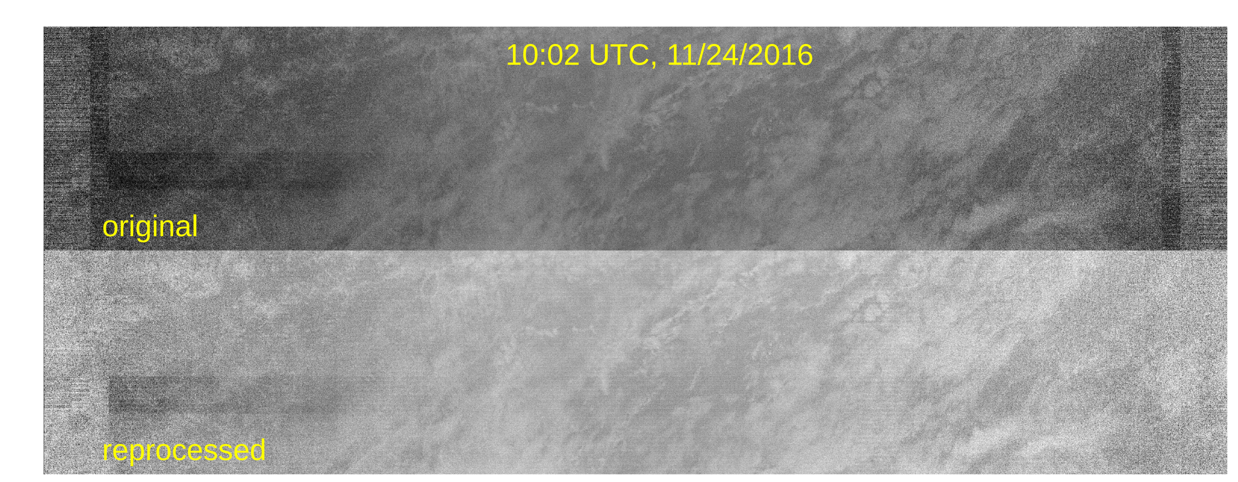

Summary

- This study summarized radiometric calibration updates for improving image quality of VIIRS DNB onboard both S-NPP and NOAA-20 satellites.
- Major improvements include:
  - Correction of striping due to detector nonlinearity
  - Continuous DNB LGS gain degradation correction by modulated RSRs
  - DNB data collected during early mission calibrated with the postlaunch LUTs
  - Straylight corrected DNB data available since early mission
  - Enhanced low light detection by the deep space based HGS dark offset
- *Reprocessed SNPP VIIRS SDR data including DNB from early mission to March 2017 are available at https://ncc.nesdis.noaa.gov/VIIRS/index.php*

References:

[1] S. D. Miller, W. Straka, S. P. Mills, C. D. Elvidge, T. F. Lee, J. Solbrig, A. Walther, A. K. Heidinger, and S. C. Weiss, "Illuminating the capabilities of the suomi national polar-orbiting partnership (NPP) visible infrared imaging radiometer suite (VIIRS) day/night band," *Remote Sensing* **5**, 6717-6766 (2013).

[2] C. Cao, X. Shao, and S. Uprety, "Detecting light outages after severe storms using the S-NPP/VIIRS Day/Night Band radiances," IEEE Geosci. Remote Sens. Lett. **10**, 1582-1586 (2013).

[3] C. D. Elvidge, M. Zhizhin, K. Baugh, and F. C. Hsu, "Automatic boat identification system for VIIRS low light imaging data," Remote Sens **7**, 3020-3036 (2015).

Acknowledgment :

This study is funded by the Joint Polar Satellite System (JPSS) program. Poster contents are solely the opinions of the authors and do not constitute a statement of policy, decision, or position on behalf of NOAA or the U.S. government

Enterprise VIIRS LST Production for JPSS Mission: Validation and Application

Yuling Liu[1] , Yunyue Yu[2], Peng Yu[1], Heshun Wang[1]

1. ESSIC/CISESS, University of Maryland, College Park, MD 2. STAR/NESDIS/NOAA, College Park, MD.

Enterprise JPSS VIIRS LST Product Introduction

NDE Land Surface Temperature Product

- Based on split window technique

$$T_s = C_0 + C_1T_{11} + C_2(T_{11} - T_{12}) + C_3\varepsilon + C_4\varepsilon(T_{11} - T_{12}) + C_5\,\Delta\varepsilon$$

T_{11} and T_{12} : the TIR split-window channel BTs
ε and $\Delta\varepsilon$: mean emissivity at the TIR spectrum, and the emissivity difference
LUT {C} dimension: Day/night, View Zenith Angle, Total Column Water Vapor

- Granule (L2) and gridded (L3) LST product for both SNPP VIIRS and NOAA 20 VIIRS
- L2 VIIRS LST has been in operational and the L3 VIIRS LST was just put into operational.

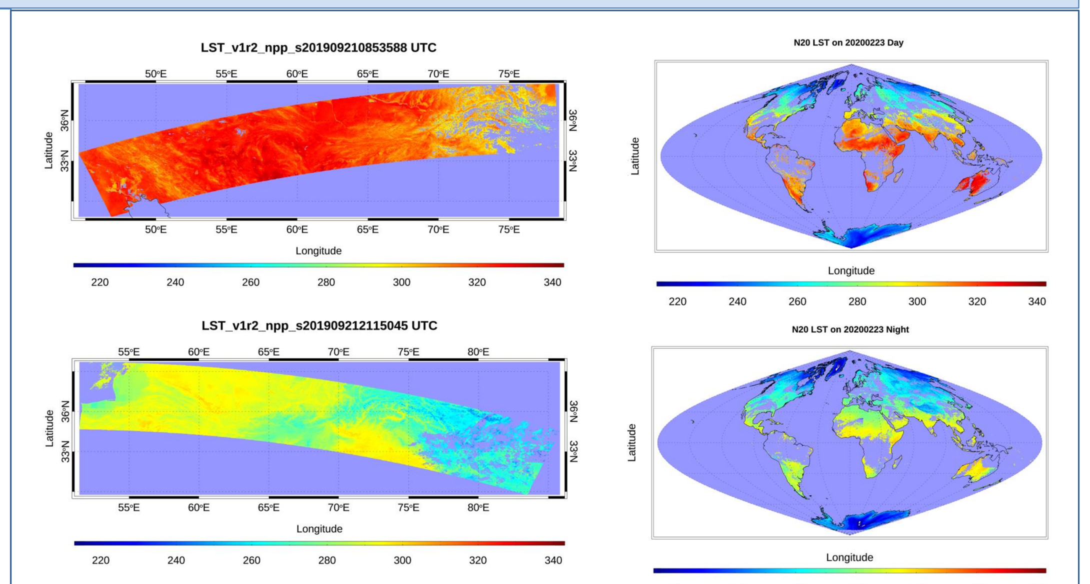

L2 VIIRS LST (left) and L3 VIIRS LST (Right)

NDE Land Surface Temperature access

- The L2 enterprise VIIRS LST is available at NOAA CLASS under group of "JPSS VIIRS Product(granule)(JPSS-GRAN)". available at https://www.avl.class.noaa.gov/saa/products/psearchJPSS_GRAN
- The L2 enterprise SNPP VIIRS data has been available since 06/06/2019 and J01 VIIRS LST has been available since 09/18/2019. Both are in the updated version v1r2 with most recent updates implemented.
- Also available at SCDR under data type "VIIRS-LST" for STAR internal users and interested groups.

Ground Validation

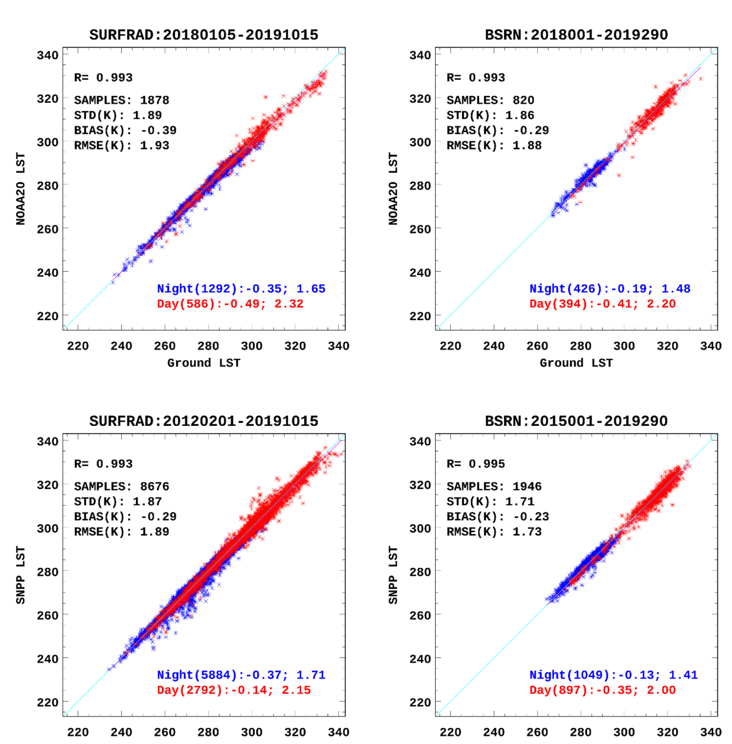

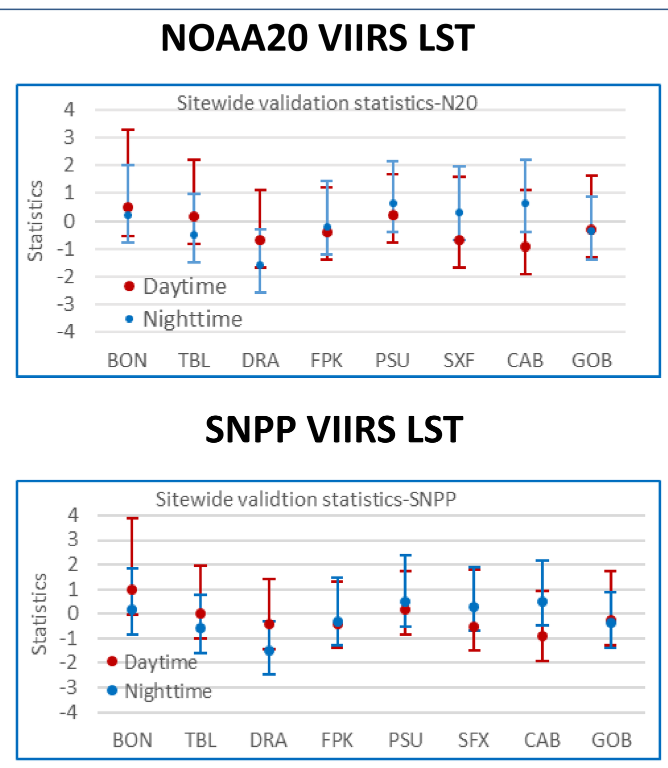

NOAA20 VIIRS LST

SNPP VIIRS LST

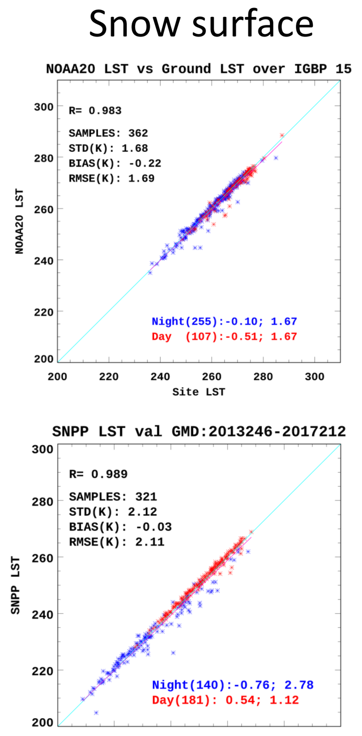

Snow surface

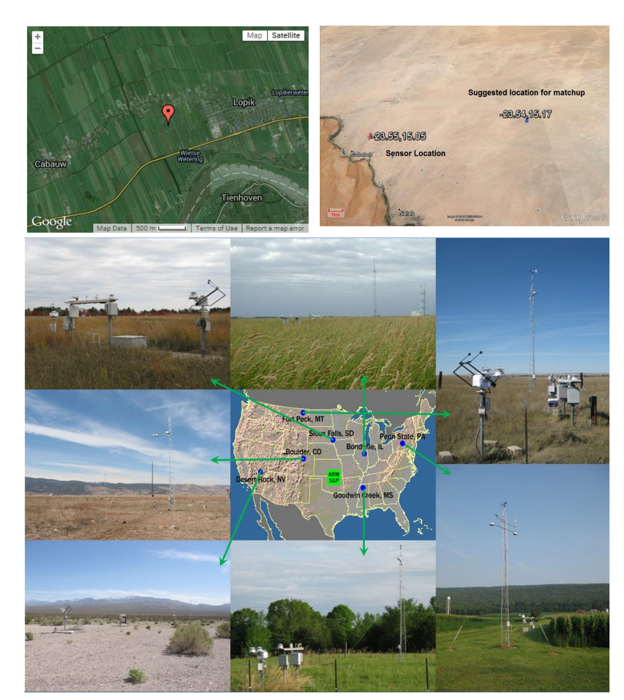

- Six sites from SURFRAD network in Continental US; two sites from BSRN network in Netherland and Namibia; one site in Summit, Greenland.
- For SNPP LST validation: over seven years of SURFRAD observations from Feb. 2012 to Oct. 2019 ; over four years of BSRN observations from January 2015 to Oct. 2019 were used. For NOAA 20 LST validation: the data covers the time period from Jan. 2018 to Oct. 2019.
- Overall good agreement; consistent performance between SNPP and NOAA20 LST; LST over snow surface is affected by cloud contamination

Long Term Monitoring

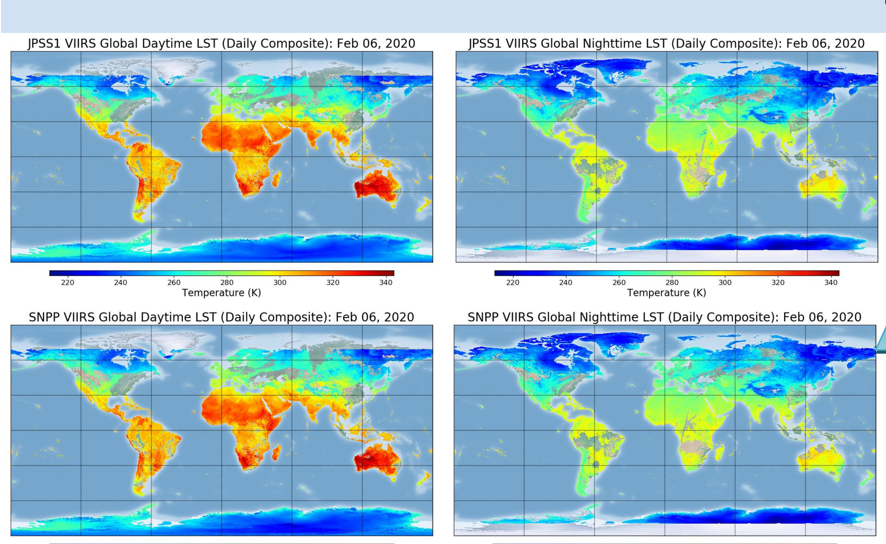

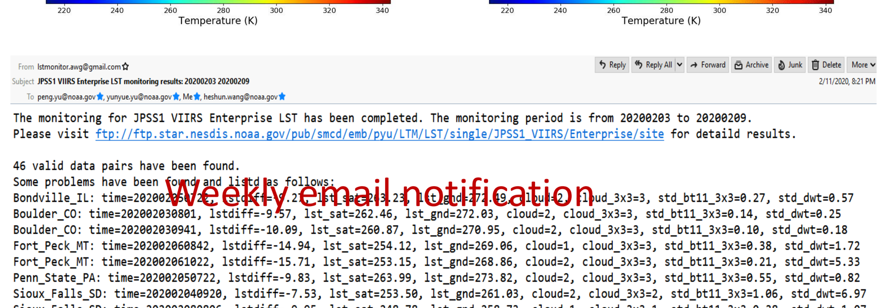

Weekly email notification

ftp://ftp.star.nesdis.noaa.gov/pub/smcd/emb/pyu/LTM/LST/single/JPSS1_VIIRS/ or /SNPP_VIIRS/

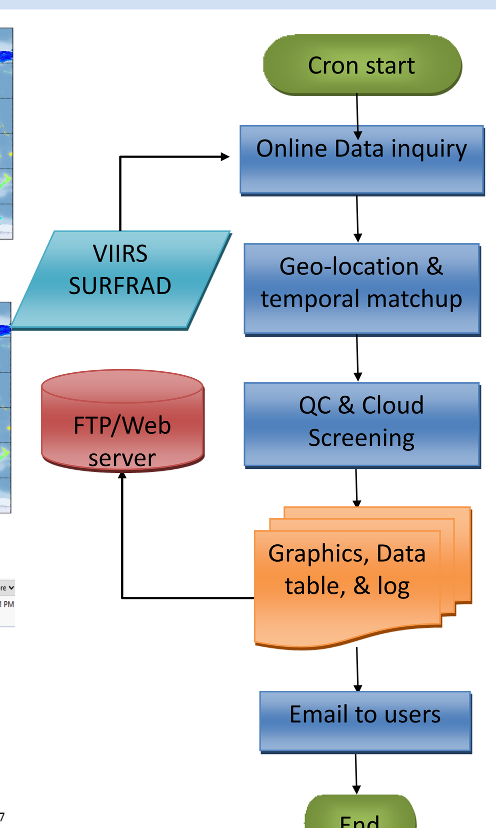

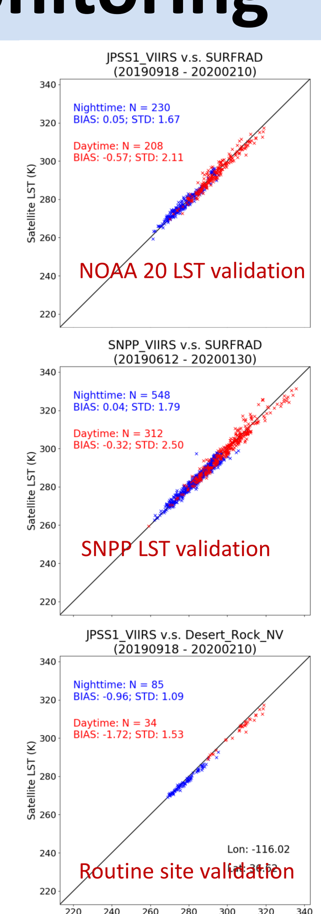

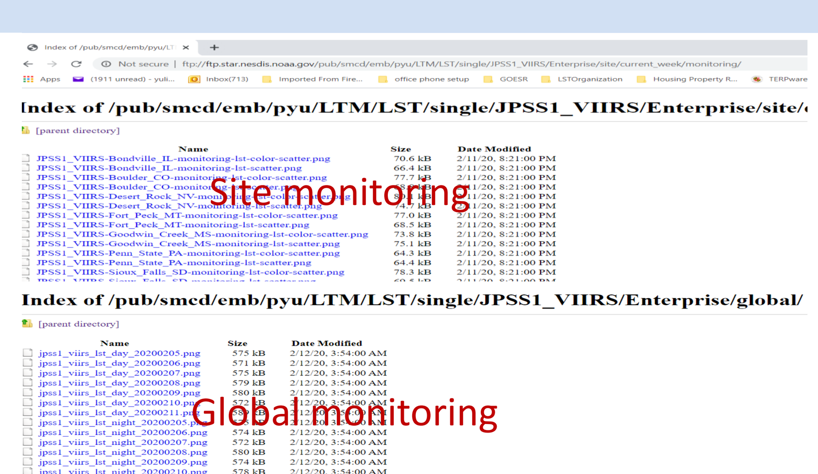

- Global LST monitoring for both SNPP and NOAA20
- Site wide monitoring and routine validation
- Provide subset data and global 5km composite data
- Various output in graphics, table and log file
- Weekly email notification with details for outliers beyond the threshold.

Cross-comparison with AQUA MODIS LST

AQUA MODIS LST Product

- MYD11A1: Split window algorithm
- MYD21A1: TES algorithm

NOAA 20 VIIRS LST product

The global L3 data in Jan, Feb, Mar and Apr. 2019 were used for the cross comparison between L3 N20 VIIRS LST and MYD11A1 LST and MYD21A1 LST. Global mean difference was analyzed for daytime and nighttime LST.

Attribute Analyzed		Analysis/Validation Result
Cross satellite Comparison	L3 NOAA 20 LST vs MYD11A1	Nighttime: 0.61(1.18) Daytime:0.38 (2.04)
	L3 NOAA 20 LST vs MYD21A1	Nighttime: -0.30(1.31) Daytime:-1.20 (2.36)

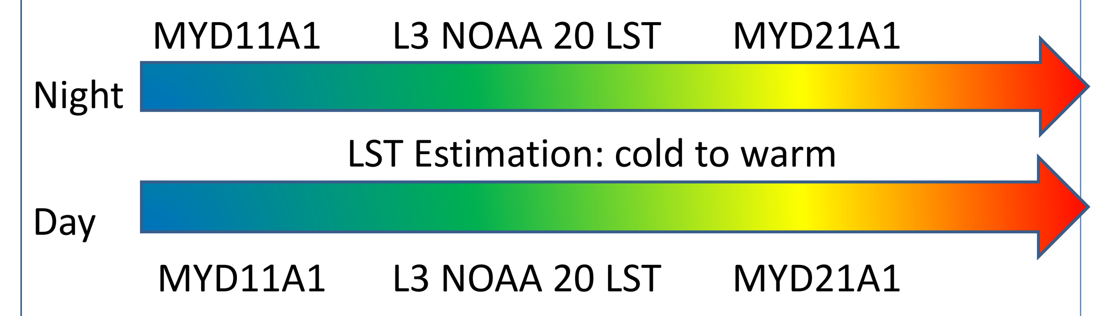

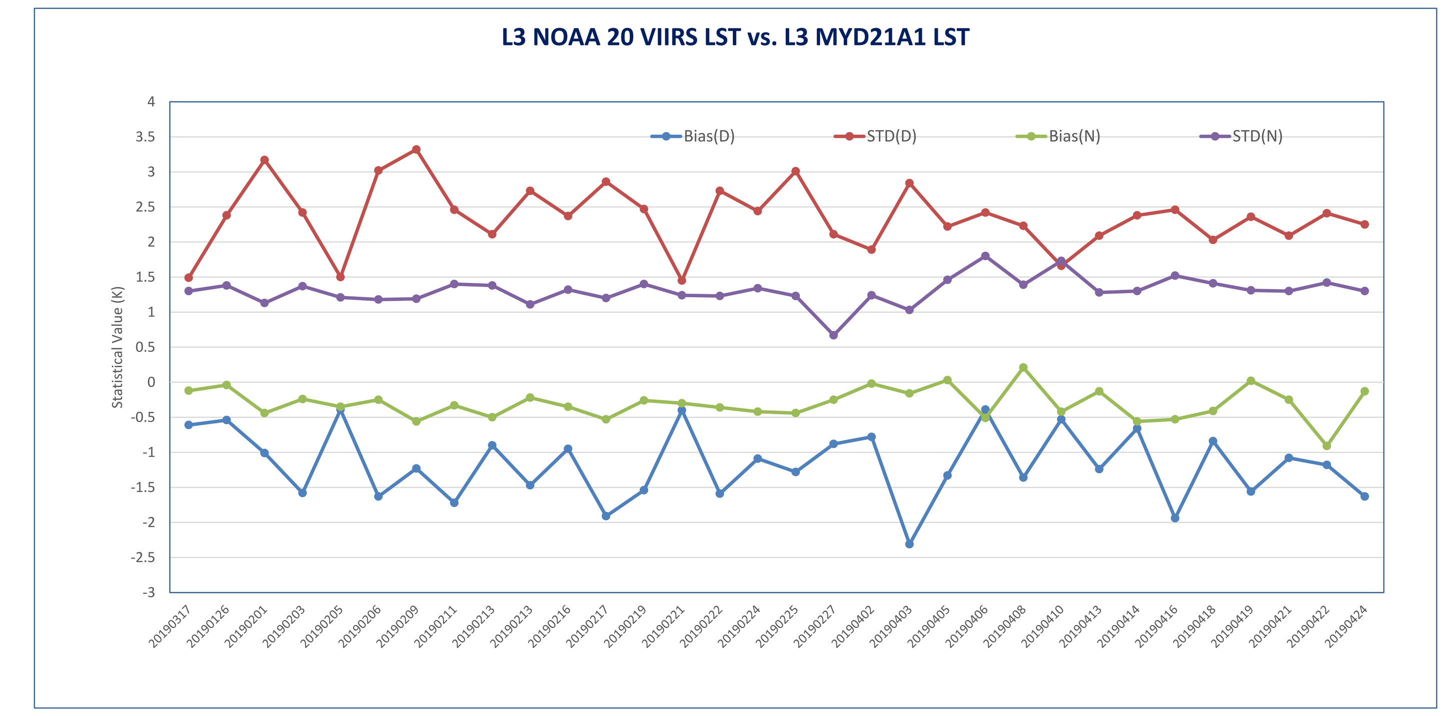

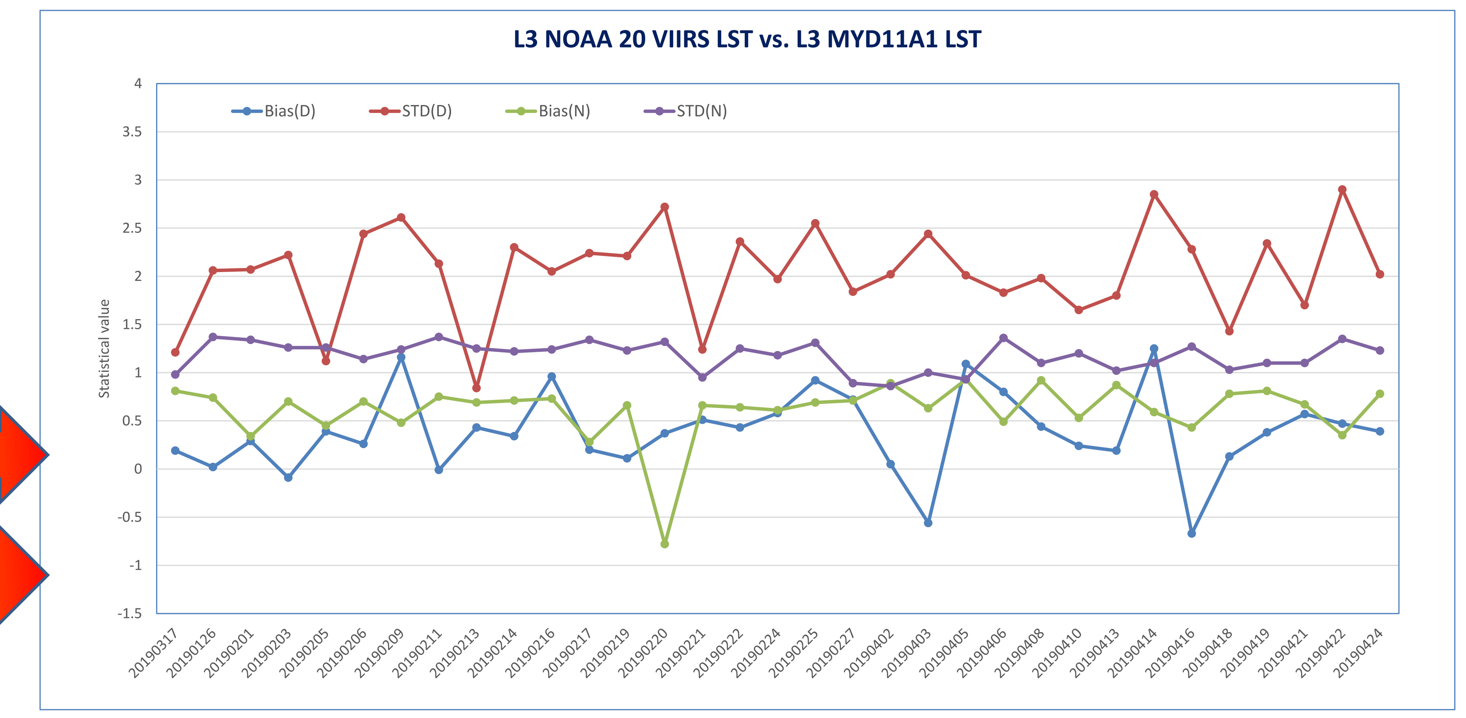

User Applications and feedback

- **NCEP/EMC Modeling**
  - VIIRS NDE LST product is in operational need for model output verification purpose
- **RTMA/URMA system data assimilation**
  - To assimilate VIIRS LST into RTMA system to adjust the 2m air temperature
- **Near real time I km SMAP soil moisture (SM) product development**
  - VIIRS LST data is used as an input in the NRT 1 km SMAP Soil Moisture Data Product development
- **Temporal and spatial variability of daytime land surface temperature in Houston**
  - SNPP VIIRS LST data is used as a reference to compare with aircraft LST observations during the NASA's DISCOVER-AQ (Deriving Information on Surface Conditions from Column and Vertically Resolved Observations Relevant to Air Quality) field campaign in September, 2013..

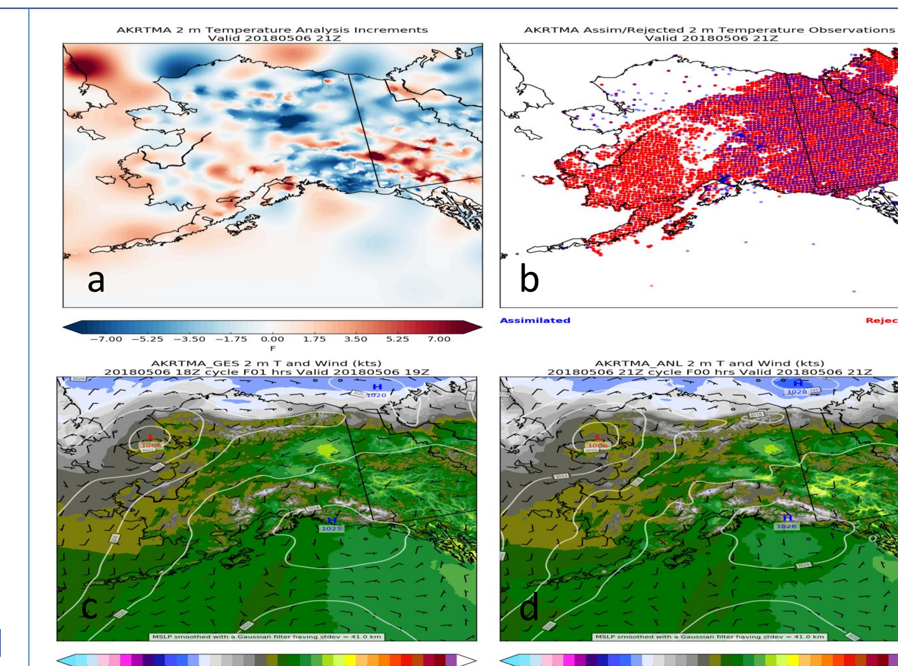

(a) The analysis increment shows the difference between the adjusted T2M after/before LST assimilation. Red color indicates an increased model T2M, blue color indicates a decreased T2M.
(b) quality control results: red dot for pixels fail the quality control; blue dots for pixels selected for assimilation
(c) Model T2M before data assimilation
(d) Model T2M after LST assimilation
The bottom two surface weather map show the adjust of T2M field looks reasonable. (Courtesy of Xiaoyan Zhang)

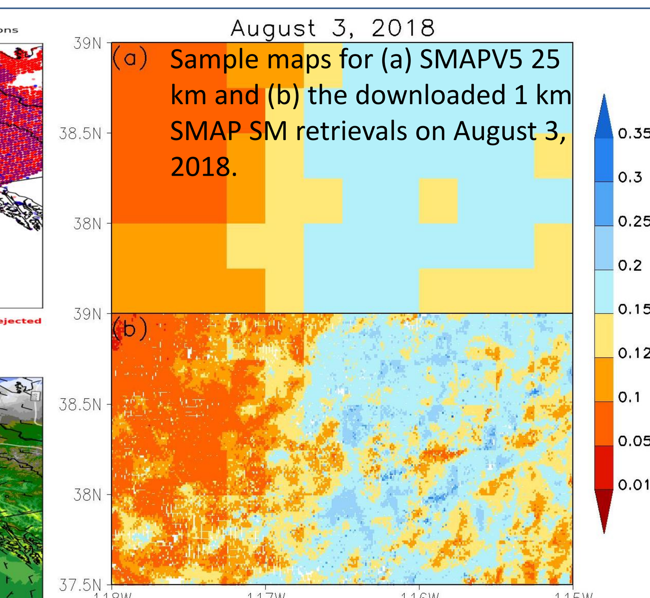

LST provides ancillary information on soil moisture distributions, and thus can be used to produce finer resolution satellite soil moisture retrievals. Particularly, agreements between the developed 1 km SM and in situ SM observations are comparable to the 25 km SMAP data, while the accuracy level is significantly improved with the advance of the fine scale satellite SM measurements. (Courtesy of Jifu Yin)

Summary

- The enterprise VIIRS LST products has a pretty good agreement with the ground measurements from SURFRAD, BSRN and GMD stations based on multiple years of data validation.
- The enterprise NOAA 20 VIIRS LST is in between the L3 MYD11A1 and MYD21A1 LST for both daytime and nighttime.
- The long term monitoring is ready for both SNPP and NOAA 20 VIIRS LST.
- LST application has been used in model LST verification, data assimilation to adjust 2m Tair and 1 km soil moisture product development etc. Ready to provide long term climate data records for users.

Enterprise VIIRS LST Production for JPSS Mission: Validation and Application

Yuling Liu[1] , Yunyue Yu[2], Peng Yu[1], Heshun Wang[1]
1. ESSIC/CISESS, University of Maryland, College Park, MD 2. STAR/NESDIS/NOAA, College Park, MD.

Enterprise JPSS VIIRS LST Product Introduction

NDE Land Surface Temperature Product

- Based on split window technique

$$T_s = C_0 + C_1T_{11} + C_2(T_{11} - T_{12}) + C_3\varepsilon + C_4\varepsilon(T_{11} - T_{12}) + C_5\,\Delta\varepsilon$$

T_{11} and T_{12} : the TIR split-window channel BTs
ε and $\Delta\varepsilon$: mean emissivity at the TIR spectrum, and the emissivity difference
LUT {C} dimension: Day/night, View Zenith Angle, Total Column Water Vapor

- Granule (L2) and gridded (L3) LST product for both SNPP VIIRS and NOAA 20 VIIRS
- L2 VIIRS LST has been in operational and the L3 VIIRS LST was just put into operational.

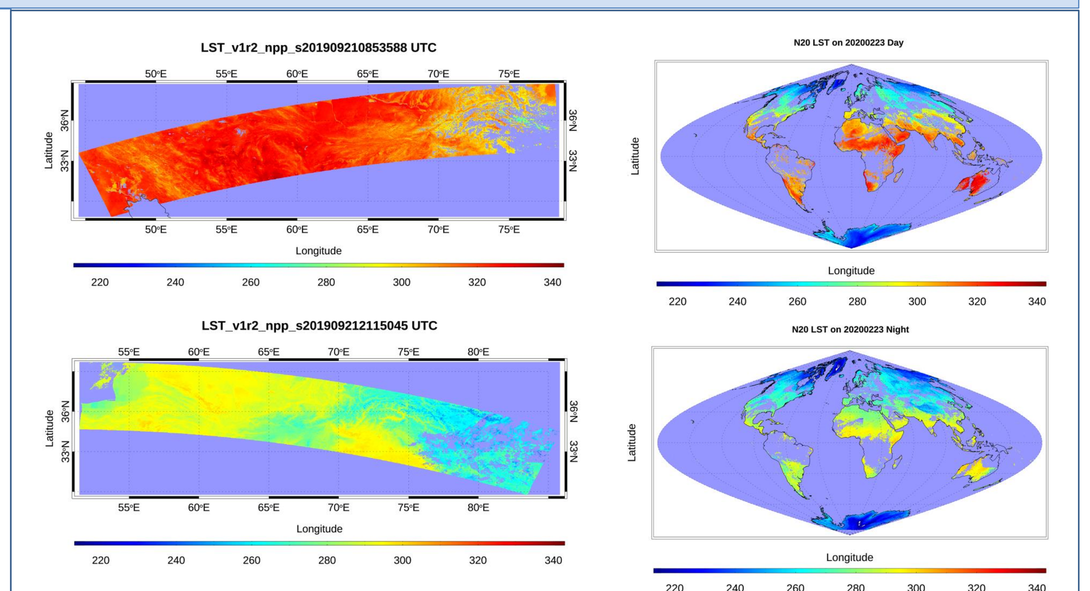

L2 VIIRS LST (left) and L3 VIIRS LST (Right)

NDE Land Surface Temperature access

- The L2 enterprise VIIRS LST is available at NOAA CLASS under group of "JPSS VIIRS Product(granule)(JPSS-GRAN)". available at https://www.avl.class.noaa.gov/saa/products/psearchJPSS_GRAN
- The L2 enterprise SNPP VIIRS data has been available since 06/06/2019 and J01 VIIRS LST has been available since 09/18/2019. Both are in the updated version v1r2 with most recent updates implemented.
- Also available at SCDR under data type "VIIRS-LST" for STAR internal users and interested groups.

Ground Validation

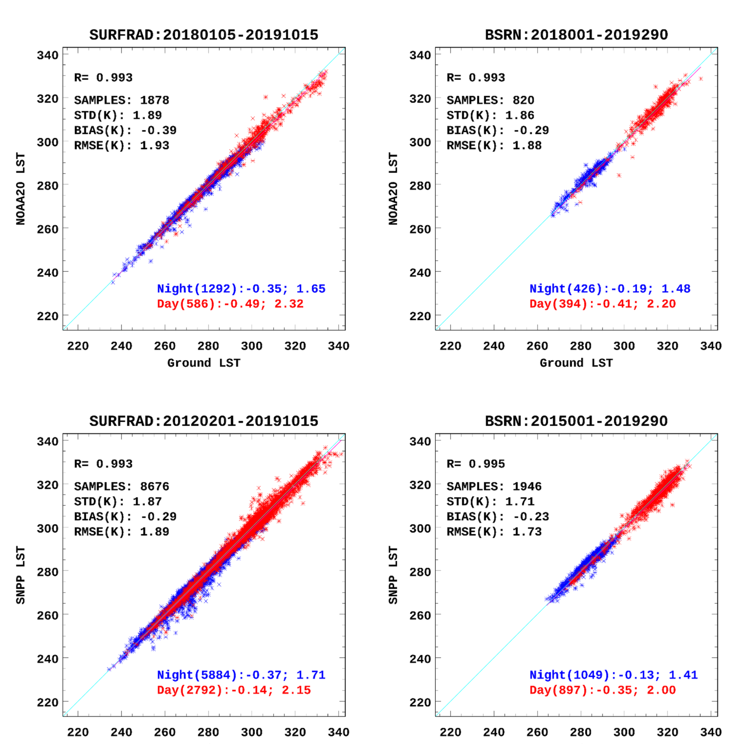

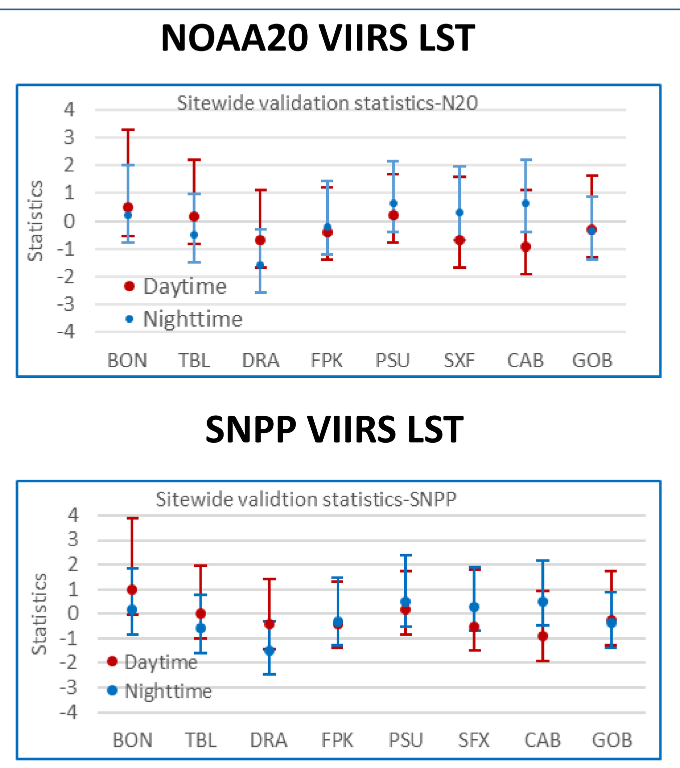

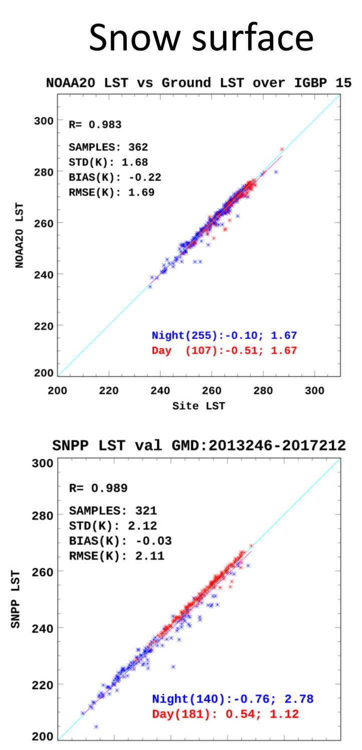

- Six sites from SURFRAD network in Continental US; two sites from BSRN network in Netherland and Namibia; one site in Summit, Greenland.
- For SNPP LST validation: over seven years of SURFRAD observations from Feb. 2012 to Oct. 2019 ; over four years of BSRN observations from January 2015 to Oct. 2019 were used. For NOAA 20 LST validation: the data covers the time period from Jan. 2018 to Oct. 2019.
- Overall good agreement; consistent performance between SNPP and NOAA20 LST; LST over snow surface is affected by cloud contamination

Long Term Monitoring

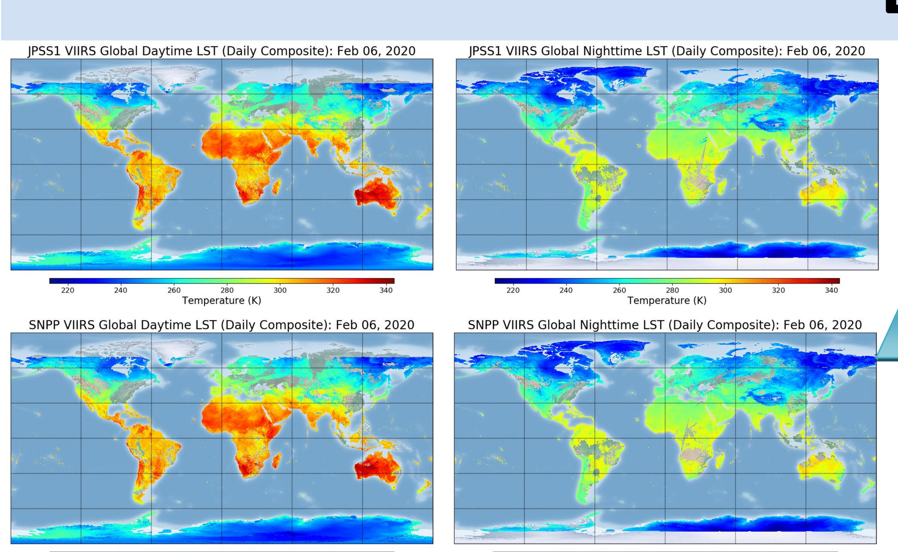

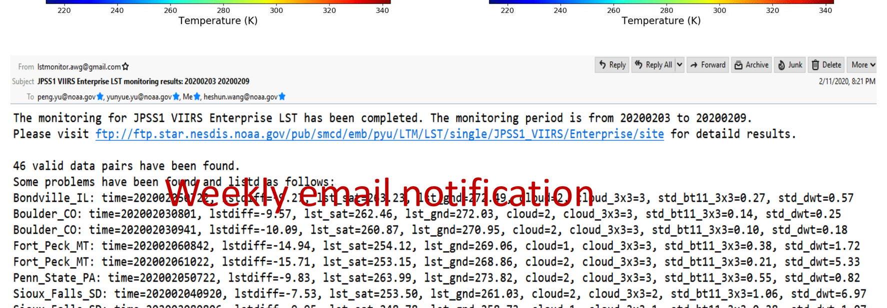

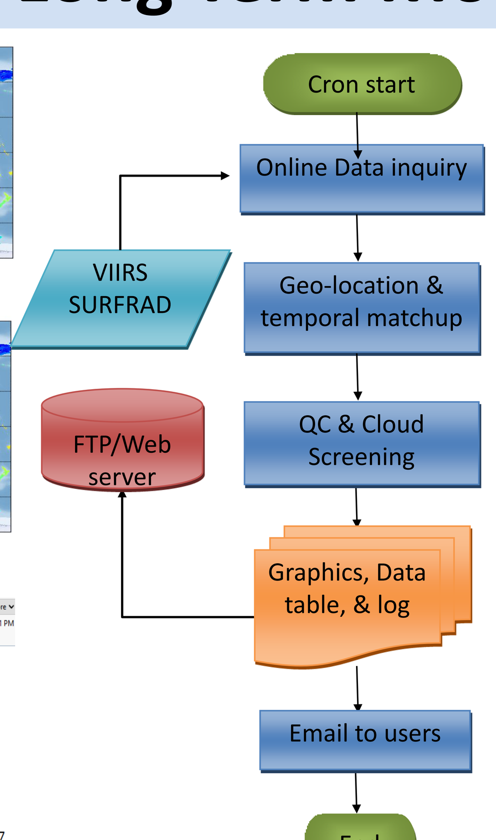

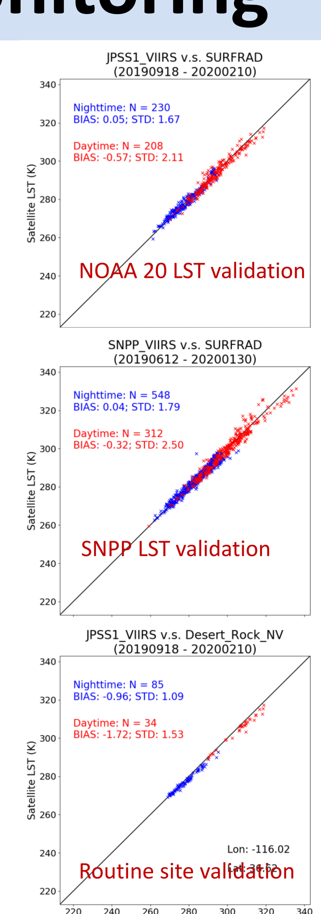

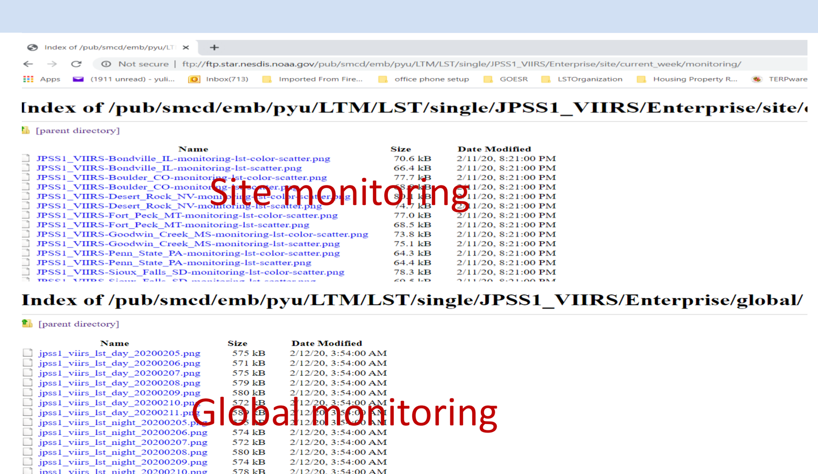

ftp://ftp.star.nesdis.noaa.gov/pub/smcd/emb/pyu/LTM/LST/single/JPSS1_VIIRS/ or /SNPP_VIIRS/

- Global LST monitoring for both SNPP and NOAA20
- Site wide monitoring and routine validation
- Provide subset data and global 5km composite data
- Various output in graphics, table and log file
- Weekly email notification with details for outliers beyond the threshold.

Cross-comparison with AQUA MODIS LST

AQUA MODIS LST Product

- MYD11A1: Split window algorithm
- MYD21A1: TES algorithm

NOAA 20 VIIRS LST product

The global L3 data in Jan, Feb, Mar and Apr. 2019 were used for the cross comparison between L3 N20 VIIRS LST and MYD11A1 LST and MYD21A1 LST. Global mean difference was analyzed for daytime and nighttime LST.

Attribute Analyzed		Analysis/Validation Result
Cross satellite Comparison	L3 NOAA 20 LST vs MYD11A1	Nighttime: 0.61(1.18) Daytime:0.38 (2.04)
	L3 NOAA 20 LST vs MYD21A1	Nighttime: -0.30(1.31) Daytime:-1.20 (2.36)

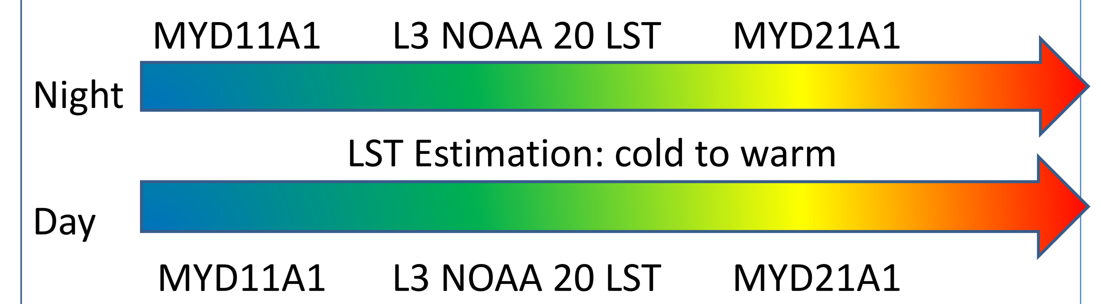

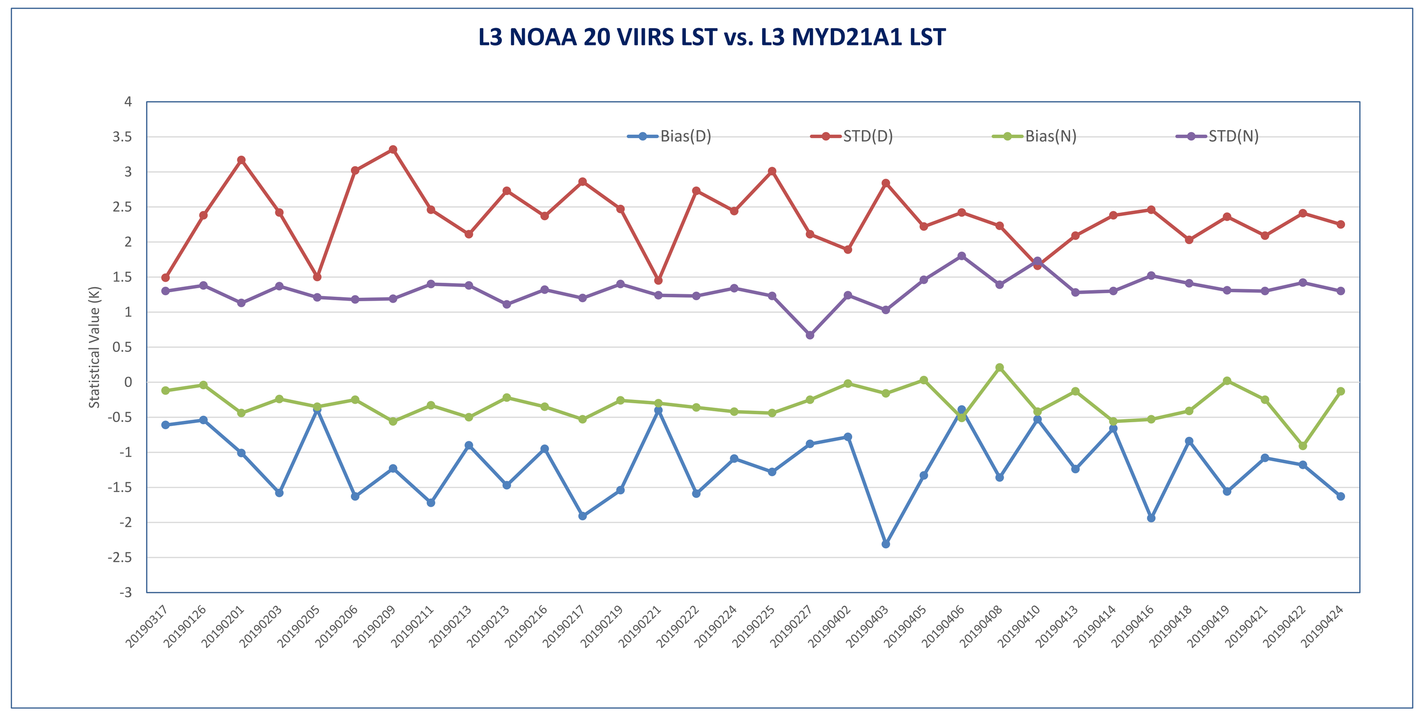

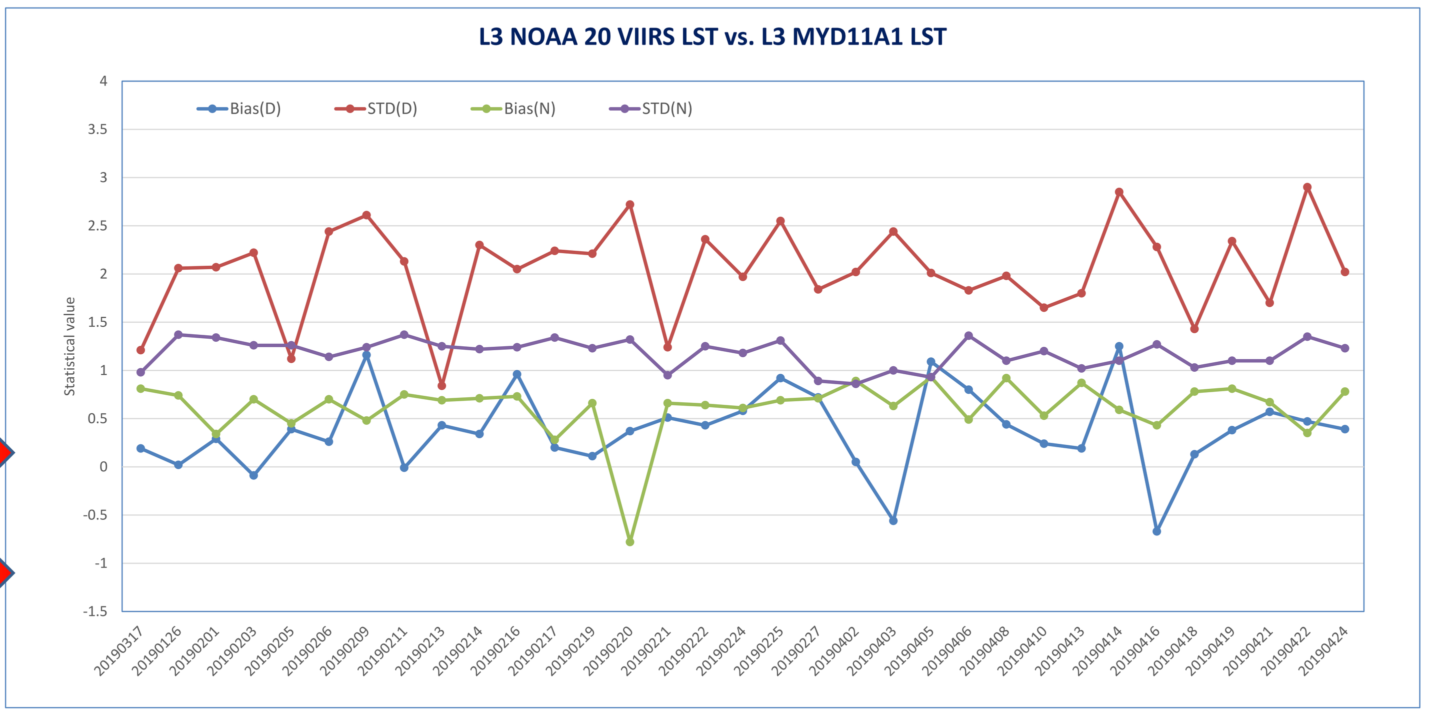

User Applications and feedback

- **NCEP/EMC Modeling**
  - VIIRS NDE LST product is in operational need for model output verification purpose
- **RTMA/URMA system data assimilation**
  - To assimilate VIIRS LST into RTMA system to adjust the 2m air temperature
- **Near real time I km SMAP soil moisture (SM) product development**
  - VIIRS LST data is used as an input in the NRT 1 km SMAP Soil Moisture Data Product development
- **Temporal and spatial variability of daytime land surface temperature in Houston**
  - SNPP VIIRS LST data is used as a reference to compare with aircraft LST observations during the NASA's DISCOVER-AQ (Deriving Information on Surface Conditions from Column and Vertically Resolved Observations Relevant to Air Quality) field campaign in September, 2013..

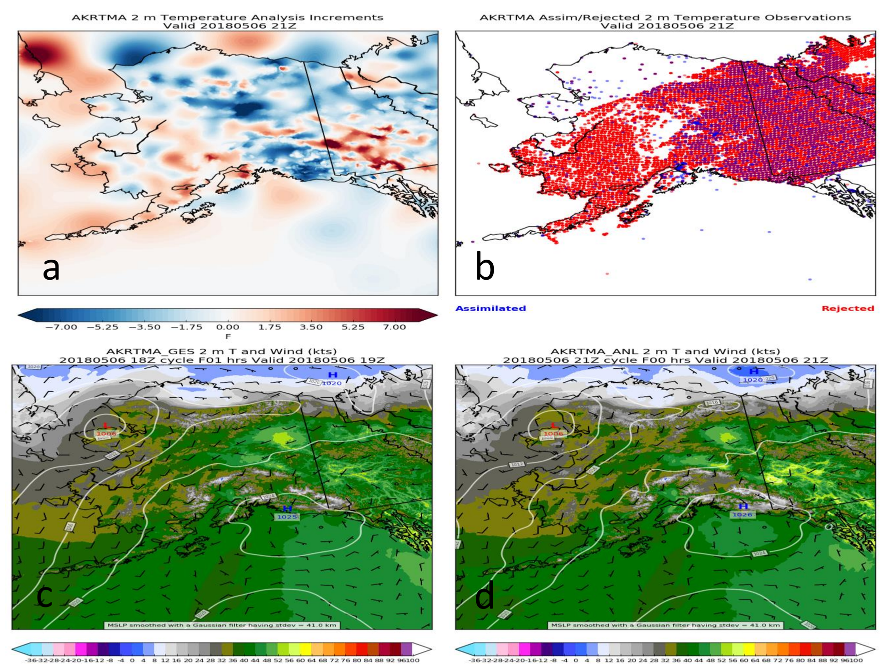

(a) The analysis increment shows the difference between the adjusted T2M after/before LST assimilation. Red color indicates an increased model T2M, blue color indicates a decreased T2M.
(b) quality control results: red dot for pixels fail the quality control; blue dots for pixels selected for assimilation
(c) Model T2M before data assimilation
(d) Model T2M after LST assimilation
The bottom two surface weather map show the adjust of T2M field looks reasonable. (Courtesy of Xiaoyan Zhang)

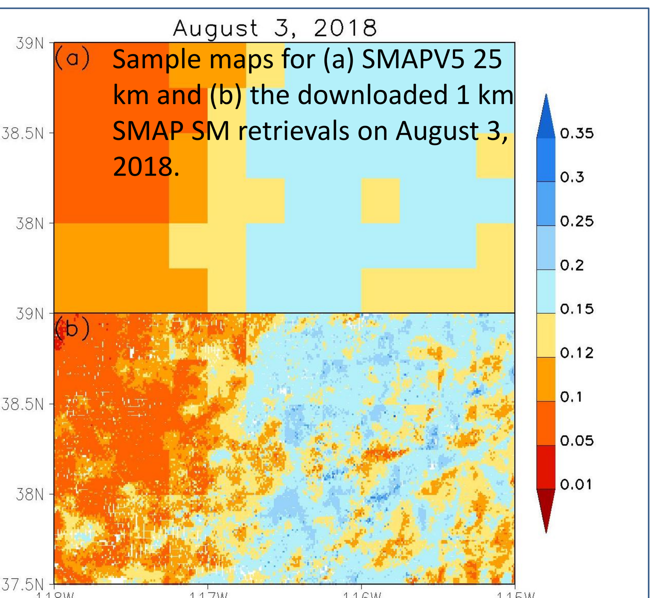

LST provides ancillary information on soil moisture distributions, and thus can be used to produce finer resolution satellite soil moisture retrievals. Particularly, agreements between the developed 1 km SM and in situ SM observations are comparable to the 25 km SMAP data, while the accuracy level is significantly improved with the advance of the fine scale satellite SM measurements. (Courtesy of Jifu Yin)

Summary

- The enterprise VIIRS LST products has a pretty good agreement with the ground measurements from SURFRAD, BSRN and GMD stations based on multiple years of data validation.
- The enterprise NOAA 20 VIIRS LST is in between the L3 MYD11A1 and MYD21A1 LST for both daytime and nighttime.
- The long term monitoring is ready for both SNPP and NOAA 20 VIIRS LST.
- LST application has been used in model LST verification, data assimilation to adjust 2m Tair and 1 km soil moisture product development etc. Ready to provide long term climate data records for users.

Blended shortwave daily mean albedo from SNPP and JPSS1 VIIRS observations

Jingjing Peng[1], Yunyue Yu[2], Peng Yu[1]

1. ESSIC/CICESS, University of Maryland, College Park, MD 2. STAR/NESDIS, NOAA, College Park, MD

ABSTRACT

- Surface Albedo (SURFALB), defined as the ratio between solar radiation reflected by Earth's surface and solar radiation incident at the surface, is a function of both solar illumination and the surface reflective properties.
- NOAA provides operational daily mean shortwave albedo over land and sea-ice surface from VIIRS data. The latest version (v1r2) S-NPP and NOAA-20 VIIRS Albedo have been available since 09/19/2019 and can be accessed from CLASS.
- The SURFALB products are also available at SCDR under data type "VIIRS-SURFALB" for STAR internal users and interested groups.
- The NOAA VIIRS albedo algorithm deploys a single clear-sky observation to estimate daily mean albedo, which is straightforward and stable for online processing. For cloudy pixels, the albedo fill value comes from a temporal filtered result which integrates information from preceding 9-days and the climatology. The clear-sky retrievals are regarded as high-quality ones.
- The SNPP and JPSS1 VIIRS albedos demonstrate slight difference due to the orbit difference, and the LUT sensitivity to angles. The inconsistency may cause some inconvenience for some users.
- Blending VIIRS albedos from SNPP and JPSS1 would increase the clear-sky observations at most locations and the percentage of high-quality retrievals.
- The current blending algorithm in test is an albedo-level-composition using L2 SURFALB data as input.

Current ALGORITHM

Direct estimation principle:

$$LSA = \alpha_0 + \sum \alpha_i r_i$$

a_i is regression coefficient for Band i, which varies with surface cover type, solar-object-view geometry angles, latitude, and day of year.

i is VIIRS band number, including the channels 1,2,3,4,5,7,8,10 and 11.

Level-2 albedo monitoring example

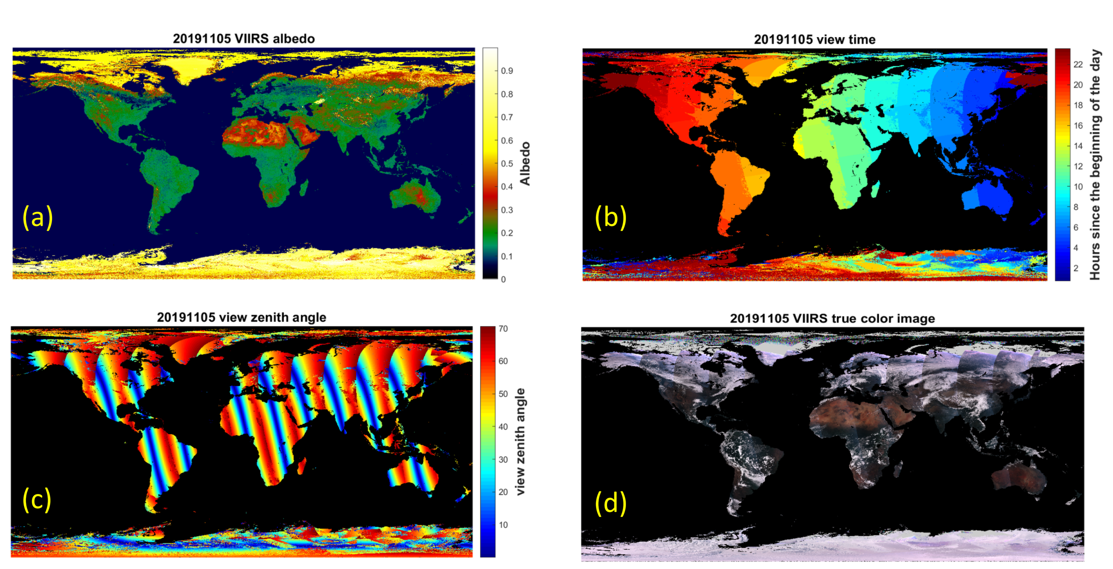

VIIRS surface albedo sample (figure a) provides a favor of the NOAA-20 VIIRS albedo product. The corresponding view time record (figure b) and view zenith angle (figure c) explains the difference existed in the TOA reflectance (figure d) used as input to the algorithm. The algorithm well handles such difference, but still with some exceptions that slight spatial discontinuity occasionally appears over Antarctic, Australia and Europe.

VIIRS surface albedo monitoring webpage

INTER-COMPARISON

JPSS1 and SNPP VIIRS albedo are compared to check their consistency, which is important for NOAA users. The global mean discrepancy shows they are generally consistent in overall magnitude, but with slight difference due to different orbit and solar/view zenith angles.

Time series of global mean difference

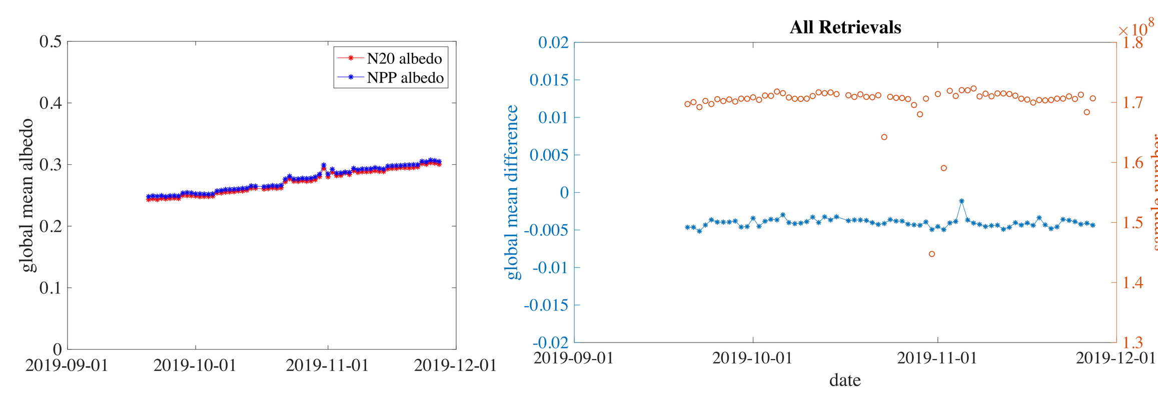

Daily comparison between related factors

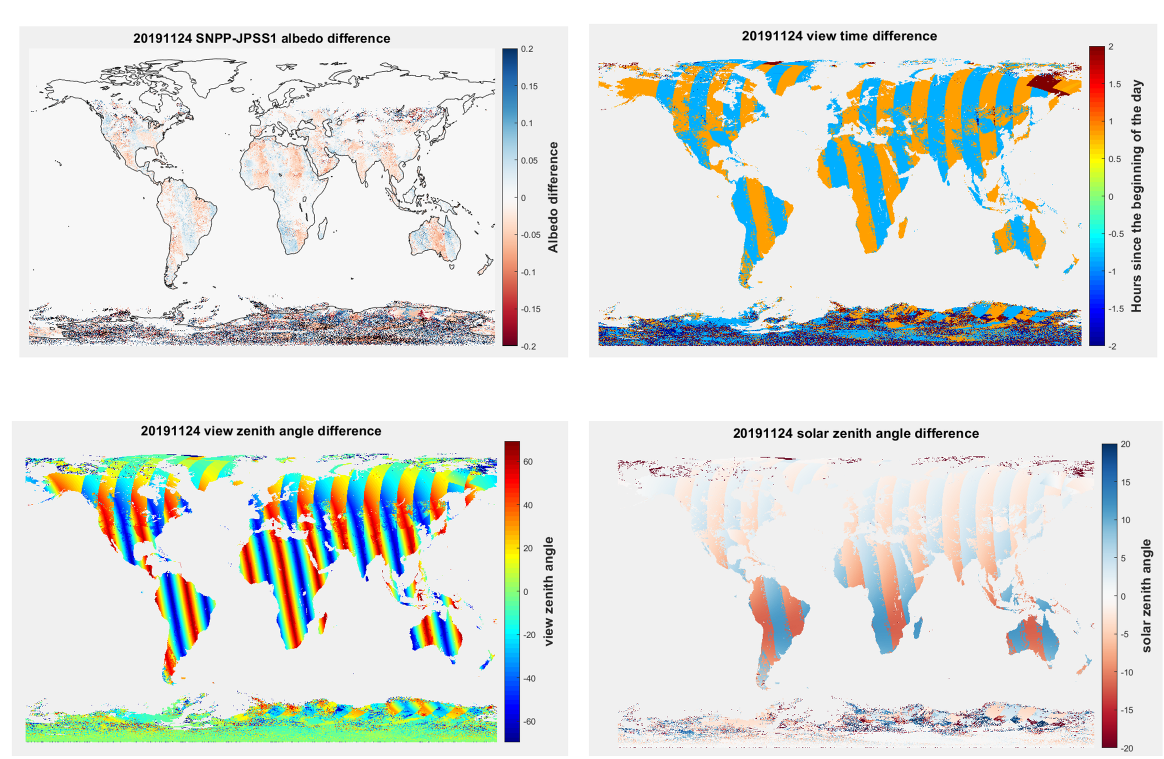

SITE LEVEL BLENDED

- Data period: Jan 01, 2018~ Oct 16, 2019 *Fort_Peck_MT*

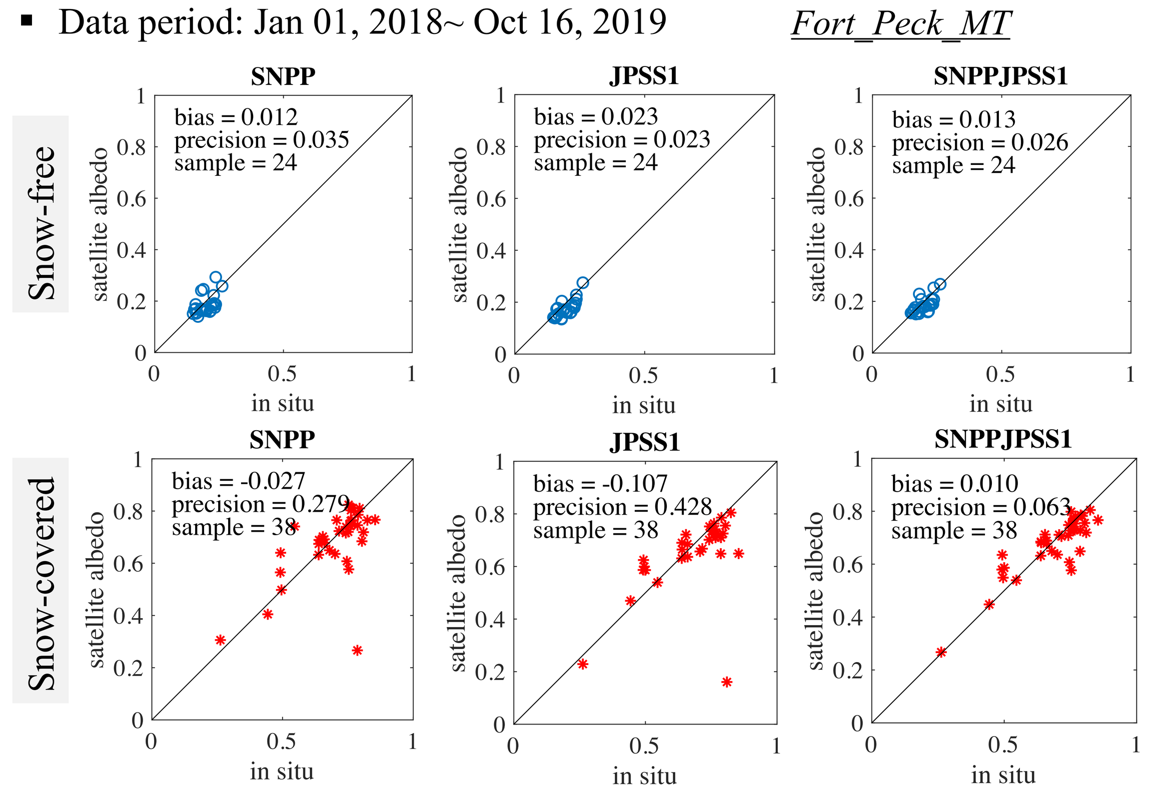

The comprison over other SURFRAD sites

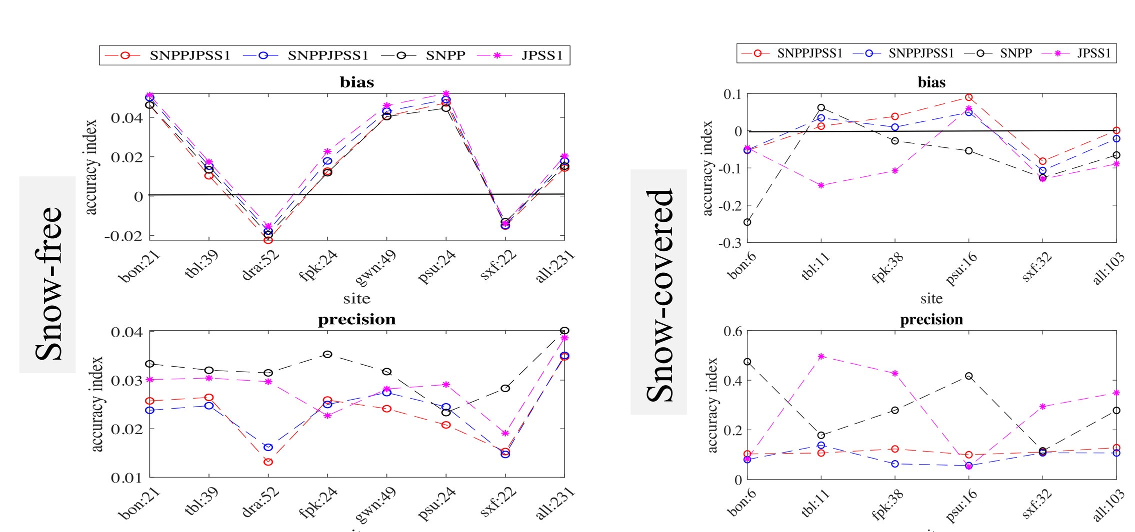

GLOBAL BLENDED

BLENDED VIIRS Global Albedo (L3 local): Feb 21 2020

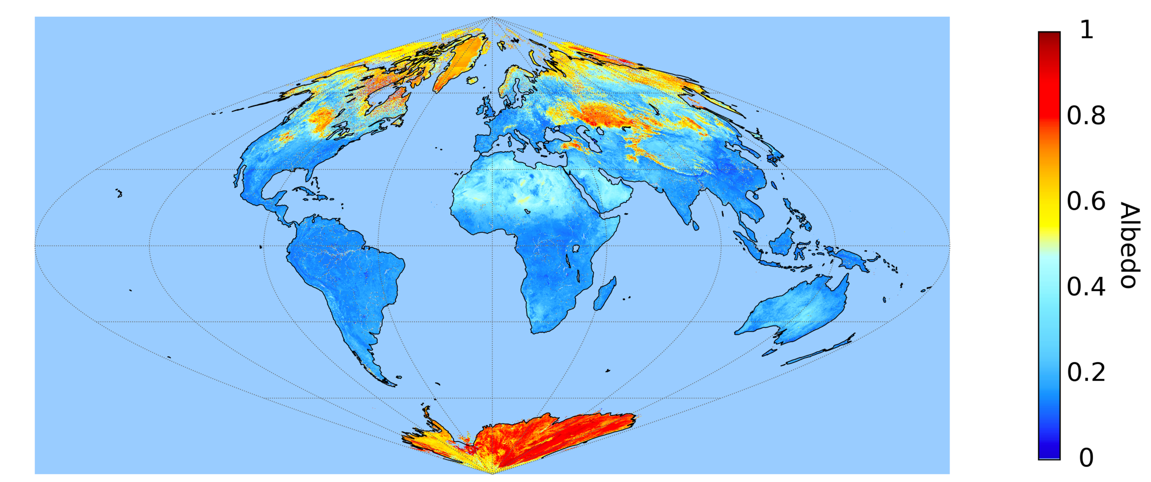

BLENDED VIIRS Global Albedo Retrieval Path: Feb 21 2020

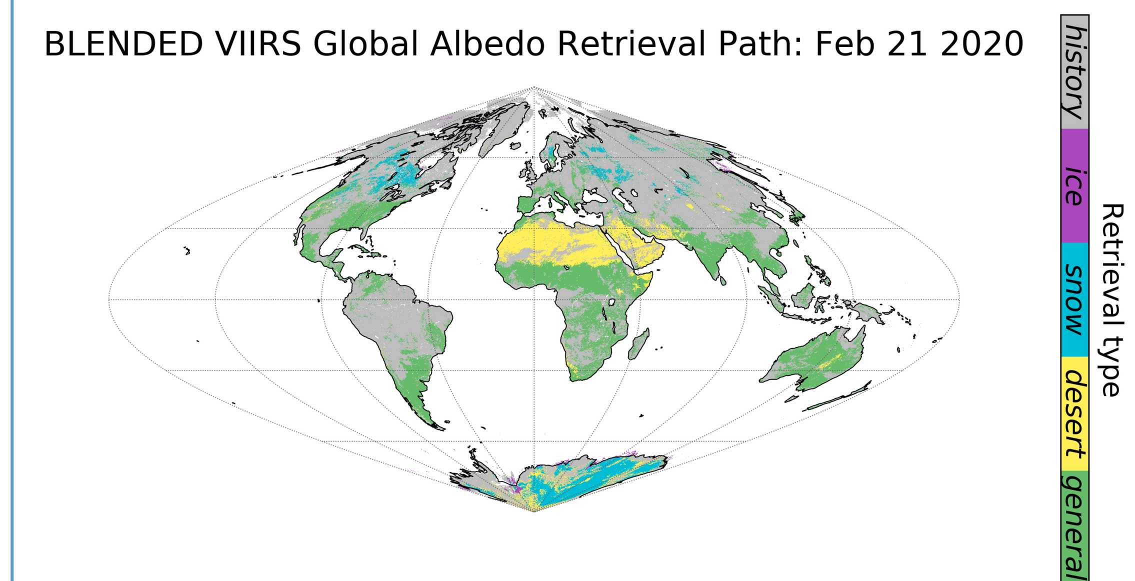

BLENDED VIIRS Albedo Retrieval Counts: Feb 21 2020

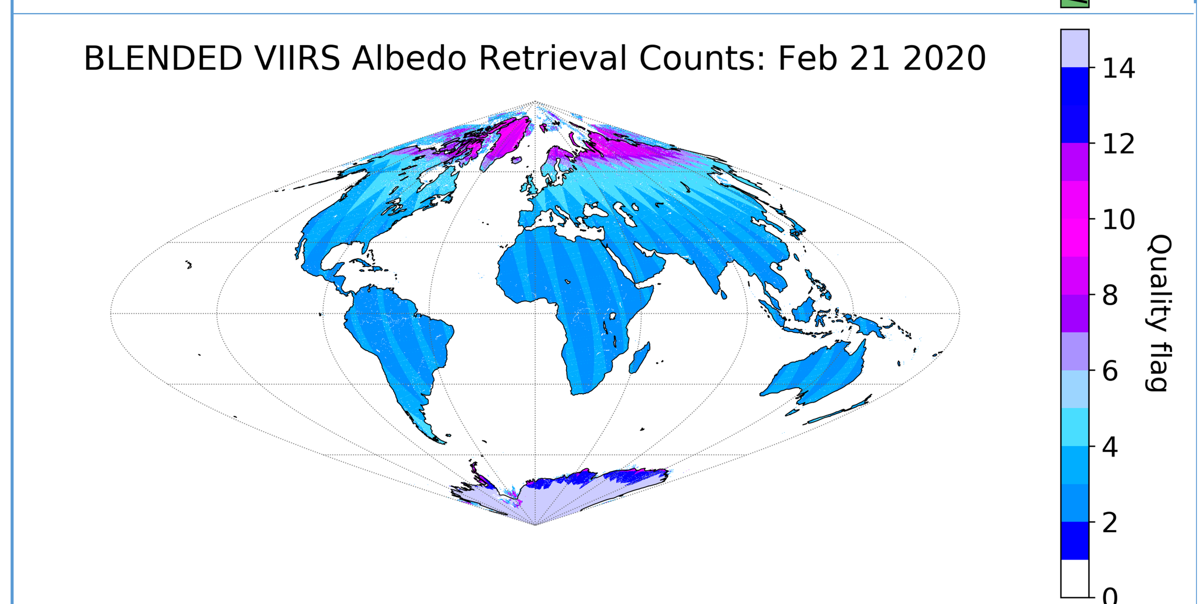

JPSS1 VIIRS Albedo Retrieval Counts: Feb 21 2020 NPP VIIRS Albedo Retrieval Counts: Feb 21 2020

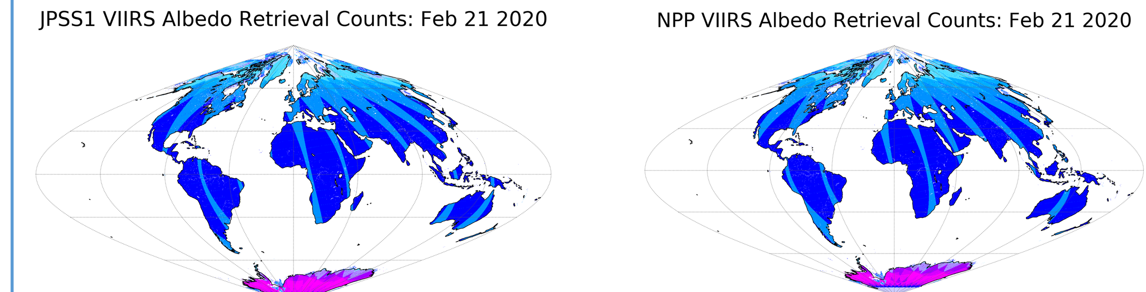

JPSS1 VIIRS Global Albedo Cloud Flag: Feb 21 2020

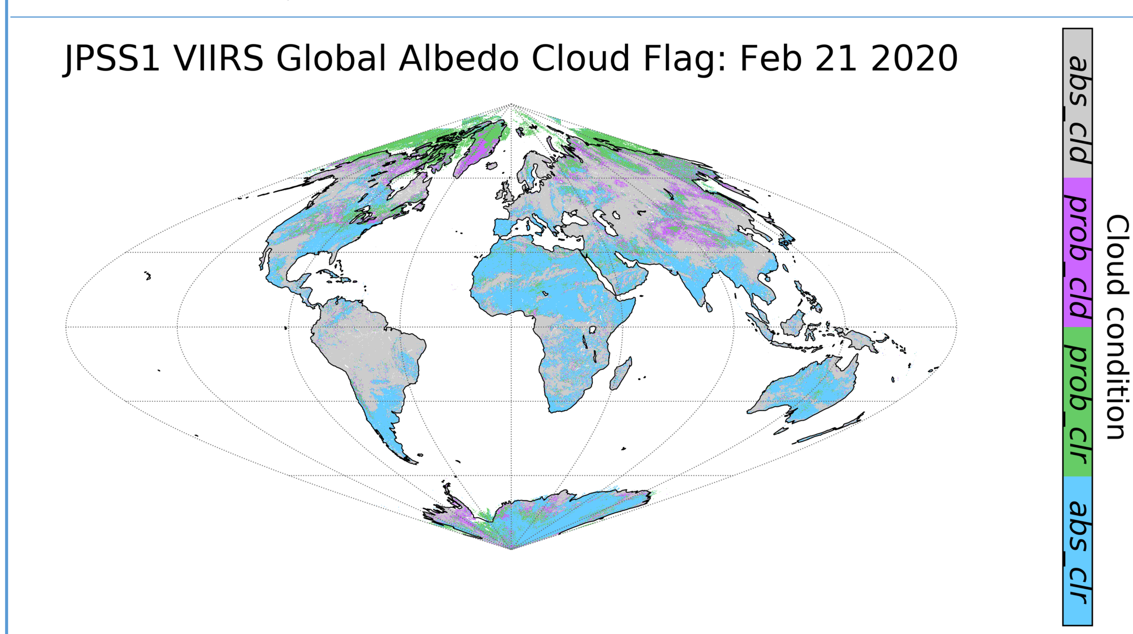

JPSS1 VIIRS Global Albedo Cloud Flag: Feb 21 2020 NPP VIIRS Global Albedo Cloud Flag: Feb 21 2020

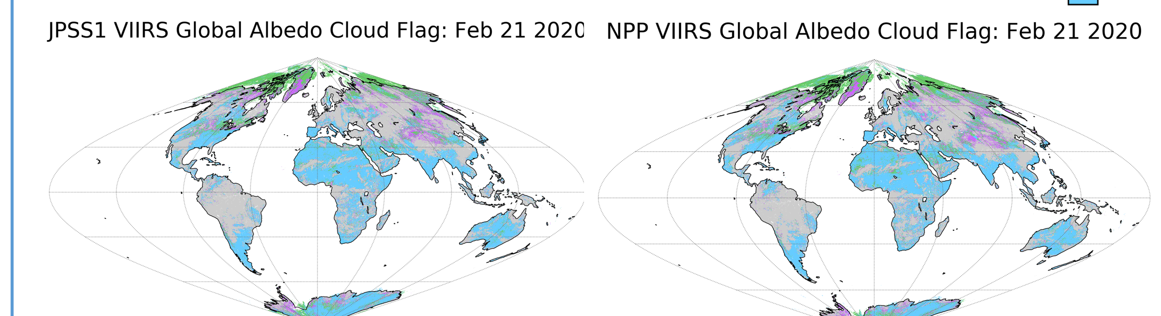

LIMITATIONS

- The V2 climatology in framework is waiting to be applied in NDE in queue, which has more complete sea-ice surface coverage. The v3 climatology is in development, which would provide more continuous result over Greenland and Antarctic.
- The site blended result is reprocessed from IDPS snow mask, cloud mask, surface type, and ice concentration, as the NDE version EDRs is only available since Sep 2019.

CONCLUSIONS

- SNPP and JPSS1 VIIRS albedo provides high-quality, comparable, and continuous retrievals.
- The single-day directly-retrieved albedo difference between SNPP and JPSS1 is attributed to the orbit difference and the sensitivity of LUT to angle difference.
- The preliminary blended-VIIRS-albedo product, from SNPP and JPSS1, is an example of data fusion to yield a unified and improved albedo product. The blended product has enhanced high-quality retrieval coverage, clear-sky observation coverage, and data accuracy compared to in-situ measurements.
- The blended albedo will be more friendly to users since it provides one better product instead of separate products from different sensors with slight inherent inconsistency.
- Various blending calculation methods would be further tested on the VIIRS daily mean albedo. The current blending algorithm is conducted at L2-albedo level, more blending algorithms at reflectance-level or L3-albedo level would also be considered.

REFERENCES

1. Peng, J. J., Yu, Y. Y., Yu, P., & Liang, S. L. (2018). The VIIRS Sea-Ice Albedo Product Generation and Preliminary Validation. *Remote Sensing*, 10(11). [10.3390/rs10111826]
2. Wang, D. D., Liang, S. L., Zhou, Y., He, T., & Yu, Y. Y. (2017). A New Method for Retrieving Daily Land Surface Albedo from VIIRS Data. *IEEE Transactions on Geoscience and Remote Sensing*, 55(3), 1765-1775. [10.1109/tgrs.2016.2632624]
3. Zhou, Y., Wang, D., Liang, S., Yu, Y., & He, T. (2016). Assessment of the Suomi NPP VIIRS Land Surface Albedo Data Using Station Measurements and High-Resolution Albedo Maps. *Remote Sensing*, 8(2). [10.3390/rs8020137]
4. Wang, D. D., Liang, S. L., He, T., & Yu, Y. Y. (2013). Direct Estimation of Land Surface Albedo from VIIRS Data: Algorithm Improvement and Preliminary Validation. *Journal of Geophysical Research-Atmospheres*, 118(22), 12577-12586. [10.1002/2013jd020417]

ACKNOWLEDGEMENT

Thank all current and former group members for their contributions to the algorithm development and the NOAA ASSISTT team for their assistance on integration.

NOAA-20 Green Vegetation Fraction (GVF) Product

Zhangyan Jiang1, Mingshi Chen[1], Corinne Carter[2], Yunyue Yu[3]

[1] IMSG at NOAA/NESDIS/STAR. [2] ESSIC/ UMD/ NOAA, [3] NOAA/NESDIS/STAR, College Park, MD, 20740.

JPSS/GOES-R Proving Ground / Risk reduction Summit, Feb 24-28, 2020, College Park, MD 20740

VIIRS GVF

- Green Vegetation fraction (GVF) is defined as the fraction of a pixel covered by green vegetation if it were viewed vertically.
- Real-time GVF is needed in the numeric weather, climate and hydrological models.
- The Suomi National Polar-orbiting Partnership (SNPP) Visible Infrared Imager Radiometer Suite (VIIRS) GVF has been operationally produced since Feb 2015 at NOAA.
- GVF are produced as a daily rolling weekly composite at 4-km resolution (global scale) and 1-km resolution (regional scale).
- As NOAA-20 (JPSS-1) data became available, the new NOAA-20 GVF product is developed and introduced in this poster

VIIRS GVF Algorithm

The GVF processing system generates daily rolling weekly GVF through the following steps:

Step 1: VIIRS swath surface reflectance data in bands I1 (red), I2 (NIR), and M3 (blue) during a calendar day (0000 – 2400 UTC) are mapped to the native GVF geographic grid (0.003 degree plate carree projection) to produce a gridded daily surface reflectance map.

Step 2: At the end of a 7-day period, the daily surface reflectance maps of the 7 days are composited to produce a weekly surface reflectance map using the MVA-SAVI compositing algorithm, which selects, at each GVF grid point (pixel), the observation with maximum view-angle adjusted SAVI (soil adjusted vegetation index) value in the 7-day period. The 7-day compositing is conducted daily using data in the previous 7 days as input data, which is called daily rolling weekly compositing.

Step 3: EVI is calculated from the daily rolling weekly composited VIIRS surface reflectance data in bands I1, I2 and M3.

$$EVI = 2.5\frac{NIR - Red}{NIR + 6Red - 7.5Blue + 1}$$

Step 4: High frequency noise in EVI is reduced by applying a 15-week digital smoothing filter (Sullivan, 1993) on EVI.

Step 5: GVF is calculated by comparing the smoothed EVI against the global maximum (EVI_∞) and minimum EVI (EVI_0) values assuming a linear relationship between EVI and GVF.

$$GVF = \frac{EVI - EVI_0}{EVI_\infty - EVI_0}$$

Step 6: GVF is aggregated to 0.009 degree (1-km) and 0.036 degree (4-km) resolution for output maps. Potential gaps on the output maps at high latitudes are filled using monthly VIIRS GVF climatology.

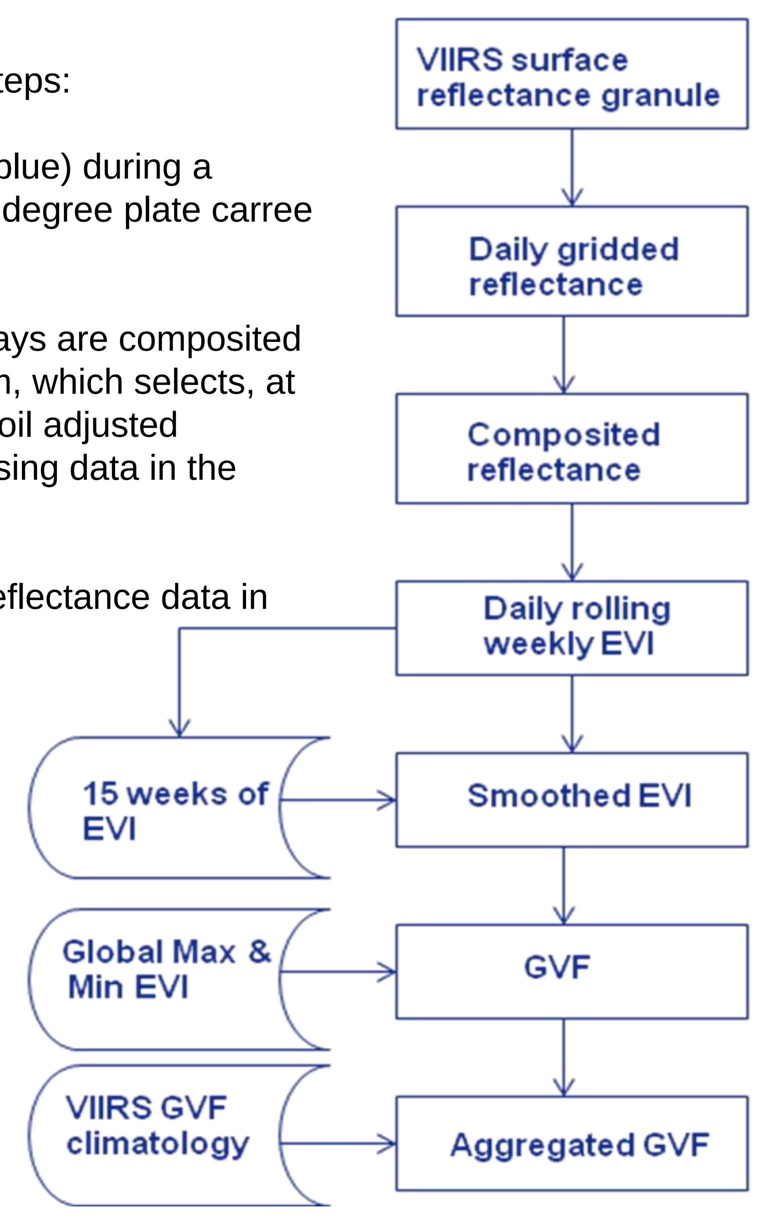

Flow chart of the GVF system

NOAA-20 Global 4-km GVF product

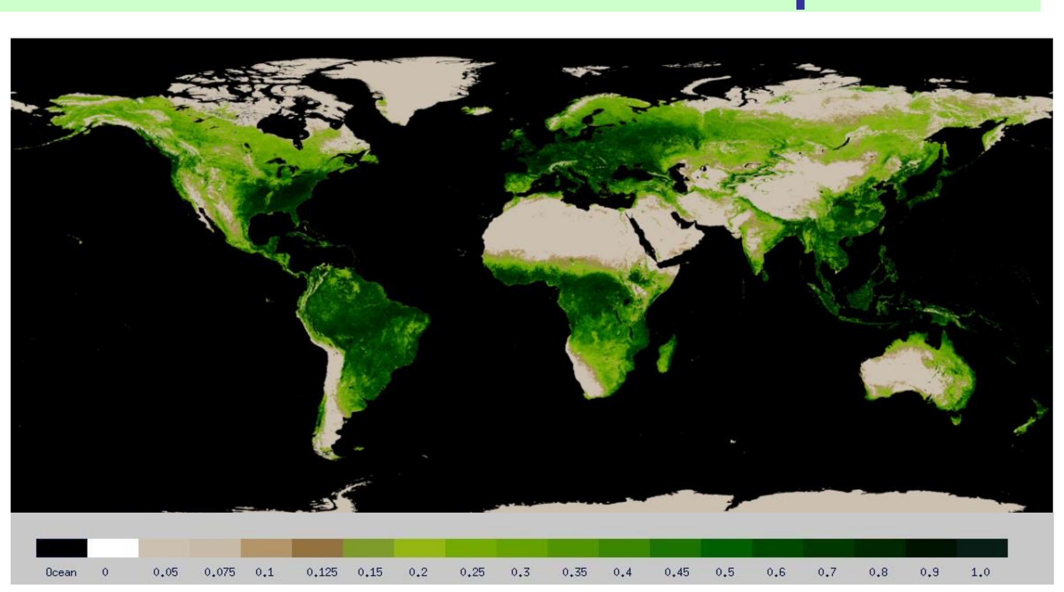

20190524-20190530

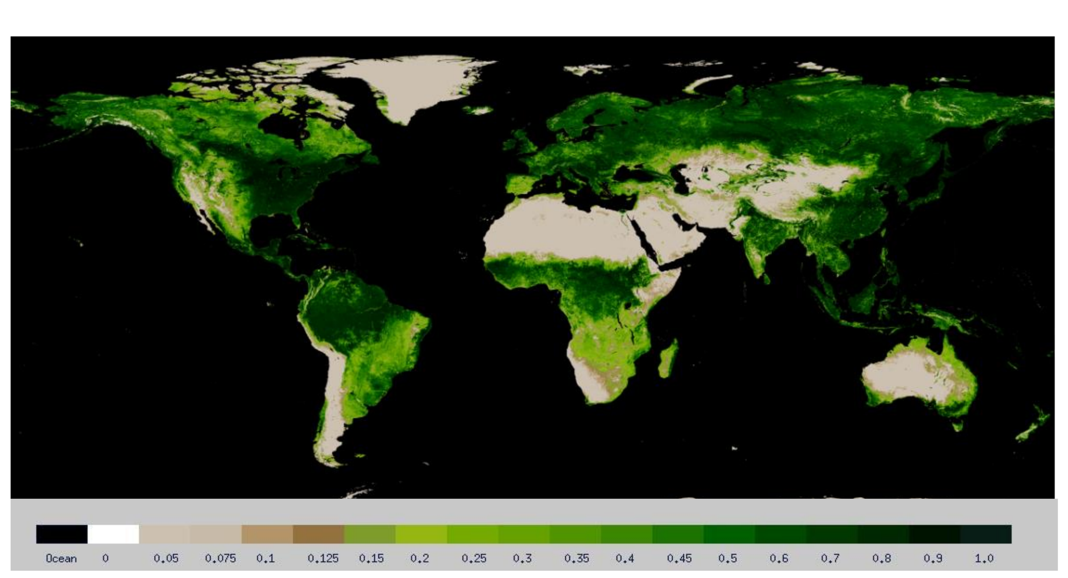

20190809-20190815

Regional 1-km GVF product

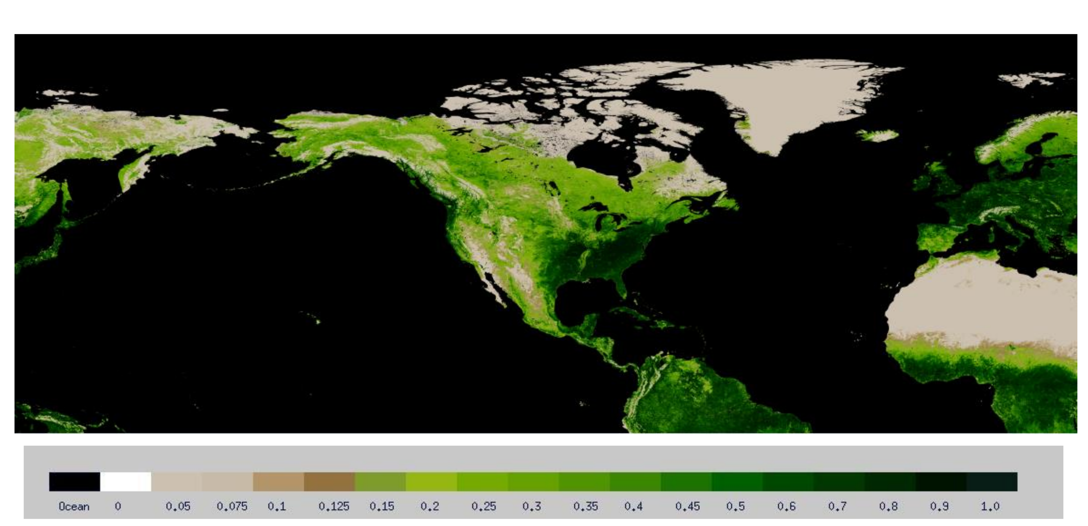

20190524-20190530

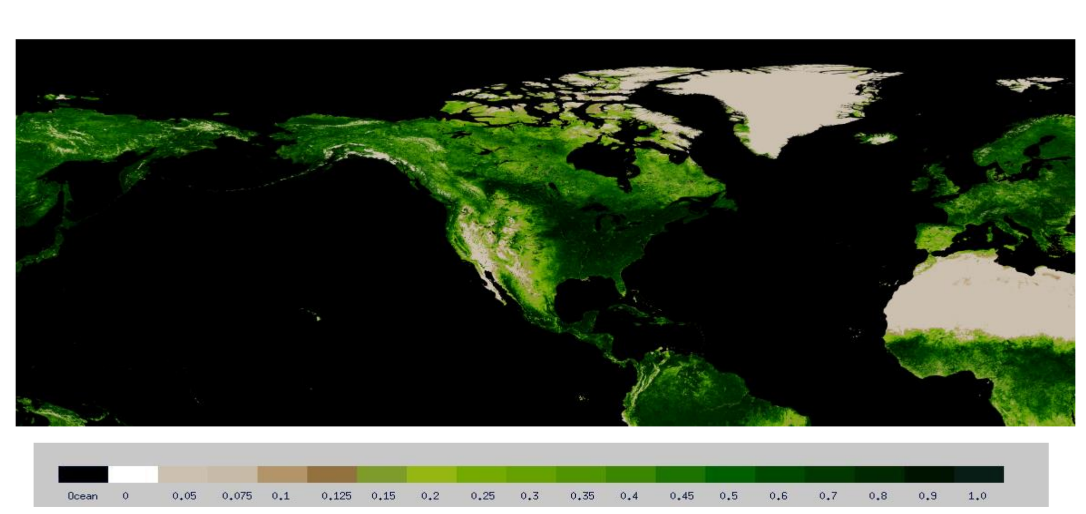

20190809-20190815

NOAA-20 GVF VS. PhenoCam GCC

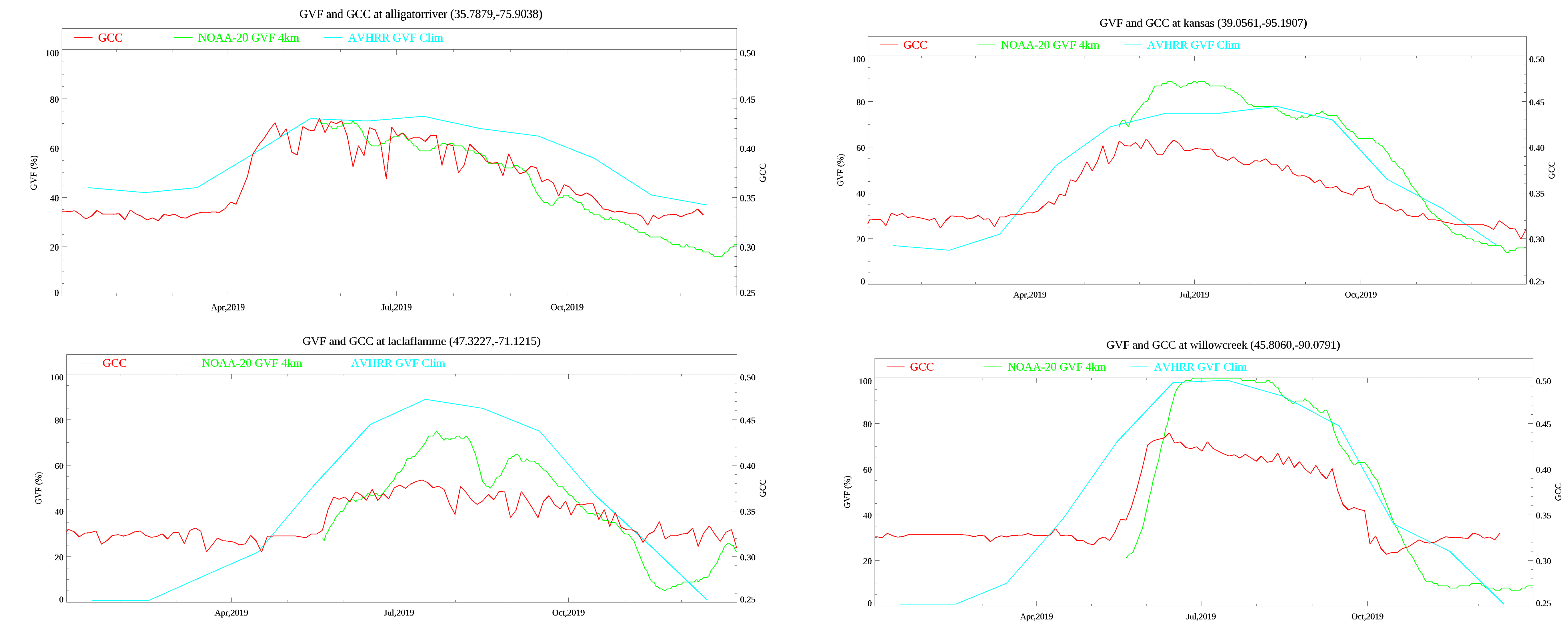

The PhenoCam Network provides automated, near-surface RGB images of canopy phenology across the North America.
(GCC) was calculated based on the daily mean R, G, B values for each site (Klosterman et al 2014; Richardson et al 2009).

GCC=G/(R+G+B)

NOAA-20 GVF time series showed similar seasonal variation as the ground measured greenness index (GCC)

NOAA-20 and S-NPP GVF comparison

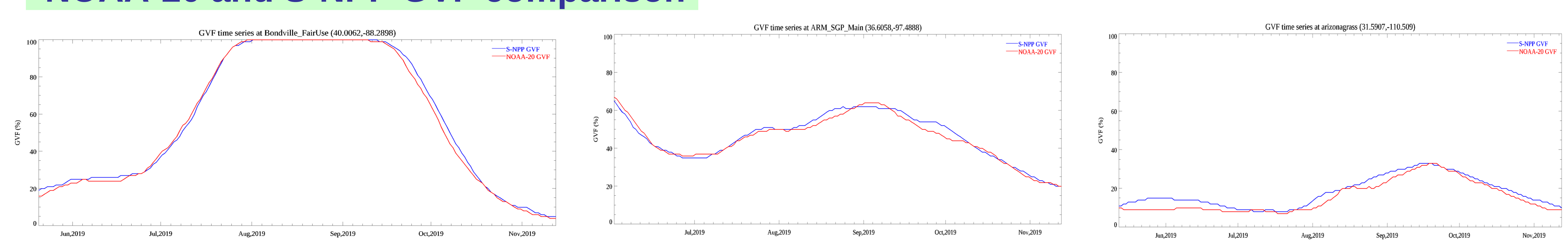

Validation

- Reference GVF data derived from 107 Landsat ETM+ images distributed globally
- Period: 1/3/2019 - 2/28/2019 (winter at north hemisphere)
- Decision-tree classification method used to classify the 30-m Landsat pixels into 3 vegetation levels (GVF=0, 0.5 or 1)
- Landsat classified images reprojected to the VIIRS GVF projection and 30-m GVF are aggregated to 4km GVF

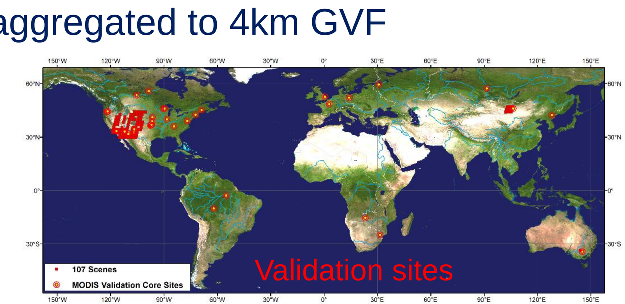

North America **Australia**

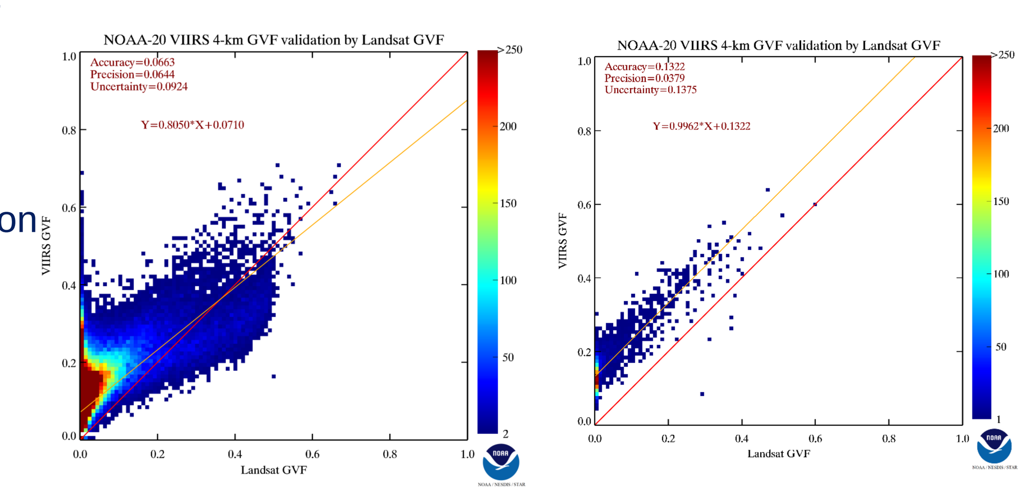

Validation of the NOAA-20 4-km GVF

Specifications		VIIRS GVF
Measurement accuracy		
Global	0.12	0.058
Regional	0.12	0.067
Measurement precision		
Global	0.15	0.063
Regional	0.15	0.076
Measurement uncertainty		
Global	0.17	0.086
Regional	0.17	0.101

Summary:

1) **The NOAA-20 VIIRS GVF system produces a global 4-km resolution GVF map and a regional 1-km GVF map once a day**
2) **NOAA-20 GVF time series showed similar seasonal variation as the ground measured greenness index (GCC)**
3) **VIIRS GVF accuracy, precision and uncertainty were lower than the specifications, indicating that the global and regional VIIRS GVF products meet the design requirements**
4) **Operational NOAA-20 VIIRS GVF product has been available for the public at NOAA comprehensive large array-data stewardship system (CLASS) since 6/4/2019 (https://www.bou.class.noaa.gov/saa/products/welcome)**

Near Rear Time One-kilometer SMAP Soil Moisture Data Product for Potential Use in National Water Model

Jifu Yin[1, 2] (jifu.yin@noaa.gov), Xiwu Zhan[2], Yanjuan Guo[1,2], Nai-Yu Wang[1, 2], Ralph R. Ferraro[2]

1. CISESS/ESSIC, UMD, College Park, MD. 2. NOAA NESDIS-STAR, College Park, MD.

Motivation: NOAA has undertaken a major effort to improve its hydrological forecast services through the development of a new National Water Model (NWM) at the National Water Center. Because of the uncertainties in model physics and input parameters, and potential errors in forcing data, the soil moisture (SM) estimates may be erroneous, resulting uncertainties in the output of the NWM. These type of model errors can be compensated for by assimilating fine resolution satellite SM observations. For operational users, the downscaling approach should be feasible for operational implementation, requiring limited ancillary information and primarily depending on readily available satellite observations. Thus, a near-real-time 1 km SMAP SM data product is proposed to be routinely generated at the NOAA-NESDIS using remotely sensed land surface temperature (LST) and enhanced vegetation index (EVI) observations.

Downscaling Approaches:
Temperature–vegetation Triangle (TRIA)
Vegetation temperature condition index (VTCI)
Soil wetness index-based Method (UCLA)

Satellite Observations: EVI &
Daytime LST (DAY)
Nighttime LST (NIGHT)
Nighttime and daytime LST difference (DTR)

TRIA_DAY	TRIA_NIGHT	TRIA_DTR
VTCI_DAY	VTCI_NIGHT	VTCI_DTR
UCLA_DAY	UCLA_NIGHT	UCLA_DTR

Fig. 1 Nine selected downscaling schemes for developing an optimal downscaling strategy.

Metrics	SMAP (25 km)	VTCI (1 km)			UCLA (1 km)			TRIA (1 km)		
		DAY	NIGHT	DTR	DAY	NIGHT	DTR	DAY	NIGHT	DTR
R	***0.642***	0.582	0.584	0.596	0.640	0.632	***0.642***	0.576	0.574	0.582
RMSE	0.089	0.091	0.092	0.086	0.084	0.086	***0.082***	0.097	0.097	0.091
ubRMSE	0.054	0.060	0.059	0.054	0.051	0.053	***0.049***	0.062	0.063	0.060

Tab. 1 Summary of the statistical comparison results when averaged across the CONUS, including correlation coefficient (*r*), RMSE (m^3/m^3), and ubRMSE (m^3/m^3) over the 1 May 2017- 30 April 2019 period. Italic bold indicates the optimal metric.

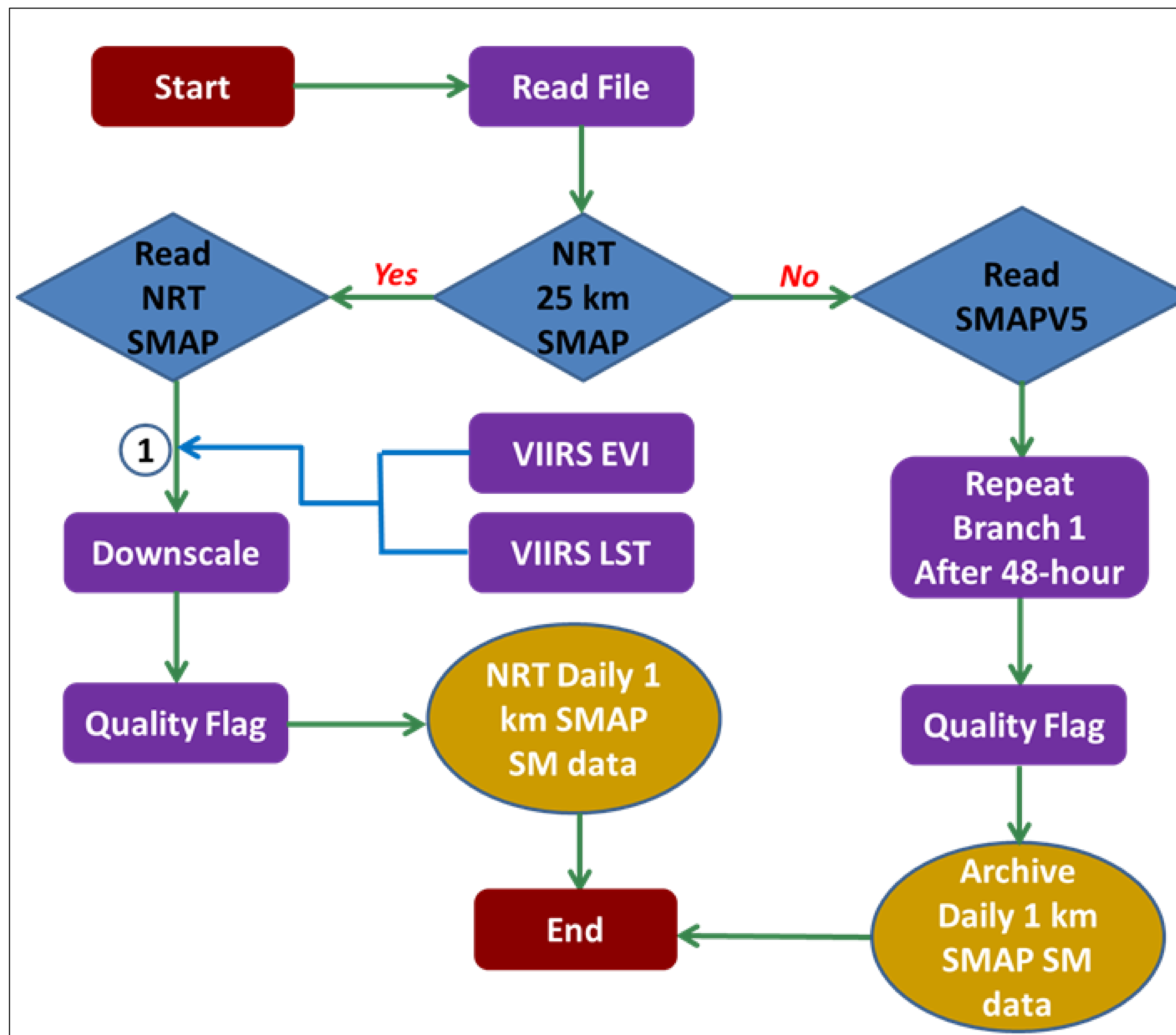

Fig. 3 Process flow of producing a NRT 1 km downscaled SMAP soil moisture map using the UCLA_DTR method.

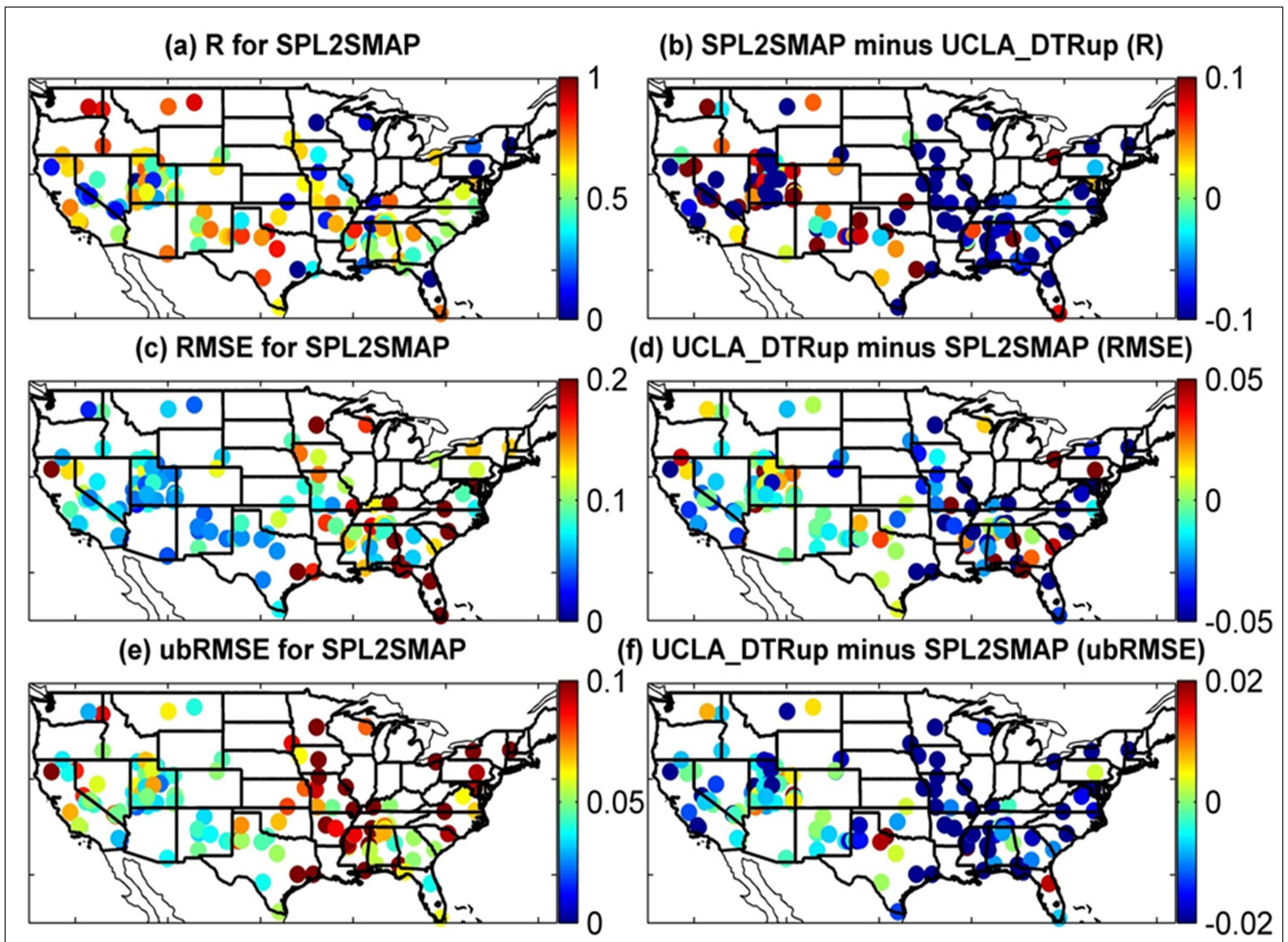

Fig. 2 With respect to the quality controlled SCAN SM observations, left column shows the metrics for SMAP/Sentinel 3 km SM product (SPL2SMAP), while the right column shows metric differences between SPL2SMAP and 3 km UCLA_DTRup during the 1 May 2017- 30 April 2019 period. Top, middle and bottom rows are for correlation coefficients (*r*), RMSE (m^3/m^3) and ubRMSE (m^3/m^3), respectively.

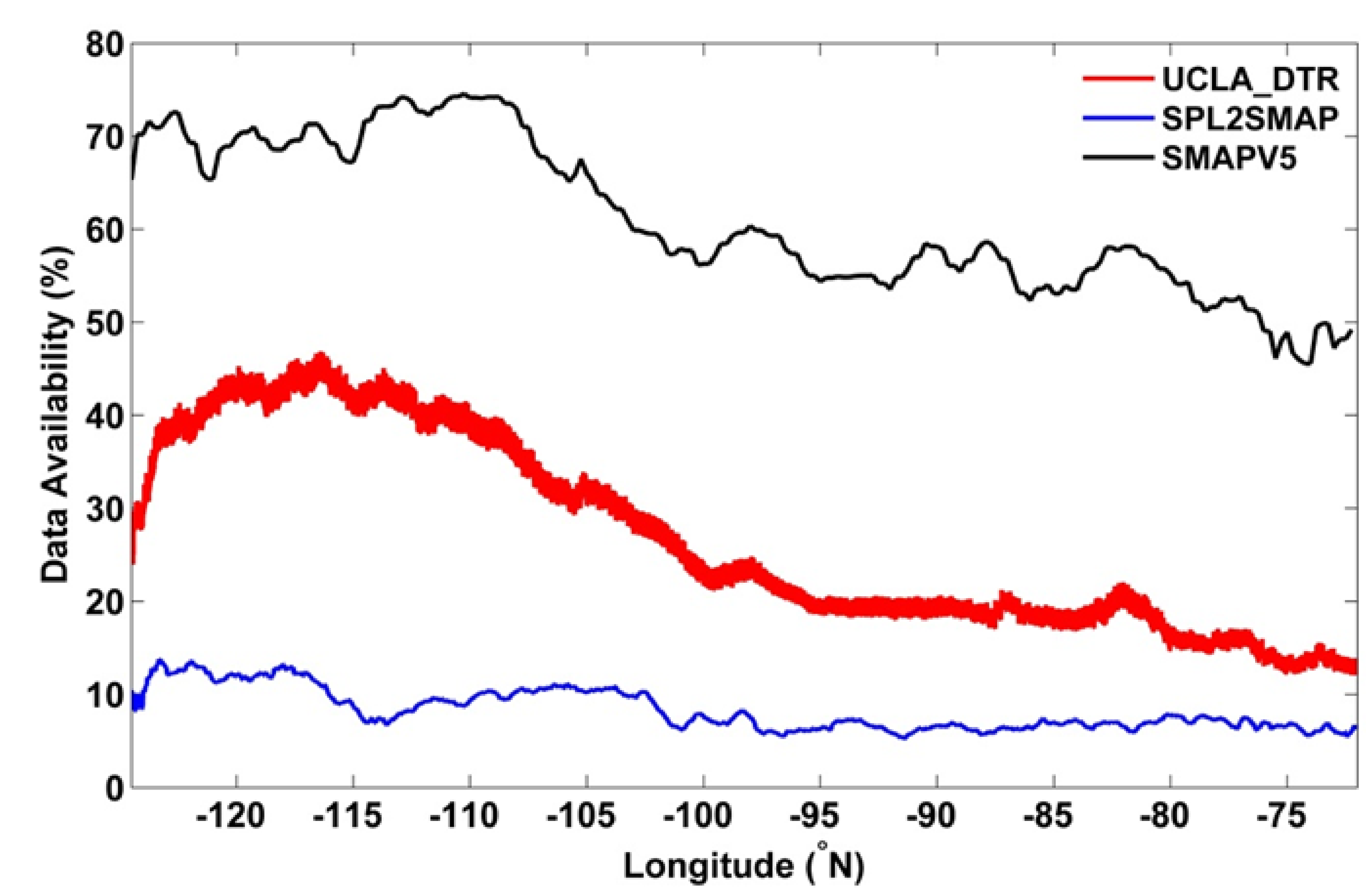

Fig. 4 Longitude-averaged data availability over the CONUS domain.

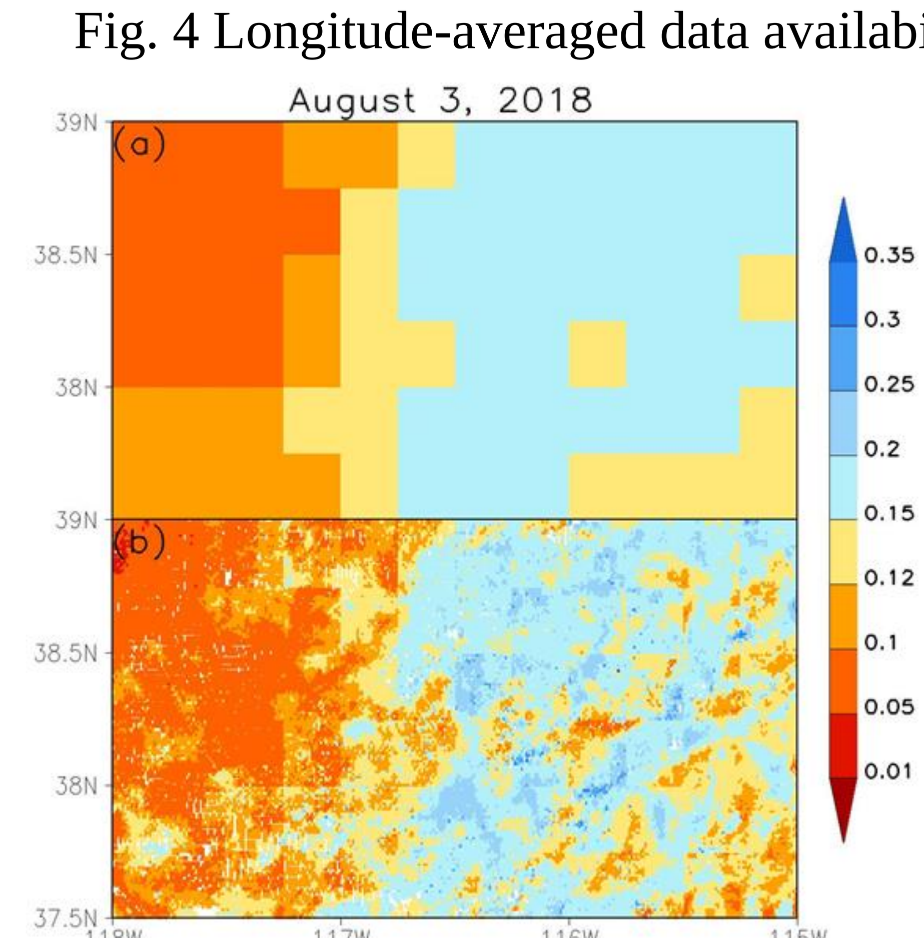

Fig. 5 Sample maps for (a) 25 km SMAP and (b) the downloaded 1 km SMAP SM retrievals over the sub-region from -118˚E, 37.5˚N to 115˚E, 39˚N on August 3, 2018.

Conclusions:

(1) The advantages of the downscaling technique include simplicity, feasibility of operational implementation, pure reliance on remote sensing measurements, computationally fast and limited ancillary information requirements.

(2) With respect to the quality controlled SCAN observations, the UCLA_DTR method showed the most successful performance out of the 9 downscaling schemes. As expected, the accuracy level is significantly improved with the advance of the fine scale satellite SM measurements.

(3) Compared to the NASA 3 km SMAP/Sentinel product, the accuracy level was significantly improved. The downscaled 1 km SMAP SM data product also provides larger data availability, although the VIIRS observations used as ancillary information can be affected by cloud coverage.

(4) Building on the results shown in this paper, a near-real-time 1 km SMAP SM data product is proposed to be developed at NOAA-NESDIS.

The Status of the GOES-R Land Surface Temperature Product

Peng Yu[1,2], Yunyue Yu[1], Yuling Liu[1,2], and Heshun Wang[1,2]
[1]STAR/NESDIS, NOAA, College Park, MD [2]ESSIC/CISESS, UMD, College Park, MD

Introduction

Land Surface Temperature (LST) is one of the key variables in the weather and climate system controlling surface heat and water exchange at the land atmosphere interface. Satellite measured LST is mostly based on thermal infrared band observations which theoretically gives the temperature at some nominal skin depth of the surface. Knowledge of the LST gives critical information on temporal and spatial variations of the surface equilibrium state and is of fundamental importance to many aspects of geosciences, *e.g.*, the net radiation budget at the Earth surface and to monitoring the state of crops and vegetation, as well as an important indicator of both the greenhouse effect and the energy flux between the atmosphere and the land.

The first Geostationary Operational Environmental Satellite-R Series (GOES-R) satellite, the GOES-16, was launched in November 2016, joined by its successor, the GOES-17, in March 2018. The Advanced Baseline Imager (ABI) onboard both platforms has 16 spectral bands (compared to five from previous GOES satellite imagers), including the Split-window (SW) channels used for LST retrieval. The LST product, as one of the baseline ABI products, has been operationally produced since January 2017. The GOES-16 LST was validated with the in-situ surface temperature estimates from the SURFRAD network and results show that the bias and precision required by the mission were met for all three LST products (CONUS, FD, and MESO). As a result, the GOES-16 LST reached its Provisional maturity in March 2018. Its GOES-17 counterpart during "cool" period reached the Provisional maturity in June 2019. This presentation will provide detailed information about the product's validation and evaluation results, their current status, and future direction.

GOES-R ABI Land Surface Temperature Product

GOES-R mission requirements for LST

Observational Requirement	LEVEL[1]	Geographic Coverage[2]	Horiz. Res.	Mapping Accuracy	Msmnt. Range (K)	Msmnt. Accuracy[3] (K)	Msmnt. Precision (K)	Refresh Rate	VAGL[4]	Extent Qualifier[5]
CONUS	T	C	2 km	1 km	213 – 330	2.5	2.3	60 min	3236 sec	LZA <70
Full Disk	T	FD	10 km	5 km	213 – 330	2.5	2.3	60 min	806 sec	LZA <70
Mesoscale	T	M	2 km	1 km	213 – 330	2.5	2.3	60 min	159 sec	LZA <70

[1] T=target, G=goal [2] C=CONUS, FD=full disk, H=hemisphere, M=mesoscale
[3]The measurement accuracy 2.5K is conditional with 1) known emissivity, 2) known atmospheric correction and 3) 80% channel correction; 5 K otherwise. [4] VAGL=Vender Allocated Ground Latency.
[5] LZA=local zenith angle.

GOES-R ABI LST Product

$$T_s = C + A_1 T_{11} + A_2(T_{11} - T_{12}) + A_3\varepsilon + D(T_{11} - T_{12})(\sec\theta - 1)$$

Data Access: https://www.avl.class.noaa.gov/saa/products/search?sub_id=0&datatype_family=GRABIPRD
GOES-16: May 24., 2017 – Present; GOES-17 LST: August 27, 2018 – Present
GOES-R LST ATBD: https://www.star.nesdis.noaa.gov/goesr/documents/ATBDs/Baseline/ATBD_GOES-R_LST_v2.5_Jul2012.pdf
GOES-R PUG: https://www.goes-r.gov/products/docs/PUG-L2+-vol5.pdf
Long-Term Monitoring Web: https://www.star.nesdis.noaa.gov/smcd/emb/land/index.php
Long-Term Monitoring FTP: ftp://ftp.star.nesdis.noaa.gov/pub/smcd/emb/pyu/LTM/single/

Product Timeline

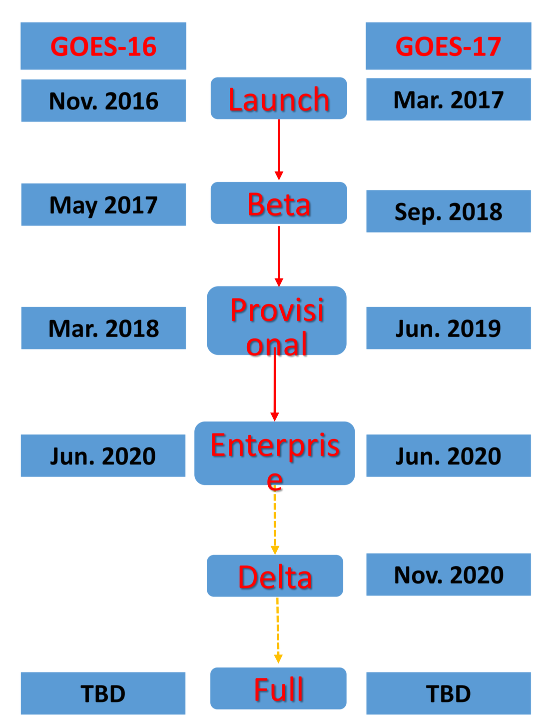

Hourly Output Frequency

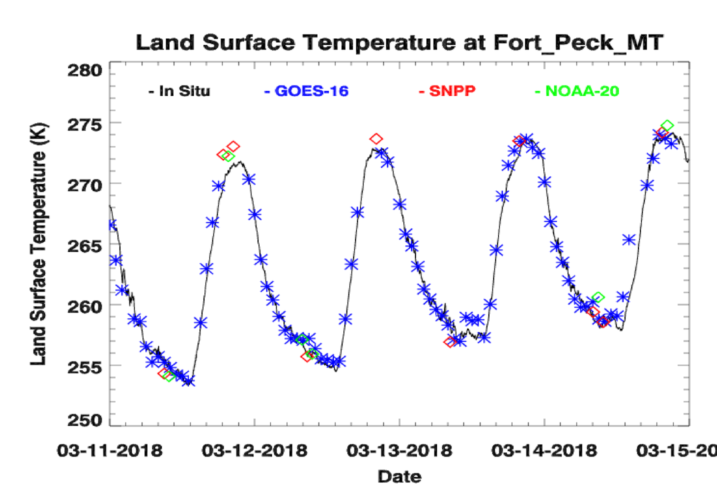

Geostationary satellites' scan frequency is higher than that of polar-orbit satellites. A comparison to LSTs combined from both SNPP and NOAA-20, the GOES-16 LST is able to more accurately characterize the LST diurnal variation.

GOES-R Coverage

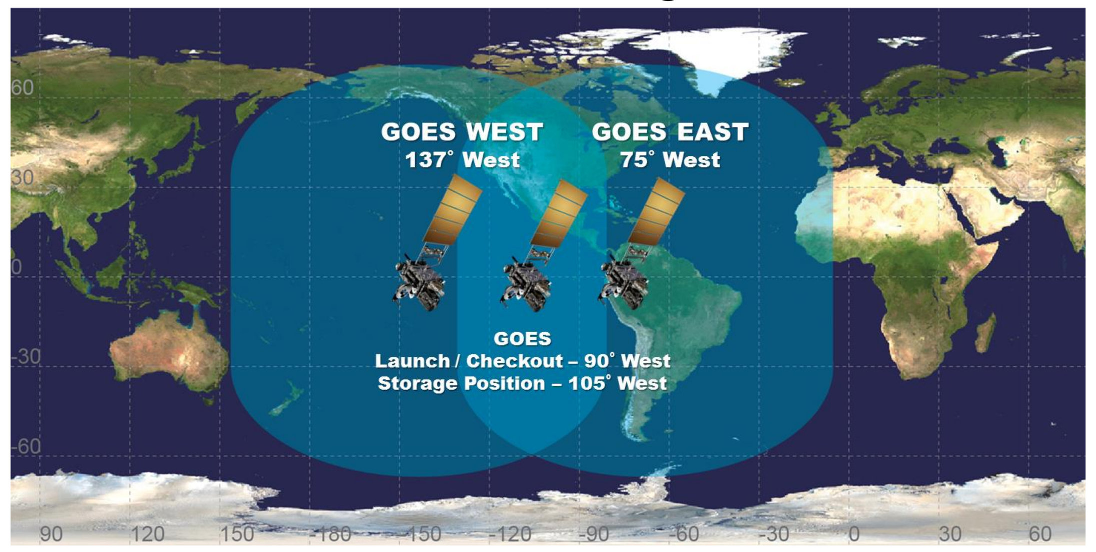

- GOES-16 at GOES-EAST
- GOES-17 at GOES-WEST
- Two platforms overlap at the CONUS
- Hourly output frequency revealed more detailed temporal evolution compared to sensors onboard polar orbiting satellites, e.g., JPSS and SNPP

Advanced Baseline Imager Scan Modes

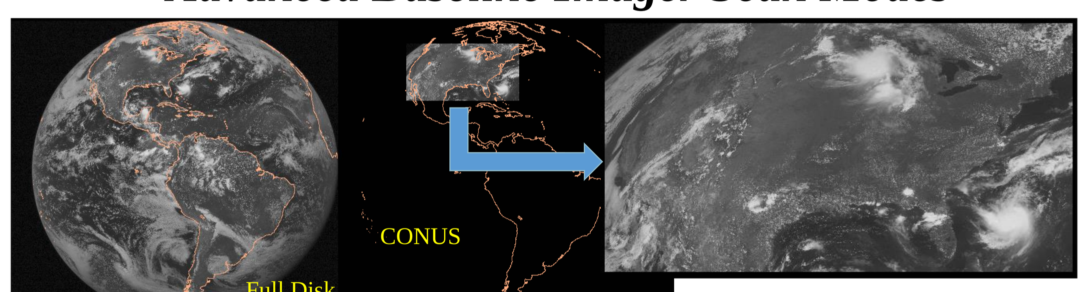

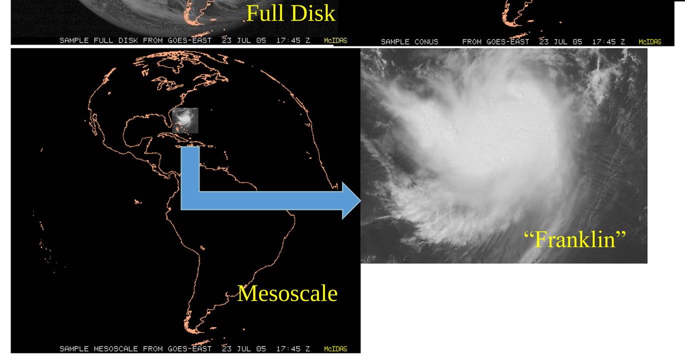

There are three scan modes for the ABI:

- Mode 3: Full disk images every 15 minutes + 5 min CONUS images + two 1–min mesoscale images
- Mode 4: Continuous Full disk every 5 minutes
- Mode 6 (Default): Full disk images every 10 minutes + 5 min CONUS images + two 1–min mesoscale images

ABI scans about 5 times faster than the previous GOES imager

GOES-R Long-Term Monitoring Output Examples

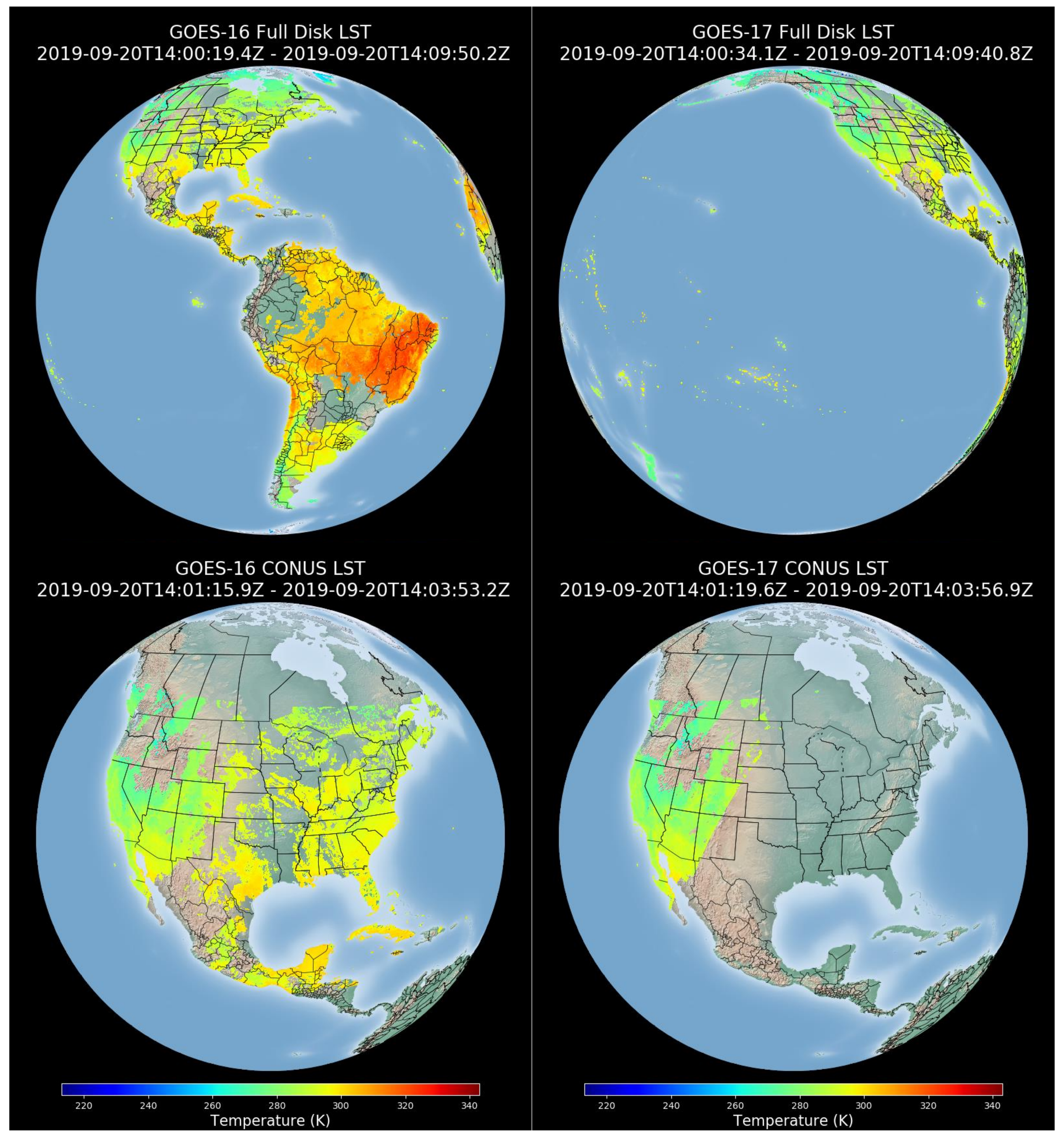

Validation Results

GOES-16 CONUS LST Validation Results

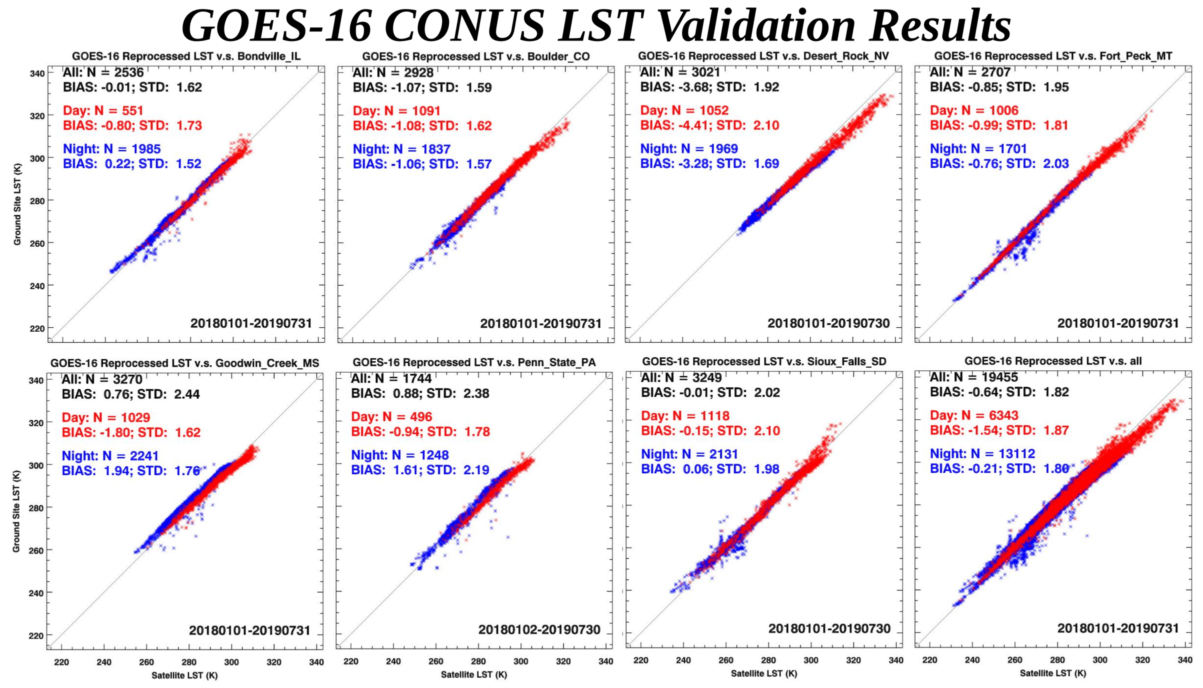

GOES-17 CONUS LST Validation Results

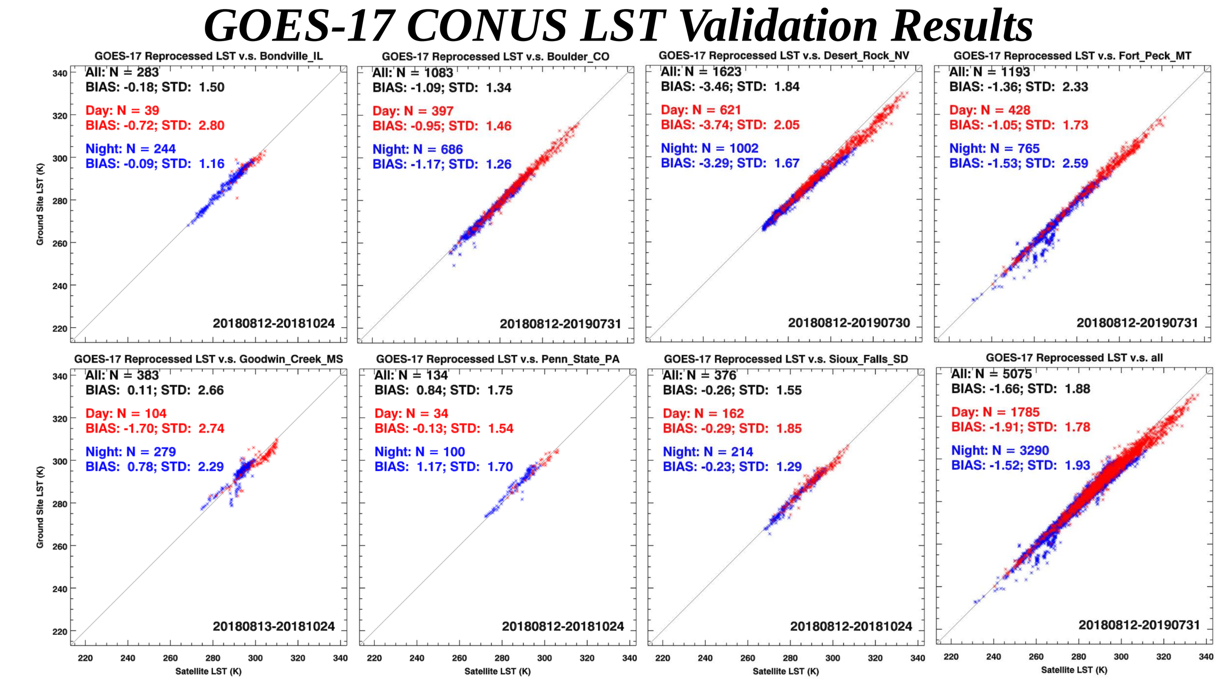

Enterprise Algorithm Evaluation with GOES-17 Data

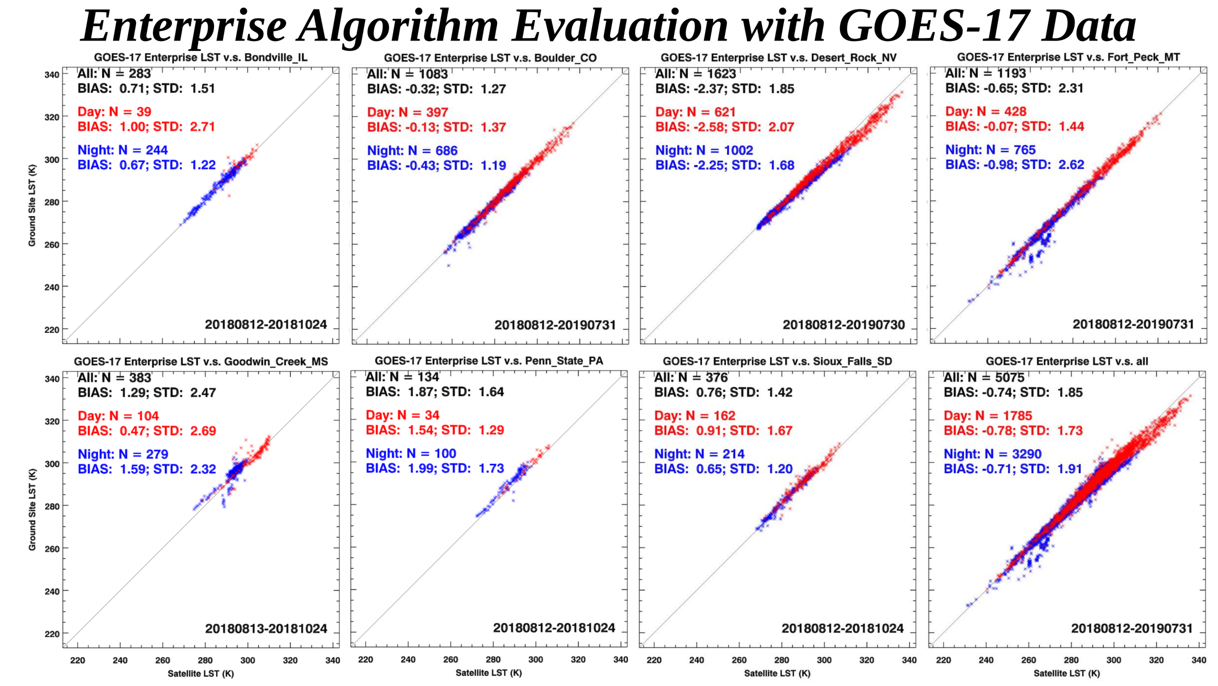

Mitigation Algorithm Evaluation with GOES-17 Data

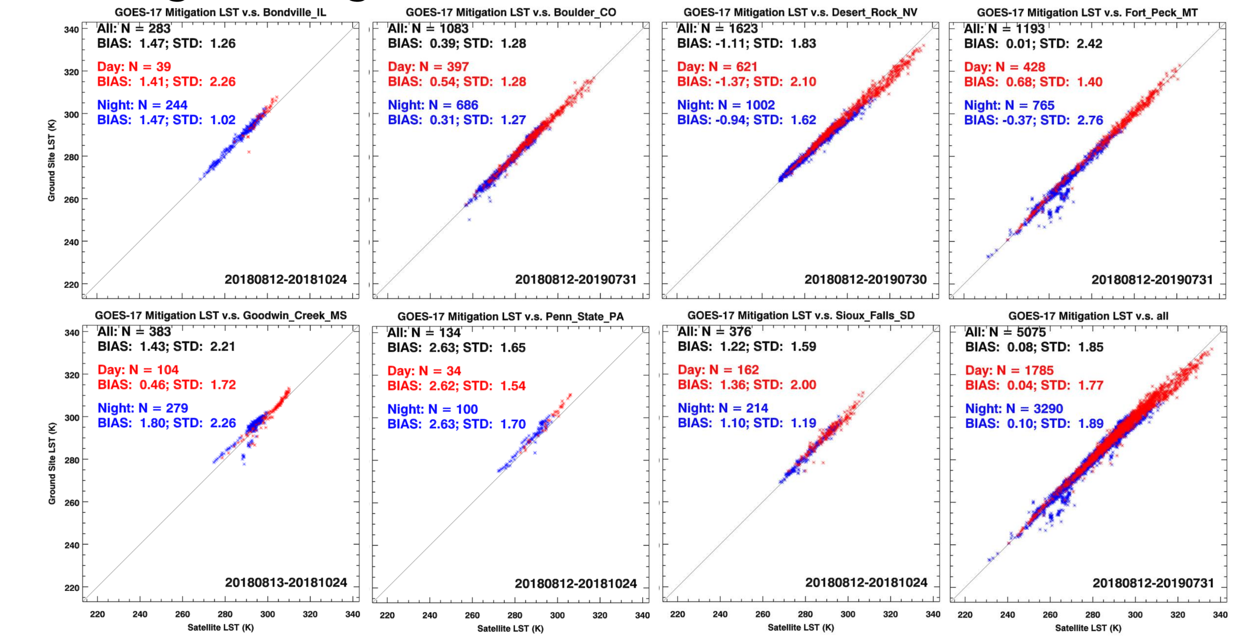

Application Examples

- GOES-R LST is used in numerical weather forecast model output verification.
- GOES Evapotranspiration and Drought System
- Urban air surface temperature model

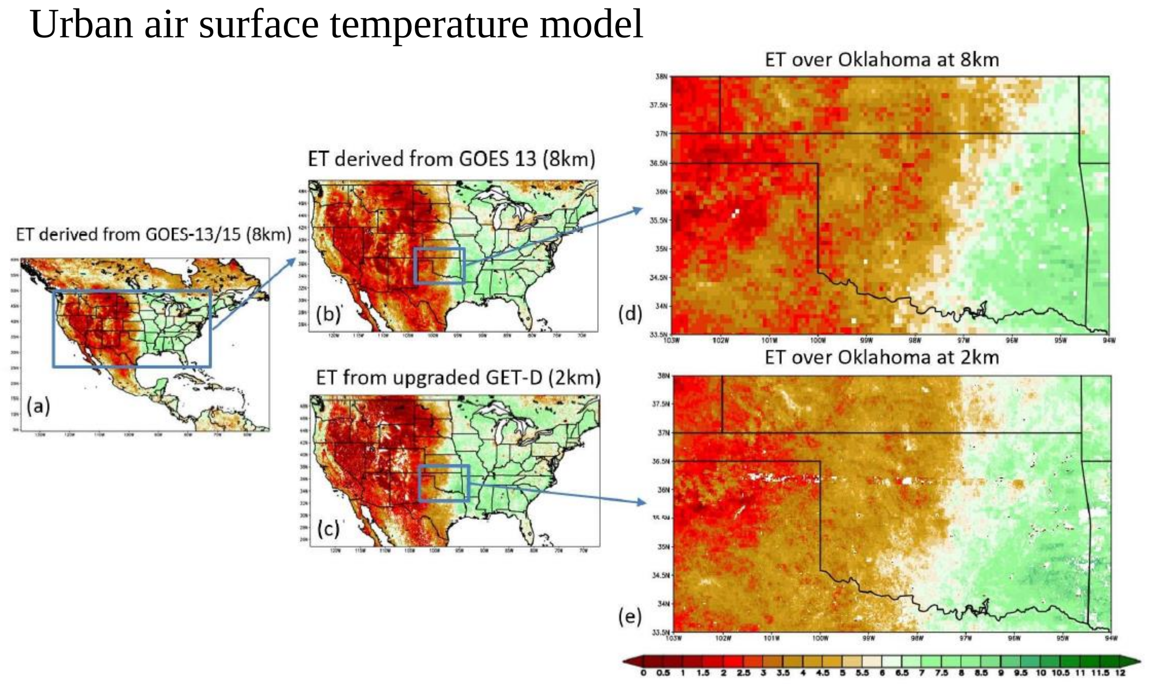

ET estimates comparis on between operational GOES-13/15 based 8 km product (a: over North America domain and b: over CONUS domain) and upgraded GOES-16 based 2 km product (c), with regional comparison over Oklahoma at 8km (d) and 2km (e). Monthly composite of July 2017 (mm/day).

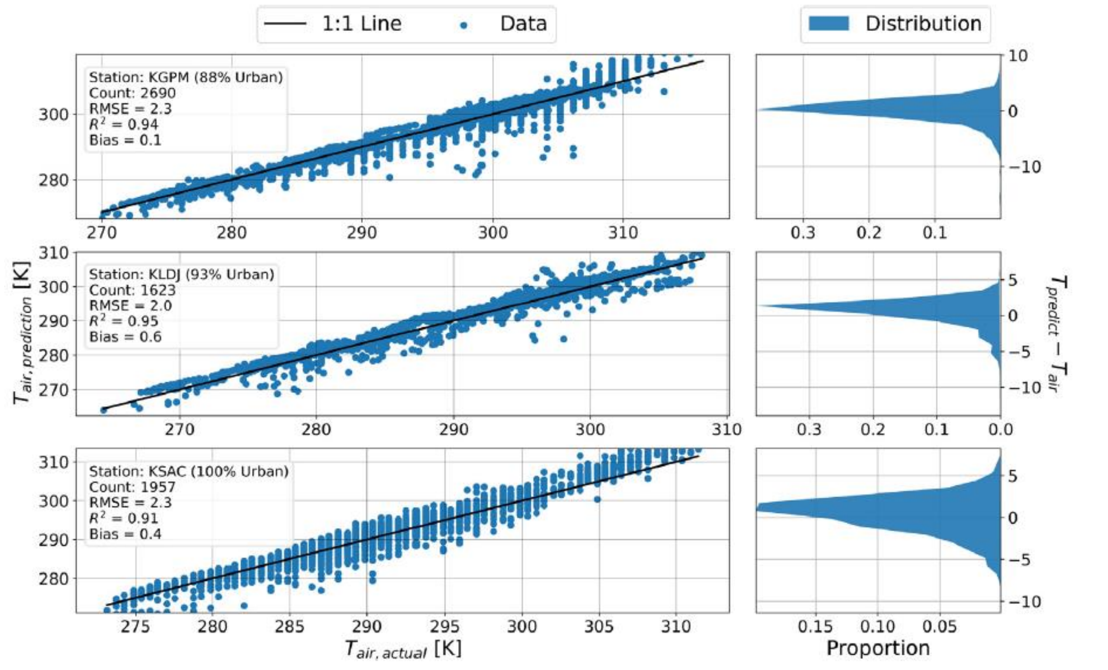

Scatter and difference plots for ground station and satellite-predicted air temperature for three individual stations in Dallas, TX (top), Elizabeth, NJ (middle),and Sacramento, CA (bottom). Each station is at least 70% urban. The scatter shows the adherence of the prediction algorithm to the true ground station temperatures. The distribution shows the distribution of the scatter.

Summary

- GOES-16 LST and GOES-17 LST (during "cool" period only) reached provisional maturity in March 2018 and June 2019, respectively. All products, FD, CONUS, and MESOs, meet the mission requirement based on the validation results.
- An enterprise LST retrieval algorithm applicable to multiple sensors has been developed and delivered to ASSISTT. The evaluation results indicate it outperforms the current baseline algorithm.
- To address the loop heat pipe overheating issue, an mitigation algorithm has been developed to improve the product quality and increase its usable period during "warm" period. The preliminary evaluation results are satisfactory.
- The Enterprise/Mitigation package are expected to be implemented in the ground system in August 2020.
- The product has been widely used in different applications

A Novel Re-Compositing Approach to Create Continuous and Consistent Cross-Senor/Cross-Production Global NDVI Datasets

STAR 2020 JPSS/GOES-R PGRR Summit Tue # 11

Wenze Yang[1*], Felix Kogan[2], Wei Guo[1], and Yong Chen[3]

1. IMSG at NOAA/NESDIS/STAR, College Park, MD *Email : Wenze.Yang@noaa.gov; 2. NOAA/NESDIS/STAR, College Park, MD; 3. GST, Greenbelt, MD

Introduction

The longest Normalized Difference Vegetation Index (NDVI) time series, produced from the Advanced Very High Resolution Radiometer (AVHRR) has ended in 2017, and there will be no continuation of AVHRR on-board afternoon satellites. NDVI from other sensors, especially the operational Visible Infrared Imaging Radiometer Suite (VIIRS), is imperative to elongate this global data set while maintaining the continuity and consistency. NDVI could be de-composited into two components: the multi-year climatology and vegetation condition index (VCI), with the former contains climate information and a majority of sensor noise, and the latter contains weather information and residual sensor noise. With the assumption that VCI from different sensors are similar, we re-composited the cross-sensor/cross-production NDVI with original VCI and the cross-sensor/cross-production climatology, and compared various cross-converted datasets with the three base NDVI datasets: two NDVI productions derived from AVHRR observation and another from VIIRS observation. As a result, the re-composited NDVI agrees well with the original NDVI spatially and temporally, with an accuracy of 0.02 NDVI unit at a global scale.

Methodology

NDVI could be de-composited into its climatology and VCI. The climatology stores Ecosystem Component and major part of Observing Noise Component, while the VCI contains Weather Component and some residual of Observing Noise Component. Similarly, NDVI from different sensor and/or different production suite could be de-composited into its distinctive climatology and VCI. With the assumption that the discrepancy of VCI from different sensors/productions could be neglected, and given corresponding sets of climatology, we can back-project, or re-composite VCI to sensor/production-specific NDVI.

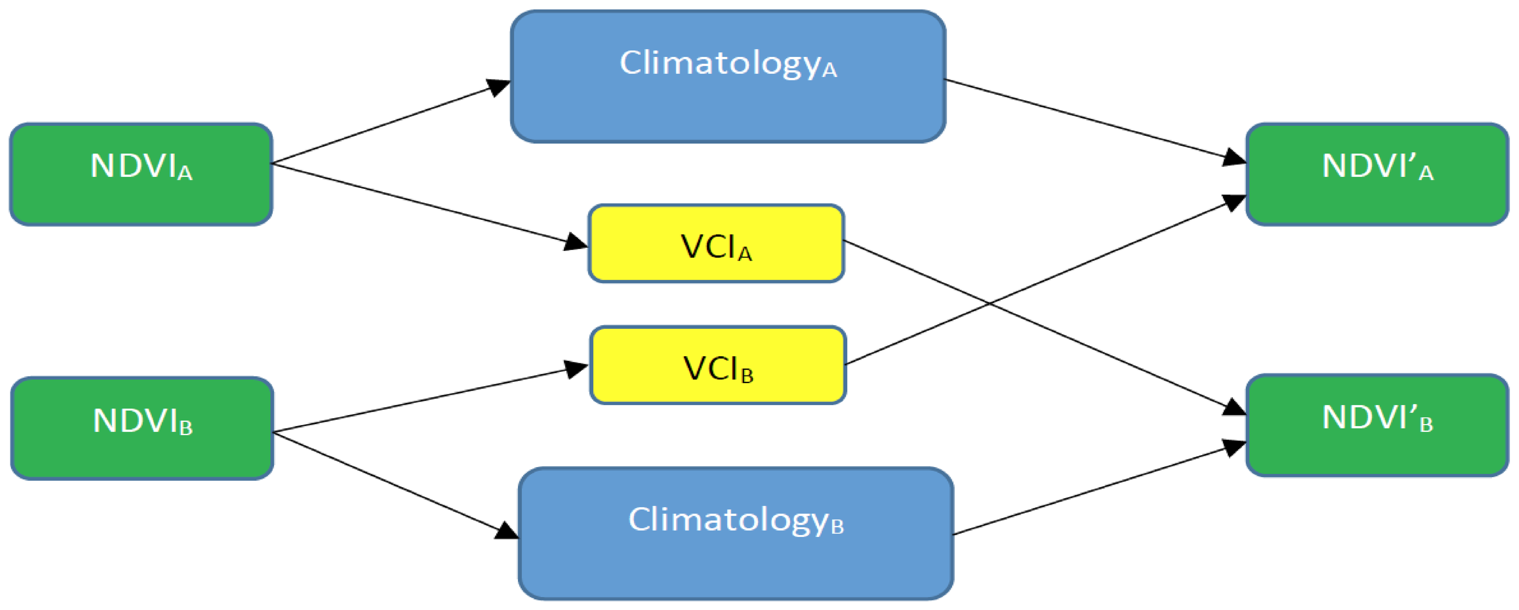

NDVI de-compositing and re-compositing through VCI.

Sensor Specific Differences

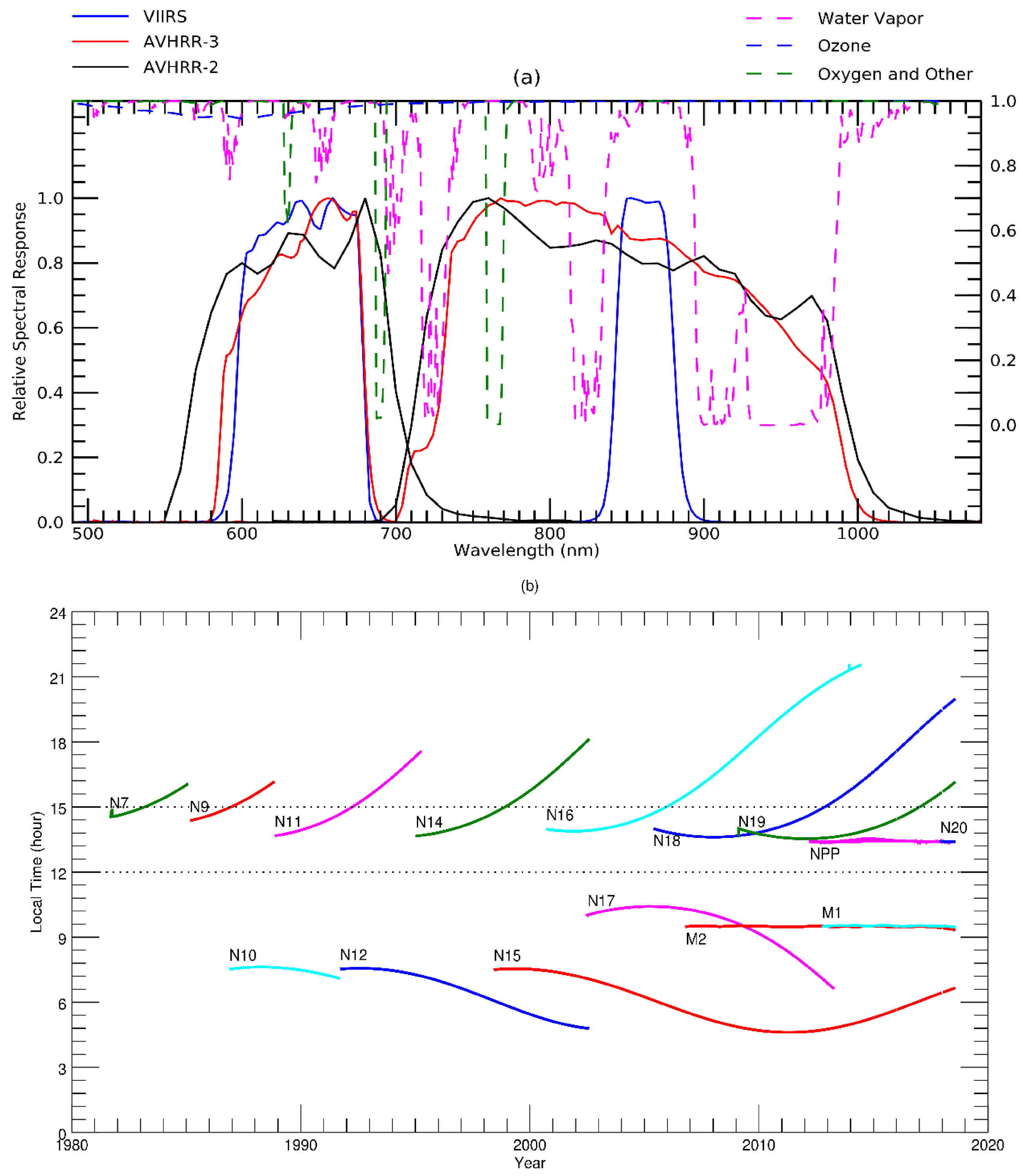

(a) Relative spectral response function of VIIRS (S-NPP), AVHRR-2 (NOAA-11) and AVHRR-3 (NOAA-19) red and NIR bands. The transmittance spectra of some selected gases are also plotted; (b) Local equatorial crossing time (LECT) of polar satellites which carry either the sensor VIIRS (S-NPP and NOAA-20) or AVHRR (the rest). In the figure, NPP is short for Suomi NPOESS Preparatory Project (S-NPP), rest N is short for National Oceanic and Atmospheric Administration (NOAA), and M is short for MetOP.

Original Base NDVI Time Series

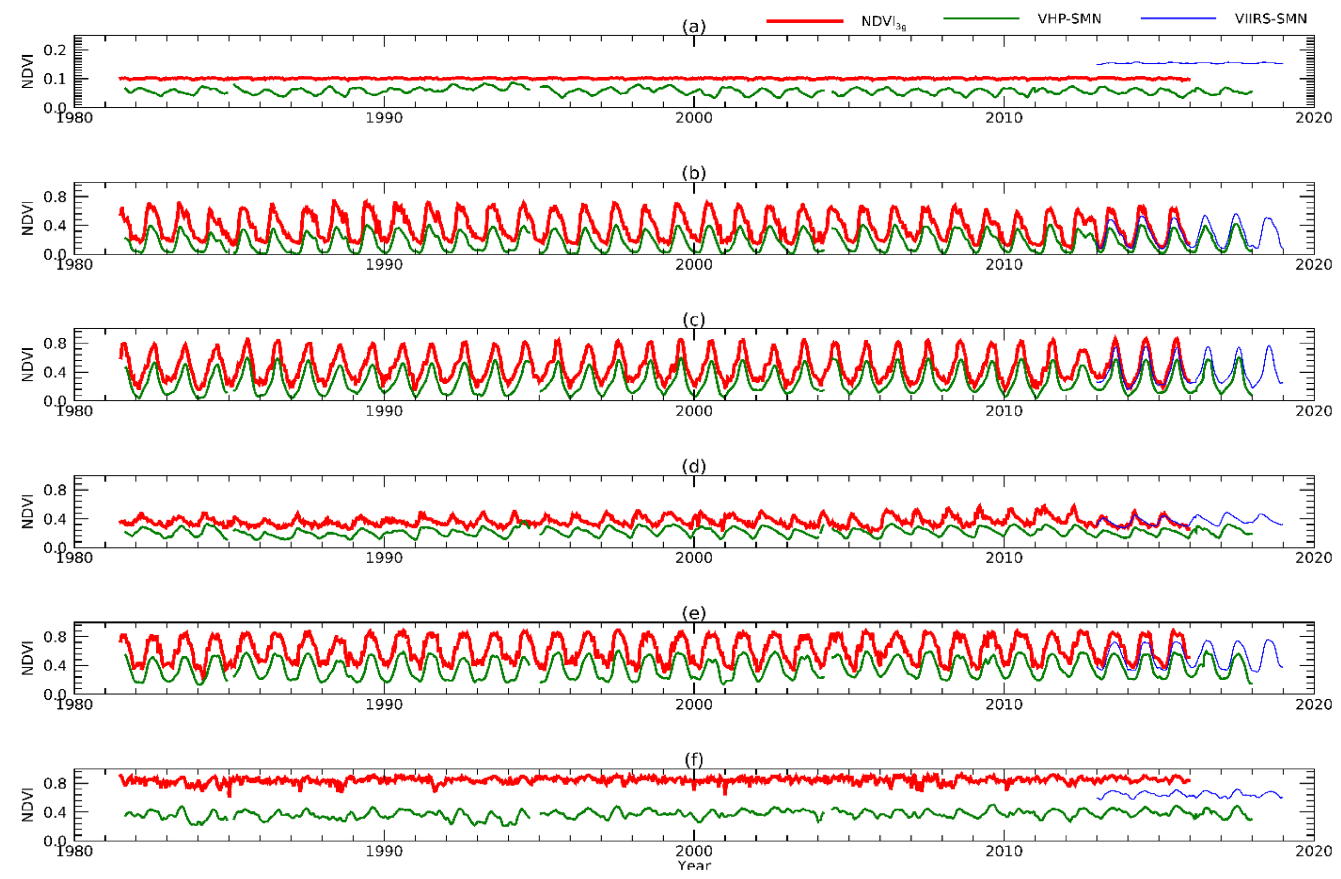

NDVI time series of 6 sites from three base datasets: GIMMS NDVI3g (1981-2015) vs. AVHRR VHP (VHP-SMN, 1981-2017) vs. VIIRS (VIIRS-SMN, 2013-2018). The 6 sites are (a) East Sahara in Libya, (b) Saratov in Russia, (c) Illinois in USA, (d) South Queensland in Australia, (e) Maine in USA, and (f) Amazon in Brazil.

Histogram of Three Base Datasets

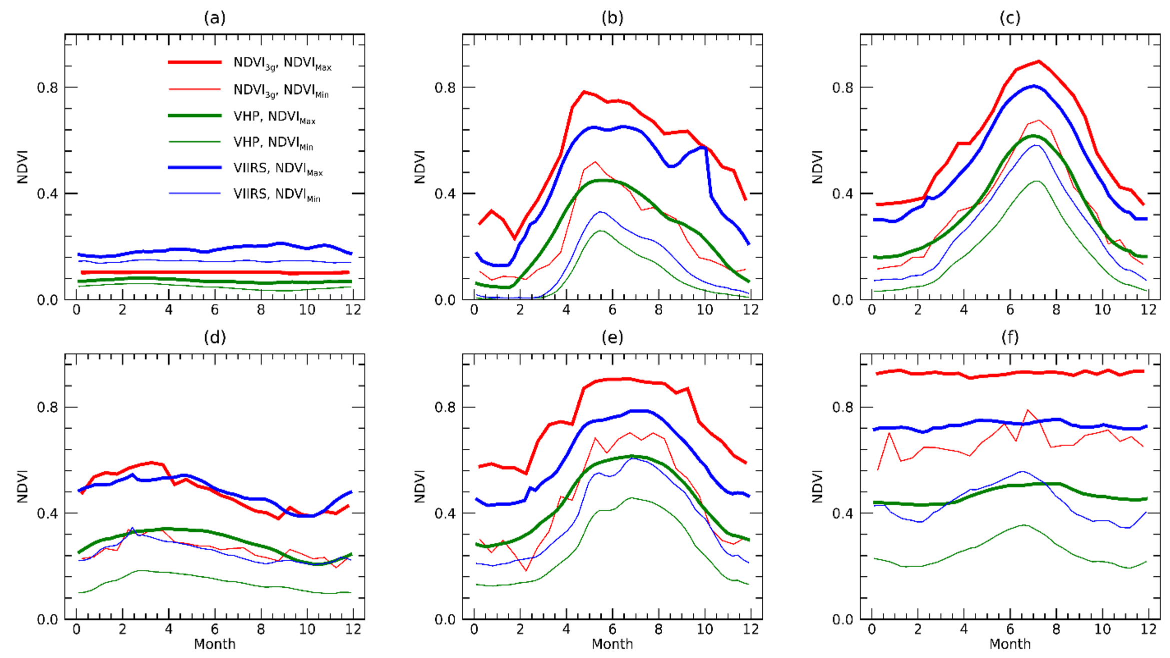

Climatology of 6 sites from the three base datasets, GIMMS NDVI3g vs. AVHRR VHP vs. VIIRS VHP. The 6 sites are the same as the previous figure.

Difference Map and Histogram

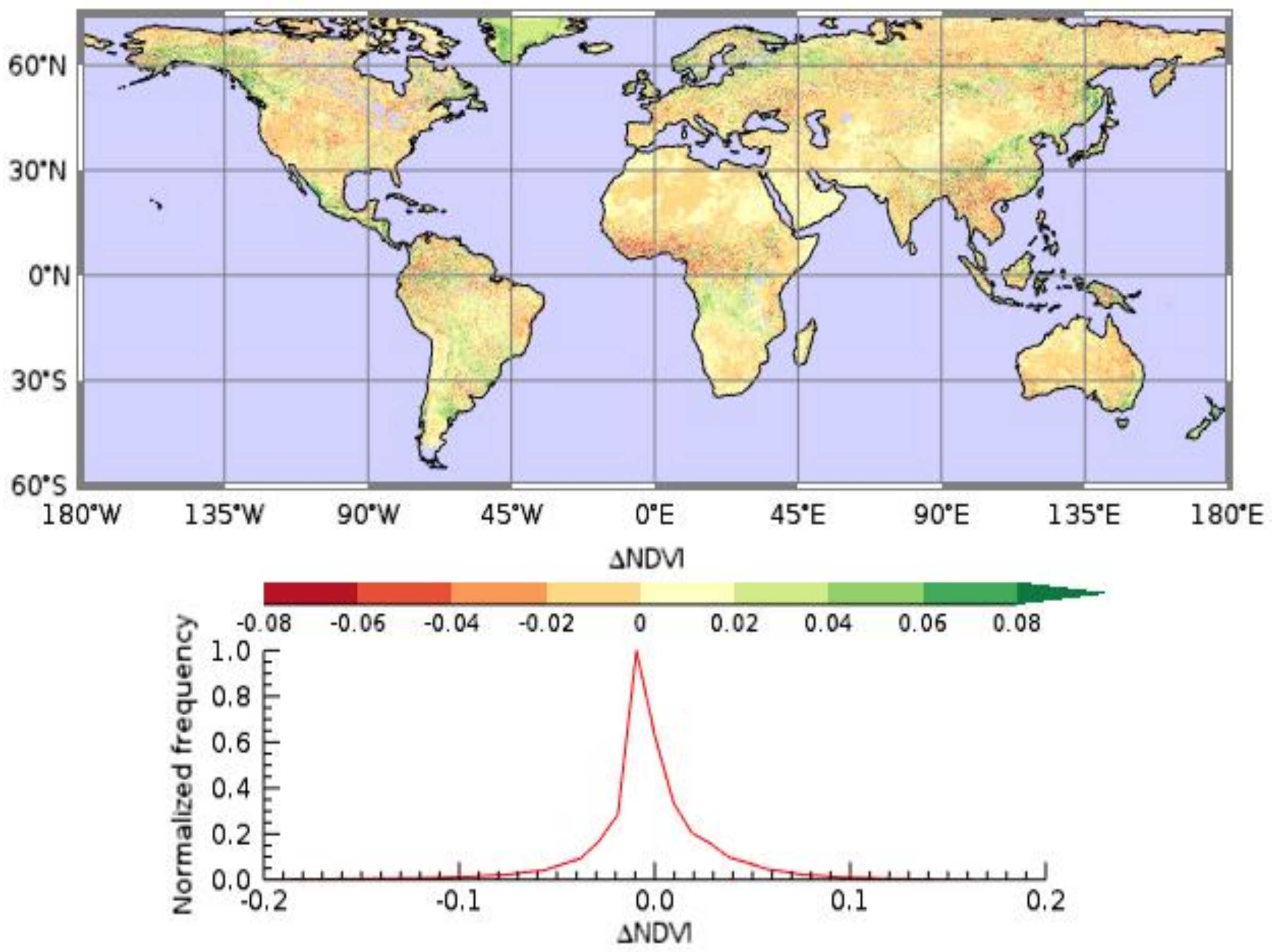

After converting NDVI from VIIRS to AVHRR VHP, we mapped its difference comparing to original AVHRR NDVI, and also plot the difference histogram.

Converted vs. Original NDVI Time Series

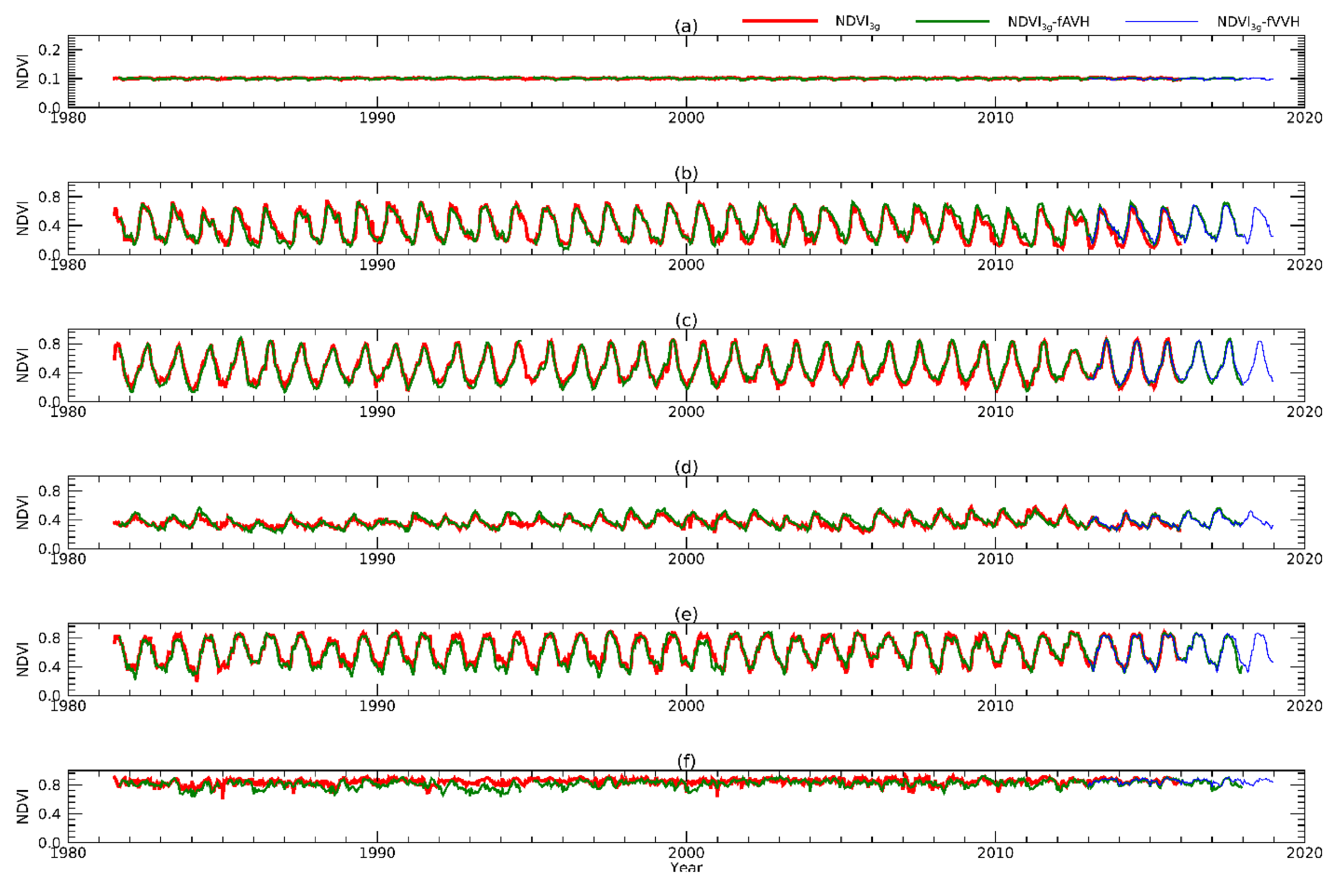

After converting AVHRR VHP and VIIRS NDVI to GIMMS NDVI3g, we compared their time series with the original NDVI3g. Note if converting to other two datasets, the comparison results are similar.

Global Surface Type Products from VIIRS

Chengquan Huang[1], Jiaming Lu[1], Weishu Gong[1], Zhenhua Zou[1], Xiwu Zhan[2]
1. Department of Geographical Science, University of Maryland, College Park, MD 20742 2. STAR/NEDSIS/NOAA, College Park, MD 20740

Summary

VIIRS observations from S-NPP have been used to generate global surface type maps on an annual basis. The primary product is an Annual Surface Type (AST) map derived using VIIRS observations acquired within one full calendar year. This product uses 17 IGBP classes to characterize the Earth's surface at approximately 1-km spatial resolution. To facilitate product use in specific applications, two additional maps are produced by reclassifying the IGBP map using the classification schemes required by those applications.

The overall accuracies of the IGBP classifications for the years between 2012 and 2018 varied between 76% and 79%, exceeding the JPSS L1RD requirement of 70%. The 2019 product is being developed with a planned release date in late summer/early fall. Future products will be produced by incorporating VIIRS data from NOAA-20 and VIIRS-like observations that will be available when the planned EUMETSAT Metop Second Generation (Metop-SG) satellite is lanuched. Togehter, these observations will greatly improve the feasibility to monitor sub-annual dynamics important for weather/climate processes, including rapid changes in surface inundation, snow/ice cover, and vegetation conditions. The VIIRS Surface Type team will explore and demonstrate capabilities for monitoring such changes.

Methods

Overall Approach

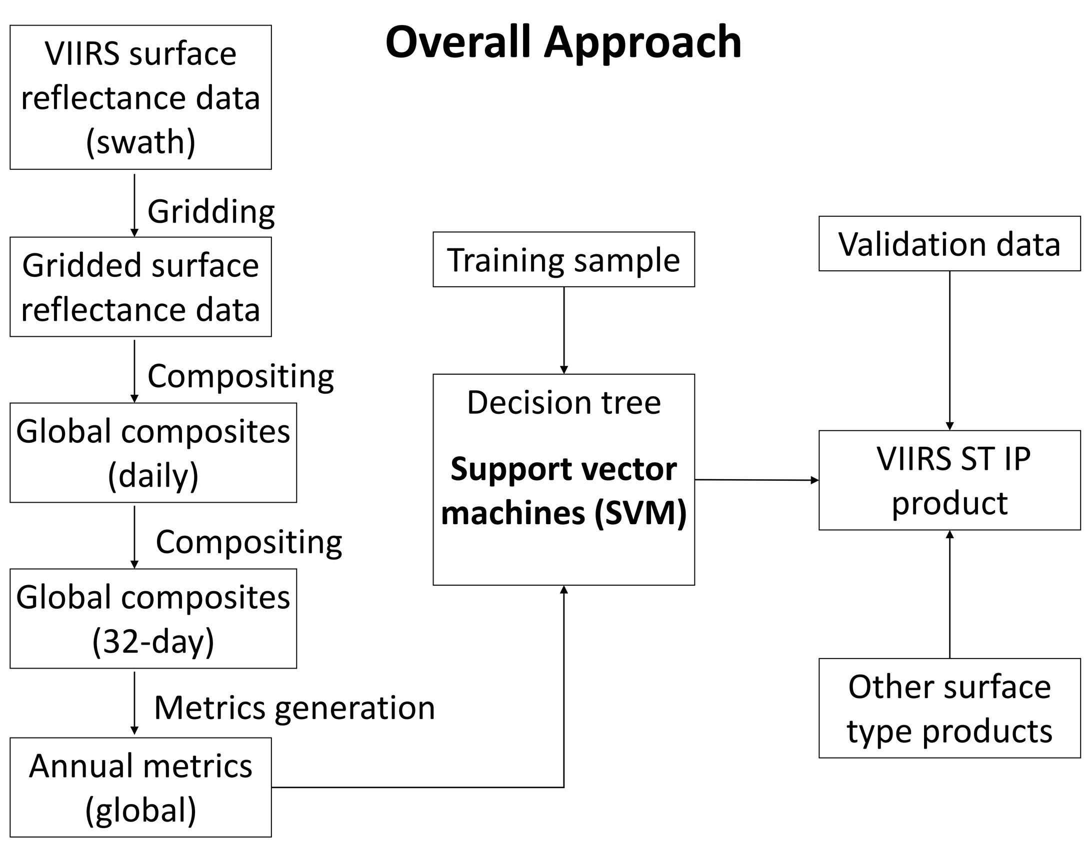

Improved Image Composting Method

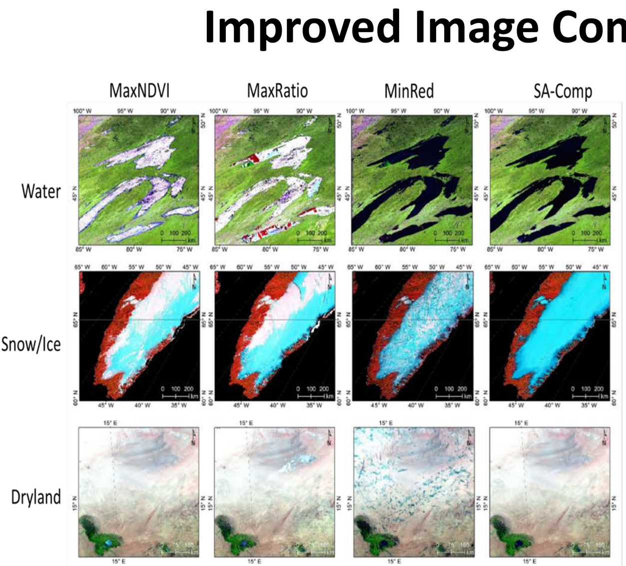

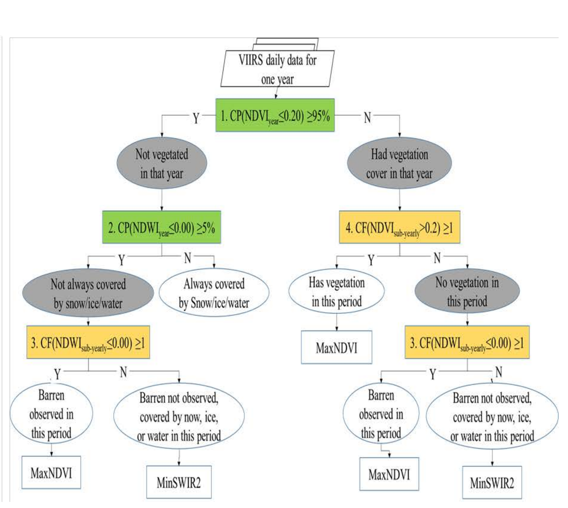

Self-Adaptive Compositing (SA-Comp) method produces clear view composites for both vegetated and non-vegetated (water, snow/ice, desert, etc.) surfaces

Advanced Classification Algorithm

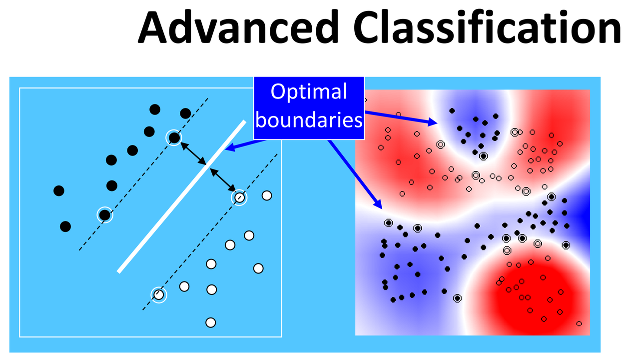

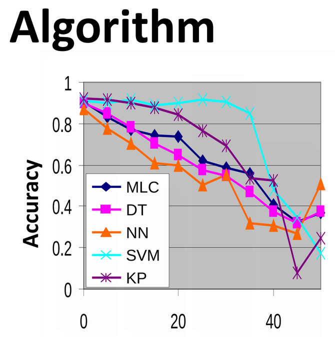

The support vector machines (SVM) method is designed to find optimal boundaries between classes, and hence is more resistant to noises and typically produces more accurate results than other classification algorithms

Publications

Zhang, R., Huang, C., Zhan, X., Dai, Q., & Song, K. (2016). Development and validation of the global surface type data product from S-NPP VIIRS. *Remote Sensing Letters, 7, 51-60.*

Zhang, R., Huang, C., Zhan, X., Jin, H., & Song, X.-P. (2017). Development of S-NPP VIIRS global surface type classification map using support vector machines. *International Journal of Digital Earth, 11, 212-232.*

Bian, J., Li, A., Huang, C., Zhang, R., & Zhan, X. (2018). A self-adaptive approach for producing clear-sky composites from VIIRS surface reflectance datasets. *ISPRS Journal of Photogrammetry and Remote Sensing, 144, 189-201, https://doi.org/10.1016/j.isprsjprs.2018.07.009.*

Results

Primary Product

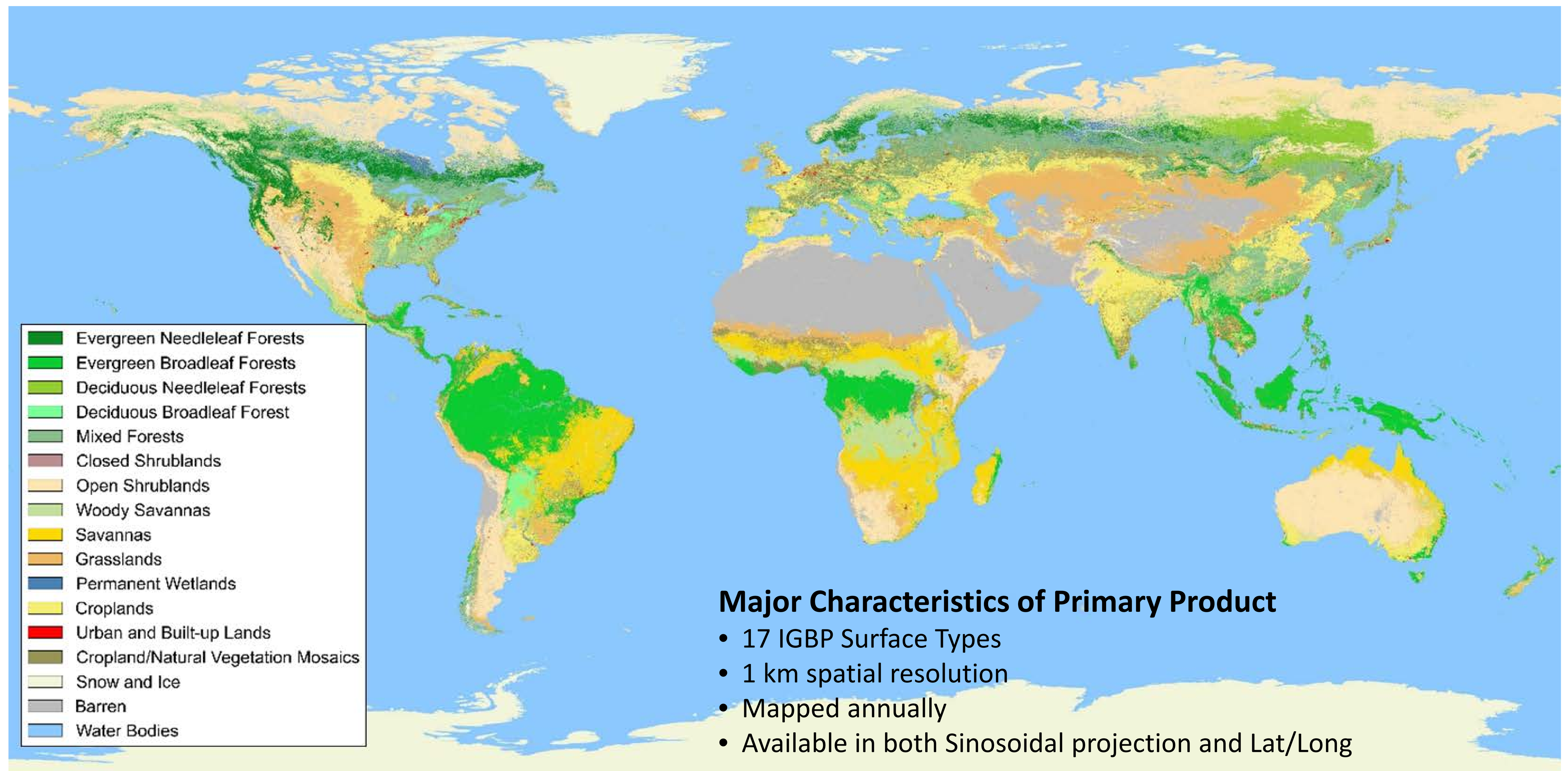

Major Characteristics of Primary Product
- 17 IGBP Surface Types
- 1 km spatial resolution
- Mapped annually
- Available in both Sinosoidal projection and Lat/Long

Application Specific Products

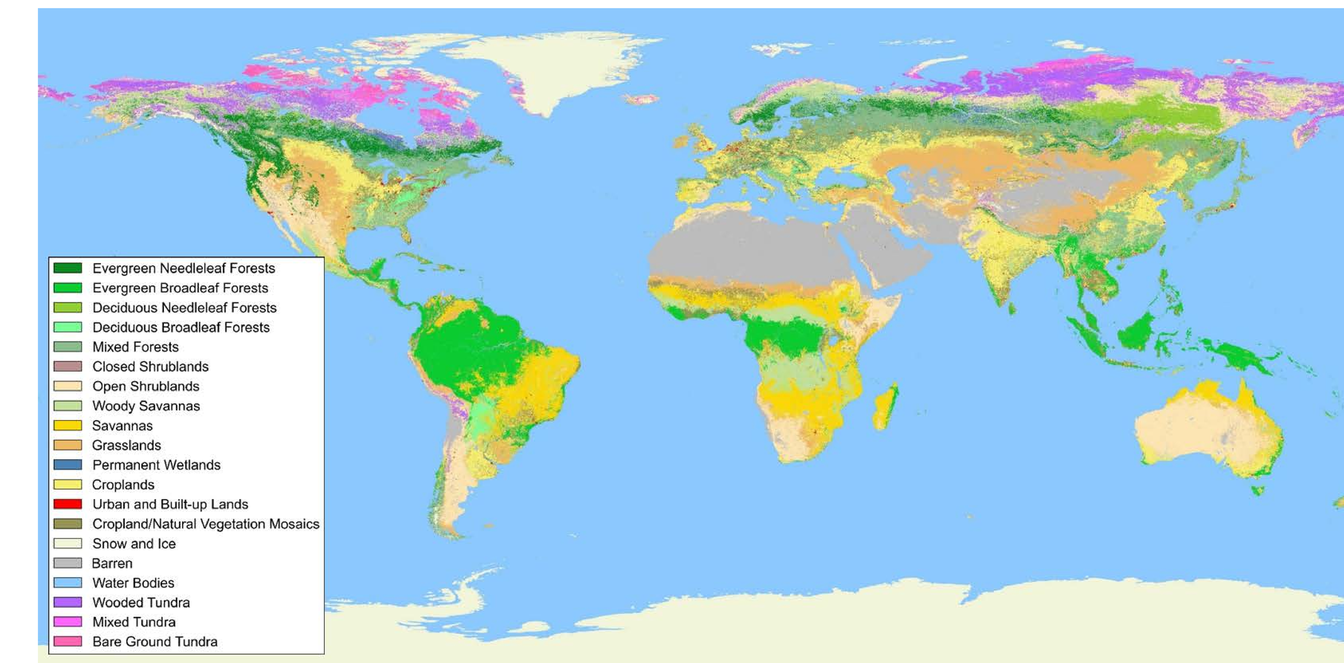

Surface Type map with classes needed to support NCEP modeling

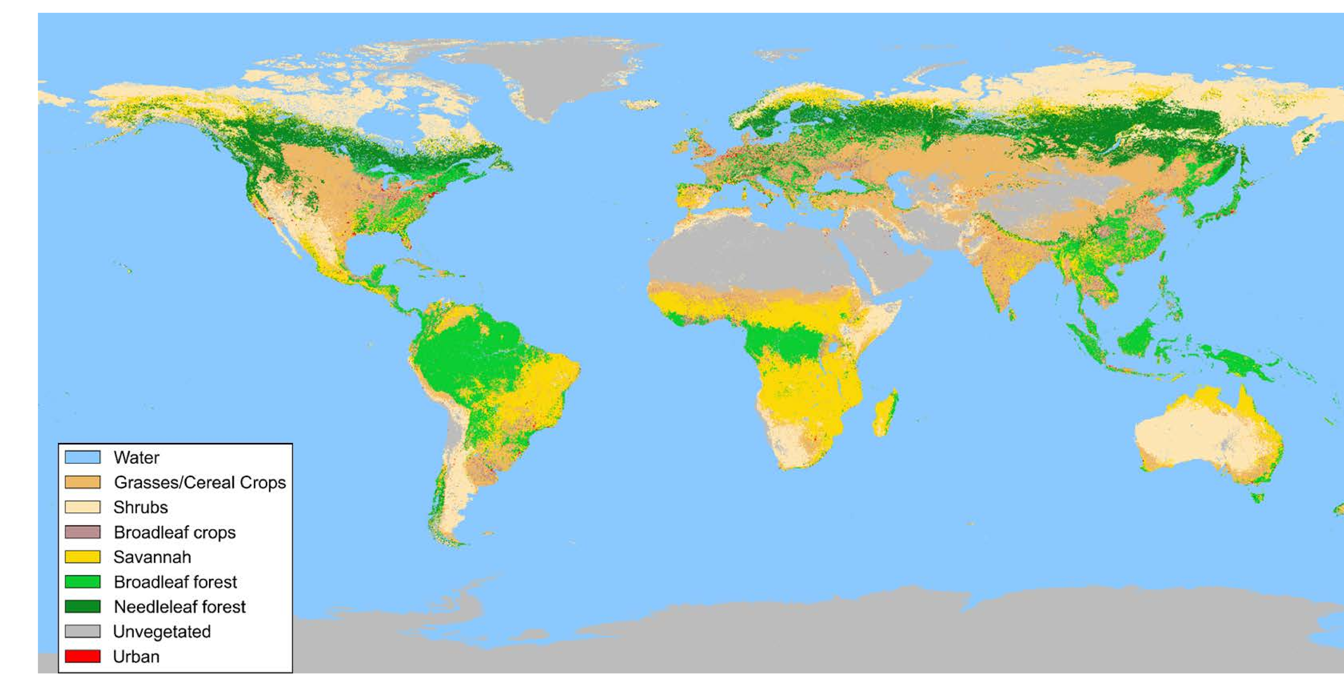

Surface Type map with classes needed to support LAI/FPAR retrieval

Reference Data

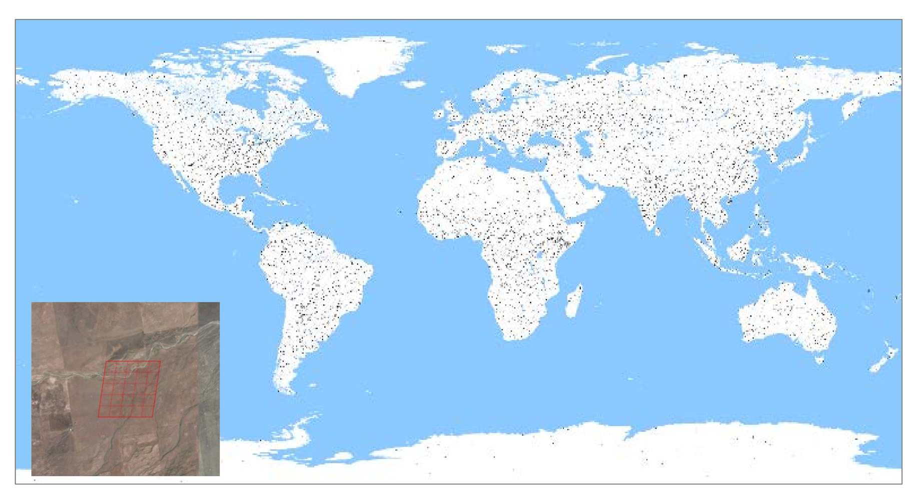

Large quantities of reference samples have been derived based on Google Earth and other available high resolution imagery
- Well distributed across the globe
- Highly reliable class labeling
- Training samples: > tens of thousands, add as needed
- Validation samples: ~6000 selected following a probability based sampling design.

Accuracy Assessment

Accuracy estimates are derived following well-established accuracy assessment protocol (Olofsson et al. 2014)
- Overall accuracies varied between 76% and 79%
- Meet the 70% JPSS L1RD requirement for the AST product
- Better than accuracies reported for MODIS land cover products

		Reference																			
		1	2	3	4	5	6	7	8	9	10	11	12	13	14	15	16	17	Total (%)	User's accuracy (%)	Producer's accuracy (%)
Map	1	2.04	0.01	0.06	0.05	0.29	0.01	0.01	0.23	0.04	0.07	0.02	0.01	0	0.01	0	0	0.01	2.86	**71.3±2.9**	**72.6±3.4**
	2	0	8.46	0	0.09	0.05	0	0	0.4	0.08	0.02	0	0.06	0	0.12	0	0	0	9.28	**91.2±1.2**	**92.6±1.1**
	3	0.05	0	1.08	0	0.13	0	0.01	0.09	0	0.02	0.02	0	0	0	0	0	0	1.41	**76.7±3.9**	**68.7±4.7**
	4	0	0.01	0.01	0.95	0.05	0	0	0.09	0.03	0	0	0	0	0.02	0	0	0	1.14	**82.8±2.8**	**42.8±3.4**
	5	0.2	0.17	0.21	0.64	3.52	0.03	0.02	0.59	0.15	0.02	0.03	0	0.02	0.33	0	0	0.02	5.95	**59.2±2.6**	**76.2±2.6**
	6	0	0	0	0	0	0.05	0	0	0	0.01	0	0	0	0	0	0	0	0.07	**70.0±6.0**	**3.6±0.8**
	7	0.22	0.02	0.07	0.05	0.19	0.48	11.64	0.51	0.36	1.24	0.17	0.36	0.02	0.15	0	0.48	0.02	16.00	**72.7±1.7**	**83.9±1.8**
	8	0.26	0.17	0.06	0.28	0.17	0.09	0.3	4.84	0.58	0.11	0.07	0.09	0.01	0.44	0	0	0.02	7.50	**64.6±1.9**	**57.5±2.2**
	9	0	0.16	0.03	0.05	0.05	0.46	0.24	1.02	5.25	0.13	0.03	0.22	0.05	0.38	0	0	0	8.08	**65.0±2.8**	**71.9±2.4**
	10	0.02	0	0.04	0.02	0.06	0.23	0.79	0.19	0.21	6.37	0	0.48	0.02	0.21	0	0.23	0.01	8.90	**71.5±1.7**	**72.1±2.1**
	11	0.01	0.02	0	0	0.01	0.01	0.06	0.05	0.06	0.01	0.48	0.01	0	0	0	0	0	0.73	**65.0±6.2**	**57.3±7.5**
	12	0.01	0.01	0	0	0.04	0.02	0.07	0.05	0.16	0.46	0.01	6.97	0.08	0.55	0	0	0.02	8.44	**82.6±1.2**	**79.7±1.7**
	13	0	0	0	0	0	0	0.01	0.01	0	0	0	0.04	0.35	0.01	0	0	0	0.42	**81.7±3.6**	**58.9±6.7**
	14	0	0.1	0.02	0.06	0.05	0.01	0.06	0.34	0.39	0.18	0	0.41	0.03	2.7	0	0.01	0	4.35	**62.0±2.1**	**53.9±2.7**
	15	0	0	0	0	0	0	0.17	0	0	0	0	0	0	0	10.19	0	0	10.36	**98.3±1.7**	**100.0±0.0**
	16	0	0	0	0	0	0	0.49	0	0	0.18	0	0.09	0	0.09	0	12.53	0	13.37	**93.7±1.4**	**94.5±0.9**
	17	0	0	0	0	0	0	0	0	0	0.02	0	0	0	0	0	0	1.11	1.13	**98.3±1.7**	**91.3±3.2**
	Total	2.81	9.13	1.57	2.21	4.62	1.4	13.87	8.42	7.31	8.83	0.83	8.75	0.59	5.01	10.19	13.26	1.21	100		

Error matrix of estimated area proportions (in percentage) for the 2014 product. Overall accuracy is 78.5 ± 0.6%.

Product Dissemination

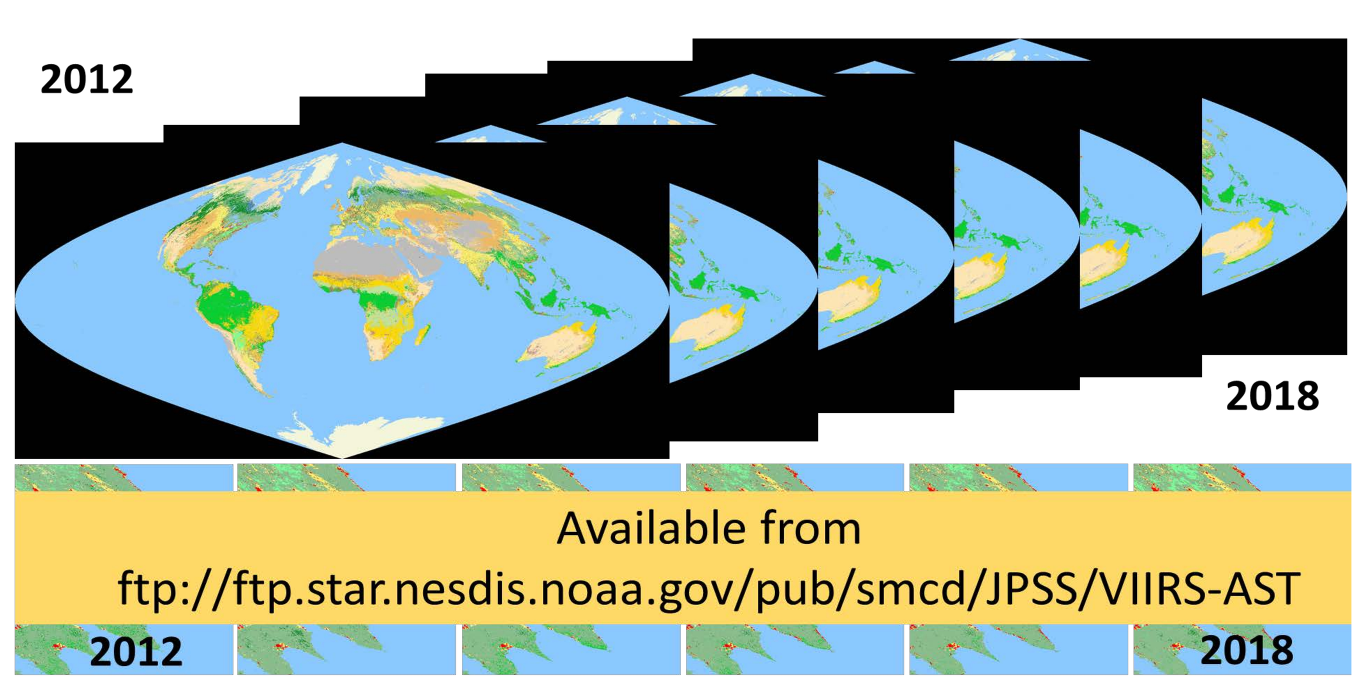

Available from
ftp://ftp.star.nesdis.noaa.gov/pub/smcd/JPSS/VIIRS-AST

Future Directions

We will focus in the following areas in our future research:
- Continue to produce the VIIRS Annual Surface Type (AST) product
- Incorporate VIIRS continuity and VIIRS-like observations
  - VIIRS continuity: NOAA-20, future JPSS missions
  - VIIRS-like observations: METImage onboard METOP-SG, AM mission by Europe
- Explore and demonstrate capabilities for monitoring sub-annual surface type dynamics
  - Focus on changes important for weather/climate processes:
    - Snow/ice, surface inundation, vegetation
  - Leverage existing/planned products/ capabilities

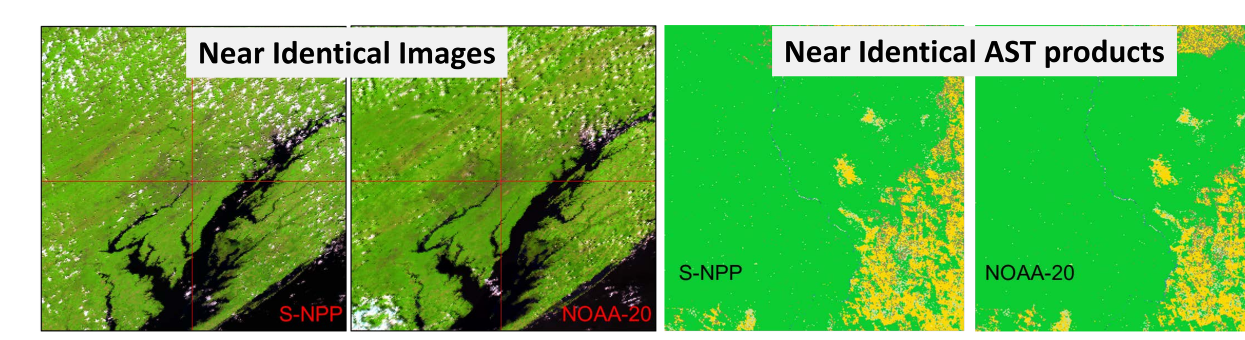

Current and planned VIIRS missions will allow continuity of the AST product

MetImage-SG			VIIRS		
Channel No	Center Wavelength (μm)	Bandwidth (FWHM in μm)	Band	Center Wavelength (μm)	Eq. Width (μm)
VII-4	0.443	0.03	M2	0.444	0.0198
VII-8	0.555	0.02	M4	0.551	0.0209
VII-12	0.668	0.02	M5	0.672	0.02
VII-16	0.763	0.01	M6	0.745	0.0146
VII-17	0.865	0.02	M7	0.862	0.0394
VII-22	1.24	0.02	M8	1.238	0.0271
VII-23	1.375	0.04	M9	1.375	0.015
VII-24	1.63	0.02	M10	1.602	0.0587
VII-25	2.25	0.05	M11	2.257	0.0467
VII-26	3.74	0.18	M12	3.697	0.192
VII-30	4.05	0.06	M13	4.067	0.165
VII-35	8.54	0.29	M14	8.578	0.324
VII-37	10.69	0.5	M15	10.729	0.99
VII-39	12.02	0.5	M16	11.845	0.866

MetImage-SG has most of the VIIRS bands (from Cao 2019)

Surface type maps updated for daily snow cove changer by integrating snow cover maps generated through the Interactive Multisensor Snow and Ice Mapping System (IMS)

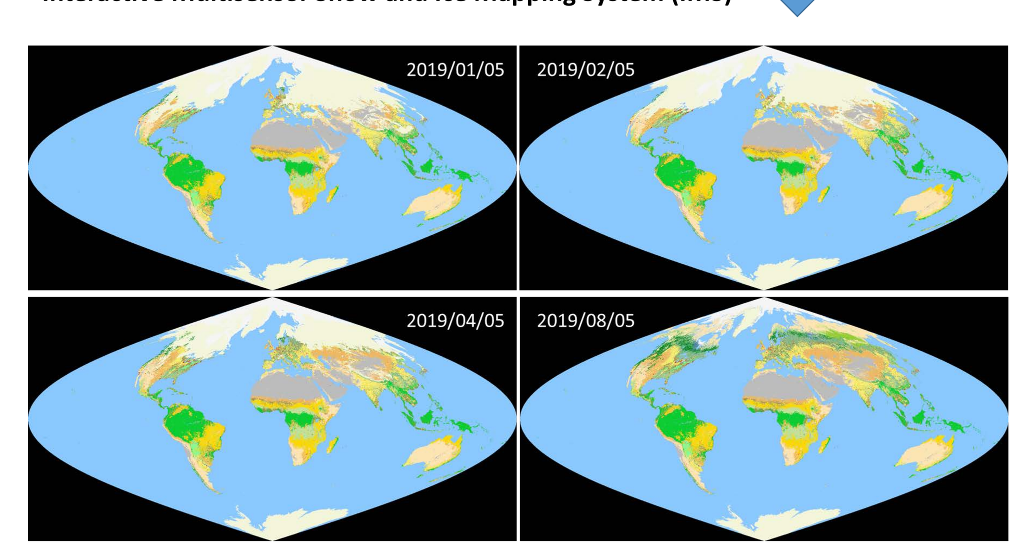

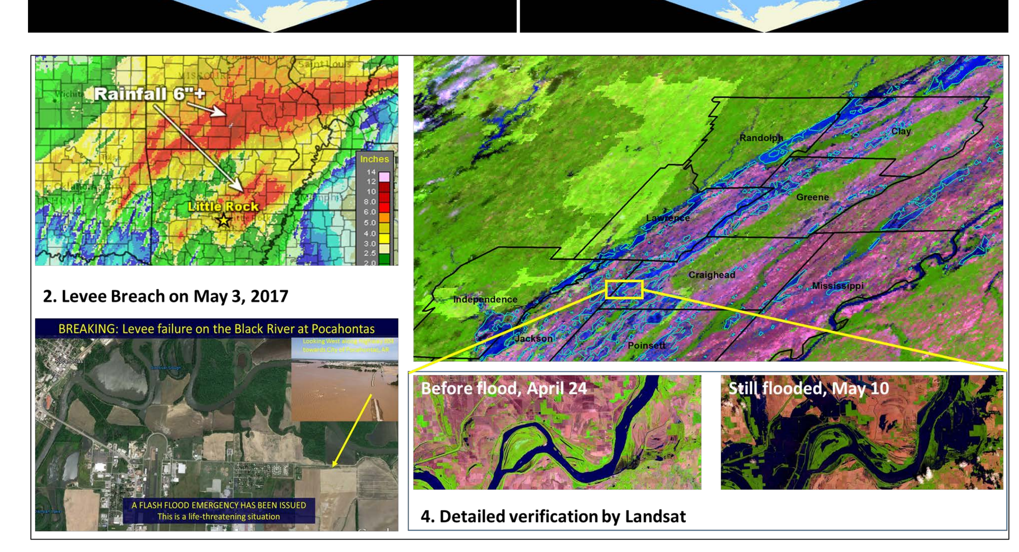

Prototype of sub-annual update of vegetation changes due to fire

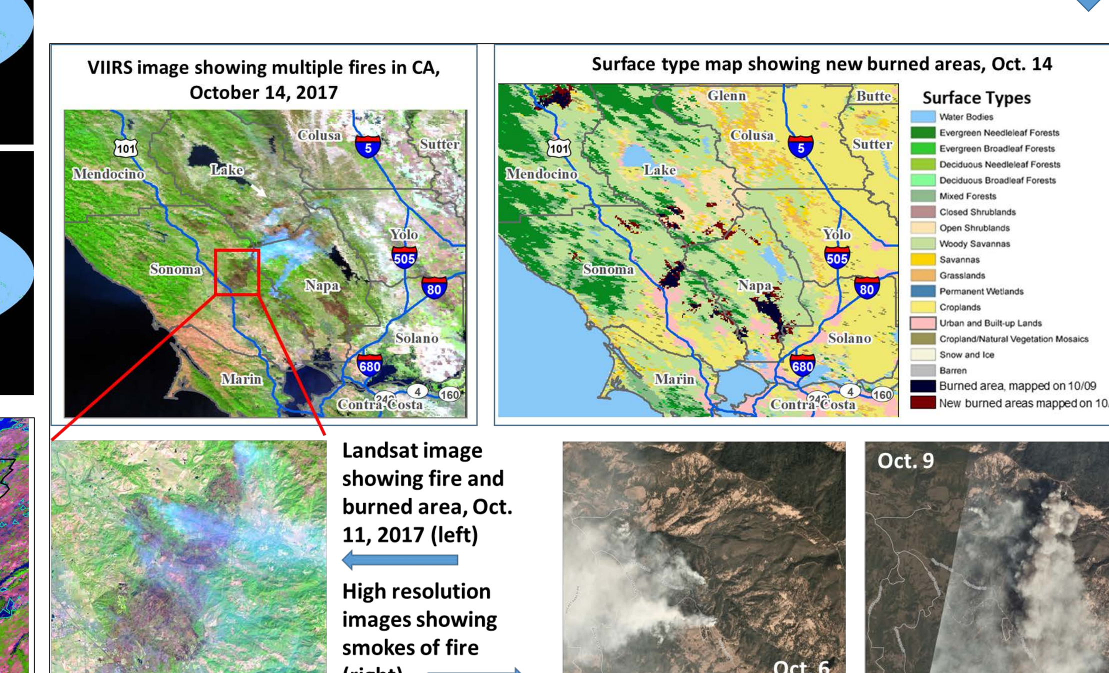

Flooding often results in large changes in surface inundation. The VIIRS Floodwater Fraction Map Products could be used to provide near daily update of surface inundation

An Evapotranspiration Data Product at 2km resolution from NOAA GOES-16

Li Fang[1,2,*], Xiwu Zhan[2], Mitchell A.Schull[1,2], Satya Kalluri[2], Istvan Laszlo[2], Peng Yu[1,2], Corinne Carter[1,2], Christopher Hain[3], Martha Anderson[4]

1 Cooperative Institute for Satellite Earth System Studies (CISESS)/Earth System Science Interdisciplinary Center, University of Maryland
2 NOAA-NESDIS Center for Satellite Applications and Research
3 NASA Marshall Space Flight Center
4 USDA Agricultural Research Service
* Li Fang lfang1@umd.edu

What is Evapotranspiration?

INTRODUCTION

- GOES Evapotranspiration (ET) and Drought (**GET-D**) has been operationally generating ET and Evaporative Stress Index (ESI) data products at 8km resolution for NCEP NWP model validation and drought monitoring
- Continuation of GET-D operation using the current high-resolution thermal observations of the Advanced Baseline Imagers (ABI) from **GOES-R series** is in high demand
- This study introduces the architecture of the upgraded GET-D system, the core model (**Atmosphere-Land Exchange Inversion model; ALEXI**) and preliminary validation results of ET product

ALEXI MODEL

- Atmosphere-Land Exchange Inversion (ALEXI) model exploits the mid-morning rise in LST from GOES to deduce the land surface fluxes, including evapotranspiration
- Implementation of the two-source energy balance (TSEB) model which balances components of energy budgets for the soil and canopy components separately

SYSTEM OUTPUTS

Variables	Spatial Resolution	Unit	Format	Description
ET	2km	mm day^{-1}	NetCDF, GRIB2, PNG	Daily ET
ET QC	2km	--	NetCDF, GRIB2	Quality control flag for retrieved ET
Fluxes	2km	W m^{-2} day^{-1}	NetCDF, GRIB2, PNG	Daily short wave down, long wave down, long wave up and net radiation
Flux QC	2km	--	NetCDF, GRIB2	Quality control flag for retrieved fluxes

PRODUCT

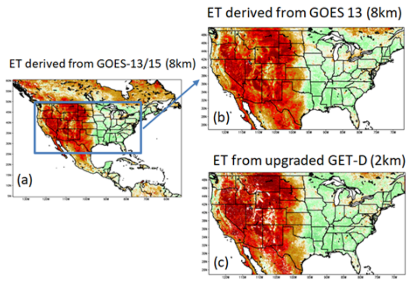

ET retrieval comparison between operational GOES-13/15 based 8km product and upgraded GOES 16 LST based 2km product; Monthly composite of July 2017 (mm/day)

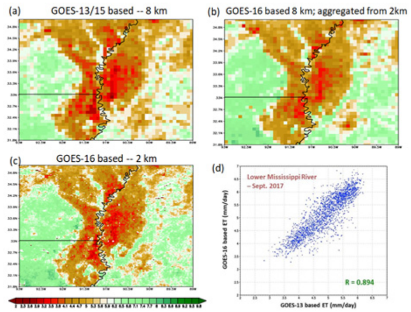

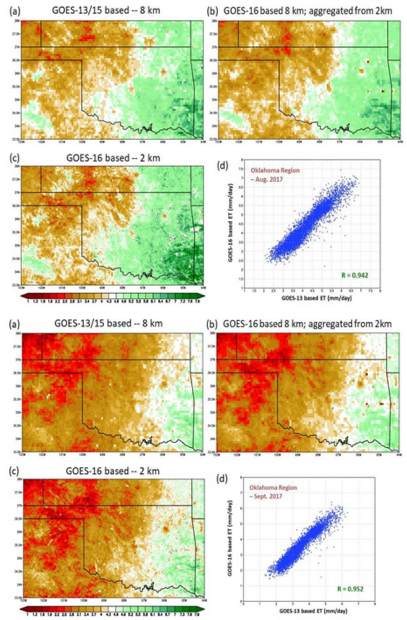

Monthly ET (mm day^{-1}) composites of: (a) the 8km estimates derived from GOES-13/15 GET-D system, (b) the 8km average aggregated from the 2km product of the upgraded GOES-16 GET-D, (c) the 2km estimates from GOES-16 GET-D, and (d) scatterplot of retrieved ET from the upgraded GET-D compared with current operation

RESULTS

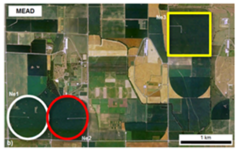

MEAD, NE Ameriflux site (S. Verma, 2010)
Rainfed and irrigation corn and soybean

Field #1: 41°09'54.2"N, 96°28'35.9"W
Field #2: 41°09'53.5" N, 96°28'12.3" W
Field #3: 41°10'46.8" N, 96°26'22.7" W

Error Statistics	Bias		RMSE		Correlation		N
Satellites	GOES-13 based	GOES-16 based	GOES-13 based	GOES-16 based	GOES-13 based	GOES-16 based	
MEADsite1	0.555	0.601	1.318	1.215	0.887	0.885	26
MEADsite2	0.561	0.546	1.094	0.906	0.860	0.885	23
MEADsite3	0.754	0.617	1.132	1.023	0.949	0.974	21
Average	0.623	**0.588**	1.181	**1.048**	0.899	**0.914**	

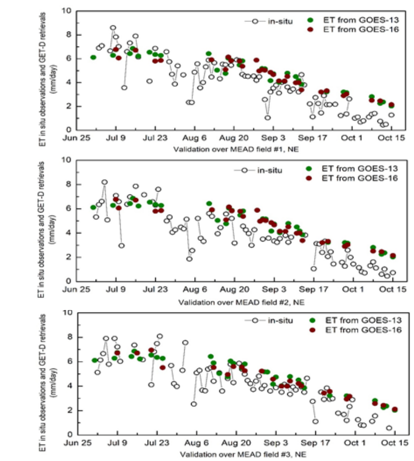

OBSERVATIONS

Name	Data Source	Resolution	Spatial Coverage	Description
GOES thermal observations	GOES-R	2km	Full Disk / CONS	Primary option: Channel 13 of GOES-16 and GOES-17 ABI L1b Radiance product (ABI-L1b-RadF) Second option: GOES LST product (OR_ABI-L2-LSTC)
Clear Sky Mask	GOES-R	2km	Full Disk	GOES-R Clear Sky Mask product (OR_ABI-L2-ACMF)
Insolation	GSIP GOES16 inso	0.125° 2km	North America	GSIP L2 real time insolation; Insolation product from GOES16
Vegetation Index	VIIRS	0.036°	Global	NESDIS GVF (inverted to LAI)
Air temperature	NARR/CFS	0.3°/0.5°	NA/Global	Surface and pressure level profiles
Specific humidity	NARR/CFS	0.3°/0.5°	NA/Global	Surface and pressure level profiles
Geopotential height	NARR/CFS	0.3°/0.5°	NA/Global	Surface and pressure level profiles
Wind speed	NARR/CFS	0.3°/0.5°	NA/Global	Surface
Downwelling longwave radiation	NARR/CFS	0.3°/0.5°	NA/Global	Surface
Solar zenith	GOES-R	2km	Full Disk	GOES-R solar zenith angles
View zenith	GOES-R	2km	Full Disk	GOES-R view zenith angle
Snow Mask	IMS	24 km	Northern Hemisphere	NOAA IMS Daily Northern Hemisphere Snow and Ice Analysis

CONCLUSIONS

- The GET-D system has been upgraded successfully to generate ET at much improved spatial resolution of **2km** over CONUS using **GOES-16** observations
- The comparison proves ET estimates from the upgraded GET-D system to be very **consistent** with the current operational products
- The **spatial correlation** between the two products reaches **0.946** averaged over CONUS domain for the studying period
- Upgraded GET-D is validated against MEAD in situ observations
- Accuracy of the new GET-D ET product is satisfactory with the bias of 0.588 mm/day and the **correlation of 0.914** averaged from three Mead sites

Fang, L.; Zhan, X.; Schull, M.; Kalluri, S.; Laszlo, I.; Yu, P.; Carter, C.; Hain, C.; Anderson, M. Evapotranspiration Data Product from NESDIS GET-D System Upgraded for GOES-16 ABI Observations. Remote Sens. ***2019****, 11, 2639.*

NOAA's New High-Resolution Sea Surface Temperature Blended Analysis

Eileen Maturi[1], Andy Harris[2], Jonathan Mittaz[3], Gary Wick[4], John Sapper[1]

1: NOAA/NESDIS, College Park, MD, 2: Univ of Maryland, College Park, MD, 3: Univ of Reading, UK, 4: NOAA/OAR/ESRL

BACKGROUND

NOAA's National Environmental Satellite, Data, and Information Service (NESDIS) generates operational geostationary Level-2P (L2P) Sea Surface Temperature (SST) products in GHRSST GDS 2.0 format GOES-16 East and GOES-15 West, Meteosat Second Generation (MSG) 11 and 8, and Himawari-8). SST product accuracy for the heritage geostationary sensors was improved with the implementation of a physical retrieval algorithm based on a Modified Total Least Squares algorithm (Koner *et al*., 2015). Additionally, the operational geostationary SST products are then blended with the polar operational SSTs to produce daily global, 5-km resolution SST analyses in GHRSST L4 format (Maturi *et al.,* 2017).

OPERATIONAL SST RETRIEVAL

History of GEO SST retrieval algorithms at NOAA/NESDIS

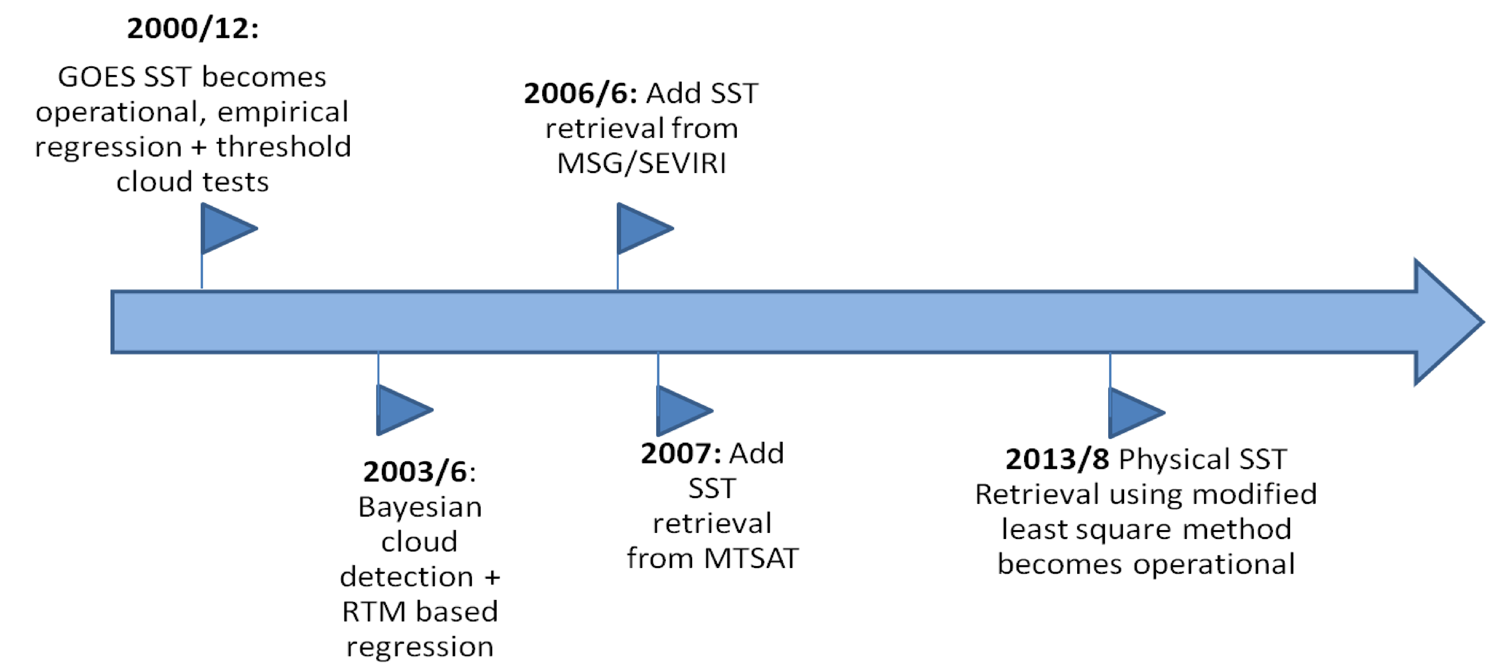

Current geostationary SST retrieval: MTLS physical retrieval + Bayesian cloud detection for clear sky (Koner *et al.,* 2015, Merchant *et al.,* 2005)

Geo-Polar Blending: A multi-scale OI with data-adaptive correlation length scale, giving a ~5-km global L4 product (Maturi *et al.,* 2017)

- Analysis is performed at 3 different scales
- Final result is interpolated from these analyses based on data density
- Preserves fine-scale features without introducing excessive noise

GEOSTATIONARY SST COVERAGE

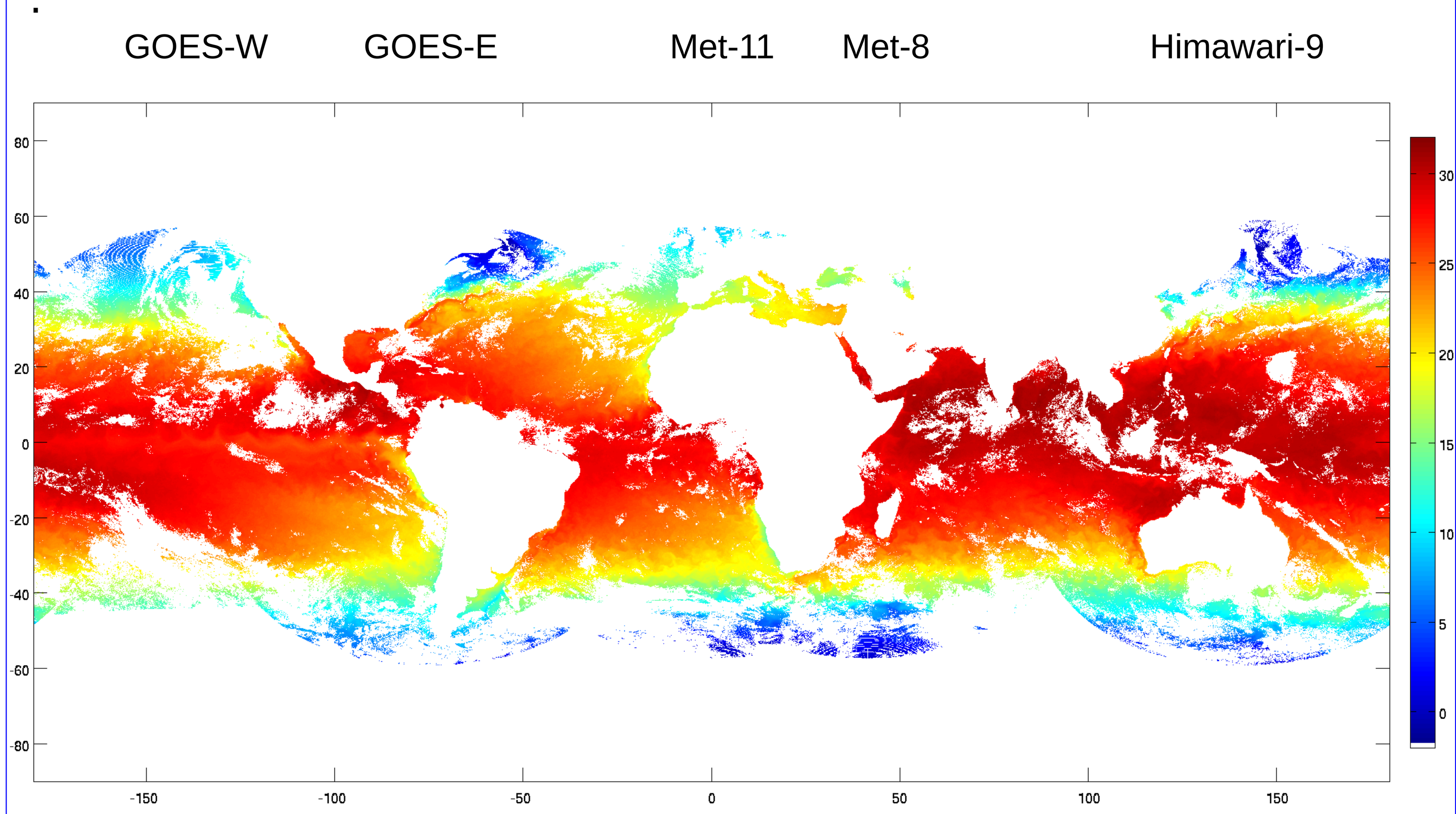

The image is a 24 hour merged composite of the Operational geostationary SST products generated by NOAA (GOES-W (15), GOES-E (16), Meteosat-11, Meteosat-8, Himawari-9). ***N.B.* The addition of Meteosat-8 has improved coverage over the Indian Ocean – important for NOAA Coral Reef Watch**

EFFECT OF DIURNAL ADJUSTMENT

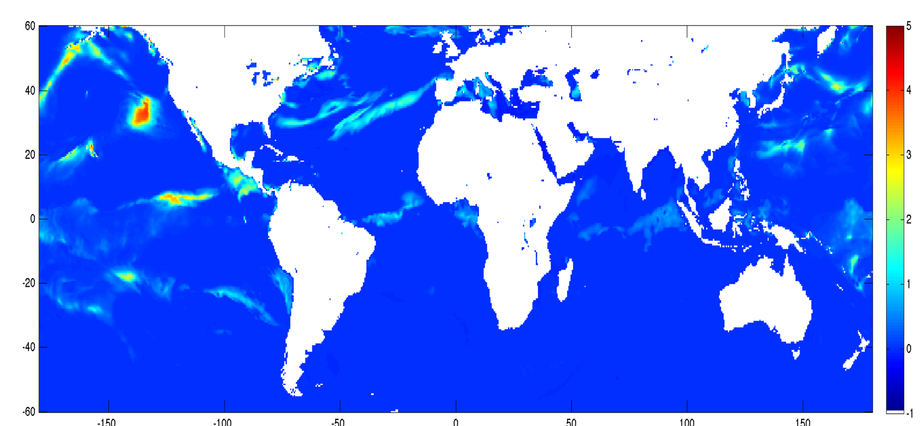

Diurnal warming amplitude calculated using turbulence model, including a parameterization for Stokes' drift

VIIRS

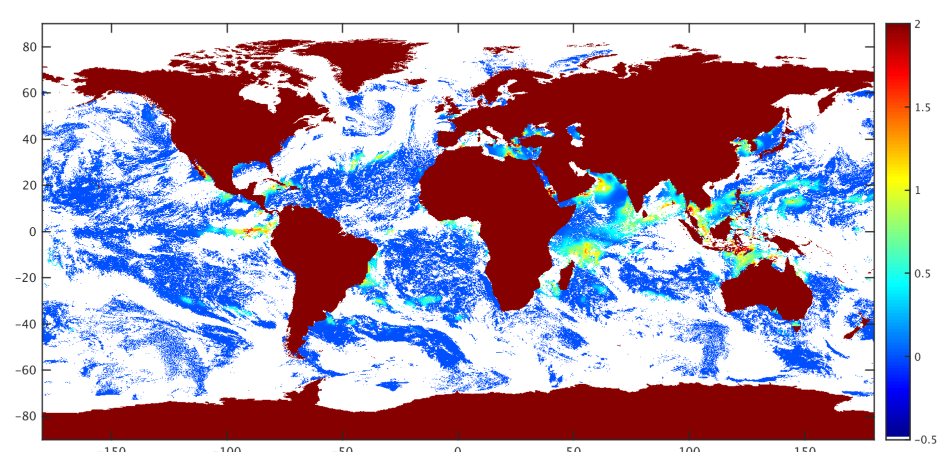

Effect of diurnal adjustment on VIIRS

BLENDED SST ANALYSIS

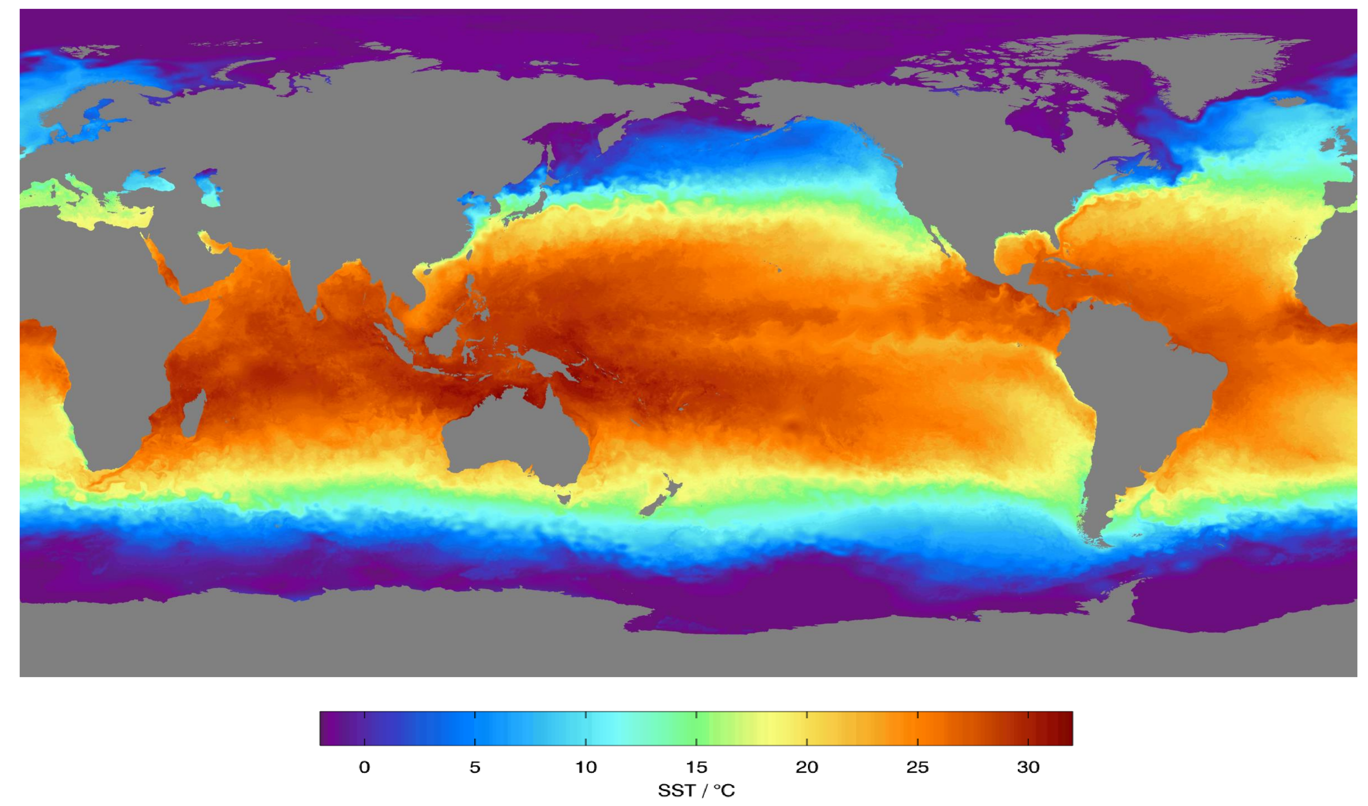

These 5-km blended SST analyses are produced daily from 24 hours of polar and geostationary sea surface temperature satellite retrievals (NPP, Metop-B, GOES-E/W, Himawari-9, and Meteosat-11). Meteosat-8 is being added over the Indian Ocean.

- Day & Night
- Night-only
- **Diurnally adjusted Day & Night**

SUMMARY

The analysis product validates to 0.3 K RMS against independent ARGO data (see https://www.star.nesdis.noaa.gov/sod/sst/squam/analysis/l4/?l4sst=CMC&ref=IQ2_AG&aggtime2=monthly&stats=SD#timeseries_dyn). The physically retrieved SST L2P inputs from the heritage geostationary imagers are an important component of the SST Analysis products. The temporal and increased data coverage of the geostationary satellites generated by a high quality SST with Standard Deviation of 0.3-.5 makes this a uniquely powerful product for many ocean applications requiring mesoscale temperature information.

Maturi E, A Harris, J Mittaz, J Sapper, G Wick, X Zhu, P Dash, P Koner, A New High Resolution Sea Surface Temperature Blended Analysis, *Bull. Am. Meteorol. Soc.*, **98**, 1015-1026, 2017

Water Quality and Bio-optical Properties Measured from the Geostationary and Polar-orbiting Satellite Sensors in the Northwestern Pacific Region

SeungHyun Son[1,2], Menghua Wang[1], & Lide Jiang[1,2]

[1]NOAA/NESDIS Center for Satellite Applications and Research, College Park, Maryland, USA
[2]CIRA, Colorado State University, Fort Collins, Colorado, USA

INTRODUCTION

The first geostationary ocean color satellite (GOCI) has the unique capability with hourly measurements during daytime to provide short-/long-term environmental monitoring in the marine ecosystem over the western Pacific region. In this presentation, we show results of GOCI-derived ocean color products from 2012 to 2019 using the Multi-Sensor Level-1 to Level-2 (MSL12) ocean color data processing system to characterize diurnal, seasonal, and interannual variations in water property. In addition, water quality and bio-optical products from the polar-orbiting ocean color satellite sensors, e.g., the Visible Infrared Imaging Radiometer Suite (VIIRS) onboard the Suomi National Polar-orbiting Partnership (SNPP) and the Ocean and Land Colour Instrument (OLCI) on the Sentinel-3A, derived using the MSL12 are compared with those from GOCI. Comparison results with the in-situ measurements from the two AERONET-OC sites located in the Yellow Sea show that over open oceans ocean color products are quite accurate and highly stable, and reasonable water property data can be derived over turbid coastal and inland waters. Furthermore, we show that GOCI measurements provide important diurnal information, while the polar-orbiting satellites provide large scale spatial coverages. Thus, measurements from the geo and polar-orbiting satellites are complementary to provide more complete picture/information of water optical, biological, and biogeochemical variations over the open ocean and coastal/inland waters.

DATA & METHODS

- The Multi-Sensor Level-1 to Level-2 (**MSL12**) ocean color data processing system has been used for VIIRS, OLCI, and GOCI data processing.
- Various parameters and lookup tables are generated, and a new atmospheric correction algorithm has been developed and implemented in MSL12 for GOCI data processing in the region (*Wang et al.*, 2012, 2013).
- GOCI and OLCI Level-1B data were processed to derive Level-2 ocean color products using the new atmospheric correction algorithm (*Jiang & Wang*, 2014).
- VIIRS ocean color Environmental Data Records (EDR or Level-2 data) were processed from the VIIRS science quality Sensor Data Records (SDR or Level-1B data) routinely using MSL12 with the NIR-SWIR combined atmospheric correction algorithm (*Wang & Shi*, 2007).

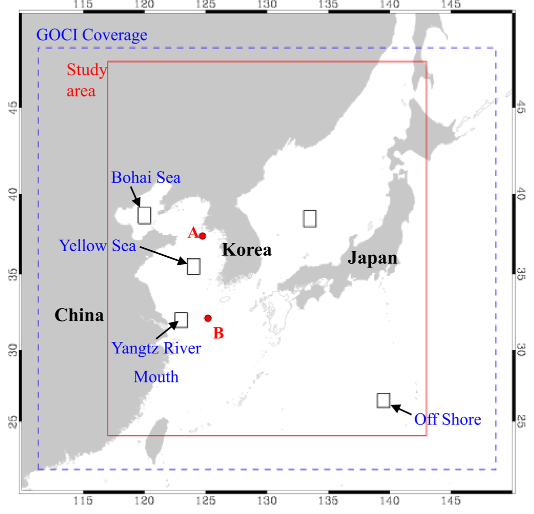

Fig. 1. Study map with two AERONET-OC sites (A-Ieodo, B-Socheongcho).

Performance of GOCI Ocean Color Products

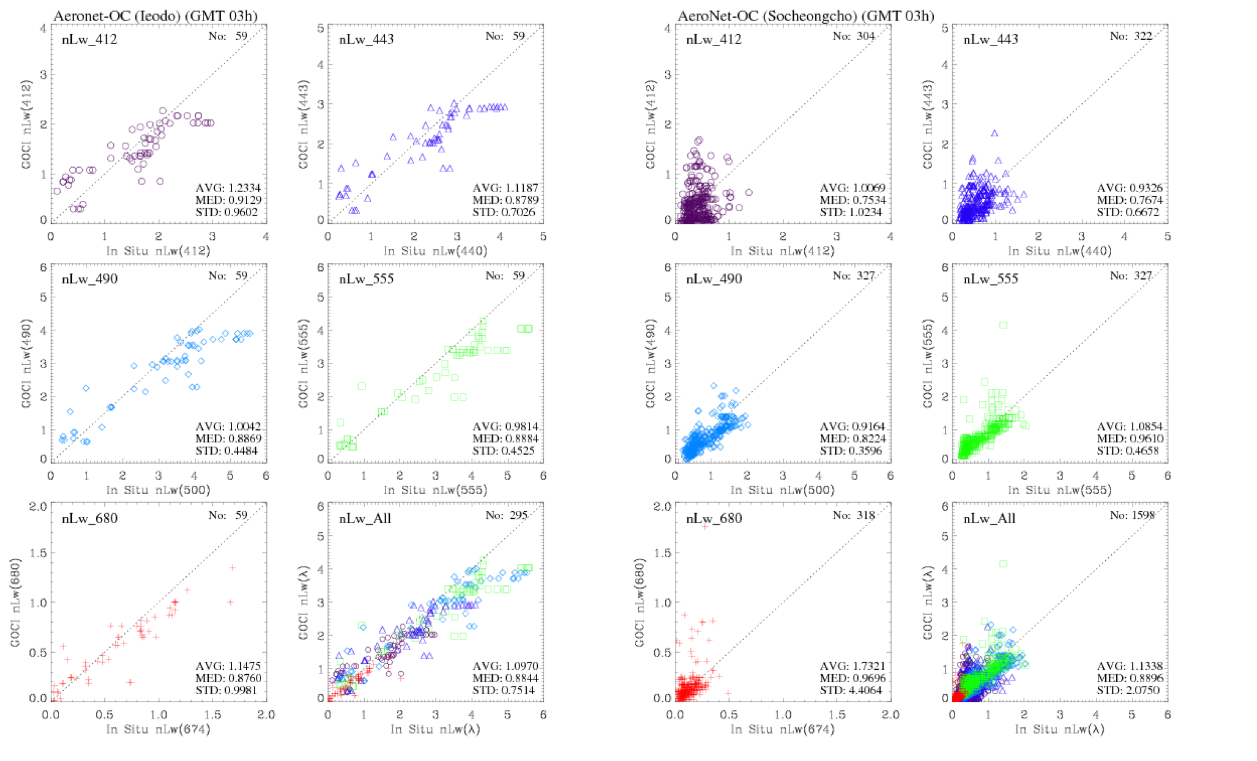

Fig. 2. Comparison of GOCI-derived $nL_w(\lambda)$ with *in situ* measurements.

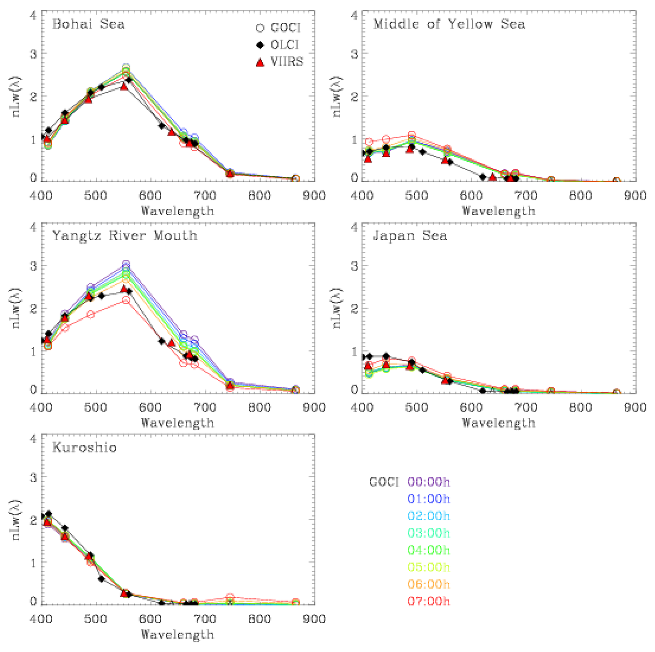

Fig. 3. $nL_w(\lambda)$ spectra from GOCI & VIIRS (Jan. 2012–Dec 2019), & OLCI (May 2016–Dec 2019) climatology composites in the five boxes shown in Fig. 1.

- Comparison results show that the GOCI-derived $nL_w(\lambda)$ data are reasonably well corresponding to the in situ measurements in the optically complex waters (Fig. 2), which are similar to those with VIIRS data.
- $nL_w(\lambda)$ spectra from GOCI (at noon), VIIRS, and OLCI climatology composites are similar in the five areas (Bohai Sea, middle of Yellow Sea, Yangtze river mouth, Japan/East Sea, and off shore waters) (Fig. 3).

GOCI, VIIRS, and OLCI Climatology Images

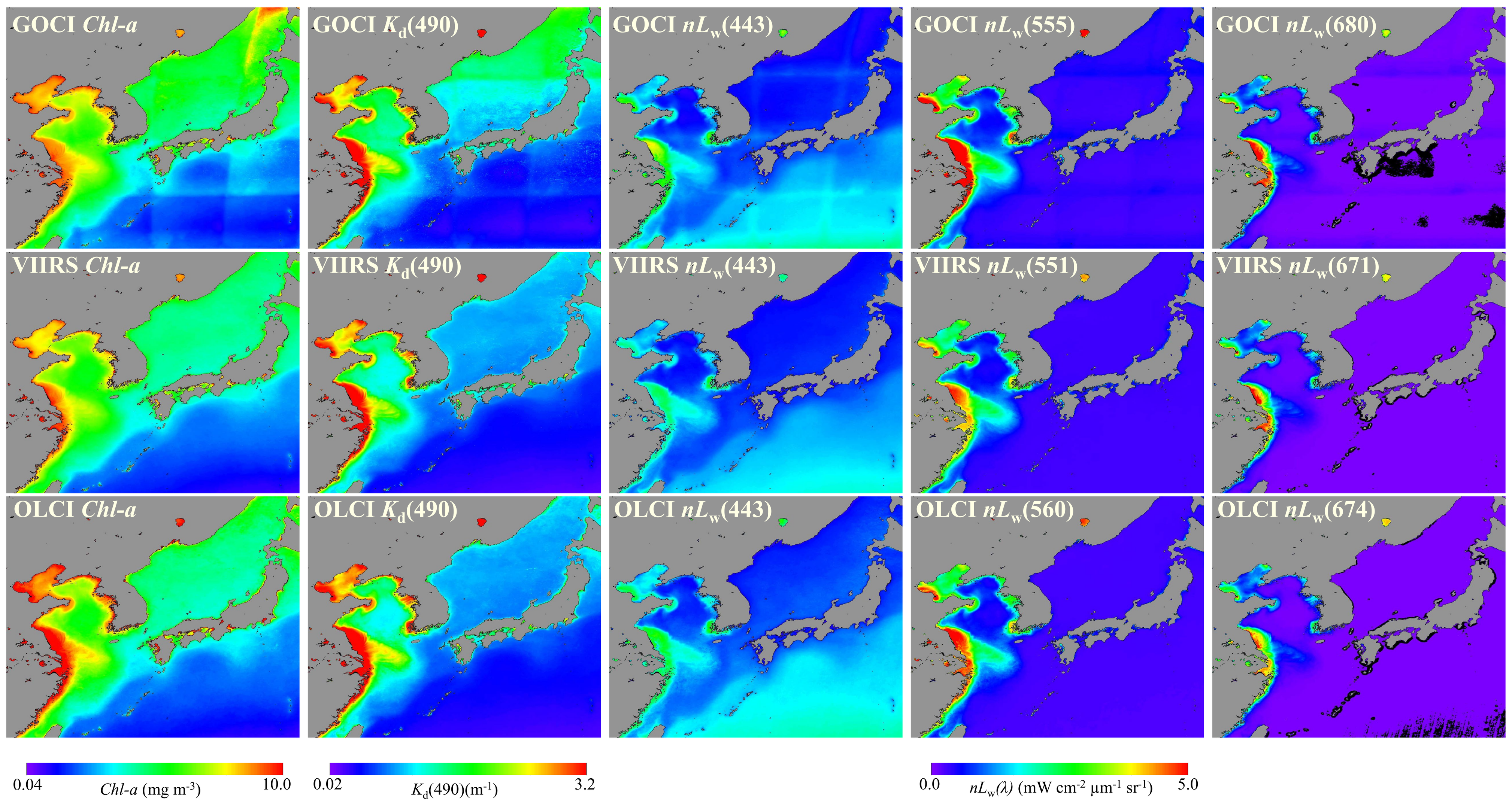

Fig. 4. Climatology Chl-a, $K_d(490)$, & $nL_w(\lambda)$ images of GOCI at noon & VIIRS (Jan 2012-Dec 2019), & OLCI (May 2016-Dec 2019).

- Overall, the GOCI-derived ocean color images are generally very similar to those from VIIRS and OLCI.
- However, there is still the boundary issue between slots in GOCI data, and significantly high values appear in the northern area in the GOCI-derived Chl-a images.

GOCI-, VIIRS-, and OLCI-derived Chl-a Seasonal Images

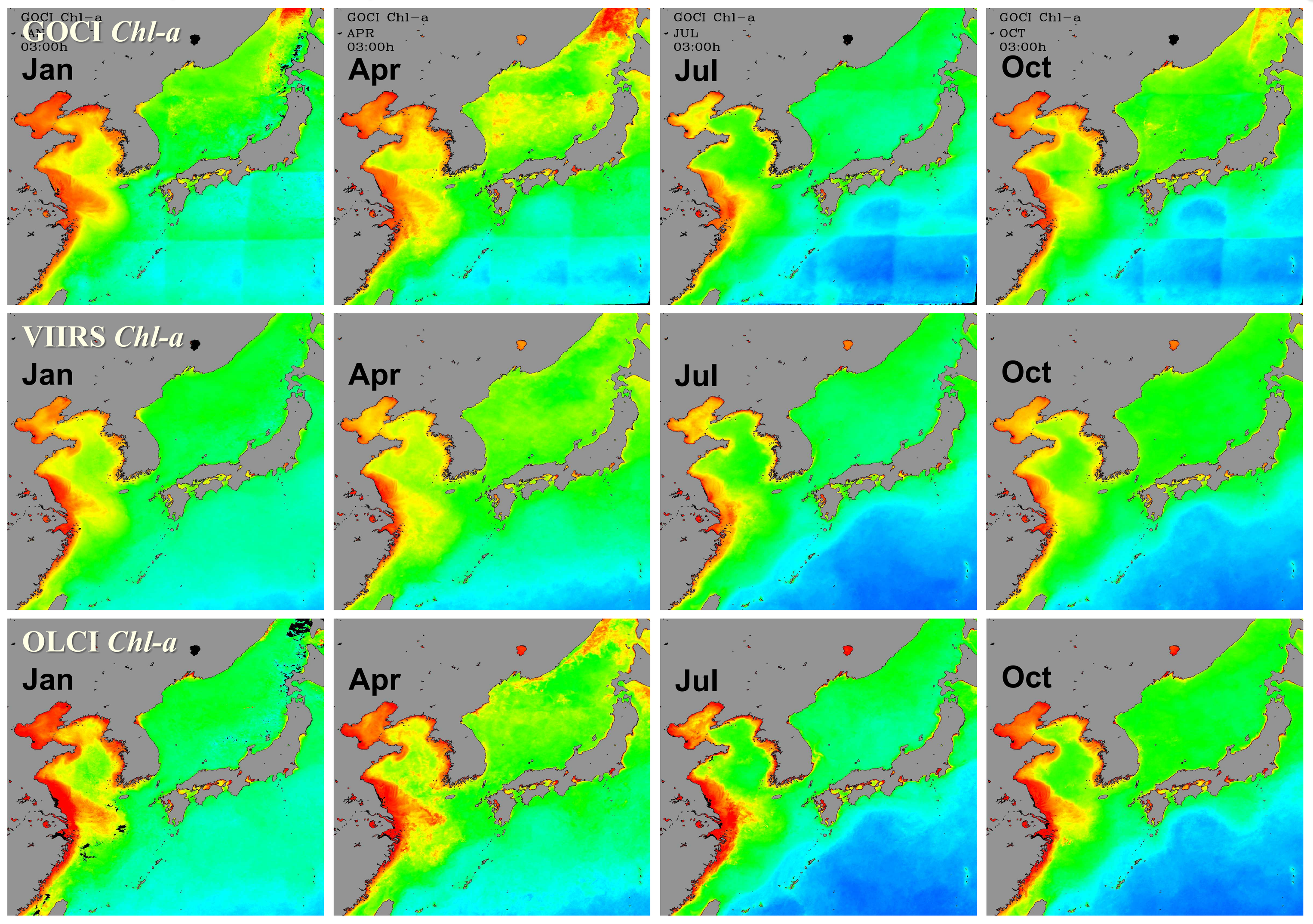

Fig. 5. Climatology monthly images of GOCI- & VIIRS- (Jan. 2012–Dec. 2019) and OLCI-derived (May 2016–Dec. 2019) Chl-a. GOCI images are at the local noon.

- GOCI-, VIIRS-, and OLCI-derived Chl-a images show similar seasonal and spatial distributions over the Northwestern Pacific Ocean.
- In general, Chl-a values are high in spring and low in summer in most waters.

Interannual Variation of GOCI-, VIIRS-, and OLCI-derived Products

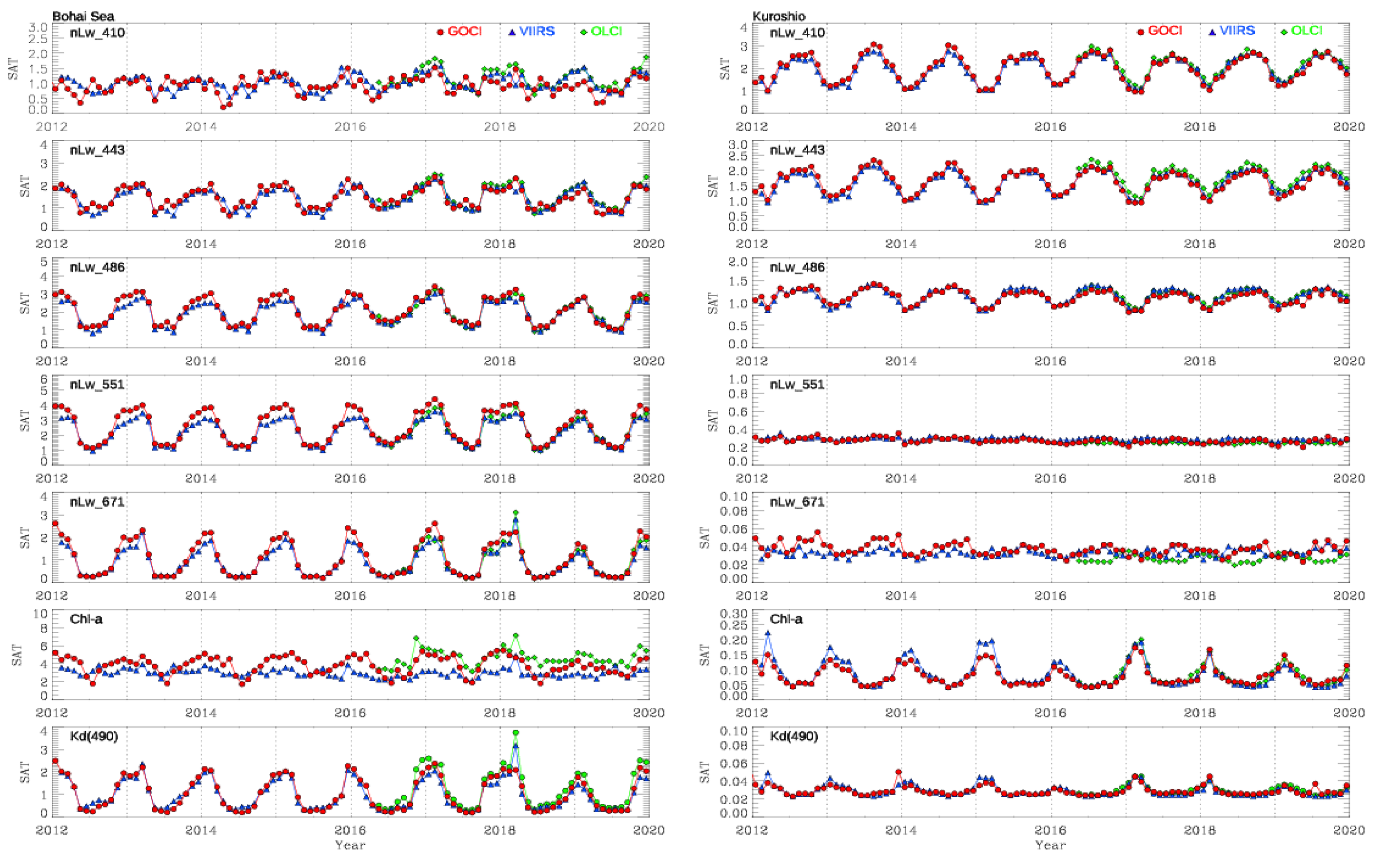

Fig. 6. Time series of GOCI-, VIIRS-, & OLCI-derived mean monthly ocean color products in highly turbid waters (Bohai Sea, left column) and the clear open ocean water (off coasts, right column).

- GOCI-, VIIRS-, and OLCI-derived ocean color products show the strong interannual variability in both highly turbid and clear open ocean waters.
- The monthly mean values are quite consistent in most of the ocean color products from the three sensors. However, there are still some discrepancies in $nL_w(\lambda)$ at blue bands and Chl-a data from GOCI, VIIRS, and OLCI data.

SUMMARY

- ➢The GOCI ocean color products for the GOCI coverage region have been derived using an iterative NIR-water reflectance corrected atmospheric correction algorithm (i.e., the BMW algorithm from *Jiang and Wang* (2014)). Time series of the monthly composite images were produced for the entire GOCI region.
- ➢VIIRS and OLCI ocean color products were also generated using MSL12 with the NIR-SWIR combined and NIR atmospheric correction algorithms, respectively. The VIIRS and OLCI ocean color data over the entire GOCI coverage region were compared with the GOCI ocean color data.
- ➢Matchup results show that GOCI ocean color data are reasonably well correlated to the in situ optical measurements in the Korean coastal waters.
- ➢In general, the temporal and spatial patterns of the GOCI-derived ocean color products are comparable to those from VIIRS and OLCI although there are still some differences. More efforts are required to improve the VIIRS, OLCI, and GOCI ocean color data quality over highly turbid coastal/inland waters.

Reference:

Jiang, L. and M. Wang (2014), Improved near-infrared ocean reflectance correction algorithm for satellite ocean color data processing, *Appl. Opt.*, 52, 6757-6770.

Wang, M. and W. Shi (2007), The NIR-SWIR combined atmospheric correction approach for MODIS ocean color data processing. *Opt. Express*, 15, 15722-15733.

Wang, M., W. Shi and L. Jiang (2012), Atmospheric correction using near-infrared bands for satellite ocean color data processing in the turbid western Pacific region. *Opt. Express*, 20(2), 741-753.

Wang, M., J. Ahn, J. Jiang, W. Shi, S. Son, Y. Park, and J. Ryu (2013), Ocean color products from the Korean Geostationary Ocean Color Imager (GOCI). *Opt. Express*, 21(3), 3835-3849.

Acknowledgments: The GOCI Level-1B data study were provided by Korea Institute of Ocean Science & Technology (KIOST) and in situ data were obtained from the NASA AERONET-OC sites. This study was supported by the NOAA Product Development, Readiness, and Application (PDRA)/Ocean Remote Sensing (ORS) Program funding and JPSS funding.

Remote sensing of shallow-water bathymetry: Leveraging multispectral satellite ocean color observations

Jianwei Wei[1], Menghua Wang[2], Zhongping Lee[3], Henry O. Briceño[4], Xiaolong Yu[3], Lide Jiang[5], Junwei Wang[6], Kelly Luis[3], Rodrigo Garcia[3]

1.NOAA/STAR; GST Inc.; 2. NOAA/STAR; 3. University of Massachusetts Boston; 4. Florida International University; 5. NOAA/STAR; Colorado State University; 6. Xiamen University

Question and Objective

Ocean color satellites allow for derivation of important biogeochemical properties for global oceans. Limited to multispectral resolution, however, it remains difficult to generate geophysical properties, e.g., water depth, over global shallow waters with the satellite remote sensing reflectance ($R_{rs}(\lambda)$). This study evaluate a new algorithm for practical application of multispectral ocean color observations to the retrieval of water depth for optically shallow waters.

	Landsat-8	SNPP	Sentinel-3A
Ocean color sensor	OLI	VIIRS	OLCI
Visible bands	443, 482, 561, 655	410, 443, 486, 551, 638, 671	400, 413, 443, 490, 510, 560, 620, 665, 674, 681
Revisit	16 days	1 day	1-3 days
Data access	USGS	NOAA	NOAA
Processing software	SeaDAS/L2GEN	MSL12	MSL12
Atmospheric correction	NIR-SWIR	NIR-SWIR	NIR

Method and Algorithm

❑ Semi-analytical approach designed for hyperspectral $R_{rs}(\lambda)$

Ocean color community has invested great effort in shallow water remote sensing with semi-analytical algorithms. An extensively tested algorithm is the so-called hyperspectral optimization processing exemplar (HOPE) (Lee et al., 1998; 1999). A shallow-water reflectance model is established as:

$$r_{rs}(\lambda) \approx r_{rs}^{dp}(\lambda)\cdot\left\{1-\exp\left[-\left(\frac{1}{\cos\theta_w}+\frac{D_0\left(1+D_1\cdot u(\lambda)\right)^{0.5}}{\cos\theta_a}\right)\cdot k(\lambda)\cdot H\right]\right\}+$$
$$\frac{\rho(\lambda)}{\pi}\exp\left[-\left(\frac{1}{\cos\theta_w}+\frac{D_0'\left(1+D_1'\cdot u(\lambda)\right)^{0.5}}{\cos\theta_a}\right)\cdot k(\lambda)\cdot H\right]$$

Five unknowns of P, G, X, B, and H can be determined by quantifying the difference between the observed spectrum, $R_{rs}^{obs}(\lambda)$, and modeled spectrum, $R_{rs}^{mod}(\lambda)$,

$$err=\frac{\left[\sum\left(R_{rs}^{mod}(\lambda_i)-R_{rs}^{obs}(\lambda_i)\right)^2\right]^{1/2}}{\sum R_{rs}^{obs}(\lambda_i)}$$

Cost function

❑ Two-spectrum optimization approach (2-SOA) for multispectral $R_{rs}(\lambda)$

Our new algorithm incorporates two independent $R_{rs}(\lambda)$ spectra measured at the same location in the spectral optimization, thus allowing to generate much improved estimation for water depth with multispectral satellite ocean color observations. The work-flow is schematically shown in below:

$R_{rs,1}^{obs}(\lambda)$ $R_{rs,2}^{obs}(\lambda)$

1st image

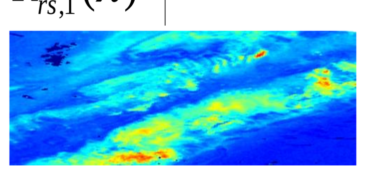

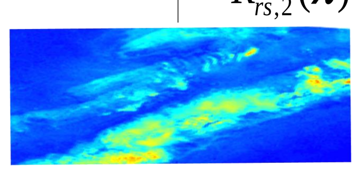

2nd image

$[P_1, G_1, X_1, B, H] \Longrightarrow R_{rs,1}^{mod}(\lambda)$ $[P_2, G_2, X_2, B, H] \Longrightarrow R_{rs,2}^{mod}(\lambda)$

$$err=\frac{\left[\sum\left(R_{rs,1}^{mod}(\lambda_i)-R_{rs,1}^{obs}(\lambda_i)\right)^2+\sum\left(R_{rs,2}^{mod}(\lambda_i)-R_{rs,2}^{obs}(\lambda_i)\right)^2\right]^{1/2}}{\sum R_{rs,1}^{obs}(\lambda_i)+\sum R_{rs,2}^{obs}(\lambda_i)}$$

Cost function

$P_1, G_1, X_1, P_2, G_2, X_2, B, H$

P: phytoplankton light absorption; G: CDOM light absorption; X: particle backscattering; B: bottom albedo; H: depth

Performance Evaluation

Hyperspectral $R_{rs}(\lambda)$ data are synthesized to cover a wide range of depths, three benthic types (coral, seagrass, and sand), and turbidity. These $R_{rs}(\lambda)$ data are then interpolated to represent the measurements for Landsat-8/OLI, SNPP/VIIRS, and Sentinel-3A/OLCI.

Parameters	Range (interval)	Levels
P	0.01–0.19 (0.03)	7
G	0.01–0.19 (0.03)	7
X	0.001–0.019 (0.004)	7
H	0.5–29.5 (1.0)	30
η	−0.5–2.5 (0.5)	7
S_{dg}	0.015	1
θ_a	30°	1
B: coral	0.005, 0.05, 0.1	3
B: seagrass	0.01, 0.035, 0.08	3
B: sand	0.1, 0.25, 0.6	3

	Lower boundary	Upper boundary	Initial value
P_1	0.005	0.35	$0.072\cdot[R_{rs,1}(443)/R_{rs,1}(550)]^{-1.62}$
G_1	0.001	0.6	$0.072\cdot[R_{rs,1}(443)/R_{rs,1}(550)]^{-1.62}$
X_1	0.0001	0.08	$30\cdot a_w(670)\cdot R_{rs,1}(670)$
P_2	0.005	0.35	$0.072\cdot[R_{rs,2}(443)/R_{rs,2}(550)]^{-1.62}$
G_2	0.001	0.6	$0.072\cdot[R_{rs,2}(443)/R_{rs,2}(550)]^{-1.62}$
X_2	0.0001	0.08	$30\cdot a_w(670)\cdot R_{rs,2}(670)$
B	0.001	0.8	0.5
H	0.1	30.5	10

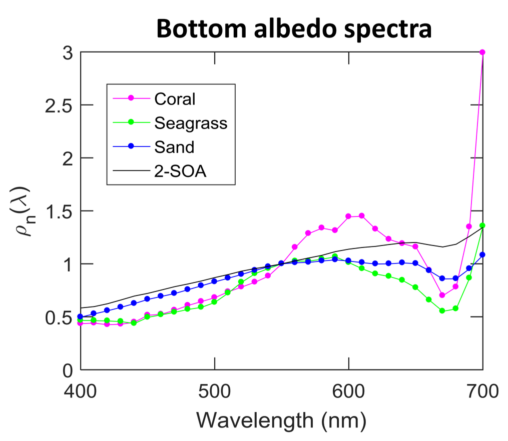

- ❖ The bottom albedo spectra for coral, seagrass, and sand were derived from Hochberg et al. (2003).
- ❖ 2-SOA uses a fixed bottom albedo spectrum (bright band) (Lee et al., 1999).
- ❖ 2-SOA used fixed lower and upper constraints and dynamic initial values.

❑ Error statistics for model-estimated water depth (0.5-30 m)

		Landsat-8\OLI			SNPP\VIIRS			Sentinel-3A\OLCI		
		coral	seagrass	sand	coral	seagrass	sand	coral	seagrass	sand
Standard	MAPE	42%	43%	21%	22%	31%	13%	22%	26%	10%
	Bias	14%	13%	7%	6%	18%	2%	5%	14%	3%
	RMSE	9.3	9.5	6.0	8.8	9.1	4.6	8.3	8.5	4.1
This study	MAPE	26%	28%	15%	14%	19%	11%	14%	16%	10%
	Bias	1%	1%	3%	4%	9%	0%	1%	5%	2%
	RMSE	8.3	8.7	5.2	7.7	8.2	4.0	7.2	7.8	3.9

MAPE: median absolute percentage error; RMSE: root mean square error.

❑ Depth-specific error statistics for model-estimated water depth

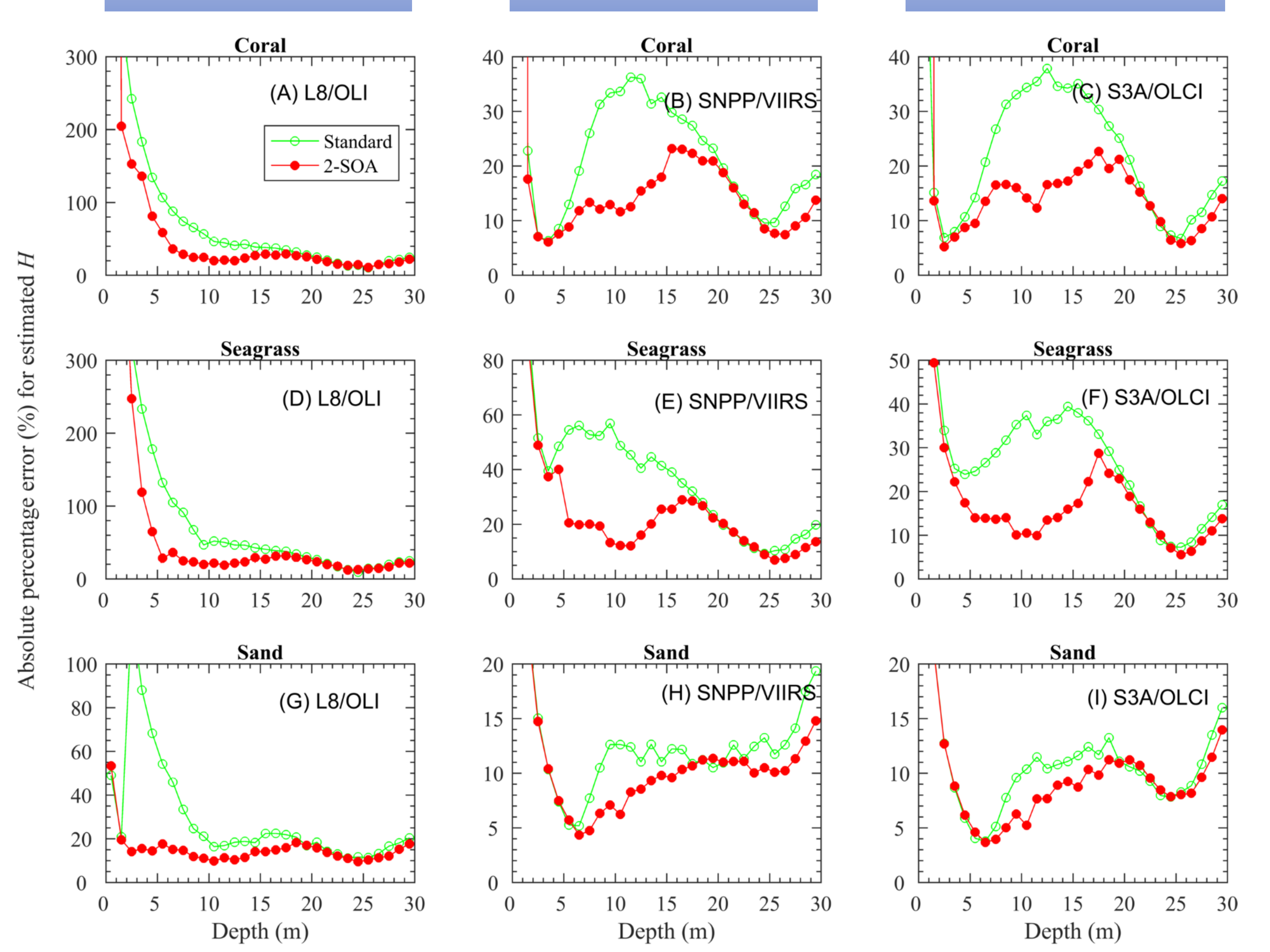

The algorithm performance varies with the range of water depth under study. Improved performance is observed for water depths over ~3-20 m in comparison to the "standard" approach.

Bathymetry from Satellite Images

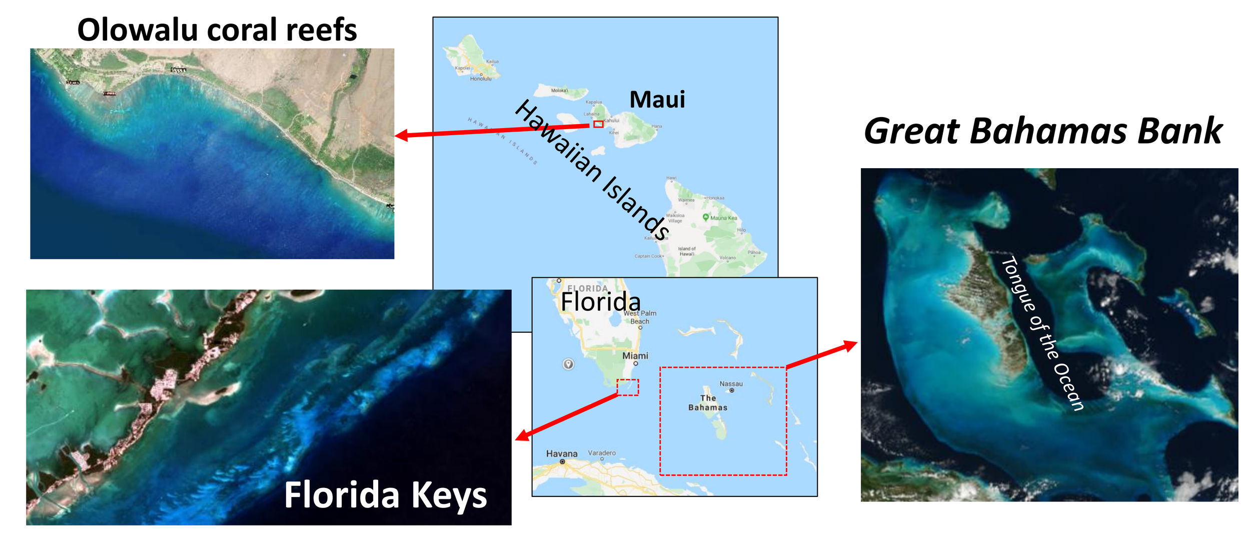

❑ Olowalu Reef (Maui, Hawaii)

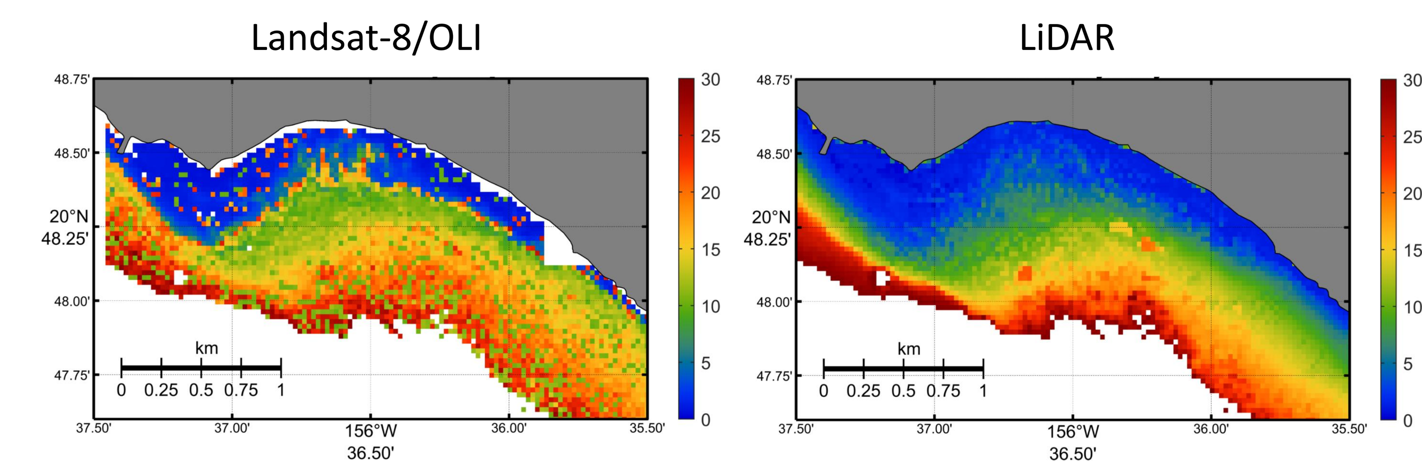

Error statistics for Landsat-8\OLI bathymetry and LiDAR data: MAPE = 40%, Bias = −17%, and RMSE = 8.4 m.

❑ Florida Keys

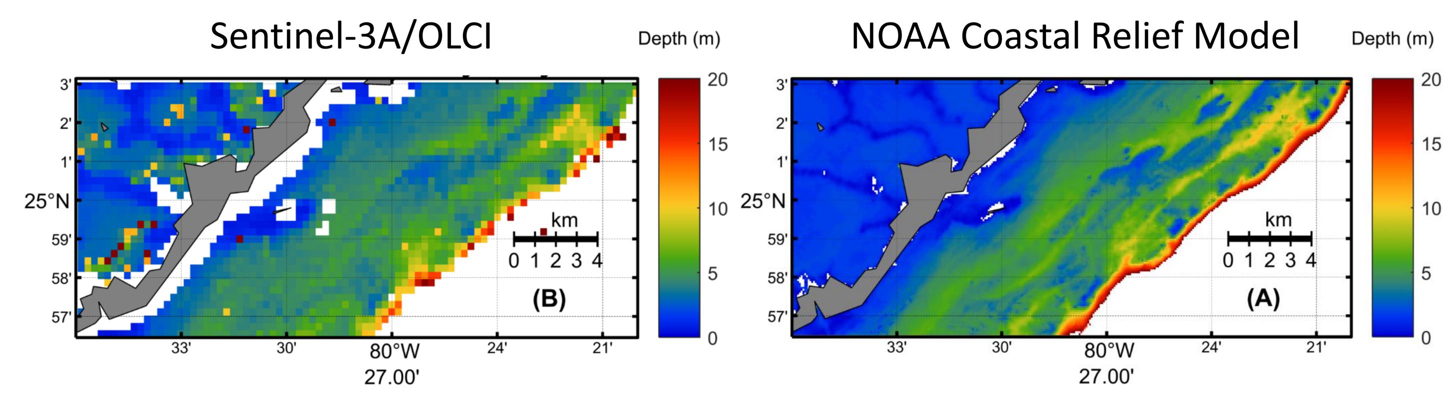

Error statistics for Sentinel-3A/OLCI bathymetry and NOAA CRM model: MAPE = 16%, Bias = −2.7%, and RMSE = 2 m.

❑ The Bahamas

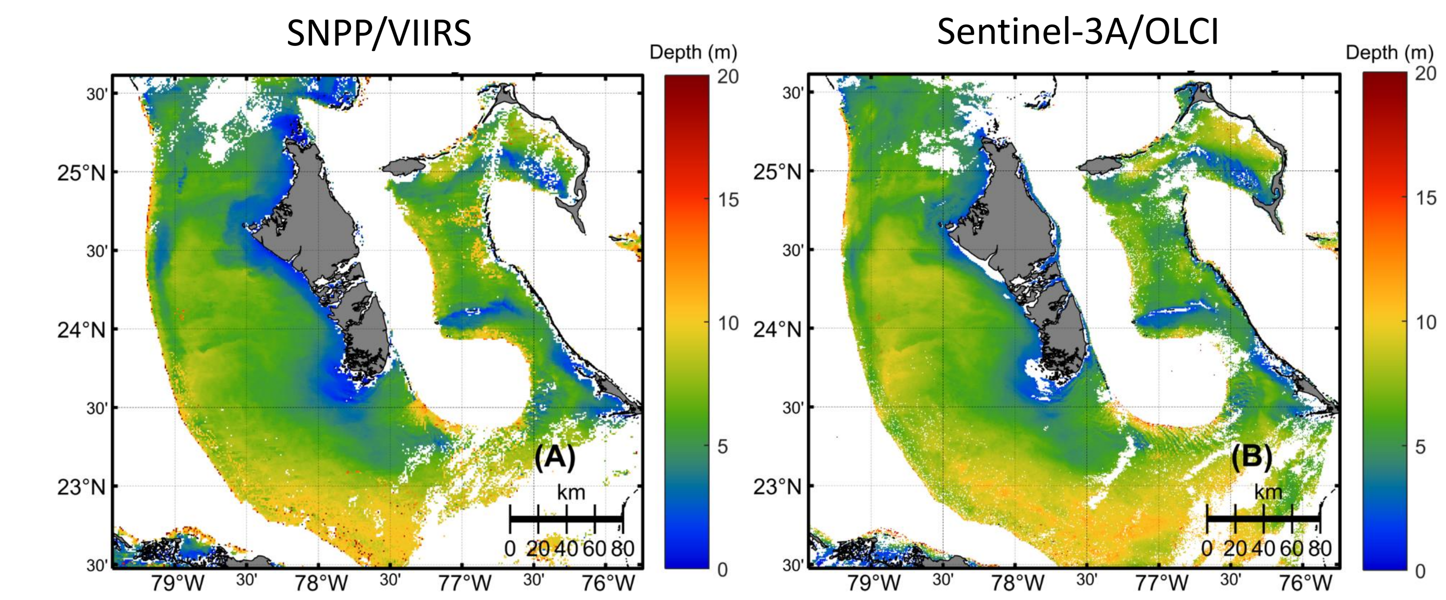

Error statistics for SNPP/VIIRS bathymetry and Sentinel-3A/OLCI bathymetry: MAPE = 9%, Bias = 8%, and RMSE = 0.57 m.

Conclusions

- ❑ A new algorithm is developed for shallow-water bathymetric estimation for multispectral satellite ocean color sensors.
- ❑ Evaluation shows substantial improvement in the estimated depth product over 0-30 m.

Acknowledgment: http://www.soest.hawaii.edu/coasts

Wildfire smoke forecasts using HYSPLIT-based emission inverse modeling system and GOES observations

Tianfeng Chai[1,2], Hyun Cheol Kim[1,2], Ariel Stein[1] , and Shobha Kondragunta[3]

1. NOAA Air Resources Laboratory, College Park, MD;

2. Cooperative Institute for Satellite Earth System Studies (CISESS), University of Maryland, College Park, Maryland;

3. National Environmental Satellite, Data, and Information Service, National Oceanic and Atmospheric Administration , College Park, Maryland

Motivation

Wildfire smoke forecasts have been challenged by high uncertainty in fire emission estimates, such as the BlueSky emission used in the current NOAA smoke forecasts (Fig. 1). We develop an inverse modeling system, the HYSPLIT-based Emissions Inverse Modeling System for wildfires (or HEIMS-fire) to estimate wildfire emissions from the smoke plumes measured by satellite observations.

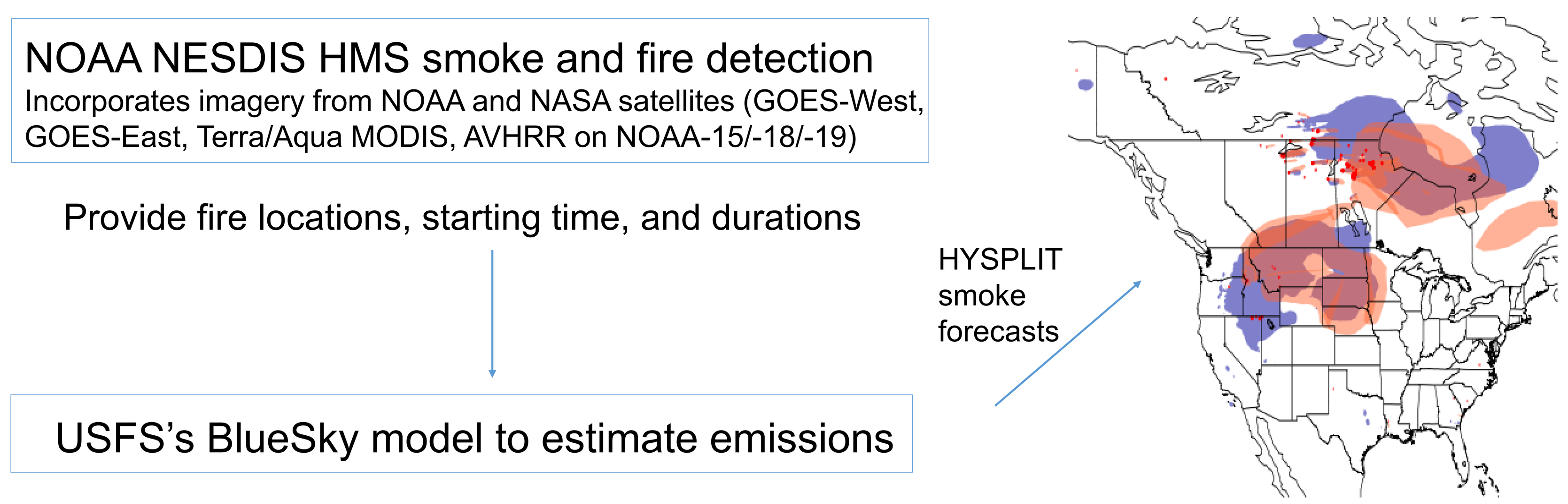

Figure 1. Current NOAA HYSPLIT wildfire smoke forecast system and comparison between HYSPLIT smoke forecasts (blue) and NESDIS HMS smoke (orange).

Methodology

In this top-down approach, the unknown emission terms are obtained by searching the emissions that would provide the best model predictions closely matching the observations. The wildfire emission locations are identified by HMS, the unknown emission rates and the release heights are left to be determined. The emission rates may vary significantly with time. Thus, the unknowns of the inverse problem are the emission rates q_{ikt} at each location i, at different height k and period t. The cost function F is defined as,

$$\mathcal{F} = \frac{1}{2}\sum_{t=1}^{T}\sum_{k=1}^{K}\sum_{i=1}^{I}\frac{(q_{ikt}-q^b_{ikt})^2}{\sigma^2_{ikt}} + \frac{1}{2}\sum_{n=1}^{N}\sum_{m=1}^{M}\frac{(c^h_{nm}-c^o_{nm})^2}{\epsilon^2_{nm}} + \mathcal{F}_{other}$$

where c^o_{nm} is the *m-th* observed concentration or mass loading at time period n and c^h_{nm} is the HYSPLIT counterpart. As shown in Equation (1), a background term is included to measure the deviation of the emission estimation from its first guess q^b_{ikt}. The background terms ensures that the problem is well-posed even when there are not enough observations available in certain circumstances. The background error variances σ^2_{ikt} measure the uncertainties of q^b_{ikt}. The observational error variances ε^2_{nm} represent the uncertainties from both the model and observations as well as the representative errors. F_{other} refers to the other regularization terms that can be included in the cost function. The optimization problem can be solved using many minimization tools, such as L-BFGS-B package, to get the final optimal emission estimates.

HEIMS-fire system

The HEIMS-fire system is shown in Fig. 2. The extensive fires in the southeastern U.S. region in November 2016 is studied here. (Fig.3).

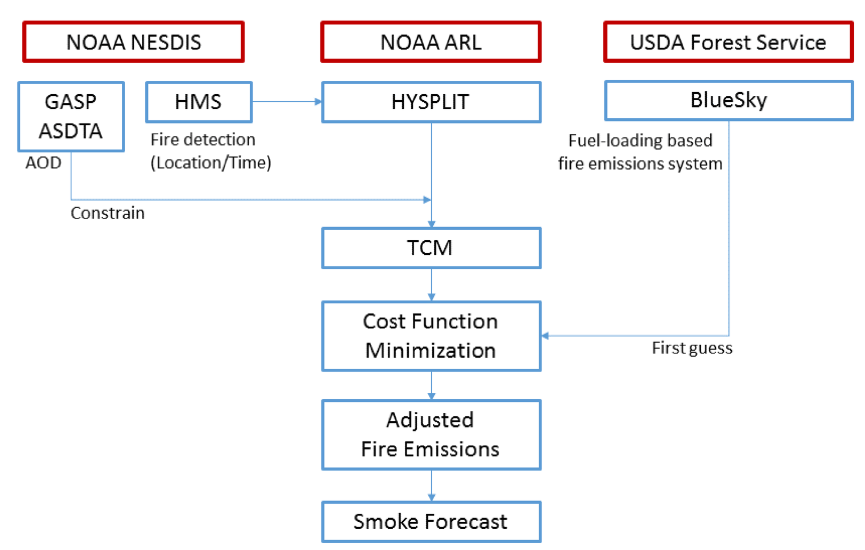

Figure 2. Schematic diagram of HYSPLIT based fire emission inverse modeling system.

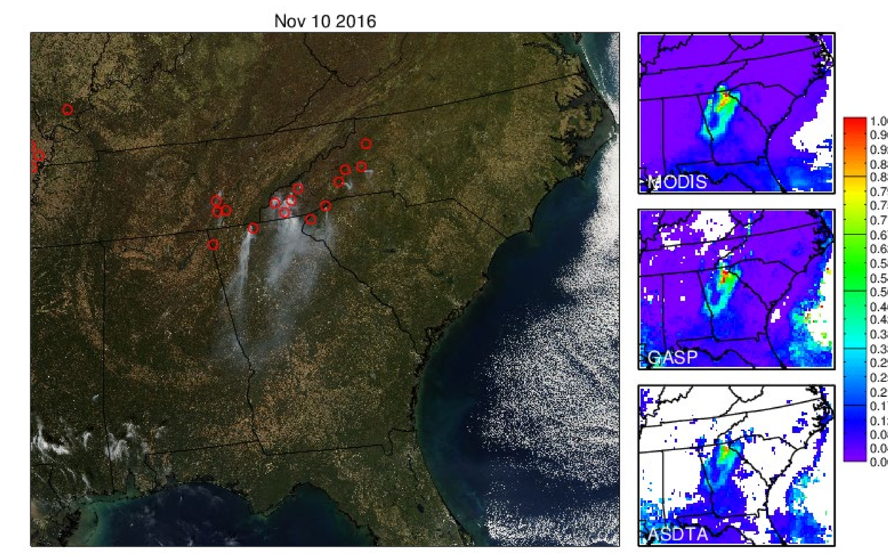

Figure 3 True-color image from MODIS (left), MODIS AOD (top right), GOES GASP AOD (middle right), and GOES ASDTA AOD (bottom right) on Nov. 10, 2016

Reconstructed smoke results

As smoke may come from distant sources, four domains of fire source inputs are considered (Fig.4). Sensitivity tests show that only including the domain 1 would generate comparable results. Using the HEIMS estimated emissions, the smoke plume predicted match the observation pretty well (Fig.5).

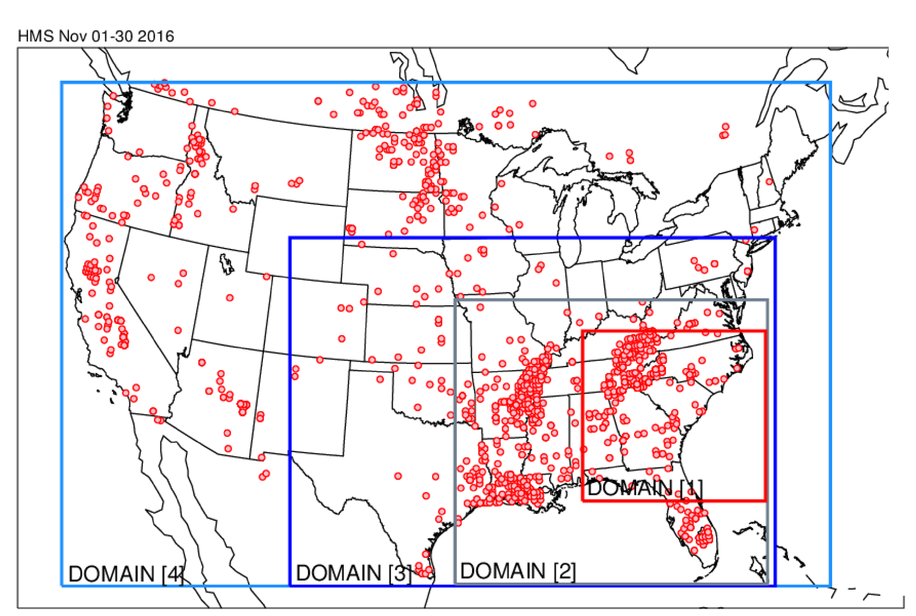

Figure 4 Four domains for fire source inputs in sensitivity tests. Red dots indicate HMS detected fire locations in November, 2016.

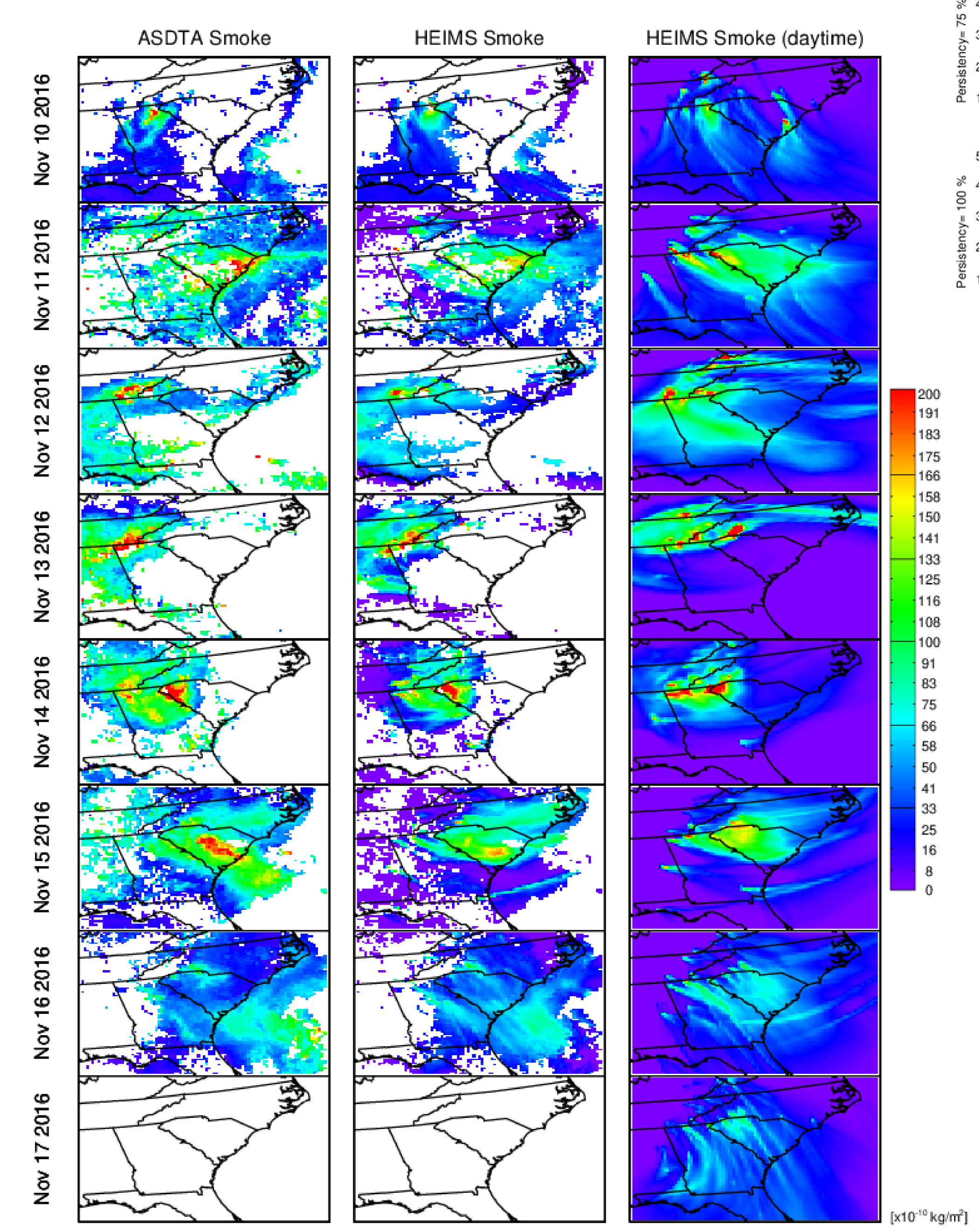

Figure 5. GOES observations (left) and HYSPLIT smoke counterparts (center). Right column shows daytime smoke predictions for the entire domain.

Hindcast

Figure 7 demonstrate the simulated fire smoke by operational NOAA HYSPLIT Smoke Forecast System (SFS) and HEIMS hindcast results on Nov. 11 and two-day forecasts for Nov. 12 and 13. Both systems reproduced well the smoke in their general patterns and intensity, as shown in ASDTA AOD and MODIS true color image. Note that the SFS assumes 75% of emissions still happen at the same location the next day, but the HEIMS uses 50% persistence assumption after sensitivity tests (Fig. 6)

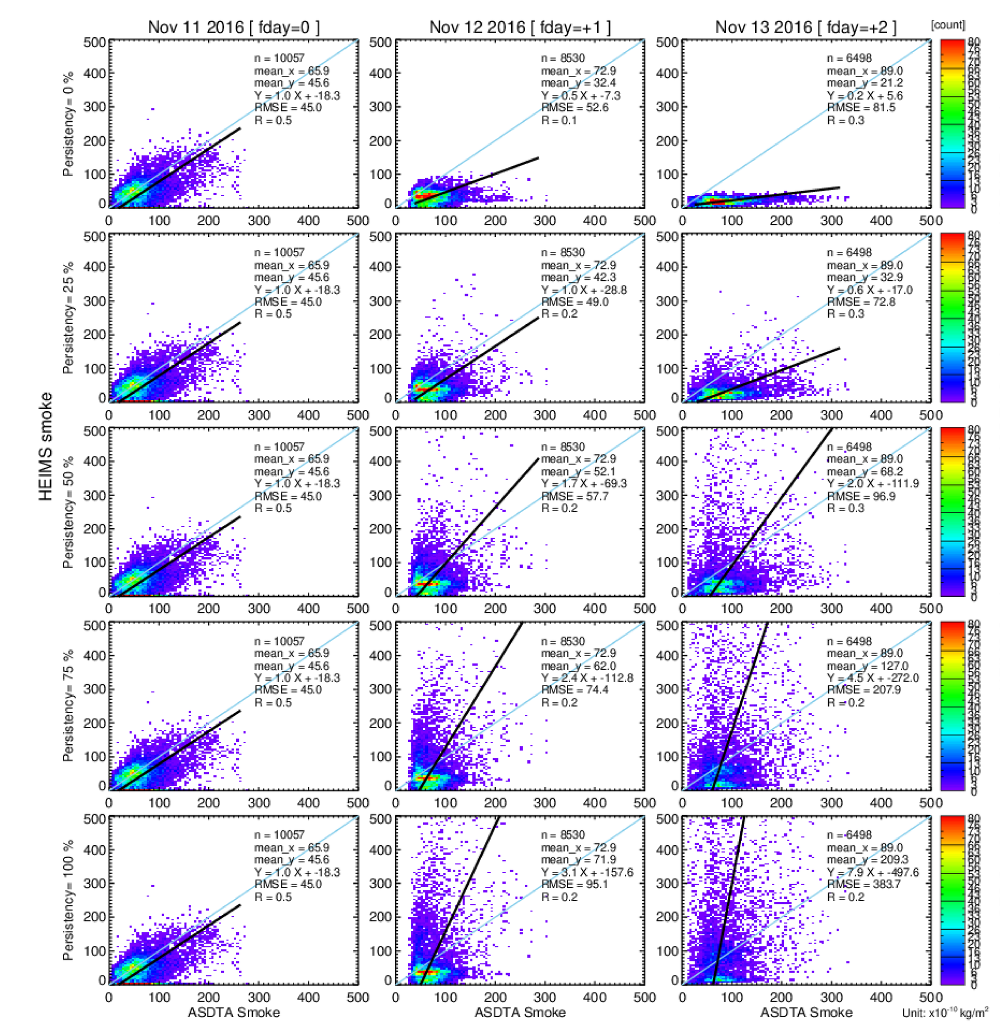

Figure 6. Effect of varying persistent rates for 2 forecast days.

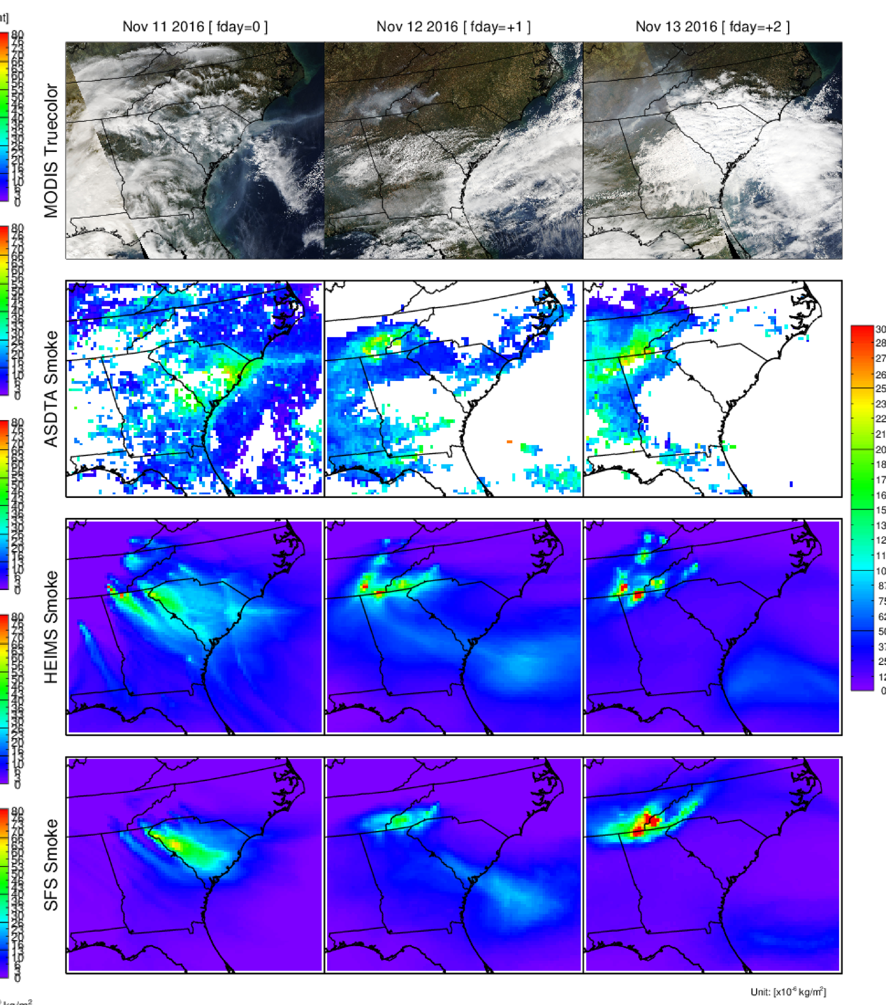

Figure 7. Observed and forecasted smoke on November 11-13. Rows 1-4: True color image from MODIS, ASDTA smoke, HEIMS smoke hindcast, and SFS smoke forecasts (from operation).

Summary and future work

Wildfire emission inversion system HEIMS-fire has been built based on HYSPLIT model, its TCM, and a cost function;
A case study using real GOES data has been performed;
High resolution GOES-16/17 data will be tested;
More evaluation will be performed using VIIRS AOD and surface PM2.5 observations;
Estimated emissions will be tested in other models, such as CMAQ and HRRR-smoke.

Contact information: Tianfeng.Chai@noaa.gov

Towards the Development of Real-time Normalized Burn Ratio (NBR) and delta NBR Imagery from GOES-16/17 and S-NPP

Emily Berndt[1], Kristopher White[2], Frank LaFontaine[3], and Royce Fontenot[4]

[1] NASA Marshall Space Flight Center [2] National Weather Service Huntsville, AL [3] Jacobs ESSCA [4] National Weather Service Albuquerque, NM

Introduction

- Burned landscapes present difficult hydrologic forecasting challenges for National Weather Service Offices
- Burned soils and landscapes can be conducive to the development of flash flooding and landslides from heavy precipitation events (Rammsey and Arrowsmith 2001)
- The severity of the burn scar can be directly related to the risk for debris flows (Cannon and DeGraff 2009) and flash flooding (Lewis et. al. 2006)
- Burned Area Reflectance Classification (BARC) map is generated to indicate the degree of burn severity, which is generated initially by high-resolution satellite imagery from sources such as Landsat, and later by labor-intensive efforts conducted at the burn scar by Burned Area Emergency Response (BAER) teams
- The challenge for operational meteorologists is that these sources of information are not readily available in near real-time
  - Landsat imagery, for example, may only be available about once every eight days, and cloudy conditions can obstruct the observation of the burn scar during a single pass.
  - BAER teams cannot conduct assessments until the wildfire has been at least 40 percent contained (up to 80 percent in some regions), and the process itself can take further days to weeks to complete depending on a number of factors
- To help remedy this lapse in knowledge, NASA SPoRT has developed the generation of NBR imagery in the Advanced Weather Interactive Processing System (AWIPS) using data from the operational GOES 16 and 17 satellites and S-NPP
- This presentation will discuss the development of the GOES- and SNPP-derived NBR and dNBR imagery and their initial evaluation by real-time decision makers

Background/Methodology

- NBR imagery takes advantage of the fact that spectral responses of near-infrared and shortwave-infrared are opposite for burned areas vs healthy vegetation.
- For near-infrared (~0.86 µm): Burned areas have low reflectance, while healthy vegetation has high reflectance.
- For shortwave-infrared (~2.2 µm): Burned areas have high reflectance, while healthy vegetation has low reflectance.

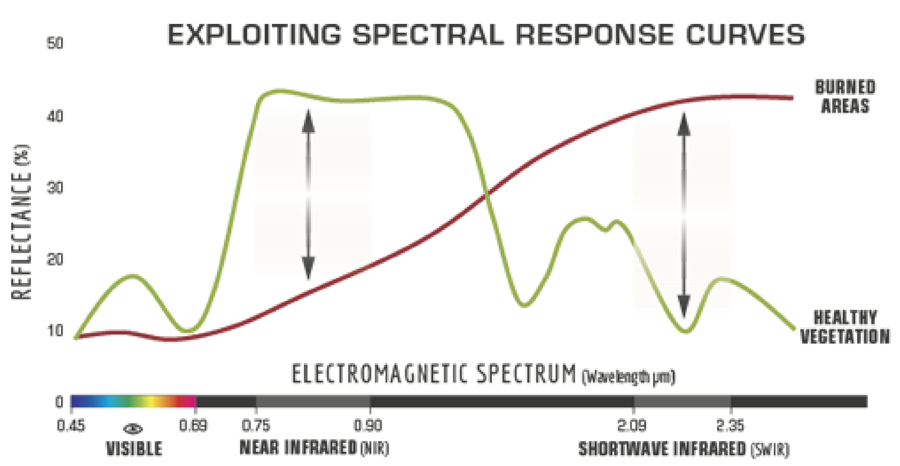

Image courtesy: https://www.fs.fed.us/eng/rsac/baer/barc.html

NBR= (0.86 µm – 2.2 µm)/(0.86 um + 2.2 um)

A couple of examples:

Healthy Vegetation…	Burned Vegetation…
0.86 = 38%	0.86 = 18%
2.25 = 15%	2.25 = 32%
NBR = (38-15)/(38+15) = 0.43	NBR = (18-32)/(18+32) = -0.28

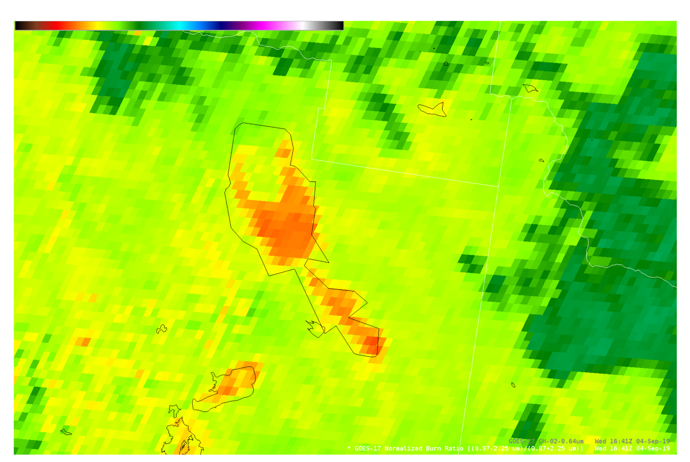

Positive values = healthy vegetation
Lower values (negative) = burned areas
NBR Image above indicates burned areas in bright yellows-reds

- The change in pre-fire and post fire NBR is known as dNBR.

dNBR = Prefire NBR – Postfire NBR

- dNBR is used to assess burn severity and vegetation regrowth compared to pre-fire conditions.
- Prefire imagery will have very high near infrared band values and very low mid infrared band values.
- Postfire imagery will have very low near infrared band values and very high mid infrared band values.
- It can be difficult to distinguish between burned and non-vegetated areas in dNBR imagery

DNBR	Burn Severity
< -0.25	High post-fire regrowth
-0.25 to -0.1	Low post-fire regrowth
-0.1 to 0.1	Unburned
0.1 to 0.27	Low-severity burn
0.27 to 0.44	Moderate-low severity burn
0.44 to 0.66	Moderate-high severity burn
> 0.66	High-severity burn

Woodbury Fire in Arizona June-July 2019

- Since NBR imagery are generated from GOES-16/17 and S-NPP bands in AWIPS, information about the burned vegetation can be observed in real-time
- Low values (bright yellow-orange-red) indicate burned vegetation severity, colors shifted to red with increased negative difference in NIR and SWIR
- High values (light green-dark green) indicate healthy vegetation, colors shifted to darker green with increased positive difference in NIR and SWIR
- Ongoing fires will generally show up as red to dark brown colors due to higher emissions in the 2.2 um band
- False returns at edges of water bodies occur in GOES-16/17 imagery due to differences in spatial resolution of 0.86 µm band (1 km) and 2.2 µm band (2 km)

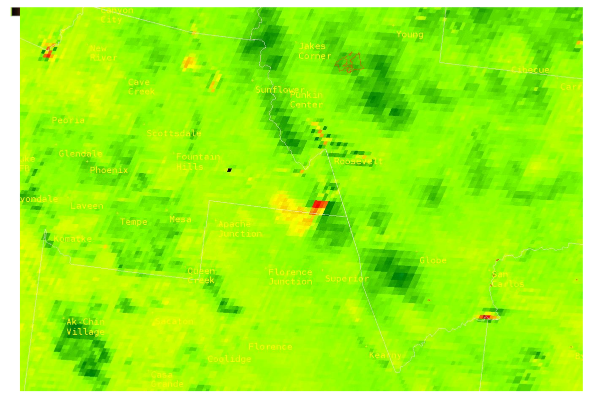

Woodbury Fire, GOES-17 NBR Image
2101 UTC 17 June 2019

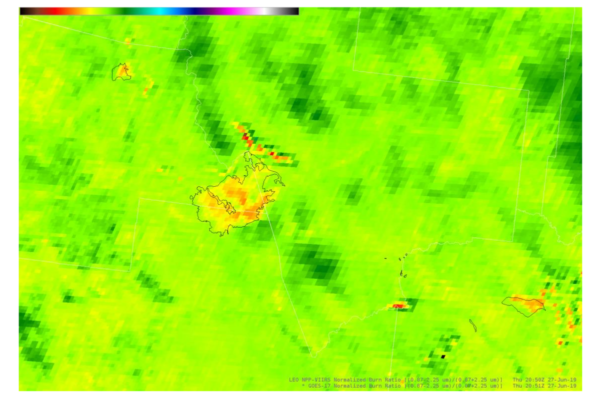

Woodbury Fire, GOES-17 NBR Image
2051 UTC 27 June 2019, with 2019 Fire Perimeters

In the GOES-17 NBR images above, notice the spread of the burn scar from 17 June to 27 June. Burn scar severity in SW portion of the Woodbury Fire remains fairly stable through the period, but the scar has spread due to the ongoing fire and the worst burn severity developed after 17 June. The fire perimeter is also shown for this fire (right) as of 27 June 2019. False NBR returns can be seen along Theodore Roosevelt Lake to the north of the Woodbury Fire. However, other burn scars can be seen in the imagery on the 27 June image (right).

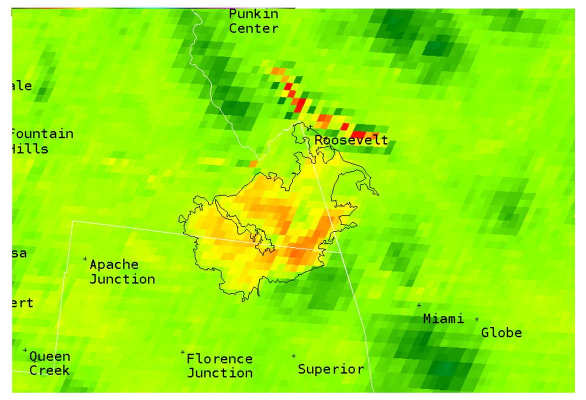

Woodbury Fire, GOES-17 NBR Image
2051 UTC 27 June 2019, with 2019 Fire Perimeters

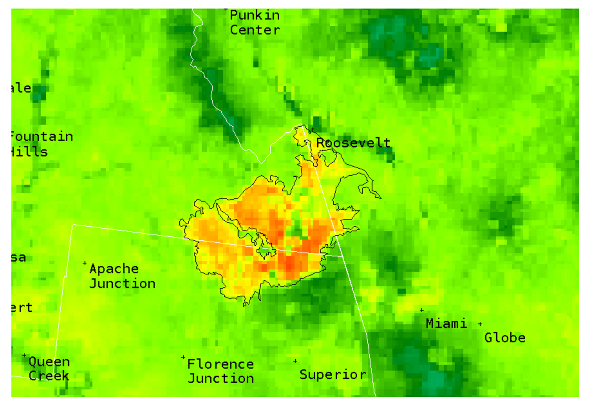

Woodbury Fire, Suomi-NPP NBR Image
2050 UTC 27 June 2019, with 2019 Fire Perimeters

In this comparison between GOES-17 NBR imagery (left) and S-NPP NBR imagery (right), notice the higher spatial resolution of the S-NPP imagery. Also, issues with false returns, such as those along Theodore Roosevelt Lake to the north of the Woodbury Fire do not occur in the S-NPP imagery as is the case with GOES imagery. However, GOES imagery has the advantage of higher temporal resolution (every 5 min), vs the S-NPP imagery, which will only generally be available once per day at any given location (clouds permitting).

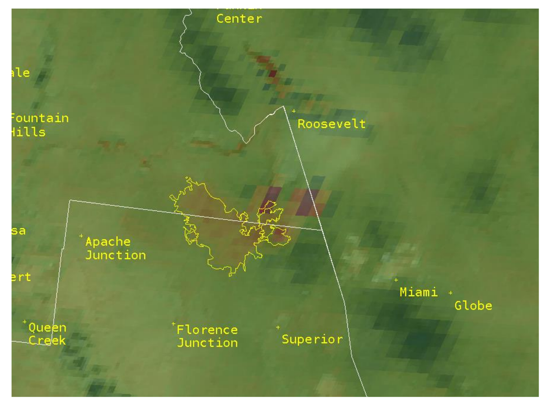

Woodbury Fire, GOES-17 NBR/Vis Image
1911 UTC 20 June 2019, with 2019 Fire Perimeter

GOES-17 NBR image with visible (0.64 µm) imagery overlays provides context for clouds and smoke, and makes the imagery appear more intuitive. Notice that smoke can be observed from the ongoing fire. The visible imagery is set to partial transparency (75%).

Timeline of Analysis for Burn Scar Severity

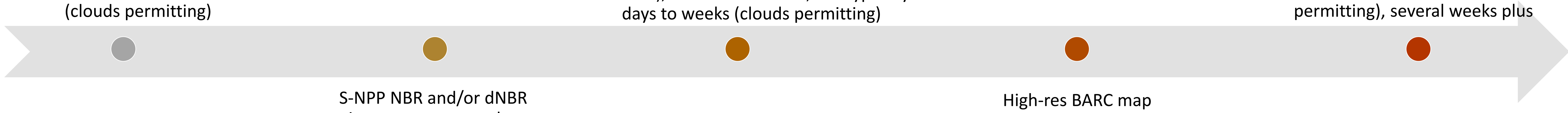

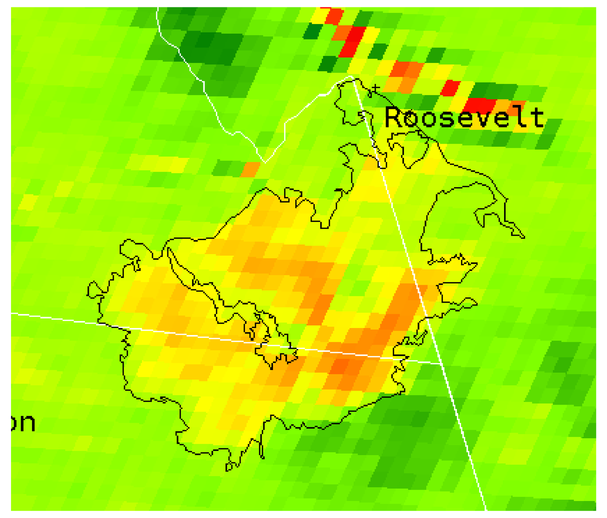

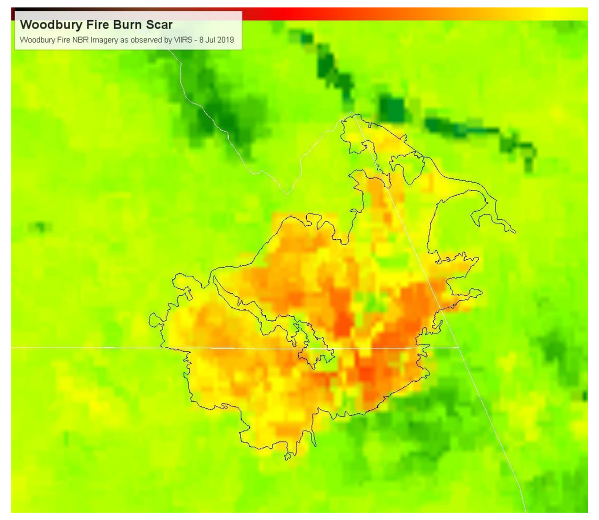

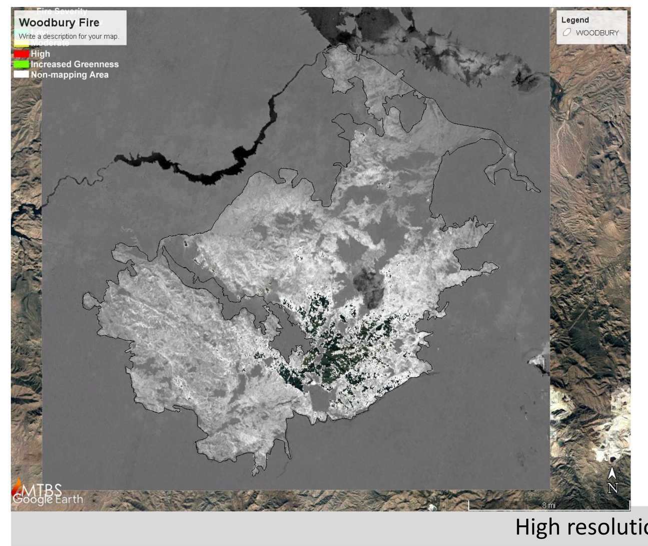

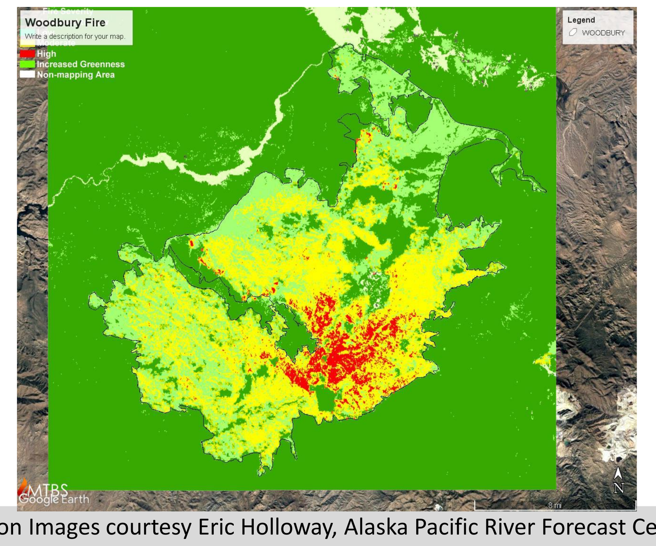

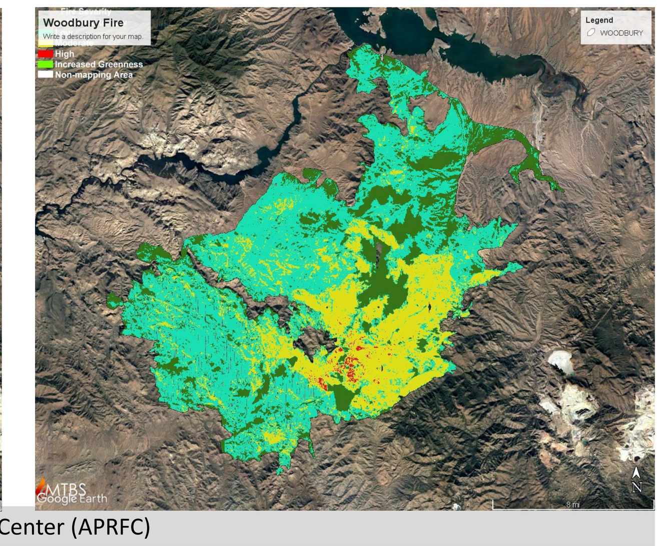

High resolution Images courtesy Eric Holloway, Alaska Pacific River Forecast Center (APRFC)

Conclusions

- Developed a process in collaboration with NWS to assess burn scar severity with new generation satellites in the early stages of fire development and growth
- Limited feedback due to lack of fires in initial test WFO (ABQ), but future users in ABQ and APRFC have provided feedback that data are sufficient to aid in decision-making.

Next Steps

- Continued testing with and feedback from NWS Western Region HQ and Albuquerque Forecast Office, planned discussions this fall
- Refine a technique for processing and disseminating GOES and S-NPP dNBR imagery in GIS format, minimizing cloud effects

References

- Field Validation of Burned Area Reflectance Classification (BARC) Products for Post Fire Assessment, Hudak et al. 2004
- Fire Severity Assessment by Using NBR and NDVI Derived from LANDSAT TM/ETM Images, Escuin et al. 2007
- Rammsey, M. S., and Arrowsmith, J. R. (2001), New images of fire scars may help mitigate future natural hazards, *Eos Trans. AGU*, 82(36), 393– 398, doi:10.1029/01EO00243.
- Cannon, Susan & De Graff, Jerome. (2009). The increasing wildfire and post-fire debris-flow threat in western USA, and implications for consequences of climate change. Landslides - Disaster Risk Reduction. 177-190.
- Lewis, Sarah A. et al. "Assessing burn severity and comparing soil water repellency, Hayman Fire, Colorado." (2006).

National Aeronautics
and Space Administration

Satellite Perspectives on Western US Wildfires in 2019: Comparison of Aerosol Retrievals from GOES and MISR, with Ground-Based Validation

Michael J. Garay and Olga V. Kalashnikova

Jet Propulsion Laboratory, California Institute of Technology, Pasadena, CA 91109

On 12 February 2019 the Geostationary Operational Environmental Satellite-17 (GOES-17) became operational as GOES-West, providing detailed observations of the Western United States from the Advanced Baseline Imager (ABI), which is the primary instrument on the latest GOES-R series of satellites. The summer and fall 2019 wildfire season in the Western US provided the first test of the aerosol retrieval capabilities of the new instrument, especially aerosol optical depth (AOD), associated with extreme fire events. At the same time, the Multi-angle Imaging SpectroRadiometer (MISR) instrument remains operational on the NASA Terra EOS satellite, yielding an unprecedented opportunity to compare simultaneous aerosol retrievals from both ABI and MISR. Validation of these retrievals is further enhanced by the deployment of additional Aerosol Robotic Network (AERONET) sun photometer sites as part of the joint NASA/NOAA FIREX-AQ field campaign, which took place in the summer of 2019.

Instruments

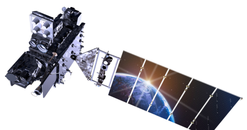

Image Credit: Lockheed Martin

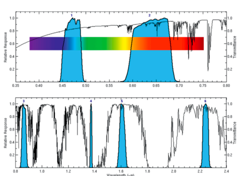

Figure from Schmit et al. (2017)

The GOES-West Satellite (GOES-17), formerly GOES-S carries the Advanced Baseline Imager (ABI) that provides sensitivity to multiple bands in the visible and shortwave infrared portion of the spectrum. This provides a new capability for aerosol retrievals that was not present with the previous generation of imaging sensors on the GOES series of satellites. Here we consider the Level 2 aerosol products designated OR_ABI-L2-AOD[F/C]-M6 from GOES-17 for the dates of 3 August through 21 August 2019 during the western phase of the FIREX-AQ field campaign.

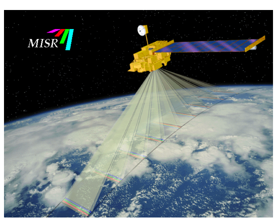

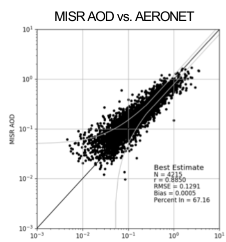

The Multi-Angle Imaging SpectroRadiometer (MISR) instrument has been operational on NASA's polar-orbiting Terra satellite since early 2000. MISR's nine cameras observe four wavelengths in the blue, green, red, and near-infrared portion of the spectrum. Together, this information is used to retrieve aerosol amount – aerosol optical depth (AOD) – over both land and water with a spatial resolution of 4.4 km as well as particle type information. Comparisons with ground-based AERONET sun photometers show that MISR AOD retrievals are of extremely high quality (Garay et al., 2020). Here we consider the MISR AS_AEROSOL product F13_0023 (Version 23).

GOES comparisons with MISR

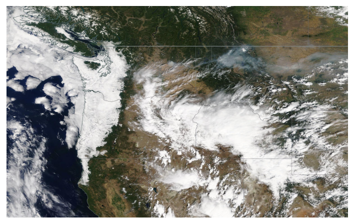

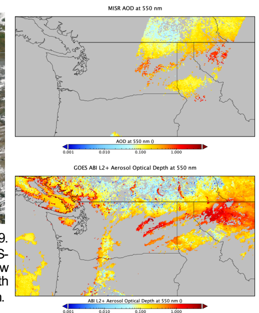

MODIS Terra view of the Pacific Northwest on 8 August 2019. Smoke from fires in Washington is clearly visible near the US-Canadian border. The aerosol retrievals to the right show generally good agreement between MISR and GOES, with somewhat more extensive coverage from the GOES algorithm.

GOES-MISR regression statistics

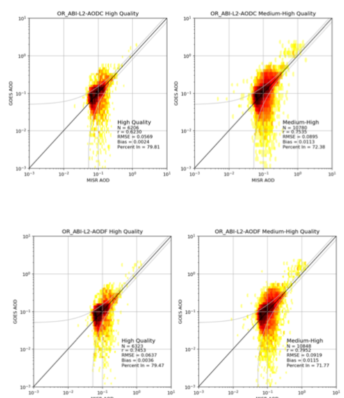

MISR and GOES data for 8 August 2019 were spatially matched within the latitude range from 31°N to 49°N to focus on the Western US. Regression plots and associated statistics were calculated for GOES CONUS (AODC) and GOES Full Disk (AODF) independently, as shown in the figures to the left. On this day, the agreement between MISR and GOES was very good, with better results when the GOES data were restricted to High Quality (DQF = 0) retrievals only, compared to Medium-High Quality (DQF <= 1),

GOES comparisons with AERONET

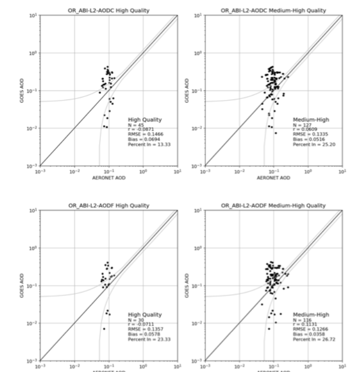

Smoke over AERONET site on 7 August 2019
Image Credit: David Giles (NASA GSFC/SSAI)

Smoke from Williams Flats Fire on 6 August 2019
Image Credit: David Giles (NASA GSFC/SSAI)

GOES data were also matched with ground-based AERONET sites for times close to the overpass time of Terra (1800–1900 UTC) for the entire time period from 3 August to 21 August 2019. The AERONET AODs were interpolated to the 550 nm reference wavelength of GOES. Some of the AERONET sites experienced heavy smoke (see photos) during the FIREX-AQ time period. Regression plots and associated statistics are more limited due to the restricted time period. These results show that the GOES aerosol products perform fairly well relative to AERONET, but the GOES aerosol retrievals tend to overestimate the AOD. However, the GOES observations provide important information on the temporal development and downwind transport of smoke during FIREX-AQ.

References

Garay, M. J. et al. (2020). Introducing the 4.4 km spatial resolution Multi-Angle Imaging SpectroRadiometer (MISR) aerosol product. *Atmos. Meas. Tech.* **13**, 593–628,, https://doi.org/10.5194/amt-13-593-2020.

Schmit, T. J. et al. (2017). A closer look at the ABI on the GOES-R series. *Bull. Amer. Meteorol. Soc.* **98**, 681–698, https://doi.org/10.1175/BAMS-D-15-00230.1.

National Aeronautics and Space Administration
Jet Propulsion Laboratory
California Institute of Technology
Pasadena, California
www.nasa.gov

Support for this research was provided by the NASA Earth Science Directorate.

Hazardous Weather Forecasting Using High Resolution Leo/Geo Soundings

W. Smith Sr.[1,2], *Q. Zhang*[2], *E. Weisz*[1], *A. DiNorscia*[2], *S. Lindstrom*[1]
[1]*U. of Wisconsin (USA)*, [2]*Hampton U. (USA)*

A system has been set up to produce in near real-time nowcasting and forecast model input data from combined Direct Broadcast Satellite (DBS) Polar Hyperspectral (PHS) CrIS/IASI and GOES ABI (PHSnABI) Data. The data is made available to potential users via the internet and through the NWS AWIPS. Studies are being performed to demonstrate severe and precipitation forecast improvements using these data. The PHSnABI observation and forecast products will be provided to weather forecasters for evaluation during the NOAA spring 2020 Hazardous Weather Testbed (HWT).

PHS and ABI Characteristics

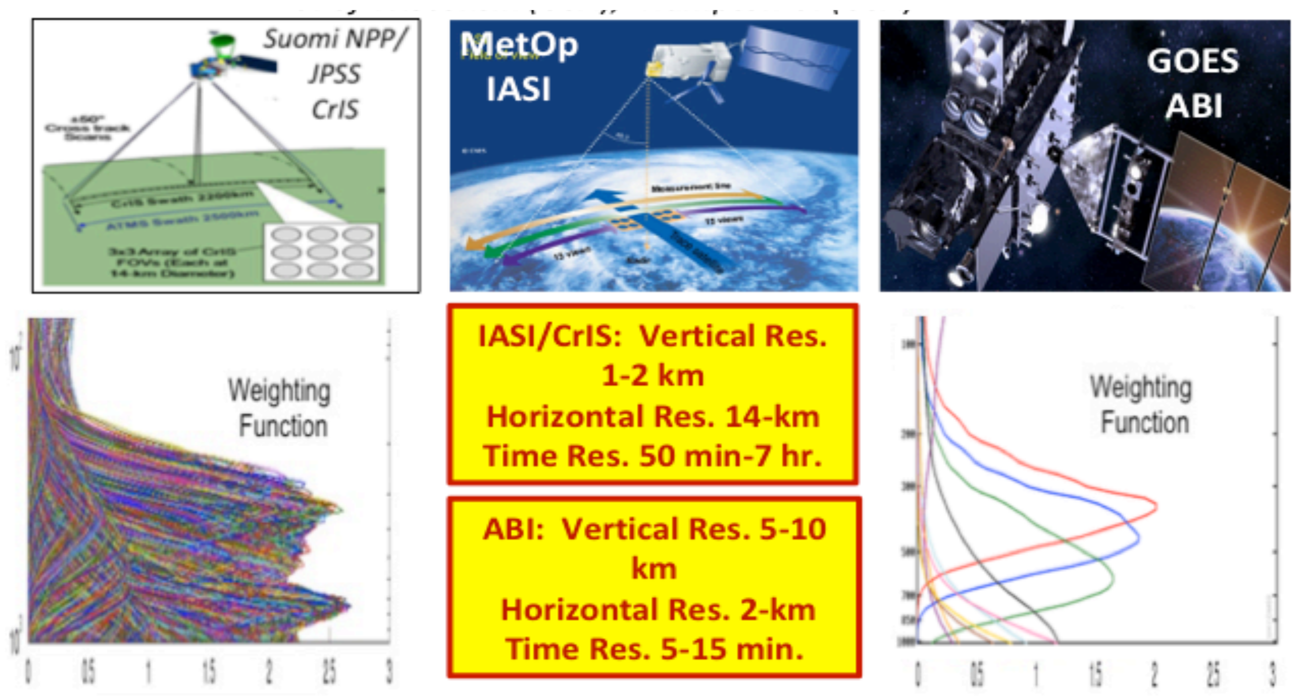

Sounding Retrieval Process

Dual Regression + De-Alias (DRDA)*

- **Alias =** Forecast Retrieval − Forecast Profile
- **DRDA Retrieval** = DR Retrieval − Alias

* Smith, W. L., and E. Weisz, 2017: Dual Regression Approach for High Spatial Resolution Infrared Soundings, in *Comprehensive Remote Sensing*, M. Goldberg, Editor, Elsevier Ltd, Langford Lane Oxford, OX5 1GB UK.

PHS and ABI Sounding Fusion

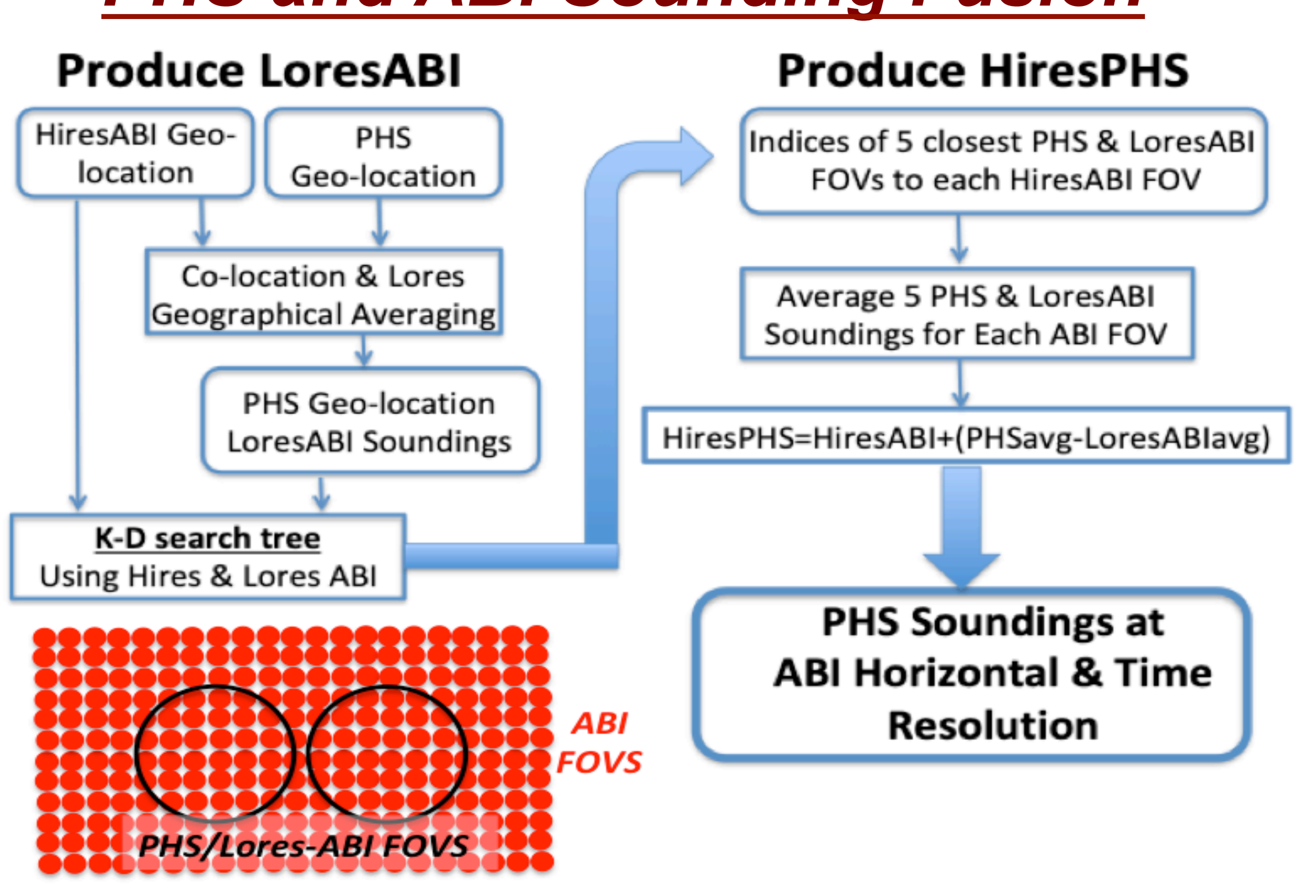

PHS and ABI Fusion Example

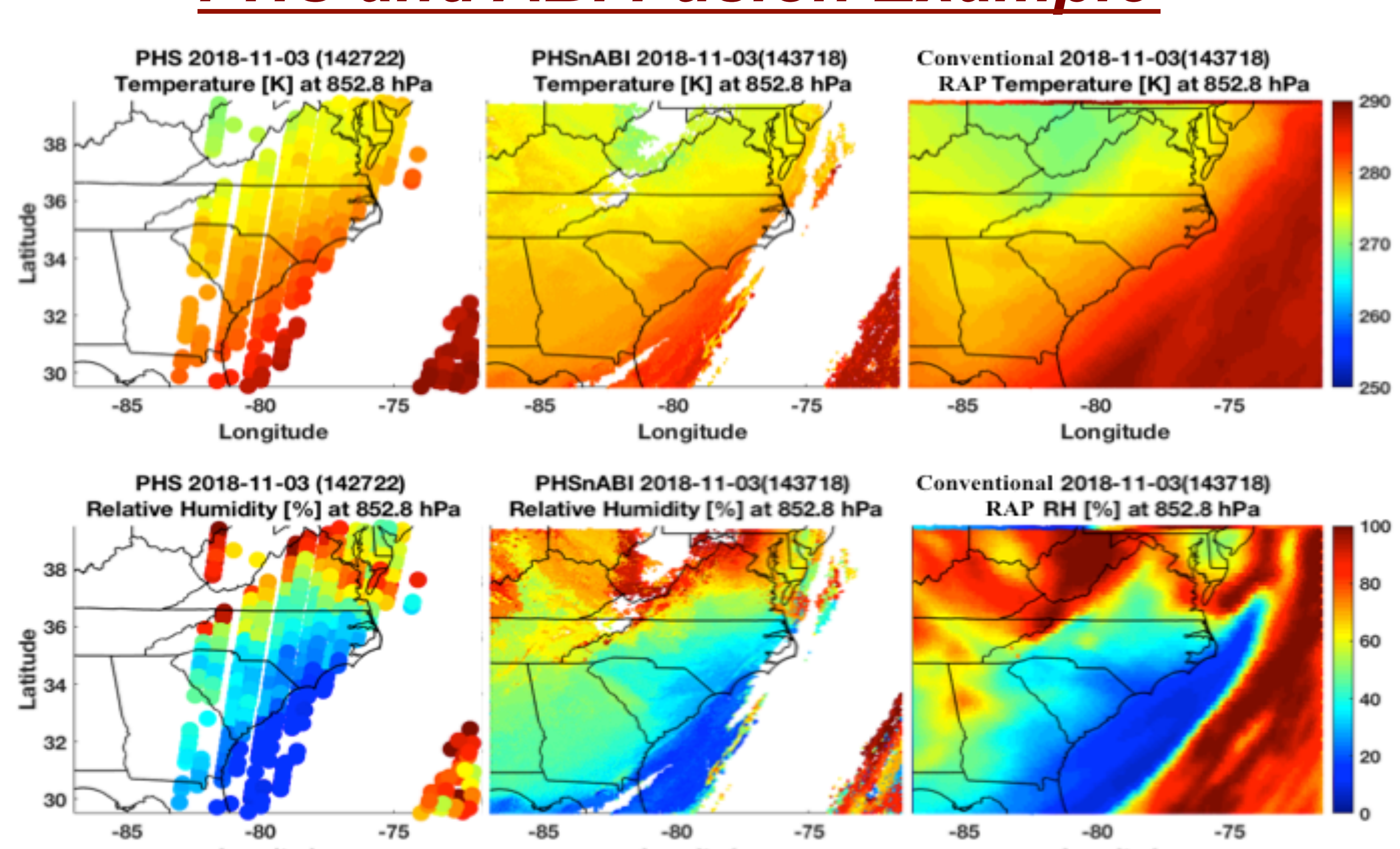

Assimilating PHSnABI

- NOAA RAP-like configured 9-Km WRF Model

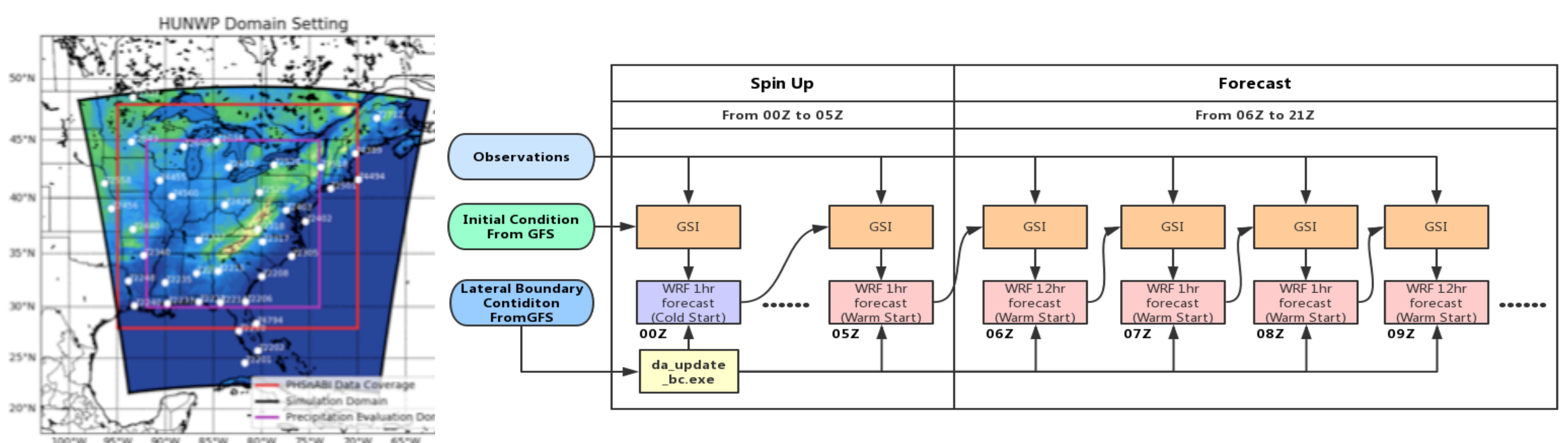

May 27/28 2019 Lifted Index & STP

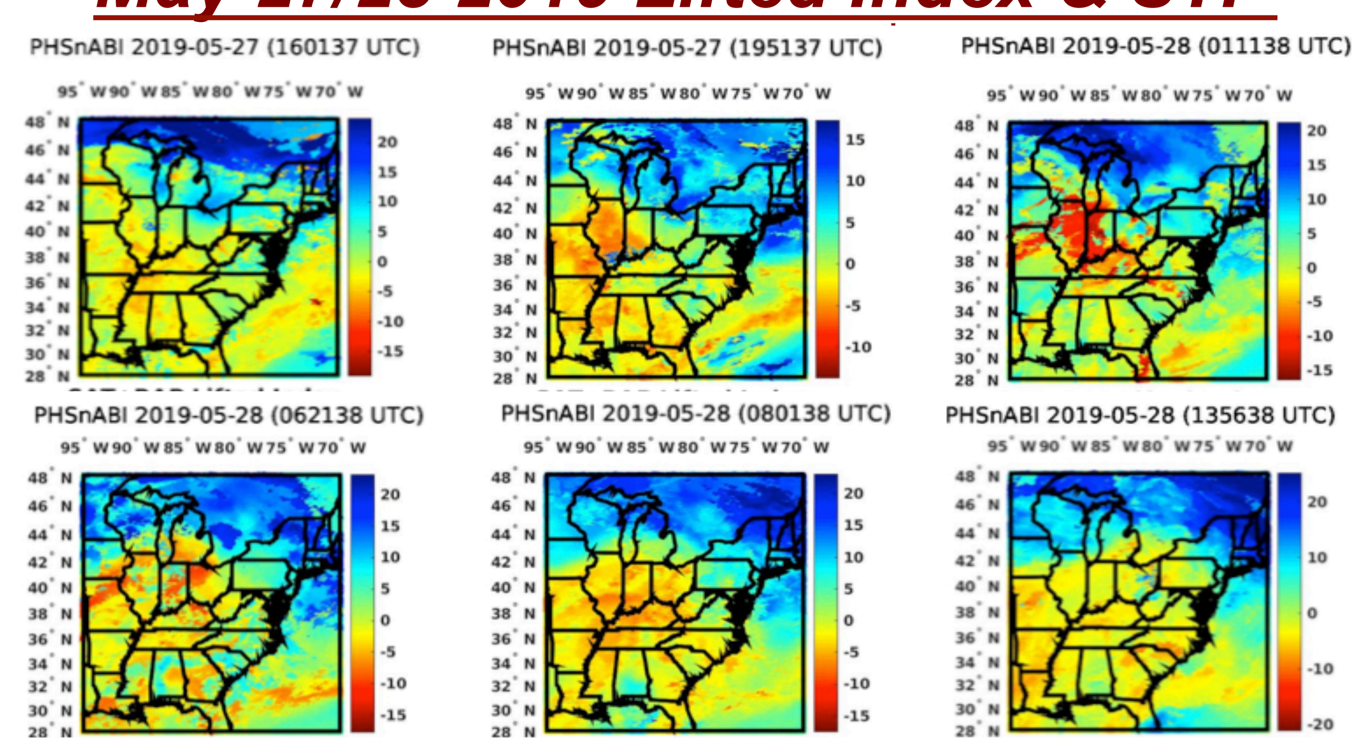

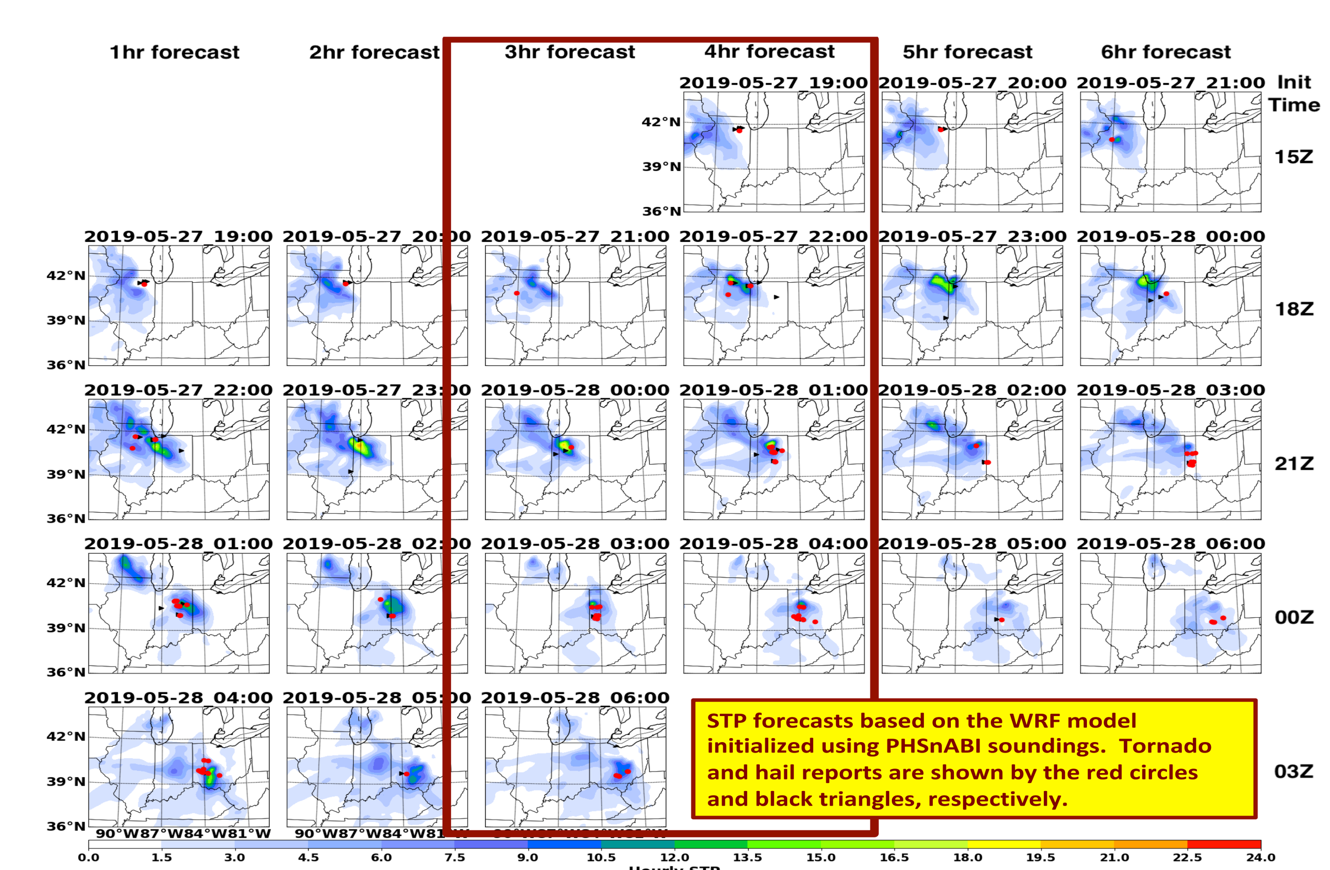

Significant Tornado Parameter (STP)

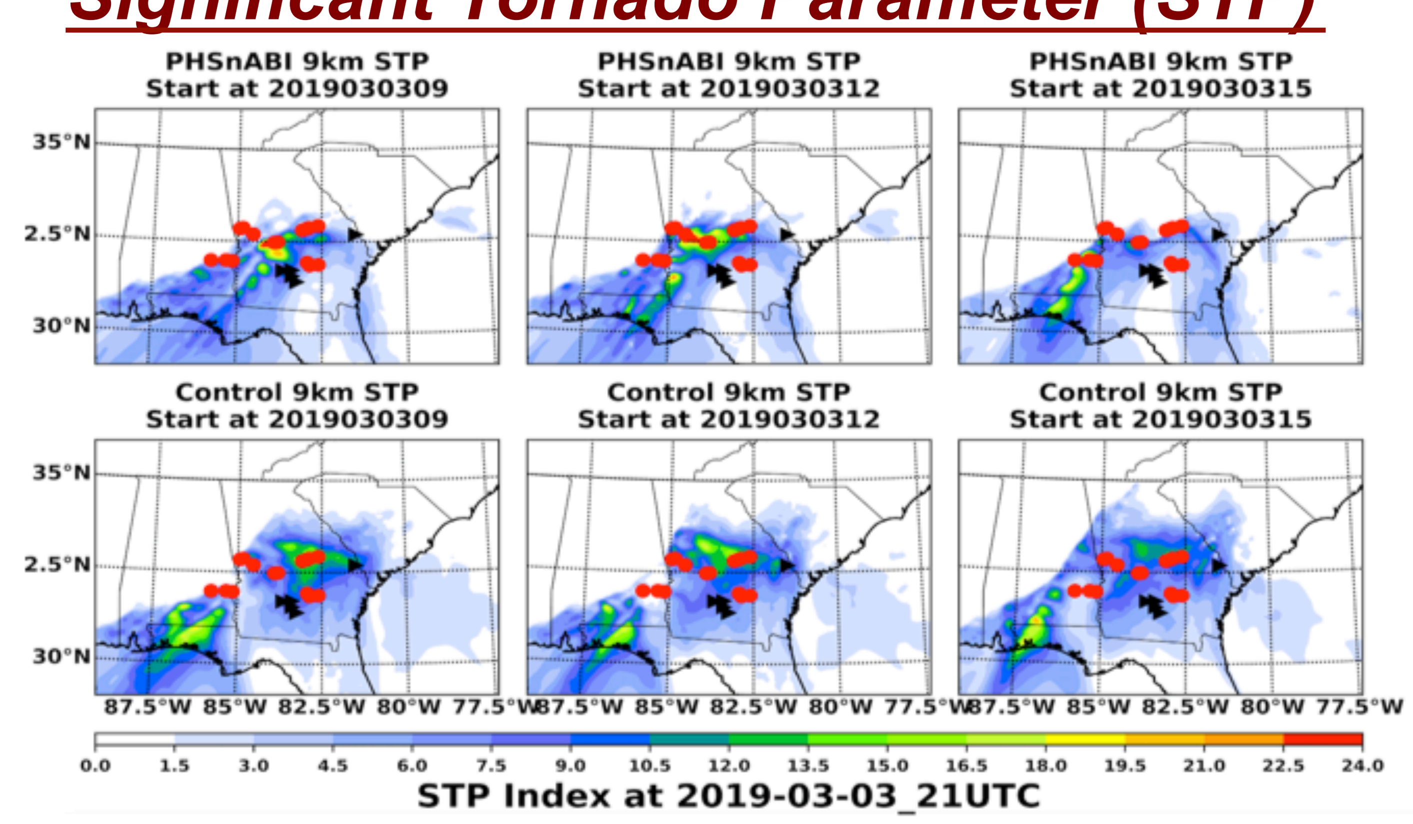

Nowcast Website (194116 UTC)

http://dbps.cas.hamptonu.edu/development/

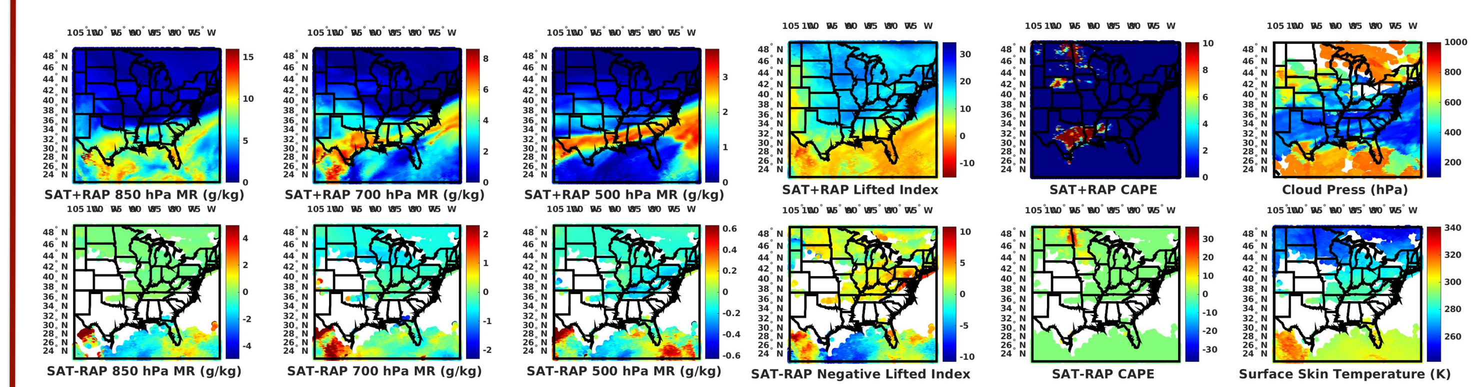

Severe Weather Research Center

8-km Numerical Weather Prediction System

CAS MainPage | HU Retrieval | UW Retrieval | Nowcast | Hourly Forecast | 6-minutes Interval dBZ | Precipitation Evaluation | Raob Evaluation

The goal of Severe Weather Research Center 8-km Numerical Weather Prediction System is to provide meteorological satellite enhanced high resolution nowcasts and short-term numerical forecasts for the purpose of warning the US population of impending High Impact Weather (e.g. tornados, hail, flash floods, tropical storms, and hurricanes). "Nowcast" products are produced from near real-time satellite soundings produced by the fusion of direct broadcast operational Polar (IASI and CrIS) Hyper-spectral Sounding (PHS) and geostationary Advanced Baseline Imager (ABI) multi-spectral sounding radiance data (PHSnABI). Numerical Weather Prediction (NWP) products are produced by the hourly assimilation of PHSnABI soundings with operational conventional weather observations into the Weather Research and Forecasting (WRF) model configured with the same physics and forecast initialization procedures used in the NOAA Rapid Refresh Prediction (RAP) NWP model. The nowcasting products which take advantage of PHSnABI soundings assimilation provide hourly Significant Tornado Parameter (STP), Most Unstable CAPE (MUCAPE), Lifted Index (LI), Accumulated Precipitation for the Central and Eastern US regions. Short-term forecast products including hourly STP, LI, MUCAPE, accumulated precipitation and 6-minutes-interval composite radar reflectivity forecasts are generated using the same background that provides nowcast products.

Initial Condition 2020/02/19 (9 UTC)

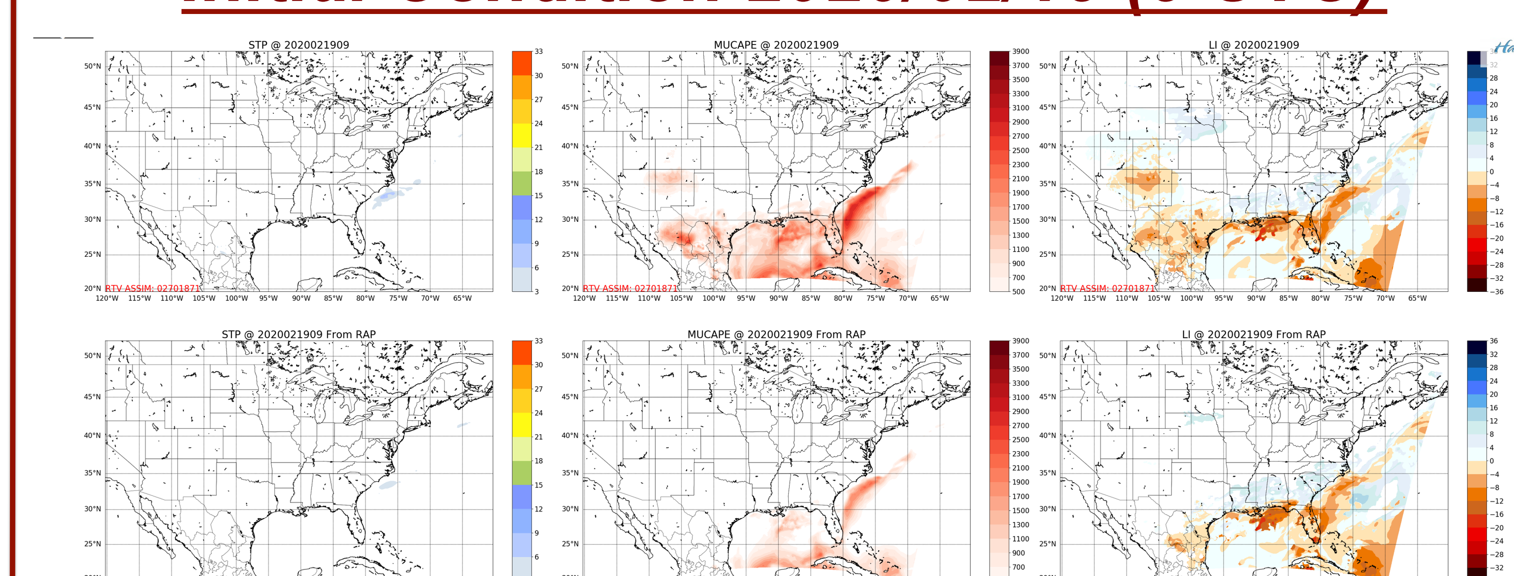

1 to 6-hour Precipitation Forecast

2020/02/19 16 - 21 UTC

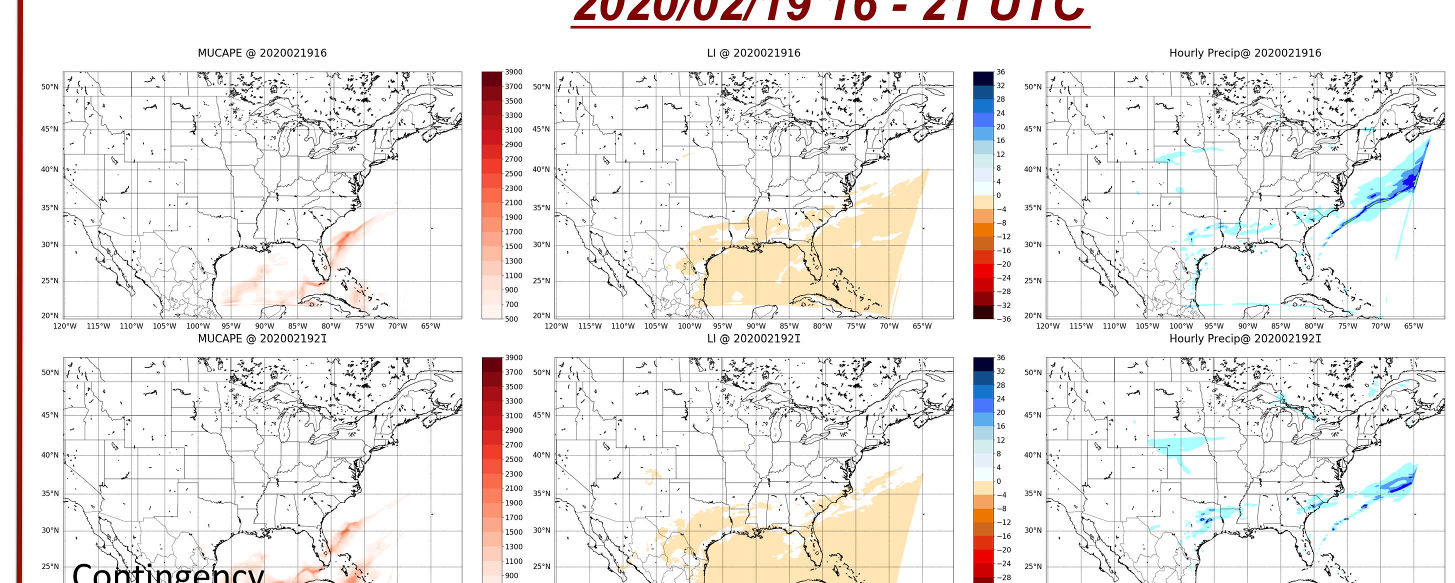

Table III. Contingency Table

		Observation	
		Happen	**Not Happen**
Forecast	**Happen**	a	b
	Not Happen	c	d

CSI=a/(a+b+c)

POD=a/(a+c)

FAR=b/(a+b)

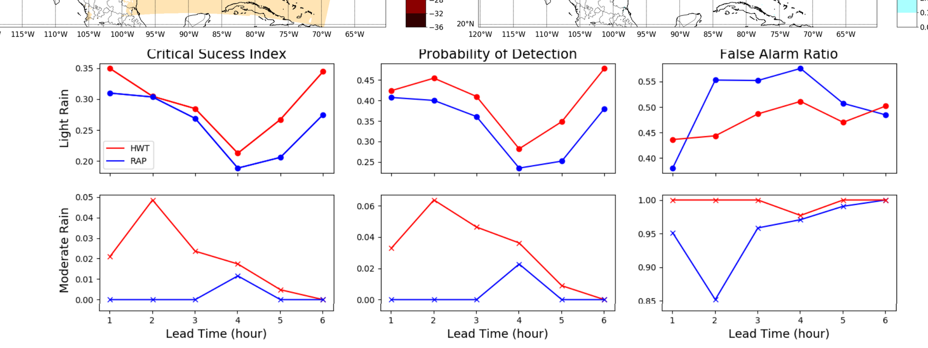

Improving Blended Total Precipitable Water (TPW) Products for Forecasters Via Advection and Inclusion of GOES-R

John M. Forsythe, Stanley Q. Kidder, Sheldon J. Kusselson, Dan Bikos, Andrew S. Jones, Louie Grasso, Ed Szoke

Cooperative Institute for Research in the Atmosphere, Colorado State University

Collaborators: Tony Wimmers (CIMSS), Limin Zhao (NOAA OSPO), Ralph Ferraro (NOAA STAR), Chris Grassotti (CISESS-Univ of MD), Andrew Orrison (NOAA WPC), Chris Gitro, Mike Jurewicz, Dan Leins (NOAA/NWS)

View near-realtime animations at: http://cat.cira.colostate.edu/ABI_TPW_FD/Merged_TPW.htm http://cat.cira.colostate.edu/GR3/GOESR_TB09_SIM_Hourly.htm htm http://cat.cira.colostate.edu/ GR3/GOES17_TB09_SIM_Hourly.htm

John.Forsythe@colostate.edu

What Do Forecasters Currently Use Operationally for Blended TPW?

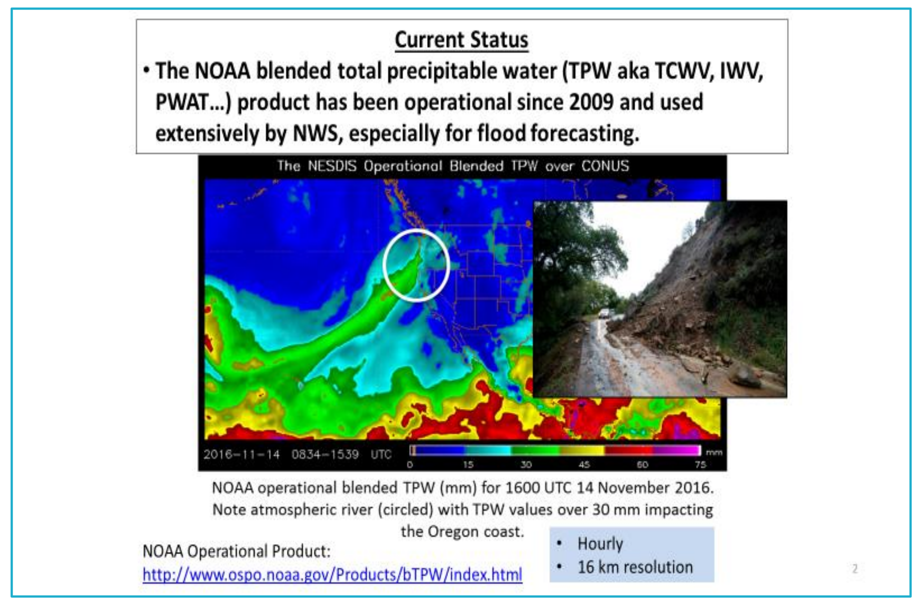

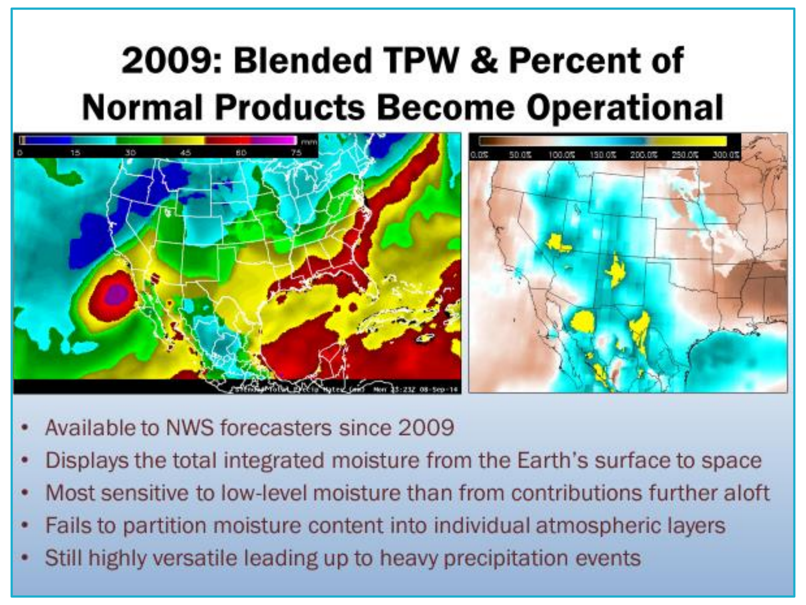

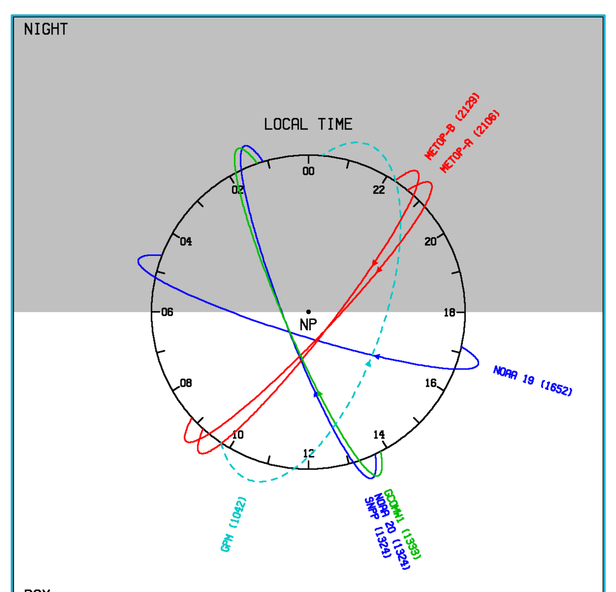

Current satellite suite used at OSPO for blended TPW. Times of ascending / descending nodes show for synsynchronous satellites. GPM precesses through all times.

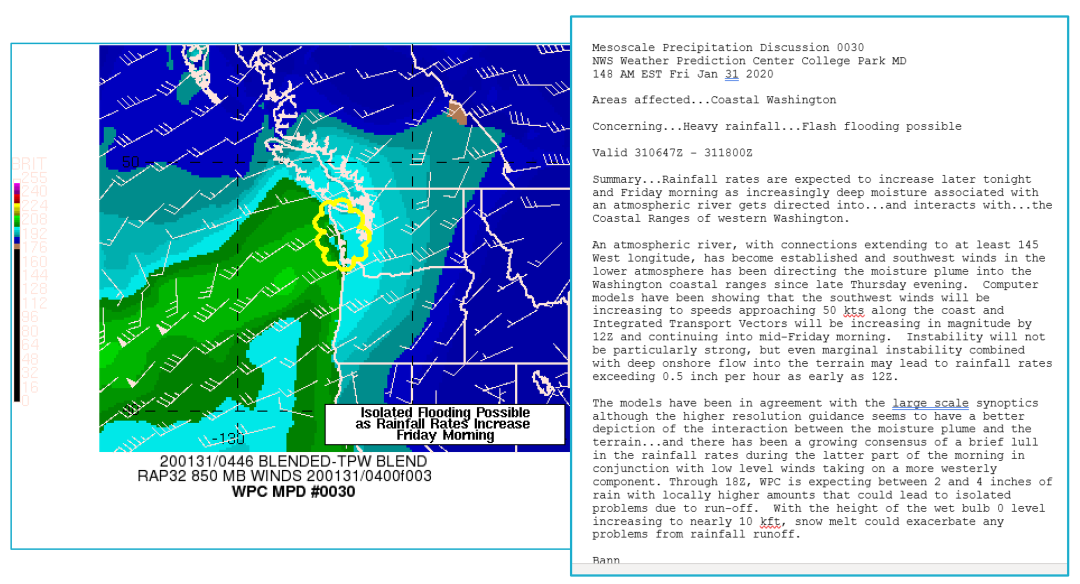

But current product does not include GOES-R data…

GOES-16 TPW Continues to Validate Well

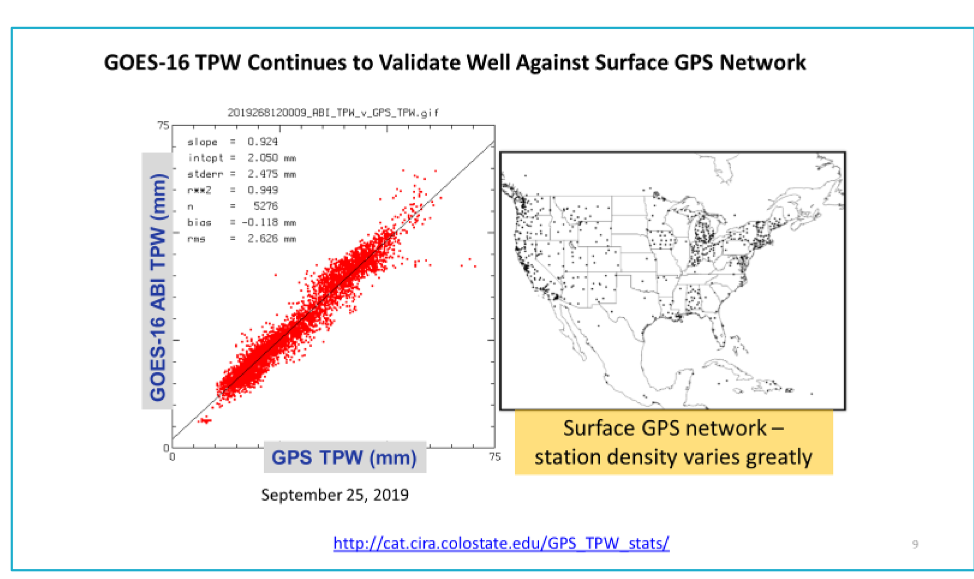

Daily validation against surface GPS stations

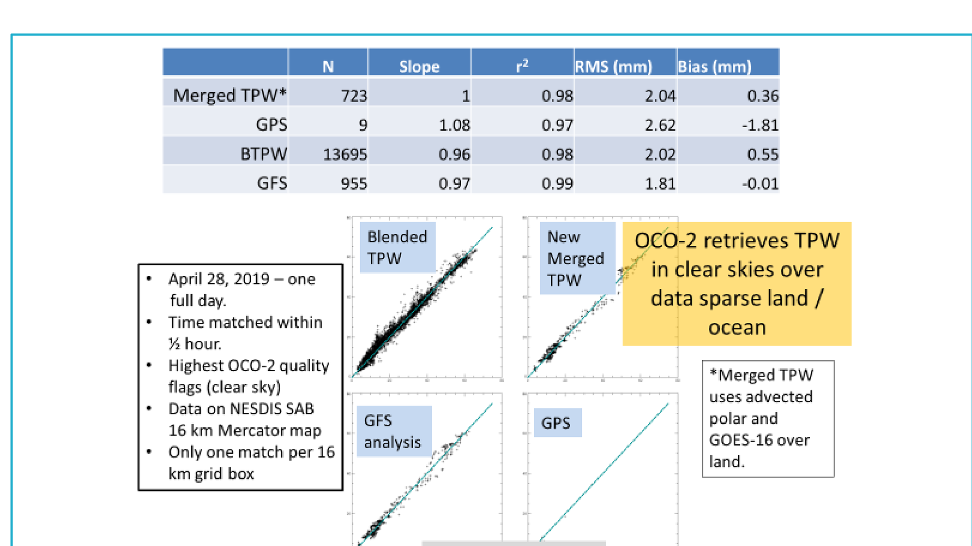

	N	Slope	r²	RMS (mm)	Bias (mm)
Merged TPW*	723	1	0.98	2.04	0.36
GFS	9	1.08	0.97	2.62	-1.81
BTPW	13695	0.96	0.98	2.02	0.55
GFS	955	0.97	0.99	1.81	-0.01

Validation against NASA Orbiting Carbon Observatory-2

Supports results in:

Schmit, T. J., Li, J., Lee, S. J., Li, Z., Dworak, R., Lee, Y.-K., et al. (2019). Legacy atmospheric profiles and derived products from GOES-16: Validation and applications. Earth and Space Science, 6, 1730–1748. https:// doi.org/10.1029/2019EA000729

Forecaster Surveys from Hazardous Weather Testbed (HWT) and Flash Flood and Intense Rainfall Experiment (FFaIR)

Questions posed to Forecasters in 2019 at Hazardous Weather Testbed (HWT - NSSL) and Flash Flood and Intense Rainfall Experiment (FFaIR - WPC)

1. Is the Merged TPW product preferable to the operational blended TPW?
2. How important is it that blended TPW be independent of forecast model TPW?
3. Is hourly temporal resolution sufficient?

NWS Forecaster Surveys of the New "Merged" Total Precipitable Water Product

Question	2019 HWT (severe wx experiment)	2019 FFaIR (flash flood experiment)
1. Did the new Merged TPW product perform better than the operational blended TPW?	(responses = 79) 68% YES 32% NO	(responses = 80) 70% - much better 12% - better 14% - same 4% - worse
2. Is hourly temporal resolution sufficient?	(responses = 35) 60 % Yes 40 % No	responses = 25) 68% Yes 12 % No (20 % N/A)
3. Would you like a TPW product that is completely independent of model moisture fields?	(responses = 35) Yes, but - 45% No, but - 40% No definitive answer - 15%	(responses = 15) Yes - 60% No - 7% Yes and No - 7% No position - 26%

How is the Merged TPW with GOES-16 Created?

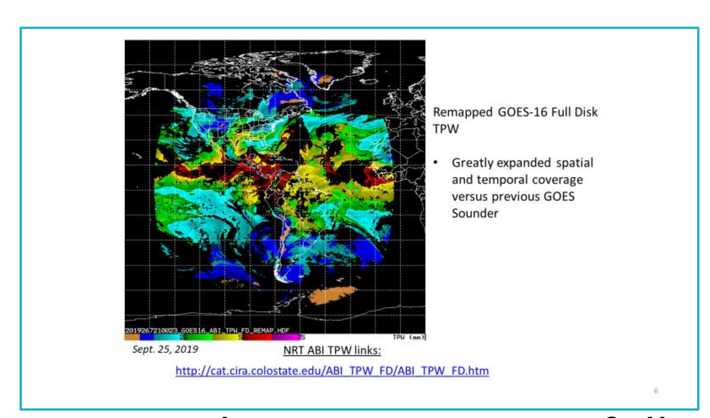

GOES-R brings 15 minute full disk coverage in clear areas – big improvement over previous sounders

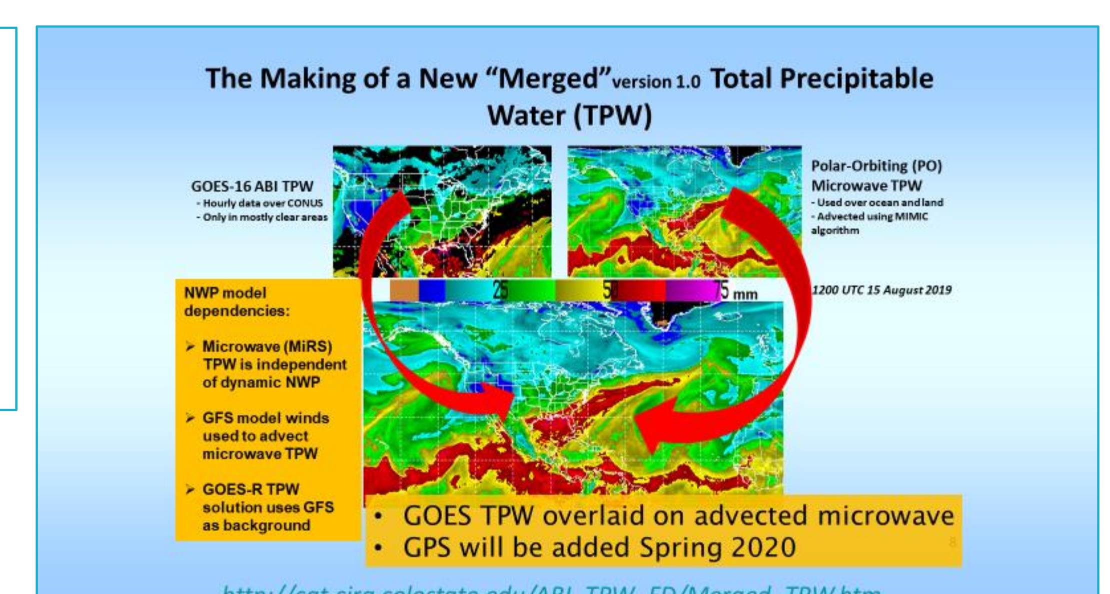

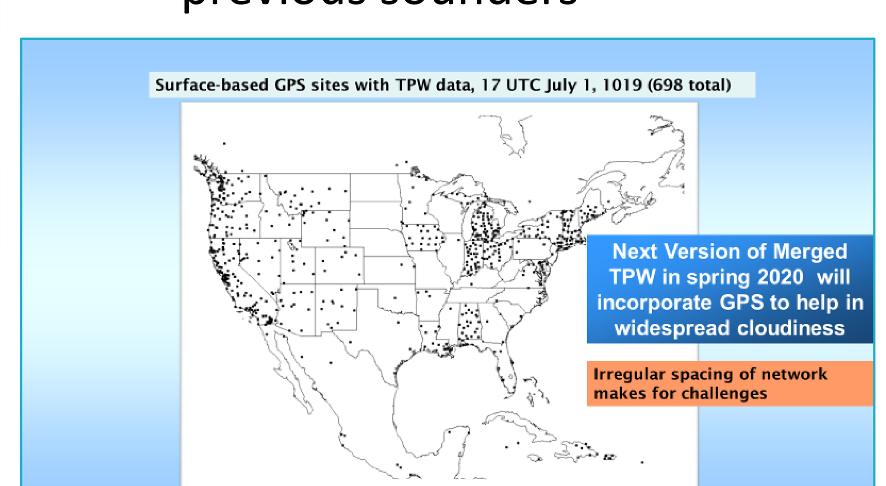

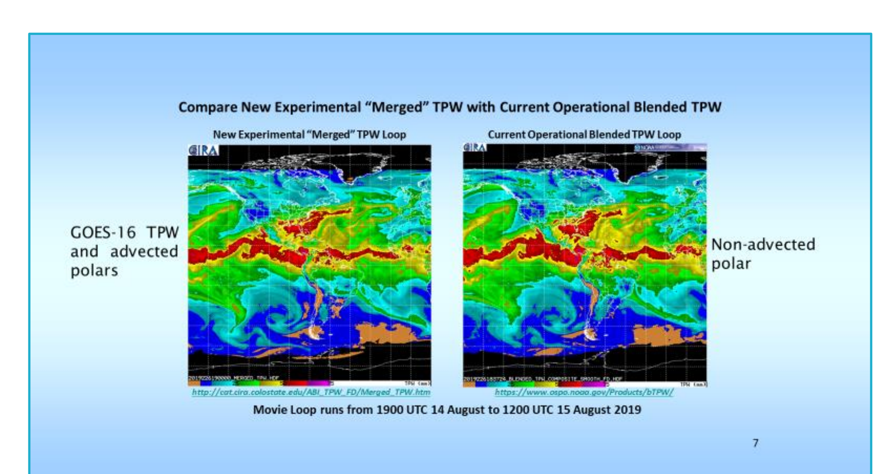

Cloud-Free Water Vapor Imagery Derived from Passive Microwave Data

Hypothesis: ABI Water vapor channels (6.2, 6.9 and 7.3 µm) simulated from microwave water vapor soundings will detect dry air masked by cirrus clouds in ABI imagery.

Configuration – Version 1 Cloud-Free Water Vapor Imagery

- Uses Advected Layer Precipitable Water (ALPW - polar satellite microwave product derived from NOAA MiRS soundings)
- GFS temperature profile
- CRTM v2.2.3
- Fixed surface and aerosol properties
- 16 km Mercator projection (same as TPW / ALPW family)
- Produced hourly for GOES-16/-17.

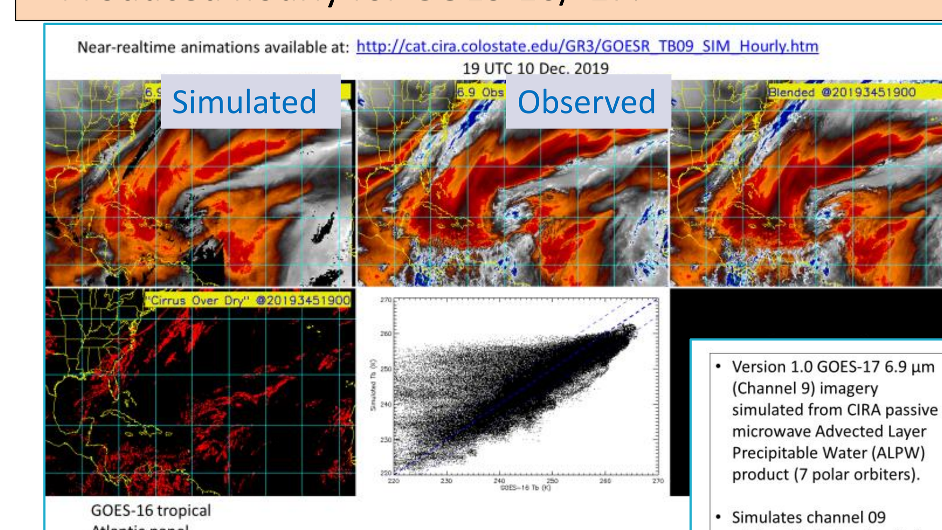

6.9 µm GOES-16 imagery

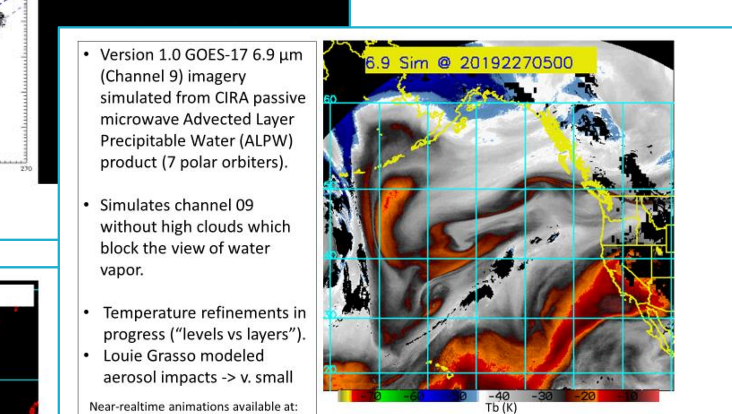

6.9 µm GOES-17 imagery

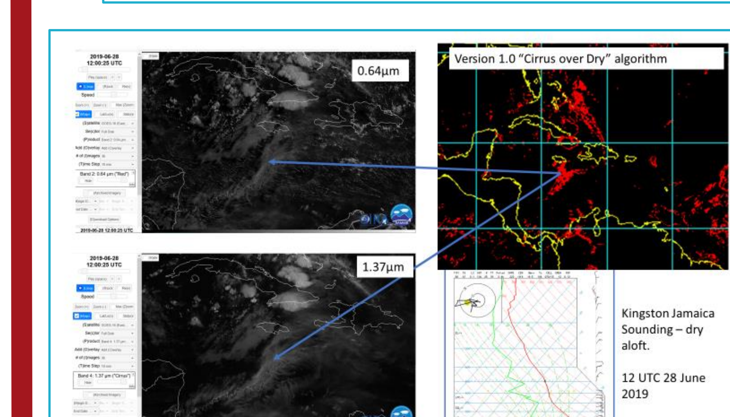

Cirrus over Dry Atmosphere

Summary and Future Work

Summary

- **A new blended TPW product which uses advection and GOES-16 in clear skies has been developed.**
- Comparisons of the GOES-16 TPW versus surface GPS and OCO-2 show low error (**RMS ~2 mm) with good temporal stability.**
- **Forecasters rated the new product higher than the current operational product.**
- **Open Question: How much model input is too much?**

Future Work

- Transition the new merged TPW into operations, including CIMSS MIMIC product.
- Survey users for applications of cloud-free water vapor imagery.

This work is supported by the NOAA GOES-R Risk Reduction and JPSS Proving Ground and Risk Reduction Programs.